Crises de liquidité endogènes dans les marchés financiers

Antoine Fosset

INSTITUT POLYTECHNIQUE DE PARIS

NNT : 2020IPPAX054

Thèse de doctorat

Crises de liquidité endogènes dans les marchés financiers

Thèse de doctorat de l'Institut Polytechnique de Paris
préparée à l'École polytechnique

École doctorale n°574 École Doctorale de
l'Institut polytechnique de Paris (ED IP Paris)

Spécialité de doctorat : Mathématiques appliquées

Thèse présentée et soutenue à Palaiseau, le 29 septembre 2020, par

ANTOINE FOSSET

Composition du Jury :

Damien Challet CentraleSupélec	Rapporteur
Fabrizio Lillo Università di Bologna	Rapporteur
Sophie Laruelle Université Paris-Est Créteil	Examinatrice
Kirone Mallick Commissariat à l'Energie Atomique	Examinateur
Jean-François Muzy CNRS & Université de Corse	Examinateur
Peter Tankov ENSAE Paris	Président
Michael Benzaquen CNRS & École polytechnique	Directeur de thèse
Mathieu Rosenbaum École polytechnique	Directeur de thèse
Jean-Philippe Bouchaud Capital Fund Management & Académie des Sciences	Co-encadrant
Alan Kirman EHESS	Invité

Remerciements

Je remercie tout particulièrement Michael Benzaquen de m'avoir pris sous sa direction et de m'avoir fait confiance pendant ces années de thèse. Grâce à son optimisme et sa motivation, j'ai pu m'épanouir pendant ces trois belles années. Mes plus grand remerciements vont ensuite à Jean-Philippe Bouchaud sans qui cette thèse n'aurait pas pu voir le jour. Son grand intérêt pour mes sujets de recherche ainsi que son aide scientifique ont été déterminants pour le déroulement de ma thése. Je remercie aussi Mathieu Rosenbaum pour ses conseils, son aide et son encadrement.

Je remercie grandement Fabrizio Lillo et Damien Challet d'avoir accepté de rapporter mon manuscrit de thèse. Je remercie aussi Sophie Laruelle, Jean-François Muzy, Kirone Mallick, Peter Tankov de faire partie de mon jury de thèse. Je suis très honoré de leur présence à ma soutenance et de l'intérêt porté pour mes travaux.

Mes remerciements vont ensuite à mes collaborateurs José Moran, Lorenzo Dall' Amico, Jean Herskovits, Davide Luzzati et particulièrement Alan Kirman pour m'avoir proposé de travailler sur les pêcheurs. Travailler avec eux a été particulièrement enrichissant et je leurs en suis extrêmement reconnaissant.

Je remercie tous ceux qui m'ont aidé d'une quelconque manière sur la rédaction du manuscrit. Merci à Mehdi et Jean pour leurs remarques scientifiques, merci à Malie et Yotam pour leur aide en anglais.

J'ai été très heureux de participer aux débuts de la chaire *Econophysix* de l'Ecole polytechnique et Capital Fund Management. Outre une expérience intellectuellement épanouissante, j'y ai rencontré Mehdi, Pierre-Philippe, Armine, Pierre, Christian, Federico, Samy, Michele et Rudy qui ont su mettre une très bonne ambiance.

Je remercie tout particulièrement le LadHyX et tous ses membres de m'avoir accueilli pendant ces années de thèse. Je suis très heureux d'avoir connu la formidable ambiance qui y règne. Un très grand merci à Kévin, Pierre, Tom Maddalena, Tom Marzin, Tullio, Benjamin, Ambre, Francesco, Blaise, Juliette, Caro, Sophie, Gabriel, Graham, Ernesto, Vincent, Thévy, Olga, Claire, Chuhan. Je remercie aussi le CMAP et les doctorants avec qui j'ai passé de bons moments : Othmane, Paul et Bastien.

Je remercie la société Capital Fund Management de m'avoir fourni un support de travail essentiel à ma thèse. Je remercie Stephen Hardiman pour tous ses conseils techniques sur les données. Cette expérience a aussi été le moment où j'ai rencontré Elise, Valentin, Amjad, Philémon, Côme et Léonard. Je remercie aussi tous les joueurs de babyfoot qui m'ont fait découvrir ce sport.

Je remercie chaleureusement mes colocs et mes amis de l'ENS pour les discussions scientifiques et tous les super moments que nous avons passé. Merci à Paul *aka* Mr CauKLM, Louise, David, Nico, Seb, Alexis, Guillaume, Manon, Emile.

Je remercie ma famille, mes parents qui m'ont transmis le goût des sciences, Mina, Malie, Juliette et Jean *aka* Jeannot l'envahisseur. Je remercie du fond du coeur tous mes cousins ainsi que tous mes amis pour leur soutien.

Abstract

Recent empirical analyses have revealed the existence of the Zumbach effect. This discovery has led to the development of quadratic Hawkes processes, which are suitable for reproducing this effect. Since this model is not linked with the price formation process, we extended it to order book modeling with a generalized quadratic Hawkes process (GQ-Hawkes). Using market data, we showed that there is a Zumbach-like effect that decreases future liquidity. Microfounding the Zumbach effect, it is responsible for a destabilization of financial markets. Moreover, the exact calibration of a GQ-Hawkes process tells us that the markets are on the verge of criticality. This empirical evidence therefore prompted us to analyse an order-book model constructed upon a Zumbach-like feedback. We therefore introduced the quadratic Santa Fe model and proved numerically that there is a phase transition between a stable market and an unstable market subject to liquidity crises. Thanks to a finite size scaling we were able to determine the critical exponents of this transition, which appears to belong to a new universality class. As this was not analytically tractable, it led us to introduce simpler models to describe liquidity crises. Setting aside the microstructure of the order book, we obtain a class of spread models where we computed the critical parameters of their transitions. Even if these exponents are not those of the quadratic Santa Fe transition, these models open new horizons for modelling spread dynamics. One of them has a non-linear coupling that reveals a metastable state. This elegant alternative scenario does not need critical parameters to obtain an unstable market, even if the empirical evidence is not in its favour. Finally, we looked at the order book dynamics from another point of view: the reaction-diffusion one. We have modelled a liquidity that appears in the order book with a certain frequency. The resolution of this model at equilibrium reveals that there is a condition of stability on the parameters beyond which the order book empties completely, corresponding to a liquidity crisis. By calibrating it on market data we were able to qualitatively analyse the distance to this unstable region.

Keywords: liquidity crises, Hawkes process, market microstructure

Résumé

De récentes analyses empiriques ont révélé l'existence de l'effet Zumbach : la tendance des prix passée augmente la volatilité future, indépendamment de son signe. Cette découverte a conduit à l'élaboration des processus de Hawkes quadratique, adpatés pour reproduire cet effet. Ce modèle ne faisant pas de lien avec le processus de formation de prix, nous l'avons étendu au carnet d'ordres avec un processus de Hawkes quadratique généralisé (GQ-Hawkes), en nous restreignant aux meilleurs prix d'achat et de vente. En utilisant des données de marchés du future sur l'Eurostoxx, nous avons montré que le couplage quadratique des prix passés existe et peut être décomposé en une contribution de la volatilité et une contribution de type Zumbach qui est l'origine microscopique de l'effet Zumbach. Ces deux contributions diminuent la liquidité future et sont responsables d'une potentielle déstabilisation des marchés financiers. De plus, la calibration exacte d'un processus GQ-Hawkes nous indique que ces couplages sont longue portée. Pour étendre notre analyse au delà du meilleur prix d'achat et de vente, nous avons introduit le spread effectif et analysé ses propriétés. Sa distribution en loi de puissance suggère que les marchés sont aux bords de la criticité. Ces preuves empiriques nous ont donc incité à faire une analyse d'un modèle de carnet d'ordres construit avec un couplage de type Zumbach. Nous sommes donc partis du modèle de Santa Fe qui supposent que tous les événements du carnet sont mutuellement indépendants et arrivent à taux constants. Nous avons introduit un couplage quadratique de type Zumbach sur les annulations d'ordres limites pour donner naissance au modèle de Santa Fe quadratique. N'ayant pas réussi à résoudre ce modèle analytiquement, nous avons fait une analyse numérique rigoureuse et prouvé qu'il existe une transition de phase entre un marché stable et un marché instable sujet à des crises de liquidité. Grâce à une analyse de taille finie nous avons pu déterminer les exposants critiques de cette transition, appartenant à une nouvelle classe d'universalité. Dans le but d'avoir des résultats analytiques, nous nous sommes orientés vers des modèles plus simples pour décrire les crises de liquidités. En mettant de côté la microstructure du carnet d'ordres, nous obtenons une classe de modèles de spread. Ces modèles consistent à modéliser le taux d'ouverture et de fermeture du spread. Nous avons analysé, d'un point de vue numérique et théorique, les propriétés de ces modèles en considérant un couplage de type Hawkes linéaire sur le taux d'ouverture du spread puis un couplage de type Hawkes quadratique. Ces modèles sont sujets à des transitions de phase ne possédant pas les mêmes exposants de celle du Santa Fe quadratique. Néanmoins ils ouvrent de nouveaux horizons pour explorer la dynamique de spread. De plus, en introduisant un couplage non-linéaire, nous obtenons un dynamique métastable : si nous attendons suffisamment longtemps une crise de liquidité arrivera. Nous avons calculé ce temps analytiquement et confronté nos résultats avec des donnés numériques. Ce scénario alternatif élégant n'a pas besoin de paramètres critiques pour obtenir un marché instable, même si les données empiriques ne sont pas en sa faveur. Pour finir, nous avons regardé la dynamique du carnet d'ordres sous un autre angle: celui de la réaction-diffusion. Nous avons modélisé une liquidité qui se révèle dans le carnet d'ordres avec une certaine fréquence. La résolution de ce modèle à l'équilibre révèle qu'il existe une condition de stabilité sur les paramètres au-delà de laquelle le carnet d'ordres se vide totalement, correspondant à une crise de liquidité. En le calibrant sur des données de marchés nous avons pu analyser qualitativement la distance à cette région instable. Au delà des crises de liquidité, ce modèle est aussi particulièrement utile pour calculer l'impact des métaordres. Nous l'avons donc numériquement étudié et montré que notre modèle reproduit bien la loi en racine *i.e.* l'impact est en racine du volume exécuté.

Mots clés: crises de liquidité, processus de Hawkes, microstructure de marché

Contents

Foreword

During my Bachelor's studies at the École Normale Supérieure, I discovered the world of statistical physics. In these academically transformative years, I became fascinated with the breadth of possibilities encapsulated by applying advanced theoretical tools on real-world physical systems. Quite naturally, the intersection between the theoretical and the applied oriented me towards the field of Econophysics. Nonetheless, at the time I felt that in order for me to truly rigorously research these topics, I should improve my theoretical background as well as my proficiency in modeling tools. Hence, I completed my Master in Financial Mathematics at École Polytechnique, which enabled me to develop expertise in stochastic calculus and statistical methods. Consequently, I harnessed my newly gained skillset and took a research-based internship at Capital Fund Management (CFM) in which I could further enhance my knowledge by studying the microstructure of financial markets and liquidity crisis. My experience in this internship led me to pursue a PhD under the supervision of Michael Benzaquen, Jean-Philippe Bouchaud and Mathieu Rosenbaum at LadHyx and CMAP.

During my PhD, I followed the footsteps of J. Donier and investigated the link between price trends and liquidity, showing that they can destabilize the market. We also developed financial supply and demand toy models which could answer these questions analytically. To do so, we considered the existence of feedback loops in our models which, inevitably, led to a high ratio of endogeneity that can trigger liquidity crises. Empirically, we examined financial market data, that was generously provided by CFM. The superb quality of the data and more importantly, the meaningful insights of CFM's researchers enabled us to analyze market destabilization in great detail at the micro scale, using self-excited models. Furthermore, addressing market stability conditions using other theoretical tools was critically important to our work. With the much-appreciated help of my former intern Lorenzo Dall' Amico, we applied a reaction-diffusion model and found critical market stability conditions. We also developed a method to calibrate this type of model on empirical data.

On a personal note, I am greatly honored to have had the unique opportunity to take part in the creation of the fantastic École Polytechnique & CFM's "Econophysics & Complex Systems Chair". More broadly speaking, witnessing the recent growing popularity of the Econophysics field thrills me as I am sure this expanding, such vibrant field will be a significant platform for cross-disciplinary cooperation that will lead to important findings. In the spirit of Agent Based Modeling, my PhD colleague José Moran and I focused on various puzzles unrelated to finance. One such case was solving the dynamics of Kirman's ants model, aiming at reproducing spontaneous herding and sudden opinion shifts. Moreover, thanks to the gracious help of Davide Luzzati and Pierre Lecointre, we analyzed a model of habit formation by self-reinforcement memory effects. Later, we collaborated with Alan Kirman, and together we extended his model by modelling fishers' decisions making.

I have chosen to put the finance parts as the main corpus of the manuscript. My agent based modeling work that is not directly related to finance nor to liquidity crisis consequently appears in the appendices. The manuscript's structure is as follows: **Chapter 1** provides an introduction to financial markets and liquidity crises. We start by presenting some previous models on which we build our own. We especially focus on self-excited models which are particularly suited for considering market endogeneity. In **Chapter 2** we present a class of models, namely General Quadratic Hawkes processes which we than calibrate on financial

data. **Chapter 3** is dedicated to theoretical and numerical analysis of an order book model which is inspired by General Quadratic Hawkes process. In order to reduce the complexity level, we introduce various spread models in **Chapter 4**, that are appropriate to analyze market stability. Then, we model the latent order book's liquidity in **Chapter 5**. All the technical details and mathematical proofs are provided in **Appendix A**, as well as additional results and plots. **Appendix B** deals with Complex Systems and focuses on a model of habit formation exhibiting self-trapping properties. In **Appendix C**, we fully solve the dynamics of Kirman's ant model. **Appendix D** contains Kirman's extended model which we develop by studying herding effects in the behaviour of fishermen.

List of papers being part of this thesis

- L. Dall'Amico , **A. Fosset**, J. P. Bouchaud, M. Benzaquen (2019). How does latent liquidity get revealed in the limit order book?. *Journal of Statistical Mechanics: Theory and Experiment, 2019*(1), 013404.

- **A. Fosset**, J. P. Bouchaud, M. Benzaquen (2020). Endogenous liquidity crises. *Journal of Statistical Mechanics: Theory and Experiment, 2020*(6), 063401.

- J. Moran, **A. Fosset**, D. Luzzati, J. P. Bouchaud, M. Benzaquen (2020). By force of habit: Self-trapping in a dynamical utility landscape. *Chaos: An Interdisciplinary Journal of Nonlinear Science, 30*(5), 053123.

- J. Moran, **A. Fosset**, M. Benzaquen, J. P. Bouchaud (2020). Schrödinger's ants: A continuous description of Kirman's recruitment model.*Available at SSRN 3575759.*

- **A. Fosset**, J. P. Bouchaud, M. Benzaquen (2020). Non-parametric Estimation of Quadratic Hawkes Processes for Order Book Events. *arXiv preprint arXiv:2005.05730.*

- J. Moran, **A. Fosset**, A. Kirman, M. Benzaquen (2020). From Ants to Fishing Vessels: A Simple Model for Herding and Exploitation of Finite Resources.*In prep.*

1

Introduction

1929's "Black Thursday" and 2010's "Flash Crash" left a deep scar in the history of Finance. These events were the result of liquidity crises, which happen when buyers/sellers are too afraid to buy/sell. Some of the most terrible liquidity crises were followed by dreadful financial and economic consequences. In an attempt to better understand liquidity crisis, we will try to model investorâs panic by extending existing models. We will first present several price and order book models that reproduce important stylized facts, that could than help us build a model that properly reproduce liquidity crises. We, therefore, start with general descriptions of financial markets, of main market participants and of financial crises. We than present several models of price and volatility. Finally, we introduce models of the limit order book, in which trading occurs on electronic markets.

Panic on Wall Street in October 1907 after a price drop on commodities. Picture from [1]

Contents

-

La science consiste à passer d'un étonnement à un autre.

Aristote

1.1 Financial markets & liquidity crises

Market participants

A market is a place where buyers meet sellers to execute transactions. The products they can buy and sell are very diversified: shares of stocks, indices, foreign exchange, derivative products (futures, options, etc.), bonds, commodities, cryptocurrency. Even though each product has its own specificity, dynamics is mainly determined by the way agents interact. Such dynamics is characterised by being very rich and complex due to the heterogeneity of market participants. Indeed, the spectrum of the time horizon of their strategies is very wide: from seconds or less for high-frequency agents to several years for low-frequency ones. A presentation of the market ecology will help us to understand and study the dynamics of the market. A full classification of the market participants would be beyond the scope of this work. Nevertheless , we can identify the following main types of agents:

- **Market makers**: they are liquidity providers. Tipically high-frequency agents, they post passive orders at the buy and sell side, then, they wait for other participants of the market to come and take their orders. As their name implies, they make the market by intermediating between slower buyers and sellers that would not be able to meet on the market at the same time. Essential to markets' ecology, some of them are paid by the exchange to ensure sufficient liquidity. Otherwise, they make money from the difference between their buying and selling quotes and are then very profitable when the price is mean-reverting. Their risk comes mainly from their inventory: if the price trends in the opposite direction of their position they lose a lot of money. They therefore adjust their price quotations to manage their risk as well as possible. The capacity of their strategies is low, but they trade very frequently, which makes them profitable on average.

- **Long investors**: they take a position on the market and re-balance their portfolio from time to time. The time horizon of their strategy is very long, around several years, and their assets under management are huge. Thus, it can take them days to buy/sell their market positions. Because of the long time horizon, executing their transactions does not require sophisticated optimization techniques. They can use different types of strategies (momentum, ETF, fundamental etc.). They are usually institutional investors or pension fund managers.

- **Brokers**: they give an access to the market to those who cannot. Their clients cannot trade themselves on the market due to a technological gap, nor the best strategy to execute large orders. Their goal is to minimize the transactions costs by splitting smartly the orders of their clients.

- **Banks**: they offer derivative products, that we can interpret as insurance contracts, to their clients and manage their risks. They have teams working on elaborating such products that will suit the needs of their clients. Nevertheless, they can also have teams that do market-making, long term investment and brokerage.

- **Other participants**: other participants can play in between all the possible strategies, on both short or long time scale.

Although technological advances have reshaped the market by providing new opportunities, the way agents trade and strategies are much the same. We can therefore say that this classification is stable over time. In what follows, we will keep in mind that market participants are **highly heterogeneous**.

Electronic markets and the limit order book

Historically, agents were physically present in the stock exchange. Such vivid scenes were well described by Emile Zola in his novel "L'Argent". Some movies also represent the market at this stage, in the "Wolf of Wall Street" of Martin Scorsese for example. As previously mentionned, the emergence of new technologies have deeply reshaped the markets. First, the market switched to Over The Counter (OTC) markets where people negotiated products via telephones. Then, the development of the internet enabled news possibilities: trading on fully electronic markets. These markets are managed by a computer that matches the orders of agents, under systematic rules. Even though some OTC markets remain, the majority are electronic nowadays. Electronic markets are believed to be an optimal setting to allow fair access to the market. It aims at a better spread of the information to everyone and reduces insider trading. On the other hand, all the trades and intentions of trades of agents are stored and the regulation uses this data to detect frauds and illegal actions. Market regulators are therefore encouraging platforms to upgrade to such automated operation. From our point of view, electronic markets have made it possible to record an incredible amount of data. By dissecting this real treasure, we have the opportunity to understand the functioning of markets in detail.

Since 2007, the emergence of Multilateral Trading Facilities has enabled agents to buy the same contracts on different electronic exchanges. Since then, electronic markets have become fragmented. We can cite "Chi-X" or "Turquoise" as competitors of the classical exchanges Euronext, NYSE, LSE etc. Offering different types of fees, their creation was made to reduce trading costs for market participants. From our perspective, it may complicate our modeling as we are interested in the aggregated market. By aggregate, we mean the sum of what happens on all the exchanges where we can buy the same asset. Nevertheless, we first need to understand what electronic markets are all about.

We chose to focus on a particular type of electronic markets: a double auction one. It offers the possibility for an agent to trade passively or aggressively. With the first option, an agent can post a buy or sell order, which consists in a number of shares at a given price and wait for a counterpart. This passive order is called a limit order. Agents can cancel their passive orders if no counterpart has yet been found. The second option, called a market order, consists of matching an existing limit order. All these limit orders are stored in the limit order book. A schematic describing it is displayed on Fig. 1.1. It represents the interaction between supply and demand on financial markets, essential to understand the price formation process. We refer to bid (*resp.* ask) side for the buy (*resp.* sell) side in the following. An important notion emerges from the order book: the liquidity. It refers to the quantity of shares available in the order book at a given time. Thus, posting a limit order in the limit order book **provides liquidity** while posting a market order **takes liquidity**. Note that some exchanges provide to their clients other fancy types of orders. More difficult to model, we restrict ourselves to exchanges and assets where only these three orders are available. Concerning market fragmentation, we assume that either we have access to the aggregated order book and if not that, the one we have is representative of the aggregated one.

Let us focus on the quantities and concepts introduced in Fig. 1.1, that are key elements for limit order book functioning. The prices on which market participants can place their

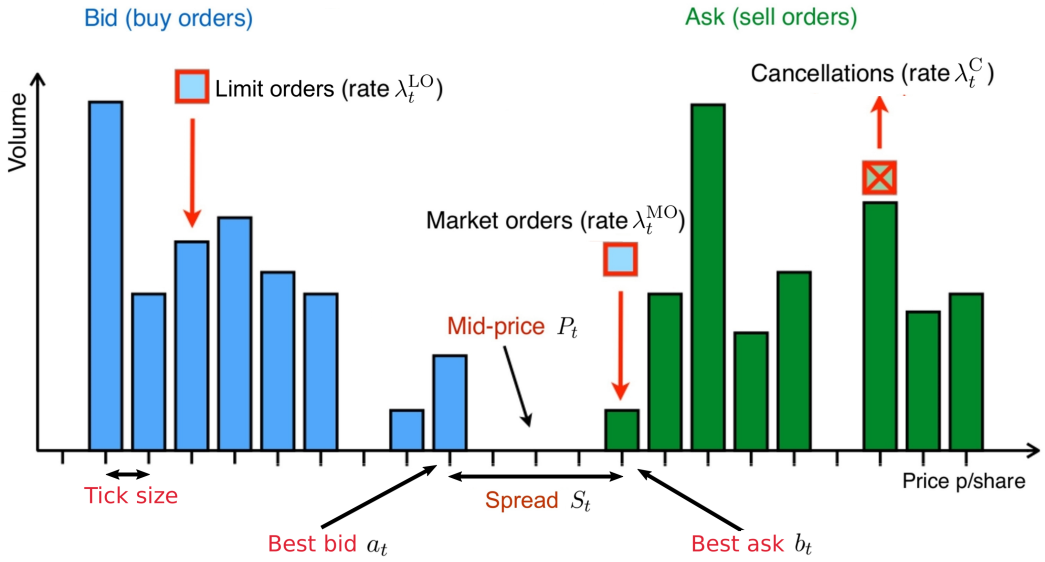

Figure 1.1: *Definition of the limit order book.*

orders are fixed: the quotation step is called the tick size. Fixed by the regulation, it varies across assets. For example, it is 0.01\$ for US stocks on NASDAQ and 1€ for the EUROSTOXX future contract. We call the best bid b_t (*resp* ask a_t) the best price of the bid (*resp* ask) side, at a time t. The spread S_t is defined as the difference between the two:

$$S_t = a_t - b_t \tag{1.1}$$

The spread is often given in tick units. We can classify assets by looking at their spread:

- **Large tick** stocks have an average spread almost equal to one, in tick units.
- **Small tick** stocks have an average spread equal to a few ticks.

The properties of the order book are different for these two types of stocks. While large tick stocks order book is full, small ticks stock order book looks sparse *i.e* some of the price levels are empty.

The "price" of the asset is formed within the order book. But presented this way, it suggests that there is one way to define it, which is untrue. To illustrate our statement, we provide a few definitions of prices that have interesting properties. First, we can define the price of the last transaction price. Not easy to use mathematically, the most common price is the mid-price:

$$P_t = \frac{a_t + b_t}{2} \tag{1.2}$$

Let's note that the mid-price only changes when the best ask or best bid changes. If the number of shares v_t^{b} at the best bid and best ask v_t^{a} are bigger than the average size of market orders, the time scale of price changes will be far bigger than the one between two order book events. If we need a price that evolves on a faster time scale, we can introduce the *micro-price* [2, 3] P_t^{micro} that accounts for supply/demand interactions:

$$P_t^{\mathrm{micro}} = \frac{v_t^{\mathrm{a}} b_t + v_t^{\mathrm{b}} a_t}{v_t^{\mathrm{a}} + v_t^{\mathrm{b}}} \tag{1.3}$$

Whatever definition of the price we choose, it is the basic information on the asset coming from the order book, that is available to all market participants. Its formation takes place

through the order book, as a dynamical interaction of supply and demand.

As we wish to model the limit order book dynamics, we will look at the rates of order book events. We define a rate as the number of events per unit of time, typically seconds. The output of an order book model will give us a dynamics of liquidity, spread and price, hoping that they will reproduce the stylized facts we want to model.

Why study financial crises?

After briefly describing markets' ecology, we ask ourselves the key question: why are financial markets so prone to crashes? Indeed, in the past decades and century, financial markets have episodically suffered from a lack of stability. Important price drops, crashes happen too frequently, shocking people's mind and sometimes leading to terrible economic outcomes. Historical review of major crashes will certainly give us insights about the mechanisms of crises. The 1920th decade was characterized by a huge growth of the economic production, built on post-war optimism. During that period, stock prices dimbed too fast and became too high relative to the underlying economic production, which caused overproduction. This mechanism created a speculative bubble that was stopped by the very infamous "Black Thursday" on October 24th 1929. On this very day, the Dow Jones suffered of a 22.6% drop at noon, followed by two consecutive drops the Monday and Tuesday after, starting then the Great Depression. The analysis of what happened this day is very important to understand the mechanism of financial crises. A great panic took the New York Stock Exchange and the liquidity of buyers *i.e.* the number of buyers vanished: market participants were too afraid to buy at any price. This mechanism made the price crash strongly. Unfortunately, this crisis spread and hit the economic sector creating recession, abnormally high unemployment, etc. The damages lasted several years, worldwide, and it took years for the economy to recover. More recently, in October 1987, the US stock market suffered from another crash of a huge intensity: the price of the Dow Jones dropped of 22.6%. To prevent the financial crisis to propagate into the real economy, the Fed injected liquidities in the financial sector. This action avoided the emergence of a global crisis but the crash spread to other foreign markets with huge drops on indices. But thanks to the Fed, this crash, called "Black Monday", was just a "liquidity crisis" and not an economic one. It had another interesting consequence: in 1998, the US government introduced a system of circuit-breakers to the stock markets. It functions as follow: when the price moves more than a given threshold, market activity halts. Unfortunately, these mechanisms could not fully prevent crises from occurring as the 21st century has already known a few, we can mention the financial crises of 2008 caused by sub-prime mortgage backed securities, the Flash Crash on the S&P500 of 2010 [4] and the Covid-19 crisis we are currently suffering from. The origins of crises vary, depending on the economic context, nevertheless, the crash itself seems universal. Panic takes the buyers leading to liquidity dry out that makes the price crash.

An interesting observation is that some crises are not triggered by economic news. The most striking example of it is the Flash Crash of the 6th of May 2010. The evolution of the price of the future on S&P500 is displayed on Fig.1.2, the S&P500 is an index composed of the 500 biggest US companies quoted on financial markets (NYSE or NASDAQ). A huge drop of almost 10% hit this asset that was stopped by circuit-breakers. Surprisingly, the price increased after market reopened with a much smaller daily price drop. No economic crisis followed this flash crash, but it spread to many other assets, where liquidity dried out and price crashed. The origin of this flash crash is due to an oversized sell order that destabilized the market. The practices of High Frequency Traders were pointed out, and they were accused of having worsened it. Other flash crashes that happened in the last decade include: the Treasury bond flash crash the 15th of October 2014, the British pound flash crash the 7th of October 2016 on the pound/dollar rate and the Bitcoin flash crash of 23rd October 2019 on the bitcoin/dollar rate for example. Nevertheless, financial markets

have always been unstable. For example, on May 28th, 1962, the S&P500 suffered a flash crash of severity similar to the that of May 6th, 2010 [5]. This happened with good old market makers and, obviously, no HFT. Upon closer scrutiny one finds that the frequency of large price moves is remarkably stable over time, see e.g. [6]. Investigating those flash crashes may help to understand better market stability. Essential to fair trading to all market participants, market stability is also indispensable for a stable economy. Past financial crises have shown that destabilized markets could trigger economic ones. Thus, understanding the mechanisms that lead to flash crashes and liquidity crises is a core subject as it can help us prevent dangerous panic on markets.

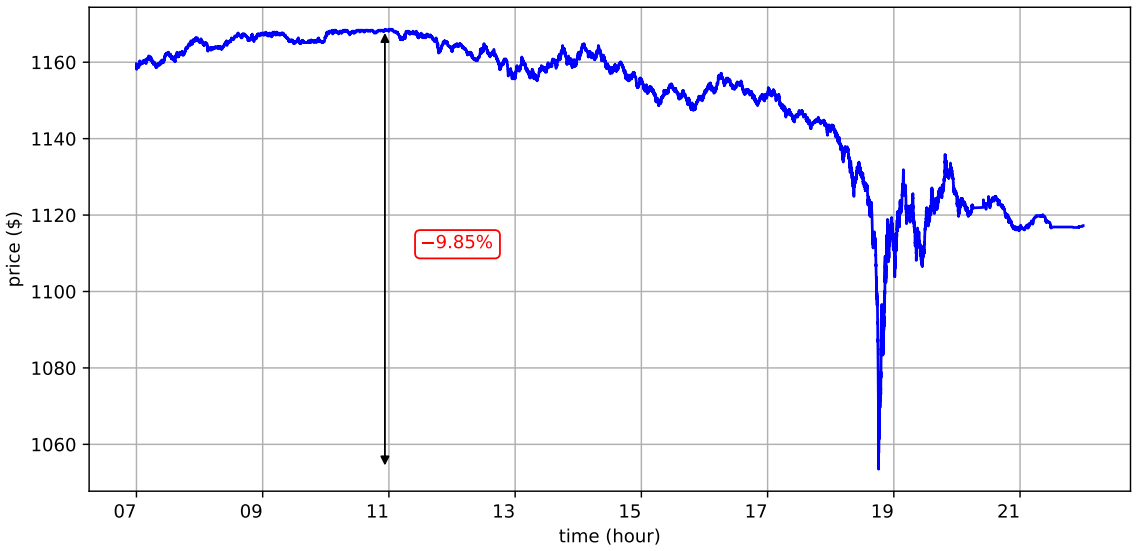

Figure 1.2: *Price of the future contract on S&P500 during the 6th of May 2010. The time are displayed in GMT+1 i.e. French time.*

The notion of panic, that remains over decades of financial industry, seems to be the key of liquidity crises. This suggests that building a model for liquidity crises requires to model the agents behind the market. The agent-based model (ABM) is actually designed for such issues. The idea consists of modeling the behaviour of microscopic agents and extracting the global behaviour of the system. This idea is very common in Statistical Physics and has been applied to many systems such as gases or bird flocks. Indeed, a gas is composed of a huge number of particles that interact at the microscopic scale. The tools of statistical Physics enable to derive the macroscopic behaviour from the microscopic ones. We wish to do exactly the same thing: understand the microscopic scale by modeling the market participants to get a macroscopic description of prices.

1.2 What drives price and volatility?

Modeling the price of an asset has been the center of interest for economists, mathematicians and physicists for many decades. This difficult challenge was the cause for the creation of many interesting models. Modeling the price strongly depends on the scale we are looking at: some people will be interested at the intraday scale while others will focus on longer scales that can range from weeks to years. In this section we present some models that have been introduced in the past. Even though some are far from accurately describing reality, it is interesting to analyze the motivation behind them. We will be especially interested in price models that can be micro founded *i.e.* that can be derived from a microscopic model. For us, a good price model is micro-founded and can reproduce long term stylized facts.

First draft of price models

Bachelier's price

The first major breakthrough in price process modeling was achieved by Louis Bachelier in this thesis "Théorie de la spéculation" [7] at the very beginning of the 19th century. By looking at the fluctuations of the price, he decided to use a very new mathematical object at this time: the Brownian motion. The underlying idea was to model these fluctuations as independent and identically distributed random variables, with a finite variance. Even though these hypotheses seem too strong, the result has some interesting properties. Mathematically speaking, we can write the price as:

$$P_t = P_0 + rt + \sigma W_t \tag{1.4}$$

with W_t a Brownian motion, r the local price trend and σ the volatility *i.e.* the amplitude of the fluctuations of the price. One interesting property of this model is that the price without its trend is **martingale**:

$$\mathbb{E}\left[P_{t+s} - P_t - rs|\mathcal{F}_t\right] = 0 \tag{1.5}$$

where $s > 0$ and $\mathcal{F}_t$ denotes the available information[1] at time t. In other words, we cannot predict price changes from past price changes. This is relatively well verified at large time scale for the price process. On the other hand, such model predicts that the price changes follow a gaussian distribution. Indeed, $P_{t+s} - P_t$ is a gaussian distribution of mean rs , variance $\sigma^2 s$ and thus a probability distribution function $\rho_{P_{t+s}-P_t}$:

$$\rho_{P_{t+s}-P_t}(x) = \frac{e^{-\frac{(x-rs)^2}{2\sigma^2 s}}}{\sqrt{2\pi\sigma^2 s}} \tag{1.6}$$

This fails to reproduce the empirical distribution of price changes, also called price returns, for two reasons. First of all, it allows the price to be negative. The simplest modification that can be achieved is to consider that the logarithm of the price follows a Brownian motion, as we will see later on. But it cannot explain the statistics of price changes on short time scales as they are not well described by gaussian variables. Nevertheless, the model of Bachelier was the precursor and the financial modelling that exploits Brownian motion and stochastic calculus to build more realistic price models.

Log normal price

The model of Bachelier allows the price to be negative[2], which makes his model not suited for long-time behavior. The simplest way to bypass this problem is to consider that the logarithm of the price is a Brownian motion:

$$P_t = P_0 e^{\left(r - \frac{\sigma^2}{2}\right)t + \sigma W_t} \tag{1.7}$$

The price follows what we call a log-normal distribution. Fig. 1.3 displays two tests of such model on the daily data of the S&P500 from 21/04/1982 to 04/06/2020. We define the daily return r_d:

$$r_\mathrm{d}(t) = \frac{P_{t+1}}{P_t} - 1 \approx \ln\left(\frac{P_{t+1}}{P_t}\right) \tag{1.8}$$

[1] Note that if $\mathcal{F}_t$ is not explicitely specified, it refers to the information generated by the price process itself.

[2] That situation could occur on commodities and energy markets after outsanding drops of demand, as a consequence of storage costs.

If we believe Eq.(1.7), then the daily returns should be gaussian. Fig. 1.3(a) checks if the logarithm of the price follows a diffusion by looking at $\mathbb{V}\left(r_d(\cdot+\tau)-r_d(\cdot)\right)$ as a function of the lag τ. When it behaves as a power law $\tau^{2\mathcal{H}}$, the exponent $\mathcal{H}$ called Hurst exponent determines the type of diffusion:

- $\mathcal{H} < 1/2$: sub-diffusion.
- $\mathcal{H} = 1/2$: normal diffusion.
- $\mathcal{H} > 1/2$: super-diffusion.

Here we find $\mathcal{H} \approx 0.48$ in favour of a normal diffusion which is based on Brownian motion. Nevertheless, Fig. 1.3(b) looks at the empirical distribution of the daily and compares it with a gaussian with same mean and variance than r_{d}. Not in agreement with the empirical distribution, we see that large events are not taken into account at all by this model. Thus, we will try to explain those large returns using other models.

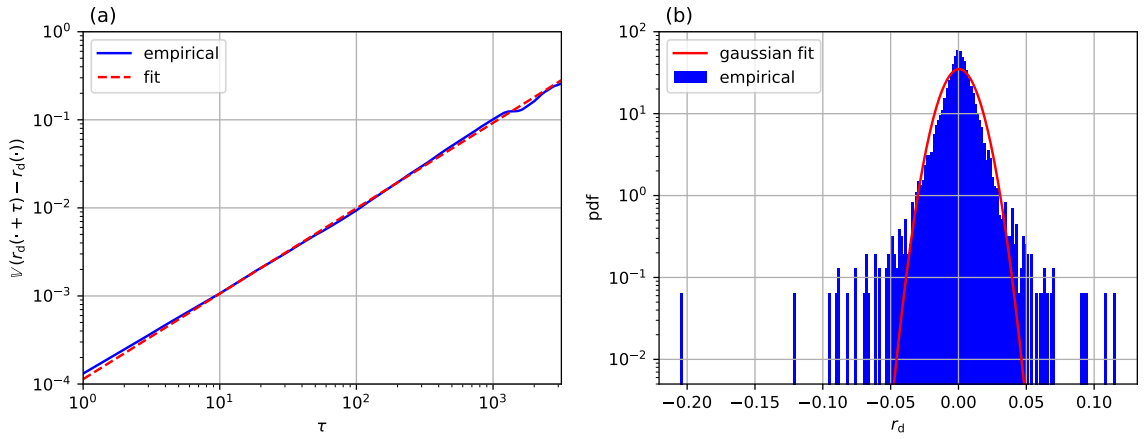

Figure 1.3: *Properties of the daily price returns* r_{d} *of the S&P500 from* 21/04/1982 *to* 04/06/2020. *(a) Scaling of* $\mathbb{V}\left(r_d(\cdot+\tau)-r_d(\cdot)\right)$ *and the a linear regression in loglog scale.* τ *is given in trading days. (b) Probability distribution function (pdf) of the daily returns* r_{d}*, with a gaussian distribution with the same mean and variance.*

Efficient price

The Bachelier's model and its extension have modeled price changes using a powerfull mathematical tool, but they did not focus on why prices change in the first place. A simple argument states that the large price changes could be explained by some external news. Let's take a simple example, if a company that sells cellphones, announces that it has over-performed by 20% more than the previous year, agents will reassess the value of the enterprise making the price suddenly increase. In practice, news can create substancial price changes if they are not expected. For example on May 1st 2020, Elon Musk tweeted that the price of Tesla, his own company, was too high. The market reacted with a 10% drop of the price during this day. An attempt of price model based on the idea asserts that the price is driven by news. The economist Eugene Fama is famous for having highlighted this point. He introduced the Efficient Markets Theory in the 1970's. His article "Efficient Capital Markets : a Review of Theory and Empirical Works" [8] reviews all the theories that make the market efficient. This concept means that the market should fully reflect the available information. The price is, then, the rational anticipation of the future of an intrinsic value P_∞. Calling

$\mathcal{F}_t$ the available information until time t and P_t the price at time t, we can write:

$$P_t = \mathbb{E}[P_\infty | \mathcal{F}_t] \tag{1.9}$$

We note that such dynamics defines a price that is a martingale for $\mathcal{F}$. One important remark we can address to this point is that the notion of information is unclear, as many features can be taken into account. Nevertheless, the way it is formulated underlies that it corresponds to news announcements that have a link with the asset. And so it does not take into account volatility, trade imbalance, etc. According to this theory, the price should move only when a piece of news appears and, in between, it should fluctuate around a constant value. If we believe this dynamics, the amplitude of the fluctuations *i.e.* the volatility, and the price changes should be explained only by the news.

Anomalous price returns: exogenous or endogenous?

The Efficient Markets Theory was first criticized by the economist Robert Shiller. His works have shown that the volatility of the market is too high to be explained by rational visions of the future. Well established in the literature [9] , this point is now considered common fact. Agents are not rational and behave due to their emotions, fears and not complex future expectations. This means that Eq. 1.9 is not well suited to describe the price dynamics with $\mathcal{F}_t$ containing the exogenous news.

Previously, we gave examples of news that have a strong effect on the price. We would like to reverse this analysis: considering large price changes, are they triggered by some news? A recent study by Joulin et *al* [10] answered this question. They measured the typical volatility σ on one minute and selected price changes bigger than 4σ. In a gaussian world, those changes could not exist. But there financial markets are full of them. Then the authors tried to link these large price changes with external news. They have drawn the following conclusions: only 5% of such price changes are triggered by external news, meaning that the other 95% are endogenous *i.e.* created by the market itself. The behavior of the volatility around a piece of news or an endogenous event is different. Indeed, while in both cases it jumps right at the event and then relaxes to ito its preceding value, the way it relaxes varies. In the first case the relaxation is a power law in time with exponent -1, whereas in the second case, the exponent is -0.5. Note that, in both cases, the market takes some time to digest the information but it takes more time for endogenous events. They lead to a persistent high volatility regime that cannot be explained by any rational theory, providing another evidence that justifies Schiller's statement: agents in financial markets are far from rational. We also note that modeling this high ratio of endogeneity will require to introduce feedback in the dynamics in order to model agents' behavior.

Volatility is a complex process that has very interesting properties, not only around large price returns. Fig. 1.4(a) shows volatility of the S&P500 over almost forty years. We have estimated it with the Parkinson estimator [11]:

$$\sigma(t) = \frac{1}{\sqrt{4 \ln 2}} \ln \left(\frac{High_t}{Low_t} \right) \tag{1.10}$$

where $High_t$ (*resp* Low_t) is the highest (*resp* lowest) value of the price during the day t. It reveals some clusters of high volatility regime and periods of lower volatility regime. Fig. 1.4(b) displays the auto-correlation of the volatility in trading days, exhibiting a power law like behavior. The auto-correlation is still relatively high after almost a lag of two years. This property explains why volatility is described as persistent. By looking at Fig. 1.4(a), the volatility seems to behave less regularly than a Brownian diffusion. In that sense, we can say that volatility is rough. A characterisation of its roughness is related to the scaling of $\mathbb{V}\left[\sigma(\cdot + \tau) - \sigma(\cdot)\right]$. The Fig. 1.4(c) shows this scaling in a log-log scale, fitted by $A\tau^{2\mathcal{H}}$. The

agreement with the fit is very strong, giving the value $\mathcal{H} = 6.7 \times 10^{-2}$. As we find $\mathcal{H} < 1/2$, the volatility is a **sub-diffusive** process. Gatheral *et al* [12] have done a full empirical analysis of this roughness and have exploited these properties to construct a theoretical framework compatible with this type of sub-diffusion. We are not going to go deeper into this model as we will not use it later, even though it provides interesting elements.

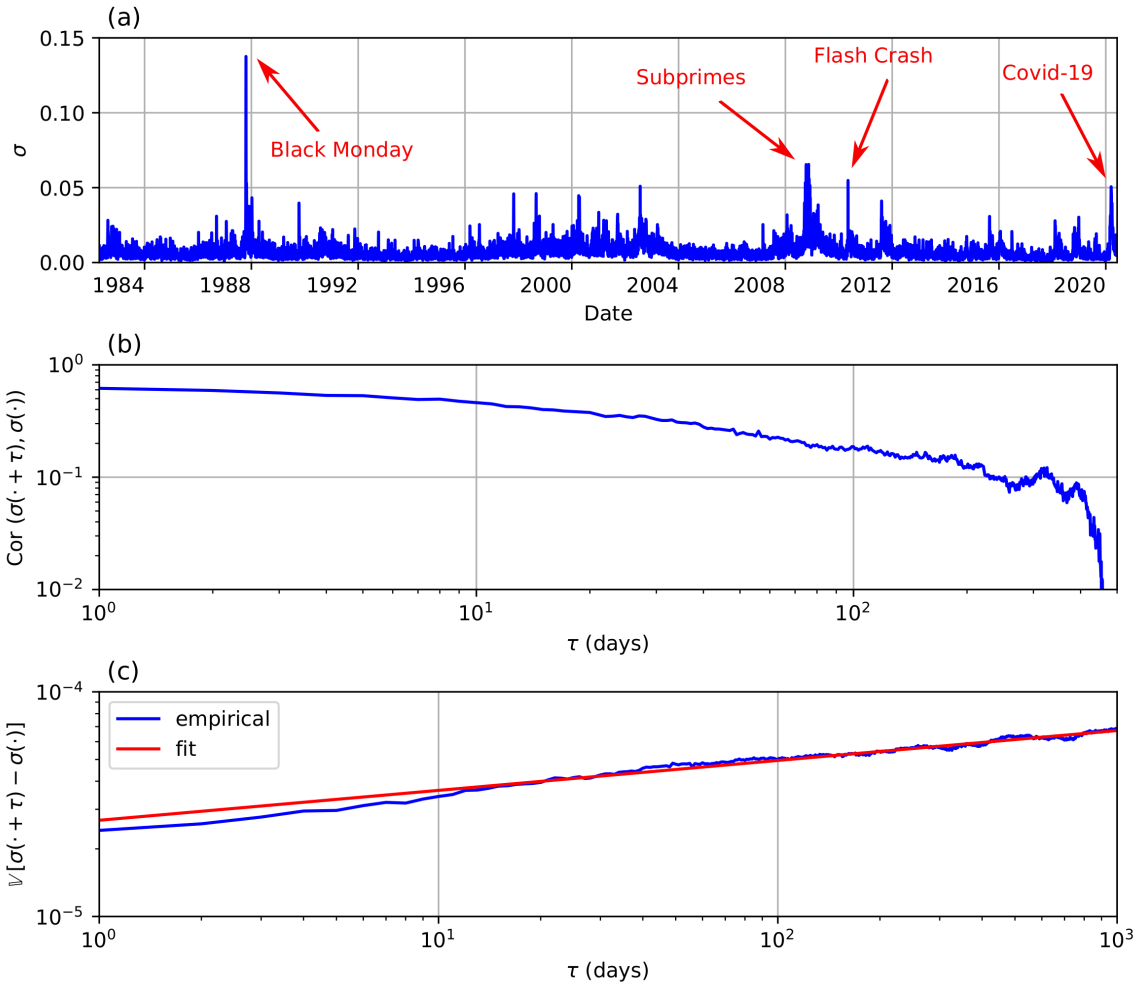

Figure 1.4: *Properties of the volatility of the S&P500 from* 21/04/1982 *to* 04/06/2020. *(a) Volatility trajectory on which we have displayed four major crises: the "Black Monday" of 1987, the subprimes crisis of 2008, the Flash Crash of 2010 and the Covid-19 crisis of 2020. (b) Auto-correlation of the volatility in trading days. (c) Scaling of* $\mathbb{V}[\sigma(\cdot + \tau) - \sigma(\cdot)]$ *with* τ *fitted by* $A\tau^{2\mathcal{H}}$, *with* $\mathcal{H} = 6.7 \times 10^{-2}$.

These two stylized facts show that the volatility and price dynamics are highly endogenous and strongly correlated. Furthermore, the power law behavior of $\mathbb{V}[\sigma(\cdot + \tau) - \sigma(\cdot)]$ is an indicator that the volatility process is critical *i.e.* it is constantly on the edge of instability. The previous models of section 1.2 cannot capture any of such behaviors as their dynamics is based on exogenous shocks only. In order to understand this near-criticality of the markets, we need to look at endogenous dynamics at the micro-scale.

Self-excited models for price dynamics

The endogeneity of the volatility indicates the presence of feedback. To develop a consistent volatility model, we can draw on what has been done in other areas of research. For example, in Physics feedback mechanisms are used in many fields: from electronics to

flocks of birds modeling. It gives birth to a wide range of models that are able to describe non-trivial dynamics. More recently, an auto-excited model has become popular in finance: the Hawkes process. Introduced by Hawkes in 1971 [13], his first goal was to analyse and predict replicas of earthquakes but it can be applied to many other fields (population dynamics, finance, etc.) as long as we model one-time events with stochastic rates. The feedback introduced by Hawkes is built on the following ideas:

- The more events happened in the past, the more likely a new one will happen.
- It takes the system some time to "forget" past events.

Before going into the details of mathematical modeling, intuition can help us to understand properties of the dynamics. Indeed, such feedback is stable if one event triggers **less than one** new event on average. Of course, this framework can be generalized to a multidimensional process, involving different types of events. We can give examples of events that we will focus on:

- Best bid and best ask changes.
- Order book events: limit order depositions, limit order cancellations and market order at a given price.

Let's turn to the mathematical presentation of this Hawkes process. We will use this formalism for the rest of the thesis, so we detail it in this section. Let $\boldsymbol{N}$ be a multidimensional counting process, N_t^i counts the number of events i before time t. We call $\boldsymbol{\lambda}$ the stochastic intensity of the process, which we can also call rate, and we can write:

$$\lambda_t^i = \lim_{dt \to 0} \frac{\mathbb{P}\left[N_{t+dt}^i - N_t^i > 0 \middle| \mathcal{F}_t\right]}{dt} \tag{1.11}$$

where $\mathcal{F}_t$ is the information generated by the process until time t. We can interpret this intensity as the infinitesimal probability of having an event at time t. One useful property is that $\left(\boldsymbol{M}_t = \boldsymbol{N}_t - \int_0^t \boldsymbol{\lambda}_s ds\right)_{t \in \mathbb{R}^+}$ is a martingale. Having introduced the formalism of point process, we turn to explanation the feedback we have mentioned before:

$$\boldsymbol{\lambda}_t = \boldsymbol{\alpha}_0 + \int_0^t \boldsymbol{\phi}(t-s) d\boldsymbol{N}_s \tag{1.12}$$

where $\boldsymbol{\alpha}_0$ is a vector and $\boldsymbol{\phi}$ is a matrix of functions. We can interpret the terms of the right-hand side (RHS) of Eq. (1.12) as follow:

- $\boldsymbol{\alpha}_0$ represents the **exogenous** rate of events.
- $\boldsymbol{\phi}$ is the feedback kernel: an event of type j that occurred at time s contributes with $\phi^{ij}(t)$ to the intensity λ_{t+s}^i.

The condition of stability is obtained by looking at the spectral properties of the matrix $||\boldsymbol{\phi}|| = \left(||\phi^{ij}|| = \int_{\mathbb{R}^+} \phi^{ij}(s) ds\right)_{ij}$. It is stable when its spectral radius $\rho_{sr}\left(||\boldsymbol{\phi}||\right)$ *i.e.* the maximum of the absolute values of the eigenvalues is strictly lower than one:

$$\rho_{sr}\left(||\boldsymbol{\phi}||\right) < 1 \tag{1.13}$$

In the one dimensional case, this spectral radius is equal to $||\phi^{11}||$ which is the average number triggered by one event, justifying our simple argument. Once we verify this stability

condition, we can show that:

$$\lim_{t\to+\infty} \mathbb{E}\left[\boldsymbol{\lambda}_t\right] = \left(\mathbb{I} - ||\boldsymbol{\phi}||\right)^{-1} \boldsymbol{\alpha_0} \tag{1.14a}$$

$$\lim_{t\to+\infty} \frac{1}{t} \mathrm{Cov}\left(\boldsymbol{N}_t, \boldsymbol{N}_t\right) = \left(\mathbb{I} - ||\boldsymbol{\phi}||\right)^{-1} \mathrm{Diag}\left(\left(\mathbb{I} - ||\boldsymbol{\phi}||\right)^{-1} \boldsymbol{\alpha_0}\right) \left(\mathbb{I} - ||\boldsymbol{\phi}||^{\dagger}\right)^{-1} \tag{1.14b}$$

where $\mathbb{I}$ is the identity matrix, Diag is the diagonal matrix from a vector and the symbol $\dagger$ represents the transpose of a matrix. Bacry *et al* in [14] have proved a functional central limit theorem, under some hypotheses on the kernels. This means that the behaviour of the Hawkes process at large time consists in a diffusion with constant trend $\boldsymbol{\Lambda} = \lim_{t\to+\infty} \mathbb{E}\left[\boldsymbol{\lambda}_t\right]$ of Eq.(1.14a) and covariances $\boldsymbol{\Sigma}_N = \lim_{t\to+\infty} \mathrm{Cov}\left(\boldsymbol{N}_t, \boldsymbol{N}_t\right)/t$ given in Eq. (1.14b):

$$\boldsymbol{N}_t \underset{t\to+\infty}{\approx} \boldsymbol{\Lambda} t + \sqrt{\boldsymbol{\Sigma}_N} \boldsymbol{W}_t \tag{1.15}$$

where $\boldsymbol{W}$ is a vector of independent Browian motions.

For a literature dedicated for the calibration of Hawkes processes, see [15, 16, 17] for many examples, with applications on financial modeling. Before going into a complex modeling, some studies have focused on the estimating $\rho_{sr}\left(||\boldsymbol{\phi}||\right)$ which can be interpreted as the **ratio of endogeneity** of the market. Hardiman *et al* [18], used a Hawkes process to count mid-price changes. After calibrating the model, they have shown that the price was critical as $\rho_{sr}\left(||\boldsymbol{\phi}||\right) \sim 1$. They have followed their analysis in second paper [19] where they have looked at the influence of many parameters on the ratio of endogeneity. One crucial result for us concerns the endogeneity during the Flash Crash of 2010: they showed that it corresponded to a burst of endogeneity, confirming the results of Filimonov *et al* [20]. Such a burst of endogeneity corresponds to a market reaching criticality.

Hawkes based models for price dynamics will provide a diffusive behavior at a large time scale, with constant volatility, incompatible with the intermittence of the volatility we see in data. As data reveals that the price is critical from a Hawkes point of view, models should take into account criticality. Jaisson *et al* have investigated in two papers [21, 22], the behavior of a Hawkes process at a large time when it reaches criticality **i.e.** $\rho_{sr}\left(||\boldsymbol{\phi}||\right) \to 1$. In the one dimensional case, the asymptotic behavior depends of the properties of the kernel:

- If $\int_0^{+\infty} t\phi(t)dt < +\infty$, the intensity of the Hawkes process converges to a CIR process, see [23] for details on the CIR model. It gives:

$$d\lambda_t = -C_1(\lambda_t - \alpha_0)dt + C_2\sqrt{\lambda_t}dW_t \tag{1.16}$$

  where C_1, C_2 are two constants and W a Brownian motion.

- If $\phi(t) \underset{t\to+\infty}{\sim} t^{-1-\mathcal{H}}$ with $0 < \mathcal{H} < 1$, the intensity of the hawkes process converges to a rough CIR process. If[3] $\mathcal{H} > 1/2$, we have:

$$\lambda_t = F^{\mathcal{H}}(t) + C_1 \int_0^t f^{\mathcal{H}}(t-s)\sqrt{\lambda_s}dW_s \tag{1.17}$$

  where $F^{\mathcal{H}}(t) = \int_0^t f^{\mathcal{H}}(s)ds$, $f^{\mathcal{H}}(t) = C_2 t^{\mathcal{H}-1} E_{\mathcal{H},\mathcal{H}}(-C_2 t^{\mathcal{H}})$, $E_{\mathcal{H},\mathcal{H}}(x) = \sum_{n\geq 0} \frac{x^n}{\Gamma(\mathcal{H}n+\mathcal{H})}$ and C_1, C_2 are two constants and W a Brownian motion. Γ denotes the Gamma function.

The second result is quite technical but the function f^H gives similar sub-diffusive results

[3] See [22] for the case $\mathcal{H} \leq 1/2$

as observed on volatility data. Furthermore, calibrating Hawkes processes on financial data usually gives power law kernels with exponents between one and two, see [16, 18], which motivates to look at such scalings.

Zumbach effect and Q-Hawkes process

Financial series are well known to be not invariant by time reversal, meaning that running financial series forward or backward in time does not lead to the same results. A glance at Fig. 1.4(a) is probably convincing enough to justify this statement. Nevertheless, the most common proof of this statement relies in the leverage effect: past large negative price returns lead to more future volatility. But large past volatility does not lead to future large negative price returns, see Bouchaud *et al* [24]. G.Zumbach has investigated other time reversal asymmetries in financial time series [25, 26]. In these papers, he highlights the so-called Zumbach effect: past price trend leads to future volatility, independently of its sign. This effect was later on confirmed by Chicheportiche *et al.* [27]. An example of the Zumbach effect is displayed on Fig. 1.5, using daily price returns defined in Eq. (1.8) and volatility defined in Eq. (1.10). We plot the correlation $\mathrm{Cor}\left(r_d^2(\cdot+\tau),\sigma(\cdot)\right)$ with a lag τ. It reveals that $\mathrm{Cor}\left(r_d^2(\cdot+\tau),\sigma(\cdot)\right) > \mathrm{Cor}\left(r_d^2(\cdot-\tau),\sigma(\cdot)\right)$ for $\tau < 0$ meaning that the effect of past square price trend on future volatility is stronger than the effect of past volatility on future square price trend. This effect does not arise from the leverage effect as conditioning on the sign of the daily return does not change this result. Note that we distinguish the **weak Zumbach effect** when $\mathrm{Cor}\left(r_d^2(\cdot+\tau),\sigma(\cdot)\right) > \mathrm{Cor}\left(r_d^2(\cdot-\tau),\sigma(\cdot)\right)$ for $\tau < 0$, from the **strong Zumbach effect** when the conditional law of future volatility explicitly depends on past returns trajectory. In the following, if not specified, we are going to discuss about the Zumbach effect for the strong Zumbach effect, by overuse of language.

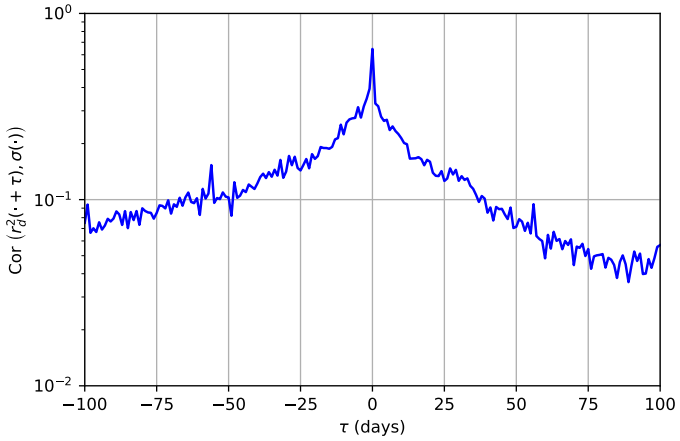

Figure 1.5: *Plot* $\mathrm{Cor}\left(r_d^2(\cdot+\tau),\sigma(\cdot)\right)$ *with a lag* τ *in days, on the S&P500 from* 02/01/1962 *to* 08/05/2020. *This curve is not symmetric by a time reversal, emphasizing the weak Zumbach effect.*

Although theoretical models can reproduce the weak Zumbach effect, such as the rough Heston model see [28], introducing a quadratic feedback term of past prices on volatility seems the natural way to get the strong Zumbach effect. The quadratic ARCH framework seems suited for this purpose, see [29, 27]. More recently, Blanc *et al* [30] coupled this framework with Hawkes processes that gave birth to a very interesting process: the Quadratic Hawkes process (Q-Hawkes). Let's consider a counting process N that counts the number of price changes. At each price change, we draw a Bernouilli variable, independent of the past, to choose the sign of the price change. Calling T_n the random times of price changes and ϵ_n

the random sign of the price change, we can write the value of the price P_t:

$$P_t - P_0 = \sum_{T_n < t} \epsilon_n dN_{T_n} \tag{1.18}$$

The intensity of the process N is given by the following equation:

$$\lambda_t = \alpha_0 + \int_0^t \int_0^t K(t,s) dP_s dP_t \tag{1.19}$$

with K a symmetric kernel. The last term of the RHS of Eq.(1.19) corresponds to the quadratic feedback. In the special case where $K(t,s) = Z(t)Z(s)$, we get:

$$\int_0^t \int_0^t K(t,s) dP_s dP_t = \left(\int_0^t Z(s) dP_s \right)^2$$

revealing the importance of the square trend on the intensity. Due to such feedback, we call Z-Hawkes these processes. As $dP_t^2 = dN_t$, the stability condition is similar to a Hawkes process: $\operatorname{Tr} K = \int_{\mathbb{R}^+} K(t,t)dt < 1$. In the Zumbach case, it reads to $\operatorname{Tr} K = \int_{\mathbb{R}^+} Z(t)^2 dt = n_Z$. A deep analysis of this model shows that it exhibits the strong Zumbach effect and that it reaches a stationary state where the volatility has a fat-tailed distribution, in the case of an exponential kernel. This fat-tailed property is a direct consequence of the Zumbach component. Indeed, in this framework, the squared volatility is equal to the intensity of the process and its distribution ρ_λ is such that:

$$\rho_\lambda \underset{\lambda \to +\infty}{\sim} Cst \; \lambda^{-\left(\frac{3}{2} + \frac{1}{2n_Z}\right)}$$

The strength of the Zumbach component diminishes the exponent of the volatility, making it critical when $n_Z \to 1$. More results and details are displayed in the article [30], exploring the interaction Hawkes with Zumbach and mathematical details are well explained in Dandapani *et al* [31].

Market impact: how much do I move the price when I buy/sell?

In the past recent year, a new stylized fact has been highlighted by a broad community of academics and practitioners. Known as the market impact, it is a consequence of interaction between supply and demand on price formation. Let's start with a simple example to understand what the market impact is: consider agents that want to buy a number Q of shares of an asset over a time horizon T. We raise the following question: what is the average price per share they will pay? Let's analyze the different ways that they can buy these shares and the costs associated with these strategies. They can decide to buy all the shares instantaneously, but it may be possible that the best ask does not contain Q shares, forcing the agents to go to the next price level which has to be higher, thus paying more than the initial price. If this amount is smaller than the available quantity at the best ask, they will pay the best ask. But, they will push the micro-price up. On average, with this strategy, the agents are going to pay more than the best ask per share and causes the price increase. They can be smarter and decide to split their order and execute a **metaorder**. Both ways of trading (with limit orders and market orders) tend to increase the micro-price and force the agents to pay more than the best price he could have on average. To conclude from this example, executing a strategy changes the price due to the finite liquidity of an asset, that creates an additional trading cost. This change of price is called the market impact, that shifts the price up (*resp* down) for buy (*resp* sell) orders.

Studying the market impact has been relevant not only for academics who wish to fully understand price formation but only practionners who attempt to reduce trading costs. In

fact, many empirical studies have focused on quantifying this market impact, converging to a very robust result: the square root law. The average change of price P_t due to signed executed volume Q_t is:

$$\mathbb{E}\left[P_t - P_0 | Q_s, s \leq t\right] \propto \sigma_{\mathrm{d}} \operatorname{sign}(Q_t) \left(\frac{|Q_t|}{V_{\mathrm{d}}}\right)^{\delta} \tag{1.20}$$

where σ_d is the daily volatility, V_d the daily traded volume and $0.4 < \delta < 0.6$ bears witness of the concave nature of market impact. The robustness of this law is indisputable as it holds on very different types of markets, equity, derivatives, cryptocurrency, etc., and not only for aggressive strategies, see [32, 33, 34, 35, 36, 37, 38, 39, 40, 41, 42]. Such universality across assets is a strong clue that this effect is created through interaction between supply and demand. Even though, some price models presented above are satisfying, the need to model supply and demand incite us to model the order book to get a joint price and liquidity dynamics.

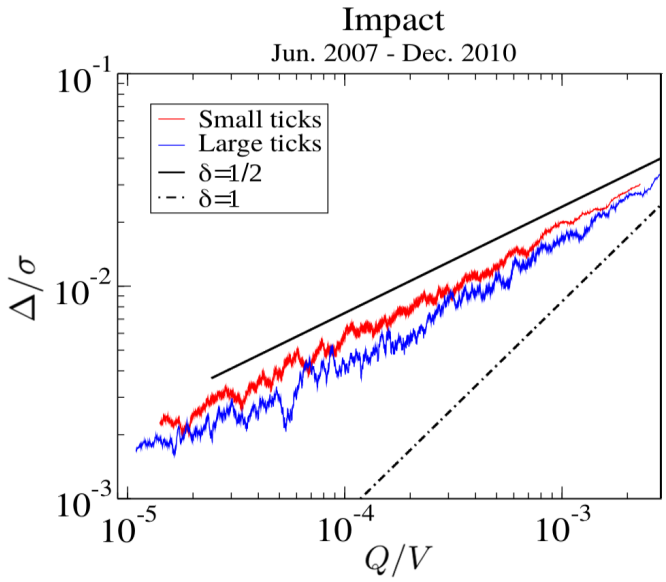

Figure 1.6: *The impact of metaorders for CFM proprietary trades on futures markets, in the period June 2007 â December 2010. This plot has been taken from Tóth et al [32]. We show Δ/σ vs. Q/V on a log-log scale, where Δ, σ and V are the market impact of a metaorder of size Q, the daily volatility and daily volume measured the day the metaorder is executed.*

1.3 Modeling the order book

Access to order book data started to be common with the development of electronic markets, in the early 2000s, opening a new area of research. Practitioners and academics have provided models of limit order book dynamics that can be tested on empirical data. This challenge seems very difficult: the order book can be seen as a multidimensional object where every price level interacts with each other. Without any strong assumption on those interactions, the curse of dimensionality will make any calibration impossible as well as model simulations. As the main activity is concentrated on the best levels, one possible way to avoid this curse consists in building a model on the best levels only, see [16] for example. Nevertheless, we wish to have a global description to describe liquidity crises. We present two order book models that do not suffer too much from dimensionality, on which we will build our work.

A discrete model: the Santa Fe model

The so-called Santa Fe model was introduced in [43, 44] by people working at the Santa Fe Institute. It belongs to a discrete modeling of the order book: the price levels are discrete as well as the number of limit orders stored in the book. The assumptions of the dynamics are the following:

- Buy (*resp.* sell) limit orders arrive with constant rate λ for price levels $p < P_t$ (*resp.* $p > P_t$), where P_t is the mid-price.
- Market orders arrive with constant rate μ at best levels only. They match an existing limit order of the opposite side and "consume" it through a transaction.
- Each limit order stored in the limit order book can be cancelled with constant rate ν.
- All the orders have the same size equal to one.
- All the events are mutually independent.
- When two orders of different types meet it gives a transaction and the two orders are annihilated through the reaction $A + B \to \emptyset$.

These dynamics are presented in Fig.1.7(a). From the hypotheses, we note that the mid-price is the reference price around which the dynamics is based. This zero-intelligence model is hard to solve analytically. Nevertheless, some interesting quantities are tractable. Far from the mid-price, we can show that the number of orders $V(p)$ in a price level p follows a Poisson distribution with parameters $V^* = \lambda/\nu$: $\mathbb{P}(V(p) = V) = e^{-V^*}\frac{V^{*V}}{V!}$. We notice that this distribution is independent of the price level p. We also can show that, far from the mid-price, gap between two occupied price levels are geometrically distributed with parameter $(e^{V^*} - 1)^{-1}$, see [6] for more details. The behavior of the order book is different depending on the value of V^*:

- $V^* \gg 1$, the order book is full. This case corresponds to large tick stocks.
- $V^* \ll 1$, the order book is sparse: many price levels are empty. This case corresponds to small tick stocks.

Taking into account what happens near the price can be achieved by adding a correction in V^* that takes into account the time spent at the best.

One major advantage of this model lies in its power of spread prediction. Indeed, the predicted spread from the Santa Fe model with the fitted parameters matches well the observed spread, see [6] for plots and more details. As the rates are assumed to be constant, fitting λ, μ and ν on data is very simple and consists in counting the number of events over the time of observation, as detailed in [6]. Not surprisingly, its predictive power fails for volatility forecasting. Indeed, there is no feedback loop in the dynamics, essential to capture the endogeneity of the volatility. We can exhibit other problems arising from this model such as mean reverting prices and the existence of a profitable market making strategies. Nevertheless, its predictive power is still impressive in comparison to the simplicity of the model. This new framework can be naturally extended in many possible ways. While state-dependency has been investigated in Huang *et al*[45] , the influence of past prices has to be answered.

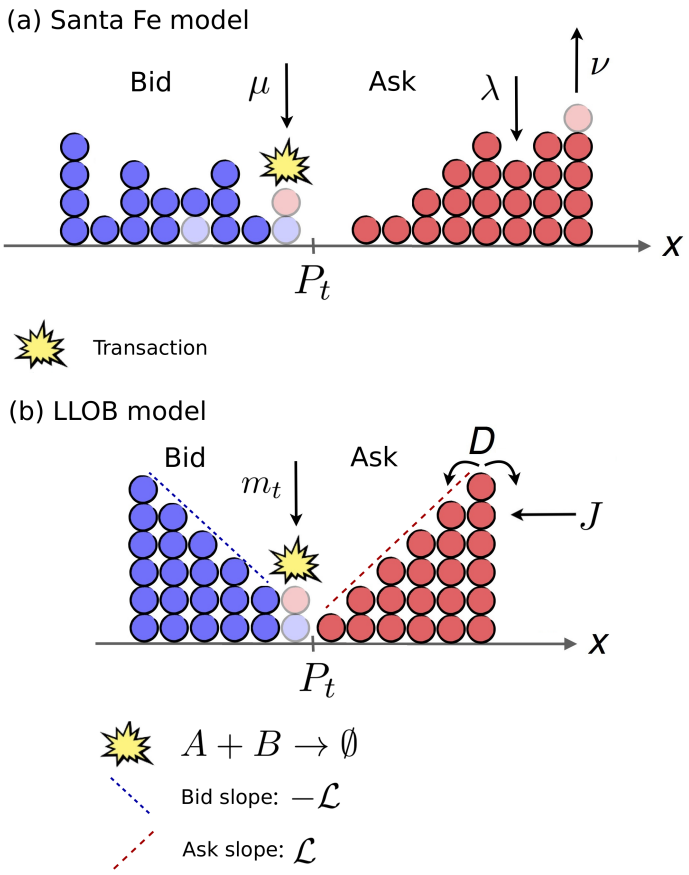

Figure 1.7: *(a) Schematic of the Santa Fe model. (b) Schematic of the LLOB model.*

A continuous model: Latent Limit Order Book (LLOB)

Reproducing the square root law is a key challenge for financial modellers. As the Santa Fe model predicts an impact roughly linear in the size of metaorders, academics have built new agent-based models that advance the understanding of this law. What is missing from the Santa Fe model is the possibility of agents to change the price of their order. Indeed, agents cannot shift their order from a price level to its neighbours. The simplest way to account for price revision consists in introducing diffusion between price levels. On the other hand, the interaction between a buy (*bid*) and sell (*ask*) order produces a transaction that deletes the existing orders in the order book. In the context of a chemical reaction, this would be written as $A + B \to \emptyset$. Literature on modeling these types of chemical reactions is wide, providing the powerful framework of the **reaction-diffusion** equations. Donier *et al* [46] have adapted this framework to model latent order books. The word latent stands for all the unobserved orders, which are counted in the order book, even if they are not yet placed in the real order book. Modeling the latent order book is much more convenient and we implicitely assume that the latent and real order book coincide close to the mid-price. Reaction-diffusion equations set a continuous description of order books, not suited for very short time scale, but very powerful for analytical results. We expect such a model to be efficient on the intraday scale and to be able to model the market impact of metaorders.

Consider latent limit order densities for bid and ask side of the book $\rho_{\mathrm{B}}(t, x)$ and $\rho_{\mathrm{A}}(t, x)$ at price x and time t. We call P_t the mid-price. The dynamics is based on the following assumptions:

- Agents place bid (*resp.* ask) limit orders with rate λ when $x < P_t$ (*resp.* $x > P_t$).

- Agents can cancel existing limit orders with rate ν.
- Agents can shift an existing limit orders through diffusion of parameter D.
- Agents can trade with a market order flux m_t at the mid-price P_t.
- When two orders of different types meet it gives a transaction, through the reaction $A + B \to \emptyset$.

The transactions are instantaneous in the market, making impossible any overlap between the two densities[4]. Then, the variable $\phi_\ell = \rho_\mathrm{B} - \rho_\mathrm{A}$ describes the whole dynamics as $\rho_\mathrm{B} = \max(0, \phi_\ell)$, $\rho_\mathrm{A} = \max(0, -\phi_\ell)$ and P_t is the unique zero of this function: $\phi_\ell(t, P_t) = 0$. The dynamics follows:

$$\partial_t \phi_\ell = D\partial_{xx}\phi_\ell + \lambda \operatorname{sign}(P_t - x) - \nu\phi_\ell + m_t \delta(x - P_t) \tag{1.21}$$

Note that we have assumed that the external news shift the order book and the mid-price of the same quantity. At stationarity, when there is no market order, the shape of the book is the following:

$$\phi_\ell^{\mathrm{st}}(\xi) = -\operatorname{sign}(x)\frac{\lambda}{\nu}\left(1 - \exp\left(\sqrt{\frac{\nu}{D}}\xi\right)\right) \tag{1.22}$$

With $\xi = x - P_t$. The stationary latent order book is **locally linear** around the price with slope $\mathcal{L} = \lambda/\sqrt{\nu D}$. This property is essential to reproduce the square root law. Let's consider an agent that trades instantly a quantity Q in a stationary order book, the shift of price Δx that matches the quantity is in book, giving $\mathcal{L}\Delta x^2 = Q$. This very simple argument enables us to get to the square root law. As linear order book seems to be the essential property to get the square root law, we decide to zoom around the price, by taking $\lambda, \nu \to 0$ with $\mathcal{L}$ constant. Eq. (1.21) is modified in:

$$\partial_t \phi_\ell = D\partial_{xx}\phi_\ell + m_t \delta(x - P_t) \tag{1.23a}$$

$$\lim_{x \to \pm\infty} \partial_x \phi_\ell = -\mathcal{L} \tag{1.23b}$$

Fig. 1.7(b) represents the dynamics in this limit. In the absence of metaorder, the order book is linear with slope $\mathcal{L}$. In the general case, it is asymptotically linear with slope $\mathcal{L}$ which means that there is a flux of orders at infinity $J = \mathcal{L}D$. Thus, we expect to get the square root law as explained above. To prove it, we solve Eq. (1.24), we apply Fourier transformation, and get the following implicit equations:

$$\phi_\ell(t, x) = -\mathcal{L}x + \int_0^t \frac{m_s}{\sqrt{4\pi D(t-s)}} e^{-\frac{(x - P_s)^2}{4D(t-s)}} ds \tag{1.24a}$$

$$P_t = \frac{1}{\mathcal{L}} \int_0^t \frac{m_s}{\sqrt{4\pi D(t-s)}} e^{-\frac{(P_t - P_s)^2}{4D(t-s)}} ds \tag{1.24b}$$

Eq. (1.24b) is a complex fixed-point equation that cannot be solved in the general case. But we can prove that there is no **price manipulation** is this setup. Nevertheless, we can develop Eq. (1.24b) in two asymptotic regimes. To determine in which regime we are, we

[4]Note that a market latency too high could occasionally lead to a reversal of the best bid and best ask.

compare the market order rate m_t with the flux of orders at infinity J. The results follow:

$$P_t = \frac{1}{\mathcal{L}} \int_0^t \frac{m_s}{\sqrt{4\pi D(t-s)}} ds \quad \text{if} \quad \forall t \quad m_t \ll J \tag{1.25a}$$

$$P_t = \sqrt{\frac{2}{\mathcal{L}} \int_0^t m_s ds} \quad \text{if} \quad \forall t \quad m_t \gg J \tag{1.25b}$$

As $Q_t = \int_0^t m_s ds$, we recognize the square-root law in the second regime. The first one gives the propagator model that was introduced in [47], compatible with the square-root for constant m_t. Fig.1.8 displays examples of price trajectory for constant meta orders $m_t = m_0$, in the two regimes, that reproduces the theoretical predictions. Note that in this figure, the time t is a proxy for the Q_t as the meta orders are constant.

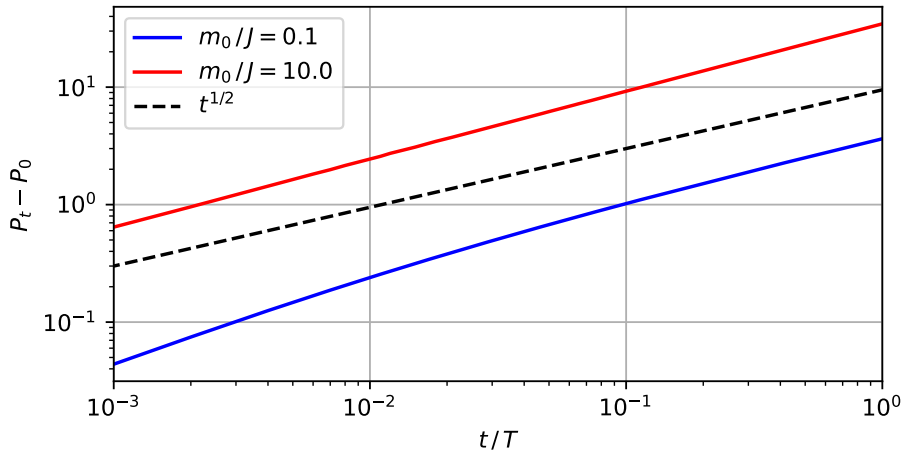

Figure 1.8: *The impact of constant metaorders ($m_t = m_0$) from Eq.*(1.24). *As the rate is constant, Q_t is proportional to t plotted on the x axis. T denotes the time horizon of the metaorders.*

This model reproduces the square-root for metaorders, opening a new range of order book models based on a reaction-diffusion framework. Indeed further extensions of this model have been achieved so far. For example, introducing heterogeneity of agents has been done by Benzaquen *et al.* [48]. Our last chapter will be devoted to the presentation of one of them.

1.4 Objectives of the manuscript

We now turn to our specific purpose: analysing liquidity crises. We address ourselves some key questions that are relevant to our work. In all our manuscript, we will systematically go from empirical investigations to numerical and analytical ones, then back and forth. Empirically speaking:

- Can we find empirical evidence at the micro-scale *i.e.* the scale of order book events that account for market destabilization?
- What are the micro foundation of the Zumbach effect?
- Can we find clues for near-critical markets?

Regarding modeling:

- How can we construct a model that reproduces some key stylized facts, such as the Zumbach effect, and that exhibits a condition for market stability?

- If there exists a transition in our model, can we characterize it by finding the condition of transition and the associated critical exponents?

- Can we calibrate our newly built model to financial data?

As we will see, the concepts and models of this introduction give us the appropriate tools to tackle these questions. In particular, we will use linear Hawkes processes and quadratic Hawkes processes to build self-excited models and the Santa Fe model or the LLOB model to describe the order book. We now briefly present our new results and explain how they are linked with the concepts of this introduction.

Our data-driven approach starts in **Chapter 2** with an empirical analysis of self-excited models on order book dynamics. The dynamics of order book events (limit order depositions, cancelations, market orders) are known to be extremely endogenous and thus it is natural to describe them by Hawkes processes. In addition, the recent discovery of the Zumbach effect has driven us to investigate the influence of past price feedback on order book events. We expect to obtain similar effects at the scale of order book events. In terms of inference, this means that we need to introduce a quadratic feedback of price changes on order book events, in the spirit of Q-Hawkes processes. To do so, we extend the Q-Hawkes process into the Generalized Quadratic Hawkes process (GQ-Hawkes) which is designed to explore such price feedback on order book events. This self-excited process has a quadratic feedback component on the price changes in addition to a Hawkes component. Then, we provide two calibration procedures and apply them to tick-by-tick order book data from the EURO STOXX contract. Both reveal a Zumback-like effect: past price trends decrease future liquidity, independently of its sign, that we can interpret as a micro foundation of the Zumbach effect. Furthermore, while using the most sophisticated one, we are able to emphasize the power law shape of the kernels that leads us to the path of near-critical markets. This idea of near-critical markets is then confirmed by introducing and studying the specific notion of effective spread.

In **Chapter 3**, we provide a self-contained order book model that takes into account quadratic feedback effects of the price process. As we focus on the dynamics of order book events, we need to have a discrete description of the order book and so we are naturally inspired by the Santa Fe model explained above. We add to this model a quadratic feedback in the arrival rates of events, in the spirit of the Generalized Quadratic Hawkes process, used in Chapter 2. For sake of simplicity, we only investigate the component where the price feedbacks the most: on the cancelations. Our hypotheses ensure that our model reproduces a Zumbach-like effect on the liquidity of the order book. Then we proceed to a numerical analysis of the model. It appears that this Zumbach-like effect at the micro level can indeed destabilize markets by drying up liquidity, if the feedback is strong enough. Then, using a scaling procedure, we prove that our model exhibits a second order phase transition. We also provide the critical exponents of this transition, revealing that it belongs to a new universality class.

The Santa Fe model is very difficult to solve analytically so it is obviously the same for our quadratic Santa Fe model. As the main difficulties come from the intricate joint dynamics of the order book events, we decide to focus on one given quantity in **Chapter 4**: the spread. Our approach consists in modeling spread opening events and spread closing events. We use the previously introduced self-excited models to build various dynamics for first ones, while we assume that the rate of second ones is constant (as we focus on destabilising events). Assuming that the events that open the spread follow a linear Hawkes process results in a dynamics with a transition between stable and unstable spread. Furthermore, we derive

an explicit stability condition and numerically compute the equilibrium distribution of the spread, in the stable phase, that appears to be exponential. Replacing the linear Hawkes process by a Q-Hawkes process does not qualitatively change the results, except that the equilibrium spread distribution is fat-tailed. Then, we investigate the effect of a non-linear Hawkes process, providing a new and interesting tool to describe the dynamics of financial markets. We show that the dynamics is meta-stable, leading to another scenario for liquidity crises in which we compute the average time of the first crash.

Chapter 2 to **4** focus on discrete order book. In **Chapter 5**, we use the continuous framework of the LLOB model. We introduce a liquidity revealing mechanism that links the latent order book with the real one. This has two major implications. First, our new model exhibits a stability condition above which lag effects due to the revealing rate is responsible for liquidity evaporation. It provides an alternative scenario for liquidity crisis as the Zumbach effect does not appear in the model. This stability condition enables us to draw a stability map from the model parameters. Then, an important buy product of our approach is that we are able to calibrate our model on financial data. More precisely, we provide a numerical scheme that infers empirical order book shapes and apply it on more than one hundred US stocks. To qualitatively quantify their stability, we display the aforementioned fits on the stability map. Finally, we numerically investigate the market impact of metaorders in this framework and show that it reproduces the famous square root law.

Take home message of Chapter 1

1. Liquidity crises. The liquidity dries out and consequently the price drops. The most striking example is the "Flash Crash" the 6th of May 2010.

2. Limit order book. It stores the buy and sell orders, in double auction electronic markets. Market participants can deposit such limit orders, cancel or execute an existing limit order via a market order.

3. Endogenous market activity. Anomalous price changes are too frequent to be explained by just a few pieces of news. Only $\sim 5\%$ is attributed to news while the others are endogenous *i.e.* created by markets themselves.

4. Hawkes process. It is a self-excited points process designed to study feedback from past events onto future ones. They are perfectly suited to study price changes and order book events.

5. Volatility. Volatility is intermittent, highly correlated and rough. These characteristics can be reproduced by a critical Hawkes process.

6. Zumbach effect. The Zumbach effect asserts that past price trends increase future volatility, independently of their sign. Quadratic Hawkes processes are introduced to reproduce this effect.

7. Market impact. Market orders move the price proportionally to the square root of the executed volume. Only some order book models can reproduce this stylized fact.

8. Santa Fe Model. Limit order depositions, cancellations and market orders are independent, constant over time and price level. This simple framework can replicate the dynamics of spreads, but not the one of the volatility.

9. LLOB. The Latent Limit Order Book model is based on a reaction-diffusion framework with $A + B \to \emptyset$. It reproduces the square-root law and opens a new field of order book models.

2

Empirical evidence of price feedback

Empirical data reveals that the liquidity flow in the order book (depositions, cancellations and market orders) is influenced by past price changes. In particular, using a minimal setting, we show that liquidity tends to decrease with the amplitude of past volatility and price trends. Then, we propose an actionable calibration procedure for general Quadratic Hawkes models of order book events (market orders, limit orders, cancellations). One of the main features of such models is to encode not only the influence of past events on future events but also, crucially, the influence of past price changes on such events. We show that the empirically calibrated quadratic kernel is well described by a diagonal contribution (that captures past realised volatility), plus a rank-one "Zumbach" contribution (that captures the effect of past trends). We find that the Zumbach kernel is a power-law of time, as are all other feedback kernels. As in many previous studies, the rate of truly exogenous events is found to be a small fraction of the total event rate. These two features suggest that the system is close to a critical point – in the sense that stronger feedback kernels would lead to instabilities.

From:
Endogenous liquidity crises
A. Fosset, Bouchaud, M. Benzaquen

And:
Non-parametric Estimation of Quadratic Hawkes Processes for Order Book Events
A. Fosset, J. P. Bouchaud, M. Benzaquen

Contents

Un problème sans solution est un problème mal posé

Albert Einstein

2.1 Introduction

The accumulation of empirical clues over the past few years provides mounting evidence that most of market volatility is of endogenous nature [49, 50, 10, 51, 52]. This obviously does not mean that significant news, such as the very recent Covid-19 crisis, do not impact financial markets, but rather that these only account for a small fraction of large price moves. Think for example of the S&P500 flash crash of May 6th, 2010 [4], see also [5], which has not been triggered by any outstanding piece of news. Furthermore, while one may argue that in some cases large drops are exogenously triggered, their amplification is often due to endogenous mechanisms [6].

The behaviorally supported idea that agents tend to overreact, especially during crises, has driven the market modeling community to fall back on self-exciting processes, better known as Hawkes processes [53]. The latter have proven to be extremely efficient to tackle the intricate dynamics of the order flow and other self-excited effects in financial markets [54, 55, 56, 57, 58, 59, 60, 61, 18, 62, 45, 63, 64, 65, 66, 20, 67]. Nonetheless, linear Hawkes processes are unable to account for an empirical finding essential to our eyes to tackle endogenous instabilities: the Zumbach effect [26, 27, 30, 28]. The latter states that past price trends increase future activity, regardless of their sign. Quadratic Hawkes processes (Q-Hawkes), inspired by quadratic ARCH processes [29, 27], were recently introduced to circumvent this issue [30, 31], and have proven key to understand fat-tails in the distribution of returns, as well as spread, volatility and liquidity dynamics [52].

The present chapter attempts to capture such feedback effects from empirical order book data. In Section 2.2, we empirically show that event rates in the limit order book are indeed affected by past volatility. Using tick-by-tick order book data from the EURO STOXX contract, we calibrate, in a minimal setting, a generalisation of the self-exciting Hawkes processes. In particular, we show that market orders and cancellations tend to increase when recent price changes are large, in turn diminishing the available liquidity, much as argued above. Then, we fully calibrate on real market data a version of the generalized Q-Hawkes process. We provide convincing evidence for the price/liquidity feedback mechanism described above and quantify its implications. In section 2.3 we briefly recall the ingredients of the model and present the non-parametric calibration procedure, inspired by the methods introduced by Bacry *et al.* [17, 16, 15]. We apply such calibration to order book data on the EURO STOXX and BUND futures contracts. In section 2.4 we present an alternative method that needs fewer assumptions to compute the overall effect of past price moves on future liquidity flow. We introduce a low rank (Zumbach-like) approximation that allows us to denoise the feedback kernels and separate the effects of trend and volatility and apply it to our futures contracts. In section 2.5, we focus on the liquidity flow and analyse spread time series in relation with adequate trend and volatility signals. In section 2.6 we conclude.

2.2 Destabilizing Feedback Effects: Empirical Analysis

In this section, we provide an empirical analysis of feedback effects within order book dynamics. Consider an electronic market with three event types only: limit order deposition (LO), limit order cancellation (C) and market orders (MO).

It is already well documented that these events strongly interact with one another. A very useful framework to describe these interactions is provided by Hawkes self-exciting point processes [53], which have already been applied to order book events in [65, 57, 45, 59, 56].

Here we want to extend these studies to account not only for activity feedback but for *price feedback* as well, in the spirit of the Quadratic Hawkes (Q-Hawkes) model of Blanc *et al.* [30].[1]

Order Book Data

In this subsection, we focus on describing the order book data we have. We have selected the EUROSTOXX, BUND, BOBL and Schatz, well know for being liquid, large tick future contract. We have selected data on regular trading hours ($9a.m.$ to $16p.m.$). The level of precision is very high: we have every order book events with a time precision of $1\mu s = 10^{-6}s$. Note that at this scale, very few events are apparently synchronized without breaking causality. It will not impact our future work as we wish to study larger time scales. We focus on the best quotes in the following, where we have the biggest number of events. Fig. 2.1(a) shows the pattern of the volatility of the EUROSTOXX and Fig. 2.1(b) displays the average rate of events Λ_{tot}. Both plot, computed other a 5 minutes bins, reveal a typical U-shape. The high activity around $2p.m.$ is due to the opening of the US market. Furthermore modeling will not take into account intraday pattern. Thus, we will normalize time intervals between two events by the average pattern: $\Lambda_{tot}(t)dt/\mathbb{E}[\Lambda_{tot}] \to dt$.

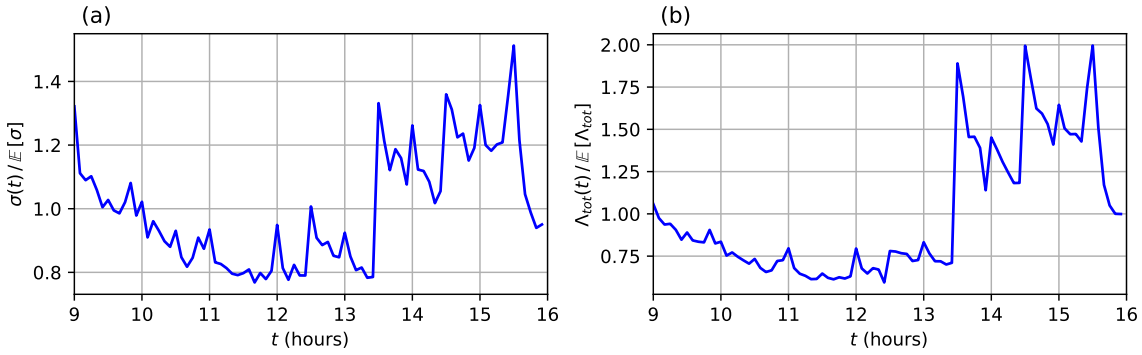

Figure 2.1: *Intraday patterns exhibiting a U-shape, on the EURO STOXX contract between* 2016/09/12 *and* 2020/02/07. *(a) pattern of the* 5 *minutes volatility. (b) pattern of the rate of events, estimated on a* 5 *minutes bins.*

Average Event Rates

Figure 2.2 displays the average order size, frequency of events and order rate (= order size × frequency) as function of the re-scaled volume at best for each event type, on the EURO STOXX contract between 2016/09/12 and 2017/04/28. The volume at best has been rescaled by the average limit order size in the same time bin, in order to eliminate intraday seasonality. In terms of time scales, we find that for EURO STOXX the average time between two events is $\tau_e = 0.03\,s$, whereas the average time between two price changes is $\tau_p = 7\,s$. In addition to the expected bid-ask symmetry, Fig. 2.2(c) reveals that the total rate of cancellations and market orders are roughly proportional to the size of the queue, whereas limit order deposition does not show any appreciable dependence on the volume at best. This observation motivates the specification of the Q-Hawkes model that we calibrate below.

A state dependent Generalized Q-Hawkes model

For the sake of simplicity, we focus on events (LO, C, MO) at the best quotes only, bid (b) and ask (a) (we do not distinguish between limit order deposition at the current best or

[1] See also [68] for a recent analysis of the complex interplay between intraday volatility spikes and negative stock market jumps.

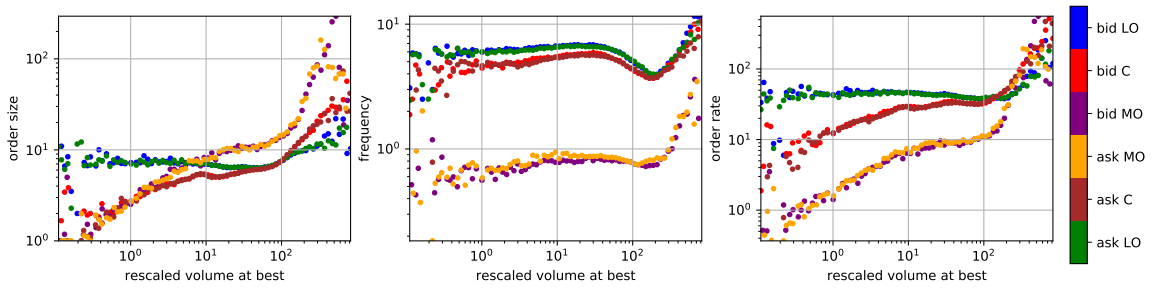

Figure 2.2: *Average order size, frequency of events and order rate (= order size × frequency) as function of volume at best rescaled by the average limit order size, on the EURO STOXX contract between* 2016/09/12 *and* 2017/04/28.

inside the spread). We therefore introduce the following six-dimensional process that counts all such events:

$$\boldsymbol{N}_t = \left(N_t^{\mathrm{C,b}},\ N_t^{\mathrm{LO,b}},\ N_t^{\mathrm{MO,b}},\ N_t^{\mathrm{MO,a}},\ N_t^{\mathrm{LO,a}},\ N_t^{\mathrm{C,a}} \right) .$$

We further assume that the time dependent intensities $\boldsymbol{\lambda}_t$ of these six processes follow the following state dependent generalized Q-Hawkes dynamics:

$$\boldsymbol{\lambda}_t = \boldsymbol{v}_t \left(\boldsymbol{\alpha}_0 + \int_0^t \boldsymbol{\phi}(t-s)\, d\boldsymbol{N}_s + \int_0^t \boldsymbol{L}(t-s)\, dP_s + \int_0^t \int_0^t \boldsymbol{K}(t-s, t-u)\, dP_s dP_u \right)_+ , \tag{2.1}$$

where dP_s is the price change at time s in tick units, $\boldsymbol{v}_t = \mathrm{Diag}\left(v_t^{\mathrm{b}}, 1, v_t^{\mathrm{b}}, v_t^{\mathrm{a}}, 1, v_t^{\mathrm{a}}\right)$ with $v_t^{\mathrm{b/a}}$ the volume at the best bid/ask in units of average limit order size. Equation (2.1) assumes that cancellations and market orders are multiplicative while limit order event types are additive, as mentioned above. Note that all kernels $\boldsymbol{L}, \boldsymbol{K}$ are 6-dimensional vectors and $\boldsymbol{\phi}$ a 6-dimensional matrix. We also assume that they ensure positive intensity whatever the past trajectory of the price. The purpose of this section is to analyse the price influence on order book event, setting aside state dependency that is fully explained in 2.2. Without a loss of generality, we can forget the dynamics of $\boldsymbol{v}_t$ and replace it by its average $\boldsymbol{v}$, as long as $\boldsymbol{v}_t$ does not depend of the past price process. So we approximate the dynamics of Eq. (2.1) by the following Generalized Q-Hawkes process (GQ-Hawkes process):

$$\boldsymbol{\lambda}_t = \boldsymbol{\alpha}_0 + \int_0^t \boldsymbol{\phi}(t-s)\, d\boldsymbol{N}_s + \int_0^t \boldsymbol{L}(t-s)\, dP_s + \int_0^t \int_0^t \boldsymbol{K}(t-s, t-u)\, dP_s dP_u, \tag{2.2}$$

For simplicity, we have overated $\boldsymbol{v}\boldsymbol{\alpha}_0 \to \boldsymbol{\alpha}_0$, $\boldsymbol{v}\boldsymbol{\phi} \to \boldsymbol{\phi}$, $\boldsymbol{v}\boldsymbol{L} \to \boldsymbol{L}$ and , $\boldsymbol{v}\boldsymbol{K} \to \boldsymbol{K}$.

The first term on the RHS of Eq. (2.2) accounts for a stationary exogenous intensity $\boldsymbol{\alpha}_0$ and the second is the classical Hawkes kernel accounting for event interactions.[2] The third and fourth terms were introduced in [30] and are new in the context of limit order book modelling. The third term is a linear feedback term from past price changes, modelling the fact that up or down price moves directly impact the rate of cancellations, market orders and limit orders. The fourth is a quadratic feedback term on the rate of order book events, which does not depend on the sign of past price changes. In [30], it was proposed to write the kernel as $\boldsymbol{K}(t-s, t-u) = \boldsymbol{K}_d \psi(t-s)\delta(s-u) + \boldsymbol{K}_1 Z(t-s)Z(t-u)$, with:

- a diagonal (in time) contribution $\psi(t-s)$, which represents the feedback of past volatil-

[2] Whereas the Hawkes contribution is not the focus of the present paper, including it is essential to obtain a reasonable explanatory power (see below).

ity on current activity, since it can be written in terms of:

$$\Sigma^2(t) = \int_0^t \psi(t-s)\,(dP_s)^2,$$

- a rank-one contribution which amounts to coupling the square of past trends, as measured by:

$$R(t) = \int_0^t Z(t-s)\,dP_s\ .$$

This is the so-called Zumbach effect: past trends, independently of their sign, lead to an increase in future activity.

In the following of this section, we will choose $\psi(s) = Z(s) = e^{-\beta s}$ for simplicity. Note that we have implicitly assumed that the shape of the diagonal contribution and rank-one contribution is the same for all the event, that we will justify in Section 2.3. One of the main empirical findings of the present study is that these two effects (volatility feedback and Zumbach effect) are indeed present and large, and capture the destabilizing feedback loop

$$\text{trends \& volatility} \quad \rightarrow \quad \text{lower liquidity} \quad \rightarrow \quad \text{more trends \& volatility}$$

as surmised in the introduction.

Calibration Strategy in a Minimal Setting

The Hawkes contribution $\boldsymbol{\phi}$ has been studied in several papers in the past (see e.g. [55]) and is now rather well understood. We first calibrate a Hawkes process without the price feedback term, i.e. setting $\boldsymbol{L}$ and $\boldsymbol{K}$ to zero in Eq. (2.2). We use the non-parametric technique introduced in [65, 15], expecting bid/ask symmetry. This means that the coefficients $\tilde{\boldsymbol{\alpha}}_0 = (\boldsymbol{I} - \boldsymbol{\phi})\boldsymbol{\Lambda}$ only depend on the type of events (and not their "sign"), and that the matrix $\boldsymbol{\phi}$ has a block-symmetry: the couplings of b→b are equal to those of a→a, and that b→a is equivalent to a→b. Our results are qualitatively similar to those reported in the literature [15, 55, 57, 65]. The matrix structure of the norm of the Hawkes feedback kernel is shown in Fig. 2.5 for the EURO STOXX contract.

Reintroducing the quadratic coupling term $\boldsymbol{K}$ leads to a much more complicated structure for the non parametric calibration problem (see [30]), in particular in the present multidimensional setting. Before implementing the full calibration scheme, we devised a simplified protocol to get some partial information on the structure of the price feedback terms. The idea is to capture the effect of local trends on the liquidity of the order book. Hence we define the net flux of orders at the bid $x = b$ or at the ask $x = a$ as:

$$dJ_t^{\mathrm{x}} := dN_t^{\mathrm{LO,x}} - dN_t^{\mathrm{MO,x}} - dN_t^{\mathrm{C,x}}.$$

From this we define the total flux and the signed flux as:

$$dI_t^{\mathrm{b+a}} = dJ_t^{\mathrm{a}} + dJ_t^{\mathrm{b}}, \qquad dI_t^{\mathrm{b-a}} = dJ_t^{\mathrm{b}} - dJ_t^{\mathrm{a}}.$$

We also introduce the forward realized flux and the forward Hawkes flux on time scale β'^{-1}:

$$F_{\beta'}^{\mathrm{x}}(t) = \int_t^{+\infty} e^{-\beta'(s-t)} dI_s^{\mathrm{x}}\ , \qquad H_{\beta'}^{\mathrm{x}}(t) = \int_t^{+\infty} e^{-\beta'(s-t)} \lambda_s^{H,\mathrm{x}} ds\ ,$$

where $\mathrm{x} = (b+a, b-a)$ and $\lambda_s^{H,\mathrm{x}}$ is the expected future activity, as predicted by the Hawkes contribution.[3] In the absence of other feedback mechanisms, one would expect any

[3] More explicitly, $\lambda_t^{H,\mathrm{x}} := \lambda_t^{\mathrm{H,LO,x}} - \lambda_t^{\mathrm{H,MO,x}} - \lambda_t^{\mathrm{H,C,x}}$, where $\boldsymbol{\lambda}^{\mathrm{H}}$ is the Hawkes intensity process calibrated

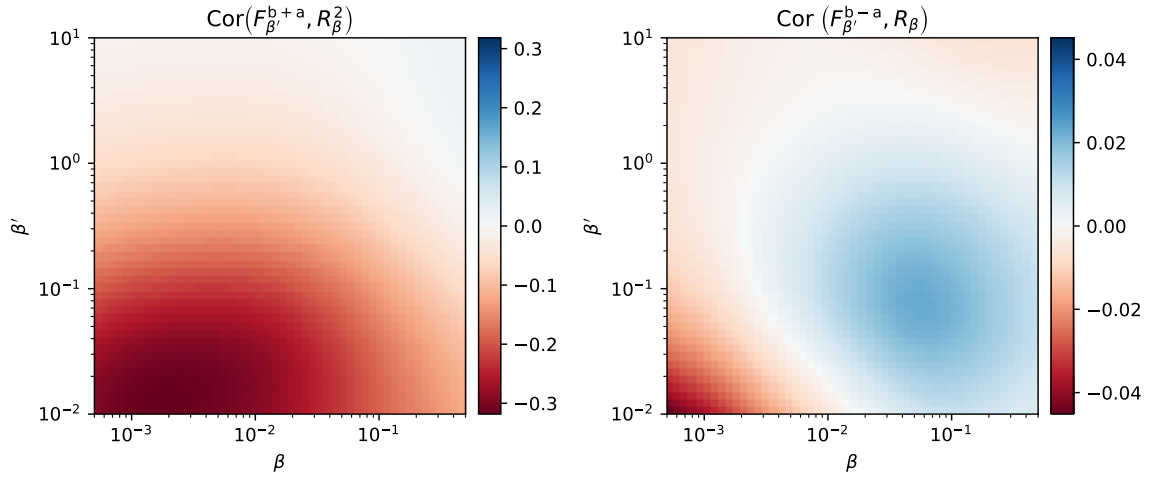

Figure 2.3: *Correlation between the trend and the total liquidity flux (left) and signed liquidity flux (right) in the plane β, β' for the EURO STOXX futures contract between* 2016/09/12 *and* 2017/04/28. *Note that the color scale is not the same in the left and in the right graph: the directional effect is weaker than the impact on the total (unsigned) liquidity.*

conditional expectation of $F^{\mathrm{x}}_{\beta'}(t)$ should simply be $H^{\mathrm{x}}_{\beta'}(t)$.

This is what we test now, by considering two conditioning variables suggested by the Q-Hawkes formalism, namely past trends and past realised volatility, as measured by the following exponential moving averages:

$$R_\beta(t) := \underbrace{\int_0^t e^{-\beta(t-s)} dP_s}_{\text{past trend}} , \qquad \Sigma^2_\beta(t) := \underbrace{\int_0^t e^{-2\beta(t-s)} (dP_s)^2}_{\text{past volatility}} .$$

By symmetry, we expect that the conditional expectations of $F^{\mathrm{b-a}}_{\beta'}(t)$ and $F^{\mathrm{b+a}}_{\beta'}(t)$ write:

$$\mathbb{E}_c[\beta' F^{\mathrm{b+a}}_{\beta'}(t) | R, \Sigma, H] = C_0 + 2\beta C_1 R^2_\beta(t) + 2\beta C_2 \Sigma^2_\beta(t) + \beta' H^{\mathrm{b+a}}_{\beta'}(t) \tag{2.3}$$

$$\mathbb{E}_c[\beta' F^{\mathrm{b-a}}_{\beta'}(t) | R, \Sigma, H] = \sqrt{\beta} C_3 R_\beta + \beta' H^{\mathrm{b-a}}_{\beta'}(t) , \tag{2.4}$$

i.e. the asymmetric part of the liquidity flow depends on the sign of the past trend, whereas the symmetric part of the flow depends both on the past volatility and on the past trend squared (i.e. the Zumbach effect). C_0, C_1, C_2 and C_3 are numerical constants. The normalisation factor β comes from the fact that $R_\beta \sim \beta^{-1/2}$ and $\Sigma^2_\beta \sim \beta^{-1}$. Note that the regression coefficients in front of the calibrated Hawkes contribution are fixed to unity, as they should be for consistency.

Results

We determine β and β' by looking at the maximum absolute correlations of $F^{\mathrm{b+a}}_{\beta'}$ with R^2_β, see Fig. 2.3 and Appendix A.1. We find $\beta = 0.001$ and $\beta' = 0.02$, corresponding to a negative correlation ≈ -0.3, indicating that *trends indeed reduce liquidity*. Note that the correlations between $F^{\mathrm{b-a}}_{\beta'}$ with R_β are one order of magnitude smaller, and in fact change sign depending on the time scales: the short time response to an up trend is adding liquidity at the ask, but the long-time response is in fact removal of liquidity at the ask. This could

above. In order to speed up the computation of $F^{\mathrm{x}}_{\beta'}$, we approximate the non-parametric Hawkes kernels by sums of exponentials.

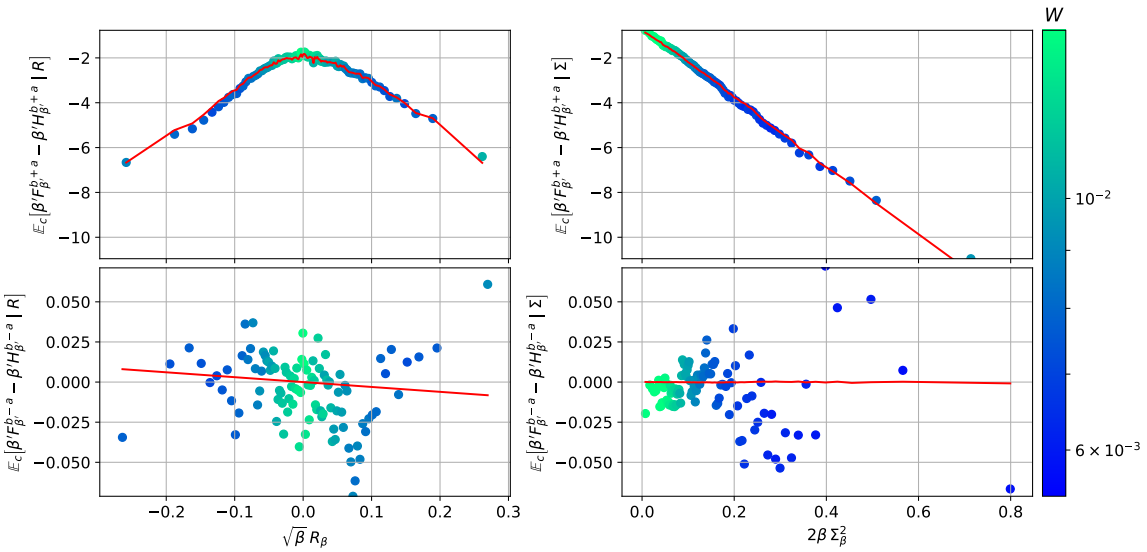

Figure 2.4: *Regressions of the incoming flux with the trend and the volatility on the EURO STOXX futures contract between* 2016/09/12 *and* 2017/04/28. *The red curves correspond to the in-sample prediction of the linear regression. Each empirical point has a weight computed from the fraction of time spent in the corresponding state.*

reflect the behaviour of different actors in the market (high-frequency traders/market makers vs. longer term traders).

Fixing $\beta = 10^{-3}$ (i.e. trends measured over 1000 seconds, similar to the time scale found in [30]) and $\beta' = 0.02$ (market response over the next 50 seconds), we find the regression coefficients C_i given in Tab. 2.1 for several futures contracts, again using the period between 12/09/2016 and 28/04/2017. The quality of the regressions in the case of the EURO STOXX is illustrated in Fig. 2.4 (similar plots are obtained for the BUND, BOBL and SCHATZ, not shown). We see that both the trend (Zumbach) effect, parameterised by C_1 and the volatility effect, parameterised by C_2, are both important to reproduce the future liquidity flow. The directional effect, measured by C_3, is much weaker, as indeed suggested by Fig. 2.3, so we will neglect it in the following.

The conclusions of this calibration exercise are that:

- Large recent price trend and volatility indeed tend to increase the rate of market orders and cancellations and lead to a decrease in liquidity. This is the main take-away message of this section.

- The quadratic feedback terms $\boldsymbol{K}$ in Eq. (2.2) is the dominant effect.

	$C_0\,(10^{-2})$	C_1	C_2	C_3
EUROSTOXX	78	−8.9	−6.7	−0.03
BUND	72	−1.7	−2.8	0.16
BOBL	13	−4.0	−0.29	0.29
SCHATZ	0.42	−2.5	0.001	0.50

Table 2.1: Values of the coefficients C_0, C_1, C_2 for the symmetric part of the liquidity flow and C_3 for the antisymmetric part, as defined in Eqs. (2.3) and (2.4). We fixed $\beta = 10^{-3}$ and $\beta' = 2 \times 10^{-2}$.

2.3 Brute Force Calibration of a GQ-Hawkes Process

Definition of the Model

We focus on a simplified version of the Generalized Quadratic Hawkes process (GQ-Hawkes) of Eq.(2.2), where the influence of the size of the queues on event rates is neglected. Nevertheless, we do not make assumptions on the structure of kernels $\boldsymbol{K}$. As pointed out in [52, 30], assuming that P_t is a martingale makes analytical calculations and numerical calibration, much more congenial. Finally, assuming as we shall do hereafter that a stationary state is reached allows us to replace the lower bound of the integrals in Eq. (2.2) by $-\infty$.

A Non-Parametric Calibration Procedure

Here we introduce a non-parametric scheme to calibrate Eq. (2.2) to real market data. Our method is an extension of the second moment method introduced by Bacry *et al.* in [17, 16], see also [27].

Covariances and Wiener-Hopf-like Equations

Before deriving the equations that will be used for the calibration, we introduce the following averages and covariances:

$$\begin{aligned}
\Delta_k dt &:= \mathbb{E}\left[(dP_t)^k\right], && \text{(2.5a)}\\
\Lambda^i dt &:= \mathbb{E}\left[dN_t^i\right], && \text{(2.5b)}\\
\chi^{ij}_{NN}(t-s)\,dtds &:= \mathrm{Cov}\left(dN_t^i, dN_s^j\right) - \Lambda^j\delta_{ij}\delta(t-s)dtds, && \text{(2.5c)}\\
\chi^{i}_{NP}(t-s)\,dtds &:= \mathrm{Cov}\left(dN_t^i, dP_s\right), && \text{(2.5d)}\\
\chi^{i}_{NP^2}(t-s)\,dtds &:= \mathrm{Cov}\left(dN_t^i, dP_s^2\right), && \text{(2.5e)}\\
\chi^{i}_{NPP}(t-s,t-x)\,dtdsdx &:= \mathrm{Cov}\left(dN_t^i, dP_x dP_s\right), && \text{(2.5f)}\\
\chi_{P^2P^2}(t-s)\,dtds &:= \mathrm{Cov}\left(dP_t^2, dP_s^2\right) - \Delta_4\delta(t-s)dsdt, && \text{(2.5g)}
\end{aligned}$$

where we have assumed for simplicity that the jumps of P and $\boldsymbol{N}$ are not simultaneous. Note that while price jumps can only occur if one order book event triggers them, the relative frequency of the latter is so much larger that this approximation is fully justified. Combining Eq. (2.2) with Eqs (2.5) yields the following set of equations for the first and second moments of the processes. Introducing the notations $||f|| = \int_{\mathbb{R}} f(t)dt$ and $\boldsymbol{K}_{\mathrm{d}}(t) := \boldsymbol{K}(t,t)$ the

diagonal part of $\boldsymbol{K}$, one obtains for $t, x > 0$ with $t \neq x$:

$$\Lambda^i = \alpha_0^i + \sum_k ||\phi^{ik}||\Lambda^k + ||K_{\rm d}^i||\Delta_2, \tag{2.6a}$$

$$\begin{aligned}\chi_{NN}^{ij}(t) &= \Lambda^j \phi^{ij}(t) + \int_{\mathbb{R}^+} \sum_k \phi^{ik}(s)\chi_{NN}^{kj}(t-s)ds \\ &+ \int_{\mathbb{R}^+} \left[L^i(s)\chi_{NP}^j(s-t) + K_{\rm d}^i(s)\chi_{NP^2}^j(s-t)\right] ds, \\ &+ \int_{[t,+\infty[^2} K^i(s,u)\chi_{NPP}^j(s-t,u-t)1_{\{s\neq u\}}duds, \end{aligned} \tag{2.6b}$$

$$\chi_{NP}^i(t) = \int_{\mathbb{R}^+} \sum_k \phi^{ik}(s)\chi_{NP}^k(t-s)ds + L^i(t)\Delta_2 + K_{\rm d}^i(t)\Delta_3, \tag{2.6c}$$

$$\chi_{NP^2}^i(t) = \int_{\mathbb{R}^+} \sum_k \phi^{ik}(s)\chi_{NP^2}^k(t-s)ds + L^i(t)\Delta_3 + K_{\rm d}^i(t)\Delta_4, \tag{2.6d}$$

$$+ \int_{\mathbb{R}^+} \chi_{P^2P^2}(t-s)K_{\rm d}^i(s)ds, \tag{2.6e}$$

$$\chi_{NPP}^i(t,x) = \int_{\mathbb{R}^+} \sum_k \phi^{ik}(s)\chi_{NPP}^k(t-s,x-s)ds + 2\Delta_2^2 K^i(t,x). \tag{2.6f}$$

Provided the number of events generated by price fluctuations is small compared to that generated by the linear Hawkes contribution, *i.e.* $\sum_{i,k} ||\phi^{ik}||\Lambda^k \gg \sum_i ||K_{\rm d}^i||\Delta_2$, Eq. (2.6b) conveniently simplifies to:

$$\chi_{NN}^{ij}(t) = \Lambda^j \phi^{ij}(t) + \sum_k \int_{\mathbb{R}^+} \phi^{ik}(s)\chi_{NN}^{kj}(t-s)ds. \tag{2.7}$$

This approximation is relatively well supported by real data for short enough times (see below). It is essential at this stage as it allows us to decouple the estimation of the Hawkes kernel from that of $\boldsymbol{L}$ and $\boldsymbol{K}$: one can first estimate $\boldsymbol{\phi}$ from Eq. (2.7) and then compute $\boldsymbol{L}$ and $\boldsymbol{K}$ from Eqs. (2.6c), (2.6e) and (2.6f). The base rate is finally obtained from Eq. (2.6a). Note that while in principle an exact calibration of Eqs. (2.6) is possible, it does not perform well on real data – but see section 2.4 below.

Micro-Price, Discretisation and Calibration Recipe

In section 2.3 we stressed that the point process P_t needs to be a martingale for Eqs. (2.6) to be valid. Yet, it is well established that the mid-price in financial markets displays substantial mean-reversion at short timescales. To circumvent this issue, we consider the volume weighted mid-price, sometimes called the **micro-price**, $P_t^{\rm micro}$, known to be closer to a martingale at high frequency [2, 3].[4] It is defined as:

$$P_t^{\rm micro} = \frac{v_t^{\rm a} b_t + v_t^{\rm b} a_t}{v_t^{\rm a} + v_t^{\rm b}}, \tag{2.8}$$

where $v_t^{\rm b}$, $v_t^{\rm a}$ denote the available volume at the best bid b_t and ask a_t respectively. To enforce further the martingale property, we use the so-called **surprise** price, that we shall henceforth denote by P_t, and which consists in subtracting to the price its (linear) statistical

[4] More refined definitions of the micro-price, even closer to a martingale, are discussed in [2].

predictability. Mathematically speaking, this reads:

$$dP_t = dP_t^{\text{micro}} - \int_{-\infty}^{t^-} \mathcal{C}_P(t-s) dP_s^{\text{micro}}, \tag{2.9}$$

where $\mathcal{C}_P(t-s) := \text{Cor}\left(dP_t^{\text{micro}}, dP_s^{\text{micro}}\right)$ denotes the price auto-correlation function.

In the previous section, we also have noted that the intensity of order book events exhibit an intraday U-shape, very much like the well known U-shaped volatility pattern, see Fig. 2.1. Computing the total intensity of events $\Lambda_{\text{tot}} = \sum_i \Lambda_i$ over 5-min bins and averaging over trading days, a U-shape is clearly visible. To avoid spurious effects related to these intraday seasonalities, we rescale time flow by this average pattern to enforce a constant rate of events in the new time variable.

In order to estimate the kernels from real order book data, one must choose a time grid t_n^H with weights w_n^H for kernel $\boldsymbol{\phi}$, such that $||\boldsymbol{\phi}|| \approx \sum_n \boldsymbol{\phi}(t_n^H) w_n^H$. We decide to use quadrature points [16] to ensure a good approximation of the integrals with a minimal number of points. Further, given that we expect power-law kernels, see e.g. [18, 16, 30], we choose a linear scale at short times that switches to logarithmic at longer times. Finally, given that typical timescales are usually quite different (see below), we choose a different time grid t_n, w_n for the kernels $\boldsymbol{L}$ and $\boldsymbol{K}$. See Appendix A.1 for more details.

Finally, the empirical covariances are usually very noisy, so we choose to smooth them using a convenient fitting function in order to obtain better behaved kernels. Concerning the volatility covariance $\chi_{P^2P^2}$, it is found to behave like a power law at large times so the chosen fitting function is[5] $A(1+t/B)^{-C}$ We also fit the logarithm of $\boldsymbol{\chi}_{NP}(t)$, $\boldsymbol{\chi}_{NP^2}(t)$ by a polynomial in $\log t$, and smooth the off-diagonal kernel, see 2.4 for details. Plots of the "raw" kernels obtained without smoothing fits are provided in Appendix. A.1. Apart from being more noisy, as expected, these raw kernels are very similar to the smoothed ones.

[5] For the EUROSTOXX, the fitting parameters are found to be $A = 1.7 \times 10^{-4}\,\$^4 s^{-2}$, $B = 81\,\text{s}$ and $C = 0.71$.

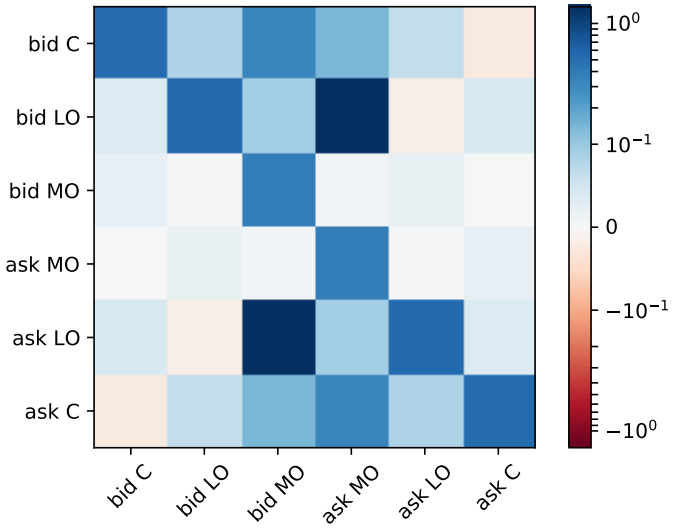

Figure 2.5: *Norms of the Hawkes kernel* $||\phi^{ij}||$ *for the EURO STOXX futures contract between* 2016/09/12 *and* 2020/02/07*, calibrated using Eq.* (2.7).

The calibration recipe then amounts to the following steps.

- Compute the surprise price from the micro-price using Eqs (2.8) and (2.9).
- Rescale time by the typical daily pattern of $\Lambda_{\text{tot}} = \sum_i \Lambda_i$.
- Estimate Δ_k, $\boldsymbol{\Lambda}$ and the covariances $\chi_{P^2P^2}$, $\boldsymbol{\chi}_{NN}$, $\boldsymbol{\chi}_{NP}$, $\boldsymbol{\chi}_{NP^2}$ and $\boldsymbol{\chi}_{NPP}$ from the data using Eqs (2.5),
- Use adequate fitting functions to smooth the empirical covariances (optional),
- Discretise and solve Eq. (2.7) to obtain the Hawkes kernel $\boldsymbol{\phi}$,
- Discretise and solve Eqs. (2.6c), (2.6e), and (2.6f) to obtain the kernels $\boldsymbol{L}$ and $\boldsymbol{K}$,
- Discretise and solve Eq. (2.6a) to obtain the base rate $\boldsymbol{\alpha}_0$.

Further details on how to solve these equations in practice are provided in Appendix A.1.

Empirical Results

We now apply the calibration procedure presented above to the EURO STOXX futures contract in the period 2016/09/12 to 2020/02/07. For this contract, the average time between two order book events is $\tau_{\text{e}} \approx 0.03s$, two orders of magnitude below the average time between two price changes $\tau_P \approx 7s$, indicating that the range of the kernels $\boldsymbol{L}$ and $\boldsymbol{K}$ is likely to be greater than that of $\boldsymbol{\phi}$, and allowing one to choose discretisation time grids accordingly. We also apply the procedure to the BUND futures contract but do not show all the (redundant) results for the sake of readability; summarising results are displayed in Fig. 2.9 and Tables 2.2, A.1 and A.2.

As specified in section 2.3, we start with the calibration of the Hawkes kernel $\boldsymbol{\phi}$. The results are displayed in Fig. 2.5 for the norms of the kernels, and in Fig. A.1 in the Appendix for the full time-dependence. The temporal decay of the kernels appears to be power law with exponent ≈ -1.5, consistent with previous reports [18, 16, 30].

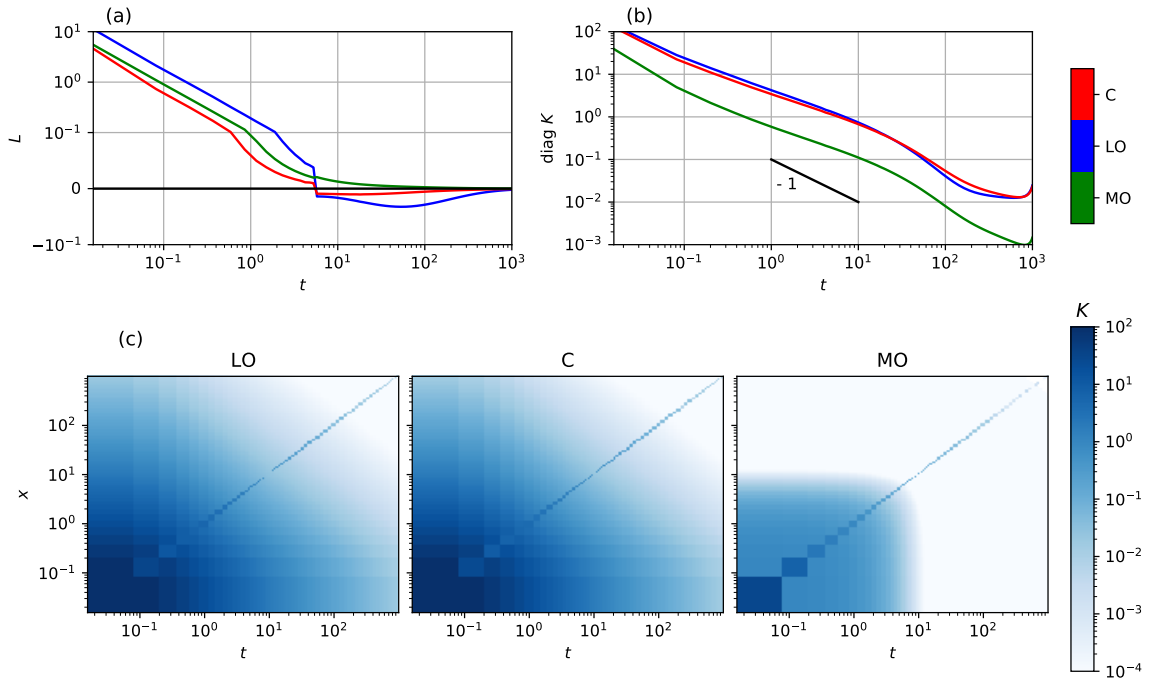

Figure 2.6: *Kernels resulting from the non-parametric calibration on the EURO STOXX futures contract between* 2016/09/12 *and* 2020/02/07. *(a) Linear kernels* $\boldsymbol{L}$. *Note that the sign is such that an up (resp. down) trend increases all the event rates at the bid (resp. ask) at short times. (b) Diagonal of quadratic kernels* $\boldsymbol{K}_{\mathrm{d}}$. *(c) Full quadratic kernels* $\boldsymbol{K}(t,x)$.

The calibration leads to a stable Hawkes process with spectral radius of $||\phi||$ (computed over 1000s) found to be ≈ 0.75 for the EURO STOXX contract and ≈ 0.74 for the BUND [55, 54]. The results show that the expected bid-ask symmetry holds with a high level of accuracy (see [52]), such that one can average the kernels accordingly to improve the statistics without loss of information.

Plugging the obtained Hawkes kernels into Eqs. (2.6c), (2.6e) and (2.6f) allow us to calibrate the kernels $\boldsymbol{L}$ and $\boldsymbol{K}$, see Fig. 2.6. Again the expected bid-ask symmetry properties hold rather well: while the linear kernel $\boldsymbol{L}$ is anti-symmetric (the effect of the positive trend on the bid is the same as that of a negative trend on the ask), the quadratic kernel $\boldsymbol{K}$ is bid-ask symmetric. We will therefore not distinguish further bid and ask events in the following.

Figure 2.6(c) shows that the quadratic contribution cannot be reduced to the diagonal part $\boldsymbol{K}_{\mathrm{d}}$ only. Indeed, the off-diagonal contribution of the kernel is non-zero and rather long-ranged. The decay of the diagonal contribution is a power law with exponent ≈ -1. Such a decay is very slow and means that $||\boldsymbol{K}_{\mathrm{d}}||$ is logarithmically sensitive to long timescales, for which we do not have much information since we only use data belonging to the same trading day to avoid the thorny discussion of overnight effects and how to treat them.

Finally, while the Hawkes and price feedback effects are difficult to compare as they do not operate on the same timescales, one can argue that the approximation presented at the end of Sec. 2.3 is well supported by data: considering a cut-off of 1000 seconds to compute the norms, one finds: $\sum_i ||K^i_{\mathrm{d}}||\Delta_2 / \sum_{i,k} ||\phi^{ik}||\Lambda^k \approx 0.06$. Another useful piece of information is the global effect of the quadratic term on order book events, measured by $\sum_i ||K^i_{\mathrm{d}}||\Delta_2$, which must be compared to the total activity $\sum_i \Lambda^i$. The ratio of these two quantities is found to be 5% for the EURO STOXX and 7% for the BUND (see Table A.2 for more details). Although not dominant, this feedback is clearly not negligible. Together with the standard

Hawkes contribution, this means that the exogenous contribution α to the total activity is only 19% of the total for the EURO STOXX (17% for the BUND). Note that this fraction is expected to decreases further as the upper cut-off of the slowly decaying kernels is extended beyond 1000 seconds (see e.g. [18]).

2.4 A Simplified Framework of a GQ-Hawkes Process

Here we present a framework which improves the above calibration in a threefold manner. As we shall see, (i) it allows to circumvent the approximation given in Eq. (2.7) which, we recall, is not perfectly satisfied by real data, (ii) it helps cleaning further the noisy off-diagonal contribution of the quadratic kernel, and (iii) it gives a more relevant measure of the global effect of price fluctuations on event rates with no longer having to consider, nor calibrate, the Hawkes contribution.

Effective Kernels

Using the resolvent method, see [16, 21], one can rewrite Eq. (2.2) as:

$$\boldsymbol{\lambda}_t = (\mathbf{I} - ||\boldsymbol{\phi}||)^{-1}\,\boldsymbol{\alpha}_0 + \int_{-\infty}^{t} \boldsymbol{\mathcal{R}}(t-s)\,d\boldsymbol{M}_s + \int_{-\infty}^{t} \bar{\boldsymbol{L}}(t-s)\,dP_s + \int_{-\infty}^{t}\int_{-\infty}^{t} \bar{\boldsymbol{K}}(t-s,t-u)\,dP_s dP_u, \tag{2.10}$$

with $\boldsymbol{M}$ a martingale satisfying $d\boldsymbol{M}_t = d\boldsymbol{N}_t - \boldsymbol{\lambda}_t dt$, $\boldsymbol{\mathcal{R}} = \sum_{n\geq 1} \boldsymbol{\phi}^{*n}$ the resolvent, $\bar{\boldsymbol{L}} = \boldsymbol{L} + \boldsymbol{\mathcal{R}} * \boldsymbol{L}$ and $\bar{\boldsymbol{K}}(t,s) = \boldsymbol{K}(t,s) + \int_0^{+\infty} \boldsymbol{\mathcal{R}}(u)\boldsymbol{K}(t-u,s-u)du$. The kernels $\bar{\boldsymbol{L}}$ and $\bar{\boldsymbol{K}}$ account for the overall feedback effect of P_t, including all subsequent Hawkes self-excited events that are induced by price fluctuations. The remarkable property of such kernels is that they solve a much simpler set of equations:

$$\chi^i_{NP}(t) = \bar{L}^i(t)\Delta_2 + \bar{K}^i_{\mathrm{d}}(t)\Delta_3 \tag{2.11a}$$

$$\chi^i_{NP^2}(t) = \bar{L}^i(t)\Delta_3 + \bar{K}^i_{\mathrm{d}}(t)\Delta_4 + \int_{\mathbb{R}} \chi_{P^2P^2}(t-s)\bar{K}^i_{\mathrm{d}}(s)ds \tag{2.11b}$$

$$\chi^i_{NPP}(t,x) = 2\bar{K}^i(x,t)\Delta_2^2, \tag{2.11c}$$

where we have again enforced that $\bar{\boldsymbol{K}}$ is symmetric. The results obtained from the inversion of Eqs (2.11) for the EURO STOXX futures contract are displayed in Fig. 2.7. These lead to similar, though slightly cleaner, conclusions to Fig. 2.6. In particular, the values of $\sum_i ||\bar{K}^i_{\mathrm{d}}||\Delta_2$ are compatible with those obtained above (taking into account the $1 - ||\boldsymbol{\phi}||$ factor, see Table A.2).

The Zumbach Factorisation

Here we further dissect the results of the calibration presented in the previous section, with the objective in particular of separating the contributions of trend and of volatility to the quadratic feedback. A meaningful approximation for the quadratic kernel $\bar{\boldsymbol{K}}$ was introduced in [30], as the sum of a purely diagonal matrix and a rank-one contribution:[6]

$$\bar{K}^i(t-s,t-u) := \bar{K}^i_{\mathrm{d}}\psi^i(t-s)\mathbb{1}_{\{s=u\}} + \bar{K}^i_1 Z^i(t-s)Z^i(t-u)\,. \tag{2.12}$$

The first term on the right hand side of Eq. (2.12) reflects feedback of past volatility on current order book events. Its contribution in Eq. (2.10) can indeed be written as:

$$\left[\sigma^i(t)\right]^2 := \int_0^t \psi^i(t-s)\,(dP_s)^2, \tag{2.13}$$

[6] The the slight abuse of notation here since the diagonal part of $\bar{K}(s)$ is in fact $\bar{K}_{\mathrm{d}}\psi(s) + \bar{K}_1 Z^2(s)$.

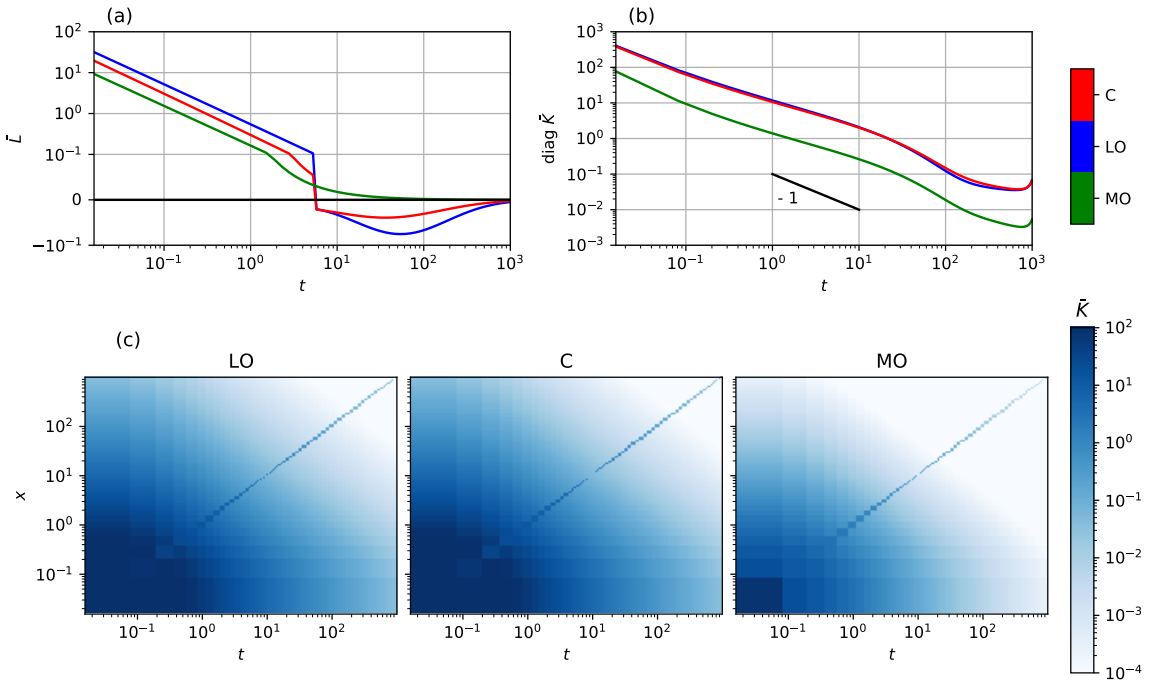

Figure 2.7: *Effective kernels resulting from the simplified calibration on the EURO STOXX futures contract between* 2016/09/12 *and* 2020/02/07. *(a) Linear kernels* $\bar{\boldsymbol{L}}$. *Note that the sign is such that an up (resp. down) trend increases all the event rates at the bid (resp. ask) at short times. (b) Diagonal of quadratic kernels* $\bar{\boldsymbol{K}}_{\mathrm{d}}$. *(c) Full quadratic kernels* $\bar{\boldsymbol{K}}(t,x)$.

The second term is in turn a reflection of the effect of past trends, as measured in Eq. (2.10) by $[R^i(t)]^2$, where:

$$R^i(t) := \int_0^t Z^i(t-s)\, dP_s. \tag{2.14}$$

This last term is reminiscent of the so-called Zumbach effect: past trends, regardless of their sign, lead to an increase in future activity. An alternative interpretation is that $[R^i(t)]^2$ is a local measure of a low-frequency volatility, to be contrasted with $[\sigma^i(t)]^2$ which is a local measure of high-frequency volatility. Note that the kernels ψ and Z are normalised:

$$\int \psi^i(s)ds = \int Z^i(s)^2 ds = 1, \tag{2.15}$$

such that the overall strength of the volatility contribution is $\bar{\boldsymbol{K}}_{\mathrm{d}}$ while that of the trend contribution is $\bar{\boldsymbol{K}}_1$.

While in practice such an approximation is, of course, not perfect, one can check that including higher rank contributions is unessential as the latter do not carry much additional signal. The rank-one kernel is obtained by minimizing $\iint \left(\bar{K}^i(s,u) - \bar{K}^i_1 Z^i(s)Z^i(u)\right)^2 \mathbb{1}_{\{u\neq s\}} dsdu$, which consists in finding the first eigenvector of a well chosen linear map, see [69] for more details. The ψ contribution is then obtained by taking the diagonal of $\bar{K}^i$ and subtracting $\bar{K}^i_1 Z^i(t)^2$. Figure 2.8 displays the kernels $\boldsymbol{\phi}$ and $\boldsymbol{Z}$ as function of time for the EUROSTOXX futures contract. As one can see, while the volatility kernel decays roughly as $1/t$, although some curvature can be observed. The Zumbach counterpart decays as $1/t$, regardless of event types (by that justifying the choice made in section 2.2, where the same functional form for all event types was assumed).

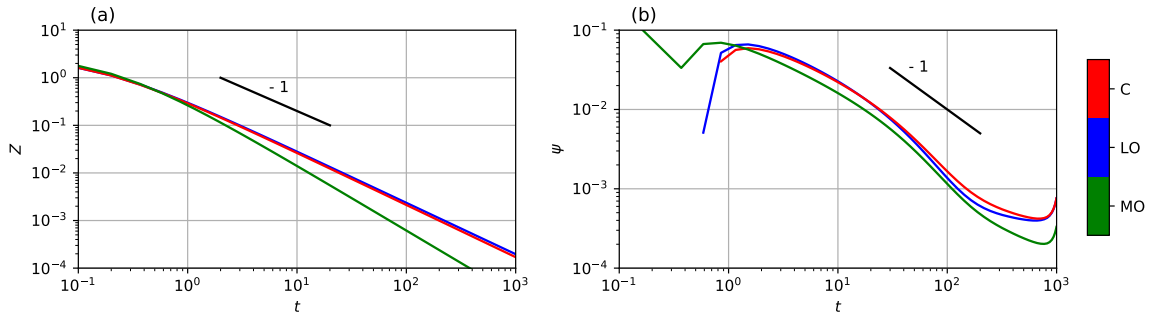

Figure 2.8: *Zumbach approximation of the effective kernel $\bar{\boldsymbol{K}}$ on the EURO STOXX futures contract between* 2016/09/12 *and* 2020/02/07. *(a) Zumbach kernel $\boldsymbol{Z}$, (b) Volatility kernel $\boldsymbol{\psi}$. Both kernels are normalised such that $||\boldsymbol{\psi}|| = ||\boldsymbol{Z}^2|| = 1$, with a cut-off in the time integrals at 1000 secs.*

2.5 Liquidity Dynamics & Crises

Quadratic Feedback on Liquidity

So far we have focused on the impact of past price moves one event rates. Here we wish to go on step further and estimate the effect of past price changes on liquidity, *i.e.* volume weighted events. For this one needs to consider order volumes. The average volumes are given in Tab. 2.2 for the different types of orders. Assuming bid/ask symmetry (consistent

	$V^{\mathrm{C,b}}$	$V^{\mathrm{LO,b}}$	$V^{\mathrm{MO,b}}$	$V^{\mathrm{MO,a}}$	$V^{\mathrm{LO,a}}$	$V^{\mathrm{C,a}}$
EUROSTOXX	10.1	9.2	7.2	8.2	9.2	10.0
BUND	4.5	4.8	4.4	4.2	4.8	4.5

Table 2.2: Average order volumes (in shares).

with the empirical results), Fig. 2.9 displays the amount of shares per second that can be attributed to the quadratic effect (both volatility and Zumbach) for each event type, namely $\bar{K}^i_{\mathrm{d}} V^i \Delta_2$ and $\bar{K}^i_1 V^i \Delta_2$ where $\bar{K}^i_{\mathrm{d}}, \bar{K}^i_1$ are obtained as explained in the previous section, V^i are given in Tab. 2.2, and Δ_2 is defined in Eq. (2.5a).[7]

Introducing the overall average quadratic liquidity flux as:

$$J_{\bar{\boldsymbol{K}}} := \left(||\bar{K}^{\mathrm{LO}}|| V^{\mathrm{LO}} - ||\bar{K}^{\mathrm{C}}|| V^{\mathrm{C}} - ||\bar{K}^{\mathrm{MO}}|| V^{\mathrm{MO}} \right) \Delta_2, \tag{2.16}$$

one consistently finds that the quadratic (price) feedback has an overall negative effect on liquidity $J_{\bar{\boldsymbol{K}}} < 0$, most of it associated to volatility, see Fig. 2.9(c).[8] In other terms, the quadratic feedback tends to decrease liquidity on average. Figure 2.9(b) shows that both the volatility and Zumbach terms have an average negative impact on liquidity (i.e. the green bars represent less than 50% of the total contribution). The Zumbach term is responsible for non-trivial long-range liquidity anomalies. In particular, Blanc *et al.* [30] showed that the price process resulting from a quadratic Hawkes process follows is diffusive with fat tailed stochastic diffusivity at large times, which can be attributed to the Zumbach effect, rather than its volatility counterpart (see also the discussion in [31]). In any case, we believe that the quadratic feedback of price trends on order book events is a crucial ingredient to understand liquidity crises. In the next section we provide a direct test of this hypothesis.

[7] The normalisation of all kernels is computed with a time cut-of at 1000 seconds.

[8] Note that the linear terms give no net contribution, i.e. $V^{\mathrm{LO}}||\bar{L}^{\mathrm{LO}}|| - V^{\mathrm{C}}||\bar{L}^{\mathrm{C}}|| - V^{\mathrm{MO}}||\bar{L}^{\mathrm{MO}}|| \approx 0$, which explains why we focus on the quadratic term). In other words, the trend has almost no linear effect on the liquidity flux at large time scales.

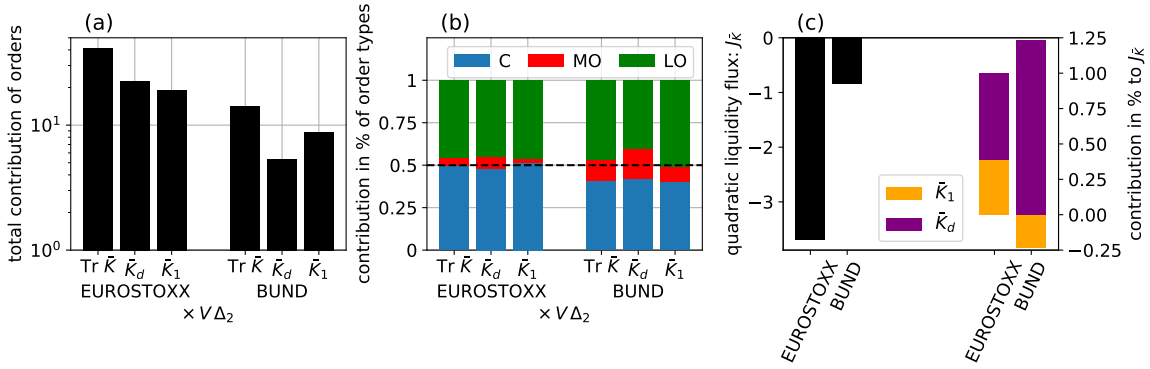

Figure 2.9: *Average quadratic contribution on the EURO STOXX and BUND futures contracts between* 2016/09/12 *and* 2020/02/07. *(a)* $\Delta_2 \sum_i V^i ||\bar{K}^i||$ *and its decomposition into* $\Delta_2 \sum_i V^i \bar{K}^i_{\mathrm{d}}$ *and* $\Delta_2 \sum_i V^i \bar{K}^i_1$. *(b) Contributions of each order type to the latter quantities. (c) Overall contribution of the quadratic effect to the liquidity flow* $J_{\bar{\boldsymbol{K}}}$ *(in shares per second), and relative contribution of the volatility and Zumbach terms.*

Spread Dynamics and Liquidity Crises

We now focus on the analysis of spread dynamics. Since the EUROSTOXX futures is a large tick contract (the spread is equal to one over 99% of the time and seldom higher than two), we characterize the dynamics of liquidity using an **effective spread** S_t^{eff} which is defined as follows. Calling $v_t^{\mathrm{a}}(x)$ (*resp* $v_t^{\mathrm{b}}(x)$) the ask (*resp* bid) volume at price level x, we construct cumulative volumes as $Q_t^{\mathrm{a}}(x) = \sum_{n \le x} v_t^{\mathrm{a}}(n)$ and $Q_t^{\mathrm{b}}(x) = \sum_{n \ge x} v_t^{\mathrm{b}}(n)$. We then choose the average volume at best V_{best} as a reference volume, and define:[9]

$$S_t^{\mathrm{eff}} := (Q_t^{\mathrm{a}})^{-1}(V_{\mathrm{best}}) - \left(Q_t^{\mathrm{b}}\right)^{-1}(V_{\mathrm{best}}), \tag{2.17}$$

where $\left(Q_t^{\mathrm{a/b}}\right)^{-1}$ denotes the inverse function of $Q_t^{\mathrm{a/b}}$. The effective spread is a natural proxy for liquidity in the close vicinity of the midprice: when the liquidity is close to its average, the effective spread coincides with the regular spread; but when liquidity is low, it can be much larger as aggregating the volume of several queues is needed to recover the reference volume V_{best}. Figure 2.10(a) displays the survival function of the effective spreads, revealing that $\mathbb{P}(S^{\mathrm{eff}}) \sim (S^{\mathrm{eff}})^{-5}$. This power-law tail is interesting for the following reason: the effective spread can be seen as a proxy for the size of latent price jumps, i.e. the jumps that are likely to happen if an aggressive market order hits the market. Hence, one expects the distribution of effective spread is not far from the distribution of price returns r, which is well known to decay as $\mathbb{P}(r) \sim r^{-4}$.

Let us now study the relation between effective spread, square volatility σ^2 and square trend R^2, as defined in Eqs. (2.13) and (2.14). Figures 2.10(b), (c) and (d) display the correlation functions $C_R(\tau) := \mathrm{Cor}\left[R(t+\tau)^2, S^{\mathrm{eff}}(t)\right]$, $C_\sigma(\tau) := \mathrm{Cor}\left[\sigma(t+\tau)^2, S^{\mathrm{eff}}(t)\right]$ and $C_{\mathcal{T}}(\tau) := \mathrm{Cor}\left[\mathcal{T}(t+\tau), S^{\mathrm{eff}}(t)\right]$ respectively, with $\mathcal{T} = R^2/\sigma^2$. Note that a causal positive impact of past trends on future spreads should translate as a strong contribution to $C_R(\tau)$ for negative τ. Interestingly, this is compatible with Fig. 2.10(b), which confirms in a model-free fashion that the Zumbach-like coupling is important: past square trends increase future effective spread, or equivalently decrease future liquidity. While also slightly asymmetric, the volatility/spread correlation $C_\sigma(\tau)$ does not reveal such a level of asymmetry (see Fig. 2.10(c)). Fig. 2.10(d) shows an even more pronounced asymmetry when we rescale the trend by the local volatility: $\mathcal{T}$ is a proxy of the autocorrelation of returns, independently of their

[9] Changing the reference volume to $2V_{\mathrm{best}}$ or $V_{\mathrm{best}}/2$ does not change the qualitative conclusions below.

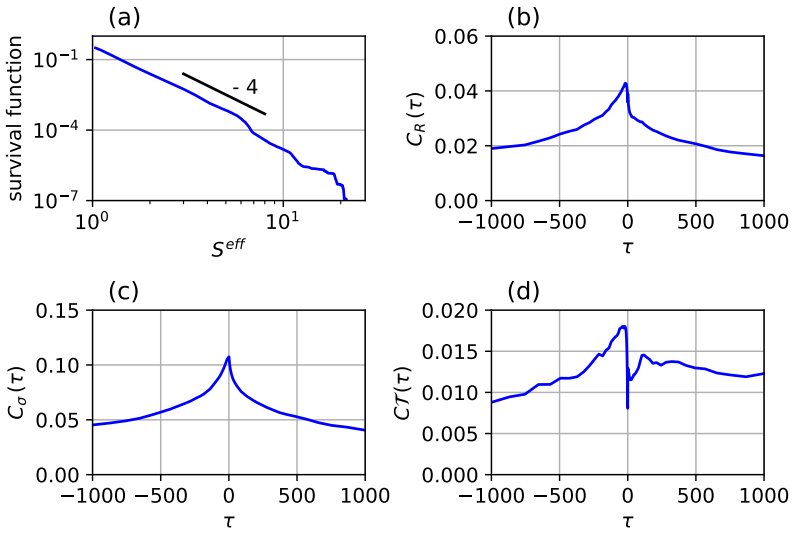

Figure 2.10: *(a) Survival function of the effective spread, showing that* $\mathbb{P}(S^{\text{eff}} > S) \sim S^{-4}$ *(b) Correlations between effective spread and past square trends (for* $\tau < 0$*) and future square trends (for* $\tau > 0$*).(c) Correlations between effective spread and square volatility. (d) Correlations between effective spread and* $\mathcal{T}$*: the ratio square trend over square volatility. EURO STOXX futures contracts between 2016/09/12 and 2020/02/07.*

amplitude. In this sense, it is a better signature of trend behaviour, as the volatility aspect of recent price changes is discarded.

2.6 Conclusion

Let us summarise what we have achieved in this chapter. We have proposed several actionable procedures to calibrate general Quadratic Hawkes models for order book events (market orders, limit orders, cancellations). One of the main features of such models is to encode not only the influence of past events on future events but also, crucially, the influence of past **price changes** on such events. We propose two methods for calibrating those models: the first one consists in a minimal setting approach while the second one fully calibrates QG-Hawkes process. Using tick-by-tick order book data on futures contracts, we have shown that the empirically calibrated quadratic kernel (describing the part of the feedback that is independent of the sign of past returns) is well described by the shape postulated in [30, 31], namely:

- a diagonal contribution that captures past realised volatility, and
- a rank-one contribution that captures the effect of past trends.

The latter contribution can be interpreted as the microstructural origin of the Zumbach effect: past trends, independently of their sign, tend to reduce the liquidity present in the order book, and therefore increase future volatility. This, in turn, contributes to increasing volatility, which may lead to a destabilising feedback loop and a liquidity dry-out.

One of the perhaps unexpected result of our calibration is that the Zumbach kernel is found to be a power-law of time for the futures contracts studied here, and not an exponential as was found in [30] for US stock prices. Hence, all Hawkes kernels in our study are found to be power-laws of time. Furthermore, as in many previous studies [20, 18, 55], the rate of truly exogenous events is found to be much smaller than the total event rate, typically

1/5 when all kernels are truncated beyond 1000 seconds, and probably even smaller when longer lags are taken into account, due to the slow decay of the kernels. These two features suggest that the system is close to a critical point – in the sense that stronger feedback kernels would lead to instabilities. In our setting, we have shown that the effective spread (which is a measure of the (il-)liquidity of the order book) has itself a power-law tailed distribution.Hence, we favour the scenario of markets poised close to a point of instability, although the detailed mechanisms that lead to such a fine tuning are still somewhat obscure. We note that the near-criticality has also been argued to be crucial to understand the "rough" nature of volatility [22, 70, 31]. We believe that understanding these mechanisms is probably one of the most intellectually challenging (and exciting) issue for microstructure theorists.

Take home message of Chapter 2

1. State-dependency. Rates of order book events are state-dependent. Our analysis reveals that limit order depositions do not depend on the number of orders at their price level, while cancellations and market orders are roughly proportional to it.

2. GQ-Hawkes process. The Generalized Quadratic Hawkes process can be calibrated on order book data thanks to a second moment method.

3. Quadratic effects. The quadratic kernels are power laws, with exponent ≈ -1 for the volatility contribution and square trend contribution, and exponent $\approx -3/2$ for the Hawkes kernels. These power laws are evidence of criticality.

4. Zumbach-like effect. The off-diagonal quadratic contribution can be factorized into a rank-one contribution, that corresponds to the feedback of the past square price trend. Such feedback diminishes future liquidity and can be interpreted as the micro-foundation of the Zumbach effect.

3

A Quadratic Santa Fe Model

In the previous chapter, we have shown, using empirical data, that liquidity tends to decrease with the amplitude of past volatility and price trends. Such a feedback mechanism in turn increases the volatility, possibly leading to a liquidity crisis. Accounting for such effects within a stylized order book model, we demonstrate numerically that there exists a second order phase transition between a stable regime for weak feedback to an unstable regime for strong feedback, in which liquidity crises arise with probability one. We characterize the critical exponents, which appear to belong to a new universality class.

From:
Endogenous liquidity crises
A. Fosset, Bouchaud, M. Benzaquen

Contents

Money, it's a gas
Grab that cash with both hands and make a stash

Pink Floyd

3.1 Introduction

It is now well established that market volatility is too high to be explained by fluctuations of fundamental value. As seen in the general introduction, a large fraction of large price jumps cannot been explained by significant news. Spectacular flash crashes, such as the infamous S&P500 flash crash of May 6th, 2010 [4], has led us to focus on a plausible general scenario of destabilising feedback loops resulting in liquidity breakdown. The previous chapter was dedicated to an empirical analysis that highlighted the feedback of square past trend and past volatility on future liquidity. Both are responsible for a decrease of liquidity and the first one micro found the Zumbach effect. To construct a possible scenario, imagine that the price has recently experienced a burst of volatility or a large trend. This creates anxiety for liquidity providers, who fear that some information about the future price, unbeknownst to them, is the underlying reason for the recent price changes. The consequence is an increased reluctance to provide liquidity: such liquidity providers become more likely to cancel their existing limit orders and less likely to refill the limit order book with new limit orders. Less liquidity is likely to amplify the future price moves, thereby creating an unstable feedback loop which might result in a runaway trajectory.

The present chapter attempts to capture such feedback effects through a stylised model for the dynamics of order books. To study the aggregate outcomes of such feedback in a minimal setting, we consider an extended version of the **Santa Fe order book model** [43, 44, 71].[1] The original model consists in a collection of N queues that evolve with constant additive limit order and market order arrival probability rates, and a constant cancellation rate per existing limit order. We introduce, in a minimal fashion, the effect of interest to us by letting the event rates feedback on past prices changes. As the empirical results of the previous chapter suggest, we use a Zumbach-like coupling as feedback from past price changes. Our numerical results strongly suggest the existence of a genuine phase transition occurs from a stable regime to an unstable regime in which liquidity crises arise, as feedback intensity is increased. We perform a finite size scaling and determine the corresponding critical exponents.

3.2 An Agent-Based Model for Liquidity Crises

The so-called **Santa Fe model** [43, 44, 71] stands among the first purely stochastic order book models, where zero-intelligence agents place their orders at random (see also [72, 45]). It was shown that this model is able to reproduce some empirical properties of order books, such as the mean bid-ask spread and mean volume profiles near the best quotes. However, the model fails to account for the empirical relation between spread and volatility (see [73, 74] and [6], Ch. 8); in fact prices are found to be strongly mean reverting, partly because of the absence of long-range correlations in the flow of market orders in the model – see the detailed discussion of this point in [32, 36, 6].

In spite of these shortcomings, the Santa Fe model is an interesting starting point for modelling order book dynamics. It consists in a collection of queues that evolve with constant

[1] The **Santa Fe model** stands among the first **zero intelligence** order book models reproducing some statistical properties, such as the mean bid-ask spread and mean volume profiles near the best quotes. Note however that the model is too simple to account for volatility levels, volume profile queues far from the best, or to solve the diffusivity puzzle [6].

additive limit and market order arrival Poisson rates, and a constant cancellation rate per existing limit order. Note that while real data is not fully consistent with additive depositions and multiplicative cancellations (see Fig. 2.2) , this simplifying hypothesis allows for easier analytical treatment, and leads to a well defined steady state order book where queues are neither empty nor of infinite size.

Here, we present an extension of the Santa Fe model where the feedback of past price changes on event rates is taken into account. As suggested by the empirical results of the previous chapter, we only retain, for simplicity, the quadratic feedback term on cancellations, neglecting all others. We also keep the initial Santa Fe specification of an additive (rather than multiplicative) rate for market orders. Numerical simulations suggest that this brings no qualitative changes to our main conclusions, which are as follows:

1. There exists a critical value of the feedback parameter α_K such that for $\alpha_K < \alpha^*$, an infinite size order book *never empties*, while for $\alpha_K > \alpha^*$ such infinite size order book *empties with probability 1*.

2. The transition appears to be of second order nature, which means that as the transition point is approached some scaling behaviour is observed. For example, the average time $\bar{\tau}$ needed for the liquidity crisis to appear in an infinite order book diverges as $(\alpha_K - \alpha^*)^{-\zeta}$ with $\zeta \approx 3$ when $\alpha_K \downarrow \alpha^*$. For a book of finite size N, this time is always finite, but diverges as N^η with $\eta \approx 3$ when $\alpha_K = \alpha^*$.

The Santa Fe Model with Feedback

Consider a grid of prices with unit tick size, with all orders of unit size.[2] This grid is divided into three parts: the bid side $\mathcal{B}_t = \{p \leq b_t\}$, the ask side $\mathcal{A}_t = \{p \geq a_t\}$ and the spread $\mathcal{S}_t = \{b_t < p < a_t\}$ where b_t and a_t respectively denote the best bid and the best ask. Market orders can only fall at the best bid and best ask; they do so with total rate 2μ, with probability $1/2$ to fall on the bid and $1/2$ to fall on the ask.

Bid limit orders fall uniformly with rate λ per tick size in $\mathcal{B}_t^+ = \{p \leq \min(b_t + 1, a_t - 1)\}$ and ask limit orders uniformly with the same rate λ in $\mathcal{A}_t^+ = \{p \geq \max(a_t - 1, b_t + 1)\}$. Orders cannot be placed inside the spread at a distance higher than one tick of the best prices.

Cancellations occur with a rate ν_t per outstanding limit order, which means that the probability that a given queue loses one order is proportional to the size of the queue. We assume that ν_t is given by a GQ-Hawkes process of the type we considered in the previous chapter, where we retain only the Zumbach term, i.e.

$$\nu_t = \nu_0 + \alpha_K \left(\int_0^t \sqrt{2\beta} e^{-\beta(t-s)} dP_s \right)^2 . \tag{3.1}$$

The case $\alpha_K = 0$ recovers the Santa Fe specification. Note that the dynamics of the different price levels are independent of one another, but described by the same parameters λ for the deposition rate and ν_t for the cancellation rate. In other words, the speed-up of cancellations when the price is trending affects *all* price levels, as empirical results of the previous chapter tell us that $\alpha_K > 0$. Then, the feedback mechanism works as follow: local trends reduce liquidity in the order book via a Zumbach-like effect. Then less liquidity not only increases the probability of a new price change but also the size of price changes, that could lead to bigger local trends. And so on and so forth. Fig. 3.1 displays a schematic that sums up this

[2] One could introduce a distribution of order size at the expense of extra complexity. We expect that if this distribution is broad enough, the character of the phase transition could change.

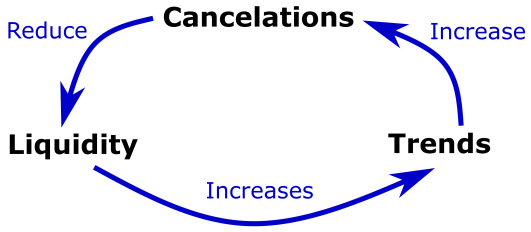

Figure 3.1: *Sketch of the feedback mechanism based on Zumbach-like effect.*

explanation. When $\alpha_K < \alpha^*$, if the spread is greater than one, we expect that the average probability of diminishing it remains higher than the one of opening it, preventing liquidity crises to occur. But if $\alpha_K > \alpha^*$, we expect the opposite and so the market to be unstable.

Numerical Simulations

To simulate the model, we take a price grid of size N ticks, and as initial condition, the equilibrium order book provided by the Santa Fe model with $\alpha_K = 0$. Then, to make the system evolve one can notice that, conditioned to the past, the system follows a multidimensional, non-homogeneous Poisson process, which is well known and easy to implement. Furthermore, for computing the integral $\int_0^t e^{-\beta(t-s)} dP_s = \sum_{T_n \leq t} e^{-\beta(t-T_n)} \Delta P_{T_n}$ efficiently, we use the the usual recursive formula to speed up the algorithm, see [54].

Dynamics: stability or liquidity crises

Figure 3.2 displays typical results in the stable phase. Note that at some point the spread opens and triggers a cascade of cancellations that empties the order book. At some point in time denoted τ_c a liquidity crisis arises, that is here defined as the first time one side of the order book is completely empty. Mathematically speaking it is defined as:

$$\tau_c = \min \left(\inf \left\{ t, \sum_{p \in \mathcal{B}_t} v_t(p) = 0 \right\}, \inf \left\{ t, \sum_{p \in \mathcal{A}_t} v_t(p) = 0 \right\} \right) \tag{3.2}$$

with $v_t(p)$ the number of orders at price p and time t. Using the finite size of the order book, we can rewrite the time of first liquidity crises as:

$$\tau_c = \min \left(\inf \left\{ t,\ b_t < 0 \right\}, \inf \left\{ t,\ a_t > N \right\} \right) \tag{3.3}$$

Eq. (3.3) shows that liquidity crises coincide with spread explosion. Fig. 3.2(c) displays a typical spread trajectory where a burst occurs. Not sufficient to trigger a liquidity crisis, it gives a example of what happens while the order book is destabilized. Fig. 3.2(d) shows the spread survival function that starts to be fat-tailed when one reaches the transition, bolstering our qualitative interpretation of the time of liquidity crises.

On the other hand, close but below the instability transition, a spread explosion goes with a sparser order book. Indeed, as the feedback from past price changes on cancellations affects all price levels, liquidity is diminished everywhere. Quantifying liquidity far from the mid-price can be achieved by computing the probability distribution function $\rho_v(t, v)$ of the variable $v_t(\infty)$ conditioned to the past price information until time t: $\mathcal{F}_t^{\mathrm{P}}$. Indeed, as we are far from the mid-price, two consecutive levels have the same law. Thus, we can forget about price changes and only focus on limit order depositions and cancellations. From these remarks, we easily derive the Fokker Planck equation that follows ρ_v:

$$\partial_t \rho_v(t, n) = \lambda(\rho_v(t, n-1) - \rho_v(t, n)) + \nu_t((n+1)\rho_v(t, n+1) - n\rho_v(t, n)) \tag{3.4}$$

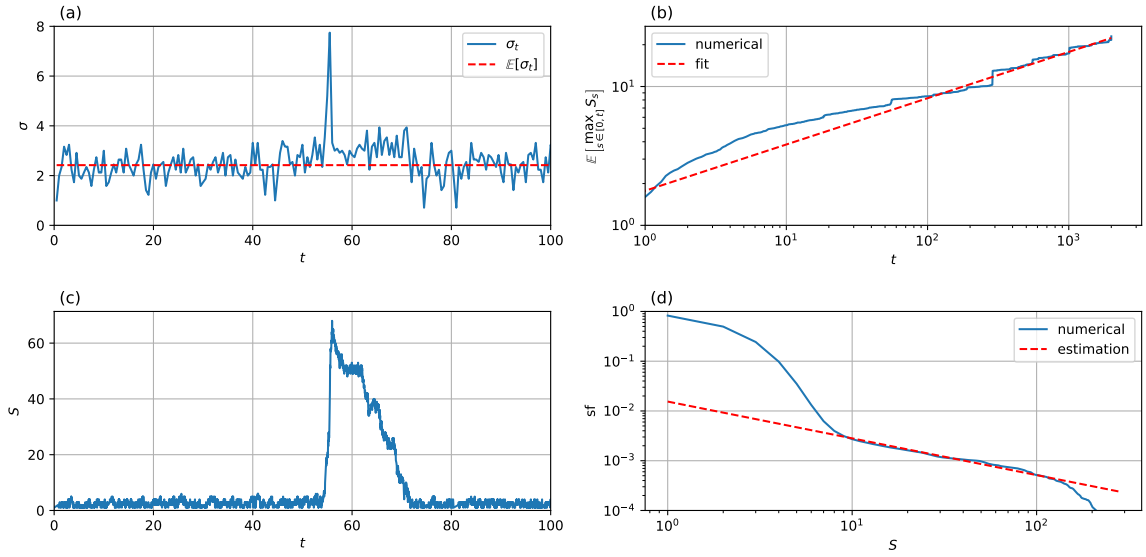

Figure 3.2: *Properties of trajectories close to, but below the instability transition ($\lambda = 10$, $\nu_0 = 0.5$ and $\mu = 20$, and $\alpha_K = 0.2$, $\beta = 1$, $T = 2000$, $N = 1000$). (a) One trajectory of the volatility exhibiting a cluster of high volatility. (b) Average maximum of the spread S as a function of time and its fit by a power-law $t^{1/\eta}$ with $\eta = 3$ for $t \geq 100$. (c) The spread trajectory corresponding to (a). (d) The spread survival function (sf), also called complementary cumulative probability distribution, decays as a power law $S^{-\kappa}$, with a cut-off that diverges as one approaches the transition α^*. The dotted line corresponds to $\kappa = 0.74$.*

Starting from the equilibrium of the Santa Fe model *i.e.* $\rho_v(0,n) = e^{-V^*}V^{*n}/n!$ with $V^* = \lambda/\nu_0$, we can show that $v_t(\infty)|\mathcal{F}_t^{\mathrm{P}}$ still follows a Poisson distribution:

$$\rho_v(t,n) = e^{-V_t^*}\frac{V_t^{*n}}{n!} \tag{3.5}$$

with $V_t^* = \frac{\lambda}{\nu_0}e^{-\int_0^t \nu_s ds} + \lambda\int_0^t e^{-\int_s^t \nu_u du}ds$, see Appendix A.2 for details. V_t^* is the average number of orders far away from the mid-price, conditioned to the price dynamics. Analyzing what happens closer to the mid-price is not tractable, but the following inequality holds: $\mathbb{P}\left[v_t(p) = n\middle|\mathcal{F}_t^{\mathrm{P}}\right] \leq \rho_v(t,n)$ for any price level p and number of orders n. Thus, the dynamics of V_t^* is a proxy for liquidity dynamics, coherent with the sketch presented in Fig. 3.1. This variable V_t^* enables a qualitative analysis of a destabilization of the order book. When the parameter α_K is close to the transition but below, large trends lead to:

- $S_t \gg 1$: large spread.
- $V_t^* \ll 1$: sparse order book.

3.3 Phase Transition and Finite Size Scaling

Exploring the parameter space (α_K, β) reveals that for $\alpha_K \gtrsim \alpha_m(\beta)$ liquidity crises arise with high probability. Figure 3.3 displays the crisis probability, defined as $\mathbb{P}[\tau_c \leq T]$, as function of α_K and β for $T\nu_0 = 200$ and $N = 280$. As expected, large feedback intensities α_K lead to unstable markets. The crossover value $\alpha_m(\beta)$ decreases as β increases, i.e. when the time scale over which trends are considered as dangerous by liquidity providers gets shorter. As expected, longer integration timescales β^{-1} lead to more stable order book, or in other terms, longer memory is a stabilising factor.

Although suggestive, Fig. 3.3 cannot be used to conclude on the existence of a true phase

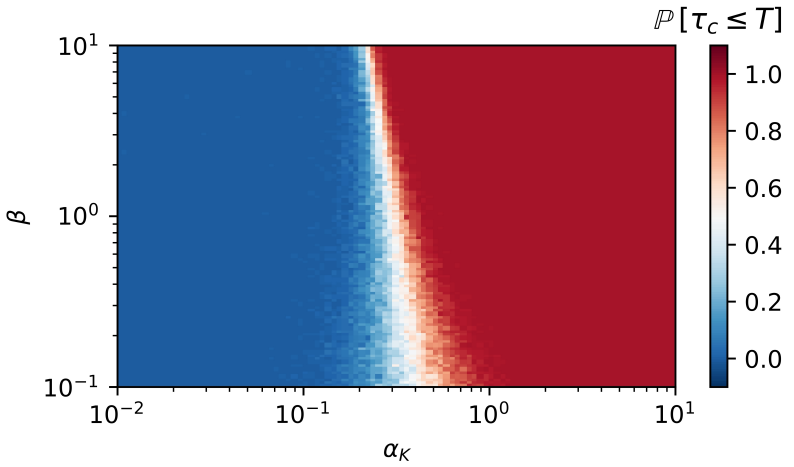

Figure 3.3: *Stability map: Crisis probability* $\mathbb{P}[\tau_c \leq T]$ *for* $T = 200$, $N = 280$, $\lambda = 10$, $\nu_0 = 1$ *and* $\mu = 20$. *The blue region correspond to a stable order book, whereas the red region corresponds to liquidity crises. The crossover line* $\alpha_m(\beta)$ *is the white sliver between the two.*

transition in the model, between a phase where liquidity crises never happen from a phase where liquidity crises always happen, provided one waits long enough. Mathematically, the question is about the behaviour of $\mathbb{P}[\tau_c \leq T]$ in the double limit $N \to \infty$ and $T \to \infty$. Clearly, for finite N, there is always a non-zero probability (perhaps very small) that the order book completely empties if one waits long enough, even when $\alpha_K = 0$. Hence:

$$\lim_{N\to\infty} \lim_{T\to\infty} \mathbb{P}_N[\tau_c \leq T, \alpha_K] = 1\,, \quad \forall \alpha_K\,.$$

If one the other hand the limit $N \to \infty$ is taken first, one may be in a situation where, for a fixed value of β

$$\lim_{T\to\infty} \lim_{N\to\infty} \mathbb{P}_N[\tau_c \leq T, \alpha_K] = \begin{cases} 1, & \text{when} \quad \alpha_K > \alpha^*, \\ 0, & \text{when} \quad \alpha_K < \alpha^*, \end{cases} \tag{3.6}$$

where α^* depends on the parameters of the model, in particular β.

Since numerical simulations can only be done for finite N and T, a common strategy is to use finite size scaling to extrapolate to infinite sizes and waiting times. If a genuine, continuous phase transition occurs at some $\alpha_K = \alpha^*$, one expects the following behaviour to hold for large enough N and T:

$$\mathbb{P}_N[\tau_c \leq T, \alpha_K] = F\left(T(\alpha_K - \alpha_m(T,N))^\zeta\right); \qquad \alpha_m(T,N) = \alpha^* - \frac{1}{T^{1/\zeta}} g\left(\frac{N^\eta}{T}\right), \tag{3.7}$$

with $F(u)$ a monotonic regular function going from 0 for $u \to -\infty$ to 1 for $u \to +\infty$, and $g(v)$ another function that goes to a constant g_∞ when $v \to \infty$ and to $+\infty$ as $v \to 0$. This scaling form has the following interpretation:

- When $1 \ll T \ll N^\eta$, $\alpha_m \approx \alpha^*$. As α_K increases, $\mathbb{P}_N[\tau_c \leq T, \alpha_K]$ evolves from 0 (no crises) to 1 (crises) in a region of width $T^{-1/\zeta}$ around α^*.
- When $T \gg N^\eta$, α_m becomes negative, meaning that $\mathbb{P}_N[\tau_c \leq T, \alpha_K]$ is close to 1 for any α_K if one waits long enough.

The comparison between T and N^η has the following interpretation: for $T \ll N^\eta$, the system cannot "feel" the boundaries of the order book because the spread has never grown so large: $S(T) \ll N$. For $T \gg N^\eta$ on the other hand, it is highly probable that the spread S has been as large as size of the order book N, meaning that a liquidity crisis has taken place. This suggests a direct way to measure η, from the dynamics of the spread that behaves as a power-law of time (see Fig. 3.2), with an exponent which should equal $1/\eta$ for consistency. This gives $\eta \approx 3$, which is compatible with the finite size scaling analysis reported in Fig. 3.4 (left inset).

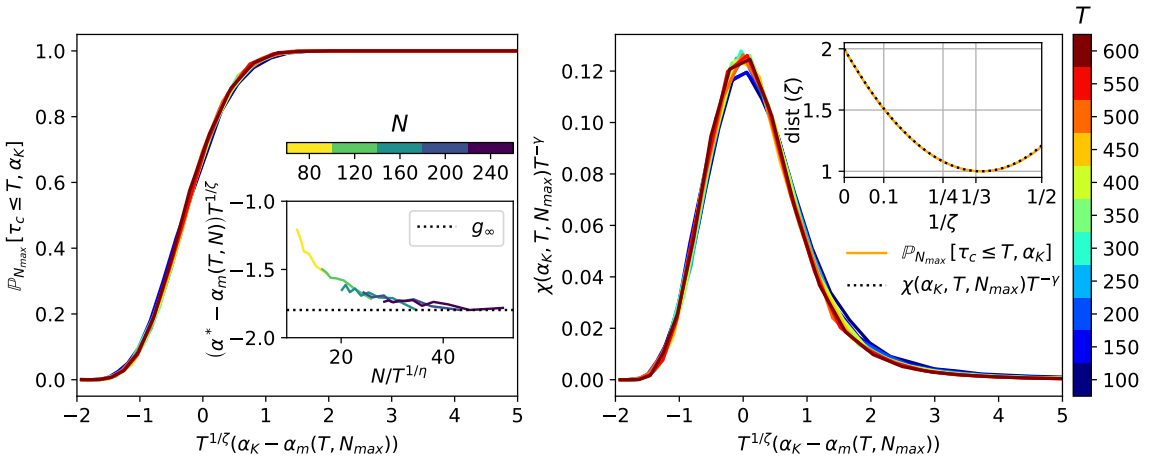

Figure 3.4: *Left: Rescaling of* $\mathbb{P}_N[\tau_c \leq T, \alpha_K]$ *according to Eq.* (3.7), *for* $\beta = 0.5$, $\lambda = 10$, $\nu_0 = 1$, $\mu = 20$, $N = N_{\max} = 240$, *and with* $\zeta = 3$ *and* $\eta = 3$. *Inset: Numerical determination of* $g(v)$, *also well described by our scaling hypothesis with* $\eta = 3$, *giving* $\alpha^* \approx 0.063$ *and* $g_\infty = \lim_{+\infty} g \approx -1.8$. *Right: Finite size scaling of* χ, *with* $\alpha_m(T, N_{\max}) :=_\alpha \chi(\alpha_K, T, N_{\max})$. *Inset: Average pairwise distance between the different curves as a function of* $1/\zeta$, *showing a minimum for* $\zeta \approx 3$ *for both quantities* $\mathbb{P}$ *and* χ.

A convenient method to pin down the values of α^* and the exponent ζ is to study the variance of the first crisis time, defined as

$$\chi(\alpha_K, T, N) = \mathbb{V}\left[\min(\tau_c, T)\right]$$

for a fixed value of β and different values of α_K, T and N. This quantity is expected to peak close to the phase transition, since for small α_K, τ_c is nearly always larger than T and $\chi \to 0$, whereas for large α_K, τ_c is small and χ is also small. The finite size scaling assumption for this quantity amounts to:

$$\chi(\alpha_K, T, N) = T^\gamma G\left(T(\alpha_K - \alpha_m(T, N))^\zeta\right), \tag{3.8}$$

where α_m is given by Eq. (3.7) with $\alpha^* \approx 0.06$ and $G(u)$ is a humped function that goes to zero for $u \to \pm\infty$. The details and justification of this procedure to find the different exponents is described in Appendix A.2. We find $\gamma \approx 2$ and $\zeta \approx \eta \approx 3$.[3] Figure 3.4 shows how all the different curves re-scale on top of each other when these parameters are fixed. We also show the quality of this rescaling as a function of ζ in the inset of Figure 3.4 (right), clearly favoring the value $\zeta = 3$.

We note that to the best of our knowledge, the numerical value of the exponents ζ, η do not seem to relate to an identified phase transition. It would be very interesting to explore

[3] Note that the value $\gamma = 2$ is not unreasonable since for $\alpha_K = \alpha^*$ one expects that τ_c is larger than T with some probability $p \in]0, 1[$, leading to $\mathbb{V}\left[\min(\tau_c, T)\right] \propto T^2$.

further the nature of this transition and (if possible) compute analytically the value of these exponents.

Although not perfect, we consider the rescaling sufficiently convincing to support our interpretation that the observed liquidity transition is a second order phase transition. This interpretation is further supported by the fact that a similar finite size scaling with the same value of the exponents ζ, η (but different values of α^*) holds for different values of the time scale β and rates λ, ν_0 and μ, and is also robust against changes in the specification of the model. This universality is a landmark of second order phase transitions.

Although our numerical evidence for such a phase transition is satisfactory, we have not found a way to bolster our results by a rigorous mathematical analysis. Indeed, even if highly stylized, the Santa Fe model with feedback is in fact quite complex. Hence, the existence of this phase transition and its second-order nature, can only be considered as conjectures at this stage. In order to make some progress, we have studied even simpler models, where the existence of a phase transition can be ascertained mathematically. This is what we discuss in the following sections.

3.4 A scenario for liquidity crises

The empirical analysis on financial data reveals that a phase transition scenario would explain liquidity crises. While the exact mechanism leading to instability is not well understood, our model can give a possible answer to this. To be relevant, markets have to sit below, but very close to the critical point and that the critical point is an attractor *i.e.* the parameter α_K is driven toward α^*. This concept, called self-organized criticality (SOC), was first introduced in [75] and developed by many in the context of game theory [76] and financial markets [77, 78, 79]. We can try to explain how SOC can be applied to this scenario. When a liquidity anomaly due to a large trend happens, the behaviour of some market participants may be altered. Indeed, thoughts of the enormous loss they may suffer increase their fears and thus their parameters α_K. On the other hand, the actions they take create arbitrages in the market, which are exploited by other market participants. This new particular environment leads to an increase of α_K with no internal mechanism that stabilizes it. On the other hand, when a liquidity crisis is triggered, the exchange can stop it using their circuit-breakers. This can be seen as a diminution of α_K which tends to stabilize the market. So when an liquidity anomaly combined with a large trend happens, two phenomena can make the critical point an attractor:

- Fear and new arbitrages increase α_K when $\alpha_K < \alpha^*$.
- Circuit-breakings decrease α_K when $\alpha_K > \alpha^*$.

that gives a scenario for a liquidity crisis with SOC. Of course, this could be explained with other arguments. The exact mathematical implementation of this mechanism is still unclear but some very recent progress open new possibilities that can be tackled. Indeed, Buendía *et al*[80] shows on one example how a dynamic system can self-organized to criticality. Adapting their ideas to our transition would consist in introducing an additional dynamic feedback onto the parameter α_K itself that makes α^* an attractor. As they deal with a physical example their additional feedback results from energy conservation. In our case, this feedback would be the consequence of P&L dynamics in agreement with our qualitative arguments.

3.5 Conclusion

Building on empirical evidence, we introduced an extension of the stylised Santa Fe model which accounts for the feedback of past price changes on event rates. Numerical simulations of our model revealed the existence of a second order phase transition, and more precisely a critical value of the feedback parameter below which an infinite size order book never empties, and above which it empties with probability one. We performed a finite size scaling analysis in order to determine the critical exponents, which does not appear to be in any of the known universality classes for 1D phase transitions.

We then pointed out that for this picture to be relevant, real financial markets would have to sit below, but very close to the critical point, consistent with the idea of self-organised criticality (SOC), a concept first introduced in [75] and developed by many in the context of game theory [76] and financial markets [77, 78, 79]. Another option would be for the feedback parameter to be itself time dependent and occasionally visit the unstable phase.

A deeper mathematical analysis aimed at deriving the critical exponents of the extended Santa Fe model presented in Section 3.2 would be highly valuable to ascertain the new universality class we exhibited numerically. For the sake of completeness, it would naturally also be of interest to couple our second order phase transition scenarii to a mechanism that draws the systems towards the critical point, building on ideas inspired e.g. by the Minority Game, see [76].

The empirical study in chapter 2 reveals that memory timescales are broadly distributed as kernels are power laws. Their effect is an important point on which we decided not to insist too much in the present study. Indeed, as we will see in the last chapter, lag effects can be extremely important destabilising factors that must be taken into account. Including these lag effects within the present framework is certainly a relevant extension worth investigating.

Take home message of Chapter 3

1. Santa Fe model with quadratic feedback. We add to the Santa Fe model a quadratic term of past price changes that feedbacks on cancellations rate.

2. Phase transition. Our model exhibits a second order phase transition that separates stable and unstable markets. The critical exponents of this transition have been characterized numerically, and it appears that this transition belongs to a new universality class.

3. Self Organized Criticality. Real markets sit just below but close to the phase transition. Simple arguments lead to think that the critical point is an attractor of the system.

4

Spread models: from Hawkes dynamics to metastable dynamics

We propose a class of models for spread dynamics that are simpler than the Quadratic Santa Fe Model. We have set aside the microstructure of the order book and focused on the spread dynamics. We map those models onto Hawkes processes for spread opening events and analyse several possibilities of feedback: linear Hawkes, quadratic Hawkes and non-linear Hawkes. With a state dependent Poisson rate for spread closing events, we show that the two first exhibit liquidity crises and we caracterize the transition. An alternative scenario is provided by a class of non-linear Hawkes process that show occasional "activated" liquidity crises, without having to be poised at the edge of instability.

From:
Endogenous liquidity crises
A. Fosset, Bouchaud, M. Benzaquen

Contents

L'argent qu'on possède est l'instrument de la liberté, celui qu'on pourchasse est celui de la servitude.

Jean-Jacques Rousseau

4.1 Introduction

In the previous chapter we have presented a Quadratic Santa Fe Model where Zumbach-like effect induces liquidity crises, through a phase transition of second order. While a numerical analysis fully characterizes this transition, we have not succeeded so far on the analytical side. We wish to introduce a simpler framework that uses the key mechanism from this feedback. An analysis of the Quadratic Santa Fe model shows that liquidity crises go with spread explosion and sparse order book. While the micro-structure of the order book is very interesting and provides a liquidity dynamics, it is responsible for the complexity of the whole dynamics. In this chapter, we restrict our attention to the dynamics of the spread, setting aside the dynamics of the microstructure of the order book. We introduce and discuss a family of simple spread models for which the liquidity crisis transition observed within the Quadratic Santa Fe model can be analyzed in more details.

We consider an order book filled with limit orders of size unity that can be cancelled or executed only at the best. As soon as a price slot is filled, no further limit order can be placed. Limit orders can thus only be placed in front of the best (inside the spread) provided the spread is open, *i.e.* $S_t := a_t - b_t \geq 2$. Note that with such simplifying hypotheses, there is no gap in the order book (apart from the spread itself) and market orders play the exact same role as cancellations.

4.2 A State-Dependent Hawkes Model for Spread Dynamics

A Simple Model

The simplest class of models consists in retaining the feedback of the spread dynamics on itself, forgetting about the price dynamics which is the main driver of the instability in the context of the Santa Fe model. Hence we also move away from the Quadratic Hawkes model we calibrated on real data in Chapter 2. The destabilizing mechanism we imagine is that spread opening events are likely to lead to more spread opening events. A simplified model reinstating the price feedback mechanism is presented in section 4.3. The model can thus be entirely characterized by the spread dynamics. We assume that the event intensities read:

$$\lambda_t^+ = \lambda_0^+ + \alpha \int_0^t \beta e^{-\beta(t-s)} dS_s^+ \tag{4.1a}$$

$$\lambda_t^- = \mathbb{1}_{\{S_t \geq 2\}} \lambda_0^- \tag{4.1b}$$

where λ^+ is the intensity of events that increase the spread, *i.e.* orders that are cancelled or executed by a market order and λ^- is the rate of limit orders reducing S_t by falling inside the spread, see Fig.4.1. Only spread opening events contribute to the feedback on λ^+, i.e. $dS_t^+ := \max(dS_t, 0)$. This highly stylized model has the advantage of being analytically tractable, while giving valuable insights on the possible phase transitions that can take place in order book models with feedback.

For $\alpha < 1$, using linear Hawkes theory, one can show (see e.g. [15]) that there exists a martingale process M_t such that:

$$S_t = S_0 + \int_0^t \left[\left(1 - \alpha e^{-(1-\alpha)\beta s}\right) \frac{\lambda_0^+}{1-\alpha} - \mathbb{1}_{\{S_s \geq 2\}} \lambda_0^- \right] ds + M_t \ . \tag{4.2}$$

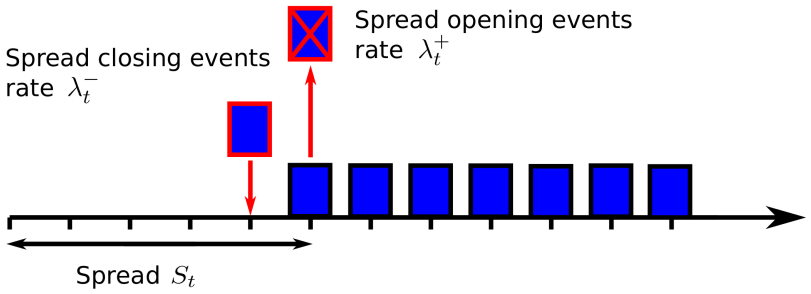

Figure 4.1: *Schematics of spread dynamics in the flat order book model.*

Introducing the parameter $\alpha_c = 1 - \lambda_0^+/\lambda_0^-$ one can distinguish between the different regimes:[1]

- $0 \leq \alpha < \alpha_c$ – The system is Hawkes-stable and the spread has a stationary distribution.
- $\alpha_c < \alpha < \alpha^* = 1$ – The system is Hawkes-stable but the spread increases on average linearly with t.
- $\alpha \geq \alpha^* = 1$ – The system is Hawkes-unstable, or "explosive".

The terminology Hawkes-(un)stable refers to the stability transition of a linear Hawkes process, that is, the transition between a regime where the intensities reach a stationary state from a regime where the number of events grows exponentially with time.

The Stable Regime

Let us first discuss the stable regime $\alpha < \alpha_c$. In the stationary state, we can prove that the probability for the spread to be open is given by:

$$\mathbb{P}[S \geq 2] = \frac{1-\alpha_c}{1-\alpha} ,$$

which goes to 1 as $\alpha \uparrow \alpha_c$. This result reproduces very well our numerical data. Although we have not been able to prove the result mathematically, numerical simulations also suggest that the full distribution of the spread is exactly geometric in this model:

$$\mathbb{P}[S = n] = \frac{1-\alpha_c}{1-\alpha}(1-r)r^{n-2} ; \qquad n \geq 2 ,$$

where r depends of α and β, see Fig. 4.2 (left). This result should in principle follow from the following equation that describes the evolution of the two-dimensional density function $\rho_t\big(S_t,\, X_t = \int_0^t \beta e^{-\beta(t-s)} dS_s^+\big)$:

$$\begin{aligned} \partial_t \rho_t \;=\; & [\lambda_0^+ + \alpha(x-\beta)]\rho_t(S-1, x-\beta)\mathbb{1}_{\{S\geq 2, x\geq\beta\}} - [\lambda_0^+ + \alpha x]\rho_t(S,x) \\ & + \lambda_0^- \rho_t(S+1,x) - \lambda_0^- \mathbb{1}_{\{S\geq 2\}}\rho_t(S,x) + \beta\partial_x(x\rho_t(S,x)) , \end{aligned} \tag{4.3}$$

see Appendix A.3. Setting the left-hand side to zero gives the stationary joint distribution of S and X. However, we have not been able to make much analytical progress, except in the limit $\beta \to 0$ where a geometric distribution for S indeed follows with $r = (1-\alpha_c)/(1-\alpha)$. Unfortunately, this approximation does not hold for $\beta \sim 1$ but works well for small β.

[1] These results are general to any Hawkes kernel ϕ provided $||\phi|| = \alpha < 1$.

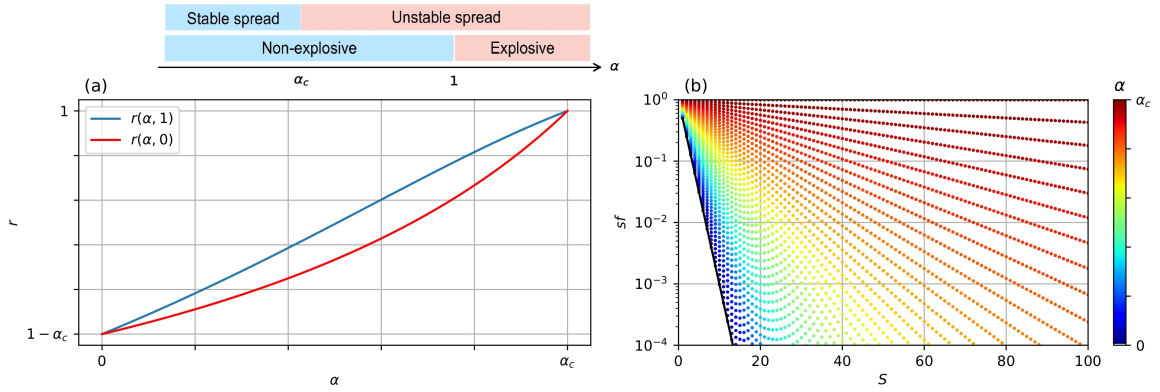

Figure 4.2: *Properties of the spread in the linear model for $\alpha < \alpha_c$, using a set of parameters $\lambda_0^+ = 1$, $\lambda_0^- = 0.5$ and $\beta = 1$. (a) Plot of $\alpha \mapsto r(\alpha, \beta)$ with $\beta = 1$ and the theoretical results of the limit $\beta \to 0$. (b) Log survival function (sf) of the spread for different values of α, suggesting an exact geometrical distribution for all α. The black curve corresponds to the theoretical equilibrium distribution when $\alpha = 0$.*

Note that in the presence of a price feedback mechanism, the spread distribution acquires a power-law tail as we observed within the extended Santa Fe model (see Appendix A.3).

Linear Spread Growth

In the interesting regime $\alpha_c < \alpha < \alpha^* = 1$ phase, one finds that the spread grows on average linearly in time, with a drift V that vanishes when $\alpha \downarrow \alpha_c$:

$$\lim_{t\to\infty} \frac{1}{t}\mathbb{E}[S_t] = V \; ; \qquad V := \lambda_0^+ \frac{\alpha - \alpha_c}{(1-\alpha)(1-\alpha_c)} \; .$$

On top of this average drift, the spread has diffusive fluctuations with some diffusion constant D defined as:

$$D(\alpha) := \lim_{t\to\infty} \frac{1}{t}\left[\mathbb{E}[S_t^2] - \mathbb{E}[S_t]^2\right] = \lambda_0^- + \frac{\lambda_0^+}{(1-\alpha)^3} \; .$$

One can thus compute exactly the probability that the spread exceeds some threshold N before time T, corresponding to an empty book in the Santa Fe model. Using standard first passage time results for the one dimensional Brownian motion [81], one has, for large N and T (and keeping the same notation as in Section 3.2):

$$\mathbb{P}_N[\tau_c \leq T, \alpha] = \int_0^T \mathrm{d}u \frac{N}{\sqrt{2\pi D(\alpha) u^3}} e^{-\frac{(N+Vu)^2}{2D(\alpha)u}} \; . \tag{4.4}$$

While the spread will eventually exceed N for large enough time, it is easy to see that:

$$\lim_{T\to\infty} \lim_{N\to\infty} \mathbb{P}_N[\tau_c \leq T, \alpha] = 0 \; ,$$

for all $\alpha < \alpha^* = 1$. In other words, the second order transition observed in the Santa Fe model with feedback is absent in the present setting. While a linear increase of the spread is interesting, it can hardly be called a liquidity "crisis". Similarly the susceptibility χ can be easily computed using Eq. (4.4) and one finds:

$$\chi(\alpha, T, N) = \mathbb{V}\left[\min(\tau_c, T)\right] = \int_0^T \mathrm{d}u \frac{N(T-u)^2\, e^{-\frac{(N+Vu)^2}{2D(\alpha)u}}}{\sqrt{2\pi D(\alpha) u^3}} - \left(\int_0^T \mathrm{d}u \frac{N(T-u)\, e^{-\frac{(N+Vu)^2}{2D(\alpha)u}}}{\sqrt{2\pi D(\alpha) u^3}} \right)^2 . \tag{4.5}$$

This gives us the same result as above:

$$\lim_{T\to\infty}\lim_{N\to\infty}\chi(\alpha,T,N)=0,$$

i.e. no liquidity "crisis". Nevertheless, it is interesting to notice that χ can be written exactly in the scaling form that we used to analyze the Sante Fe model. Indeed, the result of Eq. (4.5) can be transformed into:

$$\chi(\alpha,T,N)=T^{\gamma}\mathcal{G}\left(NT^{-1/\eta},T^{1/\zeta}(\alpha-\alpha_c)\right)\ ,$$

with:

$$\begin{aligned}\mathcal{G}(x,y)=&x\int_0^1\frac{\mathrm{d}u\,(1-u)^2}{\sqrt{2\pi D(\alpha_c)u^3}}\exp\left(-\frac{[x+uy\Lambda]^2}{2D(\alpha_c)u}\right)\\&-\left(x\int_0^1\frac{\mathrm{d}u\,(1-u)}{\sqrt{2\pi D(\alpha_c)u^3}}\exp\left(-\frac{[x+uy\Lambda]^2}{2D(\alpha_c)u}\right)\right)^2\ ,\end{aligned}$$

$\Lambda:=\lambda_0^+(1-\alpha_c)^{-2}$ and $\gamma=\eta=\zeta=2$. These exponents should be compared with the values found numerically for the generalized Santa Fe model: $\gamma\approx 2$, $\eta\approx\zeta\approx 3$.

The Explosive Regime

When $\alpha>\alpha^*=1$, the model becomes Hawkes unstable, which means in the present context that the spread increases exponentially with time. Although formally the spread never diverges in finite time, in practice there is a "liquidity crisis" as soon as $T(\alpha-\alpha^*)\propto\log N$, i.e. when the spread reaches the boundary of the order book. This would look numerically akin to a second order phase transition with exponents $\zeta=1$ and $\eta=0$, quite far from the results reported for the Santa-Fe model.

A Stabilizing Mechanism

One could expect some stabilizing mechanisms to arise when the spread becomes too large. A way to include the latter in our simple setting by substituting Eq. (4.1b) with:

$$\lambda_t^-=\lambda_0^-(S_t-1)\ , \tag{4.6}$$

meaning that there is an increased probability to introduce limit orders inside the spread when it is large. The model remains analytically tractable; the bottom line is that the Hawkes stable regime $\alpha_c<\alpha<1$ disappears: our specification is indeed able to stabilise the spread in the whole region $\alpha<1$. The Hawkes unstable regime $\alpha>1$ of course subsists and is associated to liquidity crises in an otherwise stable market ($\alpha<1$). Using the same framework as in Eq.(4.2), solving the models gives:

$$\begin{aligned}S_t=&1+e^{-\lambda_0^- t}(S_0-1)+\lambda_0^+\int_0^t ds e^{-\lambda_0^-(t-s)}\left[1+\int_0^s\mathcal{R}(u)du\right]ds\\&+\int_0^t ds e^{-\lambda_0^-(t-s)}\left[1+\int_0^{t-s}\mathcal{R}(u)e^{\lambda_0^- u}du\right]dM_s^+-\int_0^t ds e^{-\lambda_0^-(t-s)}dM_s^-\end{aligned} \tag{4.7}$$

with $\mathcal{R}(t) = \alpha\beta e^{-(1-\alpha)\beta t}$ the resolvent. From which we get the asymptotic average spread and its variance:

$$\mathbb{E}[S] = 1 + \frac{\lambda_0^+}{\lambda_0^-(1-\alpha)} \tag{4.8a}$$

$$\begin{aligned}\mathbb{V}[S] &= \frac{\lambda_0^+}{2\lambda_0^-(1-\alpha)}\left(1 + \int_0^{+\infty} e^{-2\lambda_0^- s}\left[1 + \int_0^s \mathcal{R}(u)e^{\lambda_0^- u}du\right]^2 ds\right) \\ &= \frac{\lambda_0^+}{\lambda_0^-(1-\alpha)}\left(1 + \frac{\alpha\beta(2-\alpha)}{2(1-\alpha)(\lambda_0^- + \beta(1-\alpha))}\right)\end{aligned} \tag{4.8b}$$

making clearly appear the only transition at $\alpha = 1$. By computing the two-dimensional density function $\rho_t\big(S_t,\, X_t = \int_0^t \beta e^{-\beta(t-s)} dS_s^+\big)$, we get the following Fokker-Planck equation:

$$\begin{aligned}\partial_t \rho_t &= [\lambda_0^+ + \alpha(x-\beta)]\rho_t(S-1, x-\beta)\mathbb{1}_{\{S\geq 2, x\geq\beta\}} - [\lambda_0^+ + \alpha x]\rho_t(S,x) \\ &\quad + \lambda_0^- S\rho_t(S+1,x) - \lambda_0^-(S-1)\rho_t(S,x) + \beta\partial_x(x\rho_t(S,x)) \;,\end{aligned} \tag{4.9}$$

While the variable X follows as the same stationary density than the one from the first model 4.1, the spread follows a Poisson distribution in the limit $\beta \to 0$:

$$\mathbb{P}[S = n+1] = e^{-r}\frac{r^n}{n!} \qquad n \geq 0 \;,$$

with $r = \frac{\lambda_0^+}{\lambda_0^-(1-\alpha)}$. Unfortunately, we have not succeded in solving Eq.4.9 in the general case.

Nevertheless, techniques introduced by El Euch *et al*[82] enable us to solve the dynamics in a more general case. We replace Eq. (4.1a) by:

$$\lambda_t^+ = \lambda_0^+ + \int_0^t \phi(t-s)dS_s^+ \tag{4.10}$$

where ϕ is a kernel such that $\alpha = ||\phi|| < 1$. We can show that the Laplace transform of the variables $\left(S_t^+, S_t^-\right)$ defined as:

$$\mathcal{D}(x,y,t) = \mathbb{E}\left[e^{-xS_t^+ - yS_t^-}\right] \tag{4.11}$$

follows the equation:

$$\begin{aligned}\mathcal{D}(x,y,t) = &\exp\left(\lambda_0^+\left[e^{-(x+y)}\int_0^t \overline{\mathcal{D}}(x,y,s)ds - t\right]\right) \\ &\times \exp\left(\frac{\lambda_0^+}{\lambda_0^-}e^{-x}\left[1-e^{-y}\right]\left[\frac{1-e^{-\lambda_0^- t}}{t}\right]\int_0^t \overline{\mathcal{D}}(x,y,s)ds\right)\end{aligned} \tag{4.12}$$

where the function $\overline{\mathcal{D}}$ is implicitly defined as the solution of:

$$\begin{aligned}\overline{\mathcal{D}}(x,y,t) = &\exp\left(\int_0^t \phi(s)\left[e^{-(x+y)}\overline{\mathcal{D}}(x,y,t-s) - 1\right]ds\right) \\ &\times \exp\left(e^{-x}\left[1-e^{-y}\right]\int_0^t \overline{\mathcal{D}}(x,y,t-s)\phi(s)ds\frac{\int_0^t e^{-\lambda_0^-(t-s)}\phi(s)ds}{\int_0^t \phi(s)ds}\right)\end{aligned} \tag{4.13}$$

All the technical details of the proofs are given in Appendix A.3. A very interesting extension would be to compute the dynamics at criticality ($\alpha \to 1$). We already know the behaviour of S_t^+ thanks to Jaisson *et al* [21, 22] but finding the re-scaling of λ_0^- has not been tackled yet.

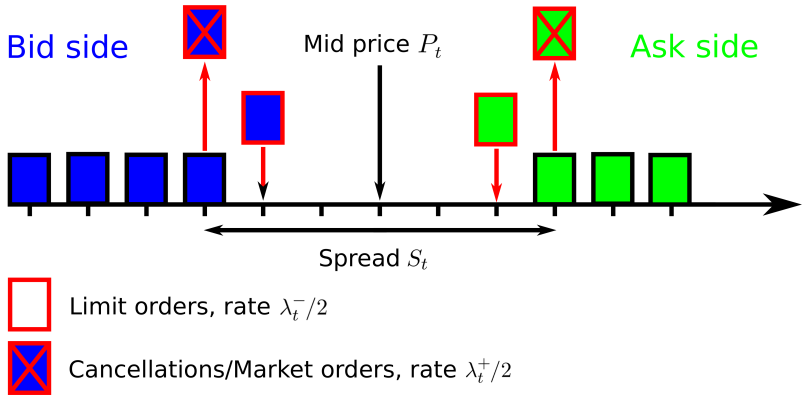

Figure 4.3: *Schematics of the flat order book dynamics with bid and ask. Note that the rate of spread closing (resp opening) event is twice the rate of limit orders (resp cancellations/market orders) because of bid/ask symmetry.*

4.3 A Model with Price Feedback on the Spread

The model presented in Section. 4.2 displays a very simple destabilizing mechanism in the mid-price reference frame, in which spread opening events trigger more spread opening events. Here, we re-introduce price dynamics to illustrate the effects of "volatility" and "trend" in the spread opening mechanism, bringing the model one step closer to the empirical study presented in Chapter 2 and the Santa Fe model of Section 3.2. In order to do so, we write the intensity of cancellations/market orders as:

$$\lambda_t^+ = \lambda_0^+ + \alpha \left(\int_0^t \sqrt{2\beta} e^{-\beta(t-s)} dP_s \right)^2 \tag{4.14a}$$

$$\lambda_t^- = \lambda_0^- \mathbb{1}_{\{S_t \geq 2\}} \, . \tag{4.14b}$$

Each event takes place with equal probability at the bid b_t or the ask a_t. The dynamics of the bid and ask are thus such that

$$\mathbb{E}\left[da_t | da_t > 0, \mathcal{F}_t\right] = -\mathbb{E}\left[db_t | db_t < 0, \mathcal{F}_t\right] = \lambda_t^+ dt/2$$

and

$$\mathbb{E}\left[da_t | da_t < 0, \mathcal{F}_t\right] = -\mathbb{E}\left[db_t | db_t > 0, \mathcal{F}_t\right] = -\lambda_t^- dt/2 \, .$$

Using the formalism introduced in [30] we are able to solve the dynamics of the system and show that there exists a martingale M_t such that:

$$S_t = S_0 + \int_0^t \left[\left(2 - \alpha e^{-(2-\alpha)\beta s}\right) \frac{\lambda_0^+}{2-\alpha} - \frac{\mathbb{1}_{\{S_s \geq 2\}}}{2-\alpha} \lambda_0^- \left(2 - 2\alpha - \alpha e^{-(2-\alpha)\beta(t-s)}\right) \right] ds + M_t \, . \tag{4.15}$$

Calling again $\alpha_c = 1 - \lambda_0^+/\lambda_0^-$, one obtains the same regimes as in Section 4.2 only replacing $\alpha^* = 1$ by $\alpha^* = 2$:

- $0 \leq \alpha < \alpha_c$ – The system is non-explosive and the spread has a stationary distribution.
- $\alpha_c < \alpha < 2$ – The system is non-explosive but the spread increases on average linearly with t.
- $2 \leq \alpha$ – The system is explosive.

Note that this transition is similar to the Z-Hawkes transition that was presented in [30]. In

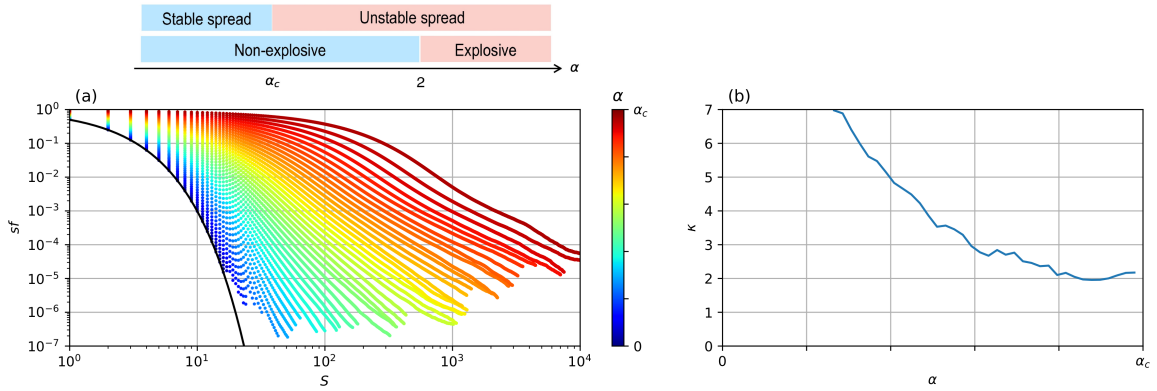

Figure 4.4: *Properties of the spread for* $\alpha < \alpha_c$ *and* $\beta = 1$, $\lambda_0^+ = 1$, $\lambda_0^- = 0.5$. *(a) Survival function (sf) of the spread. The black curve corresponds to the theoretical equilibrium distribution when* $\alpha = 0$. *For large* α, *the survival function decays asymptotically as a power-law* $S^{-\kappa}$. *(b) Tail exponent* κ *of the survival function, as a function of* α. κ *appears to saturate around* 2 *when* $\alpha \to \alpha_c$.

the $\alpha_c < \alpha < 2$ phase, the spread grows again linearly with time:

$$\mathbb{E}[S_t] \sim Vt, \qquad V := 2\lambda_0^+ \frac{\alpha - \alpha_c}{(1-\alpha_c)(2-\alpha)}.$$

In the $\alpha < \alpha_c$ phase, one finds again $\mathbb{P}[S \geq 2] = (1-\alpha_c)/(1-\alpha)$. Interestingly however, simulating numerically Eq. (4.14) we observe that the spread distribution is asymptotically fat tailed instead of geometric (see Fig. 4.4). Such a power law tail is also observed in our extended Santa Fe model close to the critical point. We note that the mid-price $P_t = (a_t + b_t)/2$ behaves like a diffusion in the two phases, with an average diffusivity D_P:

$$D_P := \lim_{t\to\infty} \frac{1}{t}\mathbb{E}\left[\sum_{s<t}(\Delta P_s)^2\right] = \frac{\lambda_0^- \mathbb{P}[S \geq 2] + \lambda_0^+}{2-\alpha},$$

One can also show that joint the probability density function $\rho\big(t, S_t,\, X_t = \int_0^t \sqrt{2\beta} e^{-\beta(t-s)} dP_s\big)$ now solves:

$$\begin{aligned}\partial_t \rho \;=\; & \left[\lambda_0^+ + \alpha\left(x - \widehat{\beta}\right)^2\right]\rho\left(t, S-1, x-\widehat{\beta}\right) + \left[\lambda_0^+ + \alpha\left(x+\widehat{\beta}\right)^2\right]\rho\left(t, S-1, x+\widehat{\beta}\right) \\ & + \lambda_0^-\left[\rho\left(t, S+1, x-\widehat{\beta}\right) + \rho\left(t, S+1, x+\widehat{\beta}\right)\right] - 2\left[\lambda_0^+ + \alpha x^2 + \lambda_0^-\right]\rho(t,S,x) \\ & + \beta\partial_x\left(x\rho\right) \;, \end{aligned} \tag{4.16}$$

where $\widehat{\beta} = \sqrt{\beta/2}$ and with the boundary condition $\forall S < 1,\ \rho(t, S, x) = 0$.

4.4 Non-Linear Hawkes Models and Metastability

We have studied in the previous section a simple spread dynamics model that maps onto a linear Hawkes process. In these models, the spread becomes unstable and grows linearly in time before the Hawkes process (i.e. the activity of the process) becomes itself explosive. One can stabilize the spread dynamics, as in the last subsection above, such that sudden liquidity crises in this model are associated to the Hawkes explosive transition.

For this picture to be correct, however, real financial markets must sit below, but very close to the Hawkes instability threshold α^*, or else one must argue that α itself is time dependent, and occasionally visits the explosive region $\alpha > \alpha^*$ before decreasing back below

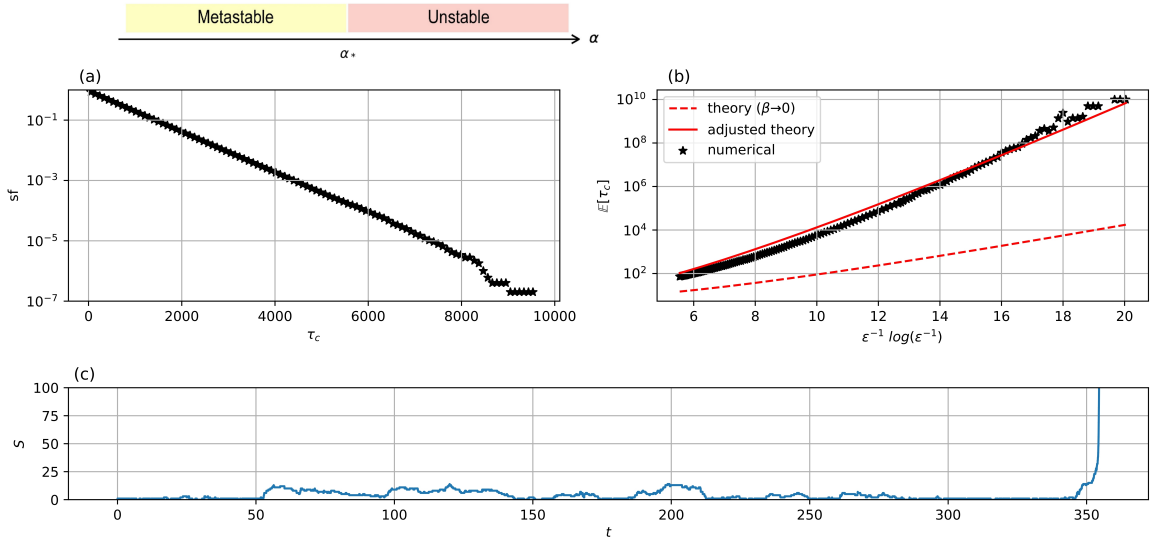

Figure 4.5: *Properties of the time of metastability when $\alpha = 0$ and $\epsilon > 0$. (a) Survival function (sf) of the time before explosion for $\epsilon = 0.2$, which is found to be exponential. (b) Evolution of the average metastability time with ϵ. The dotted red curve is the continuous time prediction given by Eq. (4.21). The plain red curve is obtained by multiplying the term in the exponential by a empirical factor 2.5. (c) Typical metastable trajectory. The set of parameters is the same that in (a): $\lambda_0^+ = 1$, $\lambda_0^- = 0.5$, $\beta = 1$ and $\epsilon = 0.2$.*

α^*, allowing the market to re-stabilise. The same remark in fact applies to the generalised Santa Fe model studied in section 3.2: if liquidity crises are indeed related to the existence of a second order phase transition, one must argue that financial markets are for some reason close to the critical point – a phenomenon called "self-organized criticality" [75] – or that the parameters fluctuate over time and occasionally push the system in the unstable phase.

Although many models in mathematical finance are tweaked such that their parameters become time dependent, we feel that this common procedure might in fact hide the inadequacy of such models. In this section, we want to explore an alternative scenario. We introduce a class of non-linear Hawkes processes that show occasional liquidity crises without either being poised at the edge of instability ($\alpha \uparrow \alpha^*$) or having a time dependent feedback parameter α.

A Model with Quadratic Feedback

Let us consider again the simplified framework of section 4.2 and generalize the feedback on spread opening events as:

$$\lambda_t^+ = \lambda_0^+ + \alpha X_t + \epsilon X_t^2 \; ; \qquad X_t := \int_0^t \beta e^{-\beta(t-s)} dS_s^+ \, . \tag{4.17}$$

When $\epsilon = 0$, this Hawkes process is non-explosive provided $\alpha < \alpha^* = 1$. But as soon as $\epsilon > 0$, the process has a non-zero probability to explode, even when $\alpha < \alpha^*$. However, interestingly, these "liquidity crises" only happen with a rate that is *exponentially small* in $1/\epsilon$, and therefore interrupt very long periods of apparent market stability – a phenomenon called "metastability" in the physics literature. This is confirmed by direct numerical simulations of the model Eq. (4.17) in Fig. 4.4. In the following section, we give an analytical description of this phenomenon.

A Continuous Time Description

In the "slow" limit $\beta \to 0$ one can write an approximate SDE for X_t. Start from the exact expression $dX_t = -\beta X_t\, dt + \beta dS_t^+$. When β is small, λ_t^+ is slowly varying and one can approximate dS_t^+ by $\lambda_t^+\, dt + \sqrt{\lambda_t^+}\, dB_t$, where B_t is a Brownian motion (for more rigorous statements, see [21]). Hence:

$$dX_t = \beta \left[\lambda_0^+ - (1-\alpha)X_t + \epsilon X_t^2\right]\, dt + \beta\sqrt{\lambda_t^+(X_t)}\, dB_t. \tag{4.18}$$

Let us write the deterministic part of this equation as minus the derivative of some "potential" $\mathcal{V}(X)$, to wit:

$$\mathcal{V}(X) = \frac{\beta(1-\alpha)}{2}\left(X - \frac{\lambda_0^+}{1-\alpha}\right)^2 - \frac{\beta\epsilon}{3}X^3. \tag{4.19}$$

Such a potential is drawn for $\alpha < 1$, $\epsilon = 0$ and $\alpha < 1$, $\epsilon > 0$ in Fig. 4.6. One clearly sees that for $\epsilon = 0$ the equilibrium $X_{\text{eq}} = \lambda_0^+/(1-\alpha)$ (that corresponds to the average intensity of the Hawkes process) is stable. But as soon as $\epsilon > 0$ the potential reaches a maximum for some value X^* beyond which it plunges towards $-\infty$. In the limit $\epsilon \to 0$, one finds that X^* is given by:

$$X^* \approx \frac{1-\alpha}{\epsilon}\ ,$$

corresponding to:

$$\mathcal{V}(X^*) \approx \frac{\beta(1-\alpha)^3}{6\epsilon^2}\ ,$$

which diverges when $\epsilon \to 0$. This picture allows one to describe the dynamics of the model for $\epsilon > 0$ in intuitive terms: for a very long time, X_t will oscillate around its equilibrium value X_{eq} until some rare fluctuation of the Brownian noise dB_t is able to bring X_t close to the top of the high barrier X^*. In such rare circumstances, X_t escapes the stable valley and runs all the way to $+\infty$ in finite time, corresponding to a "liquidity crisis".

The theory of high barrier crossing under the influence of noise is very well understood. In the present case, the final formula for the average first escape time τ_c (corresponding to the "emptying of the book" as in section 3.2) is given by [83, 6]:

$$\mathbb{E}[\tau_c] \approx 2\pi \left(\frac{D(X_{\text{eq}})}{D(X^*)|\mathcal{V}''(X^*)\mathcal{V}''(X_{\text{eq}})|}\right)^{1/2} \times \exp\left(\int_{X_{\text{eq}}}^{X^*} \mathrm{d}x \frac{\mathcal{V}'(x)}{D(x)}\right)\ , \tag{4.20}$$

with $D(X) := \frac{\beta^2}{2}\left(\lambda_0^+ + \alpha X + \epsilon X^2\right)$. The expansion to second order in ϵ gives:

$$\log \mathbb{E}[\tau_c] \underset{\epsilon\to 0}{\approx} \begin{cases} -\dfrac{2}{\beta}\left[\dfrac{1-\alpha+\log\alpha}{\epsilon} + \dfrac{\lambda_0^+}{\alpha^2}\log\dfrac{1}{\epsilon}\right] - \dfrac{1}{2}\log\dfrac{1}{\epsilon} & \text{if} \quad \alpha > 0 \\ \dfrac{1}{\beta\epsilon}\left(\log\dfrac{1}{\epsilon\lambda_0^+} - 2\right) & \text{if} \quad \alpha = 0\ . \end{cases} \tag{4.21}$$

Hence, as announced, the time before a crisis is exponentially large in ϵ^{-1}, with logarithmic corrections for $\alpha = 0$. Another prediction of this approach is that in the limit $\epsilon \to 0$, the time-to-crisis becomes a Poisson variable with mean $\mathbb{E}[\tau_c]$, as indeed found numerically (see Fig. 4.5(a)).

Our analytical result compares well with our numerical results in terms of the overall dependence on ϵ, but the numerical prefactor inside the exponential is off by a factor ~ 2.5. This can be traced to the fact that our numerical simulations are in a regime where $\beta/\lambda_0 = O(1)$, whereas the theoretical analysis is done in a regime where $\beta/\lambda_0 \to 0$. (see [84] and [6], section 5.4, where a similar phenomenon is present).

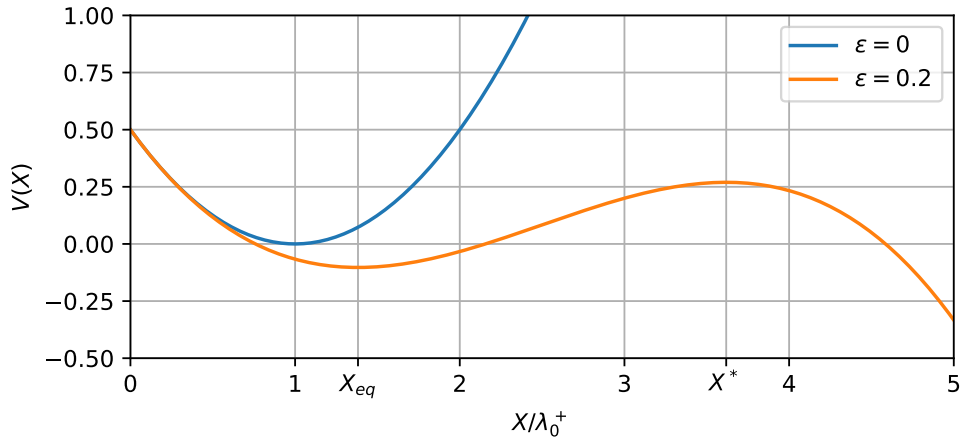

Figure 4.6: *Plots of the potential as given by Eq.* (4.19) *with* $\lambda_0^+ = 1$ *and* $\alpha = 0$.

4.5 Conclusion

In order to bolster the results of our previous chapters with analytical arguments, we then considered a class of simple models, where the existence of a phase transition can be verified mathematically. Setting aside the dynamics of the order book, and focusing our attention to the dynamics of the spread, we presented a model which can be mapped onto a linear Hawkes process in which spread opening events are likely to lead to more spread opening events. We exhibited three dynamic spread regimes as function of feedback intensity: stable, linearly increasing, and exploding spread. We argued that the second regime could be stabilised and that in such a case, and within some parameter range, a phase transition from stable to unstable spread exists, much like in the Quadratic Santa Fe model presented before, but with major quantitative differences. This simple model can be extended by introducing a quadratic feedback from price changes, without qualitative change on the three dynamics. This feedback only makes the distribution of the spread (and the volatility) fat-tails, closer to the results of the Quadratic Santa Fe model.

Finally, we presented an alternative scenario which needs no *a priori* proximity to the instability threshold, nor a time dependent feedback parameter. The model is a non-linear Hawkes process for which liquidity crises are “activated" events within a metastable phase. A continuous time description allowed us to derive the typical crisis frequency as function of the model’s parameters, and show that this time can be much longer than the microscopic time of the model. Even if metastability is an elegant modeling for modeling liquidity crises, it is not compatible with the calibration of GQHawkes on order book data that displays power-law. The alternative “activated” scenario would rather suggest a bimodal distribution with a hump at large effective spreads that we do not see on empirical data in Chap 4.

Take home message of Chapter 4

1. Spread models. This class of models consists in a flat order book where limit orders can be placed in front of the best, and cancellations can occur at the best only.

2. Spread opening events. Spread opening events are assumed to be a Hawkes process: linear or quadratic in price changes or non-linear.

3. Spread closing events. Spread closing events rate depend on the state of the spread as limit orders cannot be placed when the spread is closed.

4. Phase transition. These models feature different phases (stable, unstable) that are mathematically characterized.

5. Non linear Hawkes and metastability. A non-linear Hawkes process for spread opening events results in metastable phases.

5

Revealing liquidity in the latent order book

Latent order book models have allowed for significant progress in our understanding of price formation in financial markets. In particular they are able to reproduce a number of stylized facts, such as the square-root impact law. An important question that is raised – if one is to bring such models closer to real market data – is that of the connection between the latent (unobservable) order book and the real (observable) order book. Here we suggest a simple, consistent mechanism for the revelation of latent liquidity that allows for quantitative estimation of the latent order book from real market data. We successfully confront our results to real order book data for over a hundred assets and discuss market stability. One of our key theoretical results is the existence of a market instability threshold, where the conversion of latent order becomes too slow, inducing liquidity crises. *Finally we compute the price impact of a metaorder in different parameter regimes.*

From:
How does latent liquidity get revealed in the limit order book?
L. Dall'Amico , **A. Fosset**, J. P. Bouchaud, M. Benzaquen

Contents

I would like to thanks Lorenzo Dall' Amico who did a fantastic work on this project.

Je dis, argent trop cher
Trop grand
La vie n'a pas de prix

Téléphone

5.1 Introduction

The recent discovery of the square root law has prompted the financial community to propose new models for price formation. As presented in the general introduction 1.3, a new class of agent based models (ABM) has become a very powerful tool to gain insight into its origins. Given that the instantaneous liquidity revealed in the limit order book is very small (less than 1% of daily traded volume), **latent** order book models [32, 36, 85] build on the idea that revealed liquidity chiefly reflects the activity of high frequency market makers that act as intermediaries between much larger **unrevealed** volume imbalances. The latter are not revealed in the limit order book in order to avoid giving away precious private information, until the probability to get executed is large enough to warrant posting the order close to the bid (or to the ask). Within this class of ABM, reaction-diffusion models (see e.g. [86, 46, 48]) have proved very successful at reproducing the square root law in a setup free of price manipulation.However, one very important question is yet to be addressed if one is to connect such models with real observable and quantifiable data: what is the relation between revealed and latent liquidity and what are the mechanisms through which latent liquidity becomes revealed? These issues are the subject of the present communication. We propose a simple dynamic model to account for liquidity flow between the latent and revealed order books. We introduce two ingredients that are to our eyes essential to reproduce realistic limit order book shapes: (i) the incentive to reveal one's liquidity increases with decreasing distance to the trade price, and (ii) the process of revealing latent liquidity is not instantaneous and lag effects may be an important source of instability, as real liquidity is found to vanish in certain regions of parameters. In addition to providing an alternative scenario for liquidity crises, we show that our framework allows one to infer the shape of latent (unobservable) liquidity from real (observable) order book data. This is important because the concept of a latent order book is sometimes criticized as a figment of the theorist's imagination. Having more direct indications of its existence is comforting.

In section 5.2 we present the model and derive the governing equations. In section 5.3 we compute the stationary states of the limit order book both analytically and numerically. In section 5.4 we calibrate our model to the order books of over a hundred assets and discuss market stability as function of incentive to reveal and conversion rate. In section 5.5 we compute the price impact of a metaorder and discuss its behavior. In section 5.6 we conclude.

5.2 A mechanism for latent liquidity revealing

Our starting point is the reaction-diffusion latent order book model of Donier *et al.* [46] (see also [44]). In their setup, the latent volume densities of limit orders in the order book $\rho_{\mathrm{B}}(x,t)$ (bid side) and $\rho_{\mathrm{A}}(x,t)$ (ask side) at price x and time t evolve according to the following rules. Latent orders diffuse with diffusivity constant D, are canceled with rate ν, and new intentions are deposited with rate λ. When a buy intention meets a sell intention they are instantaneously matched: $\mathrm{A}+\mathrm{B}=\varnothing$. The trade price p_{t} is conventionally defined through the equation $\rho_{\mathrm{B}}(p_{\mathrm{t}},t)=\rho_{\mathrm{A}}(p_{\mathrm{t}},t)$. Donier *et al.* showed that the resulting stationary order book is locally linear (around the price). In particular, in the infinite memory limit $\nu,\lambda\to 0$ while keeping $\mathcal{L}:=\lambda/\sqrt{\nu D}$ constant, one obtains $\rho_{\mathrm{A}}^{\mathrm{st}}(\xi)=\rho_{\mathrm{B}}^{\mathrm{st}}(-\xi)=\mathcal{L}\xi$ for

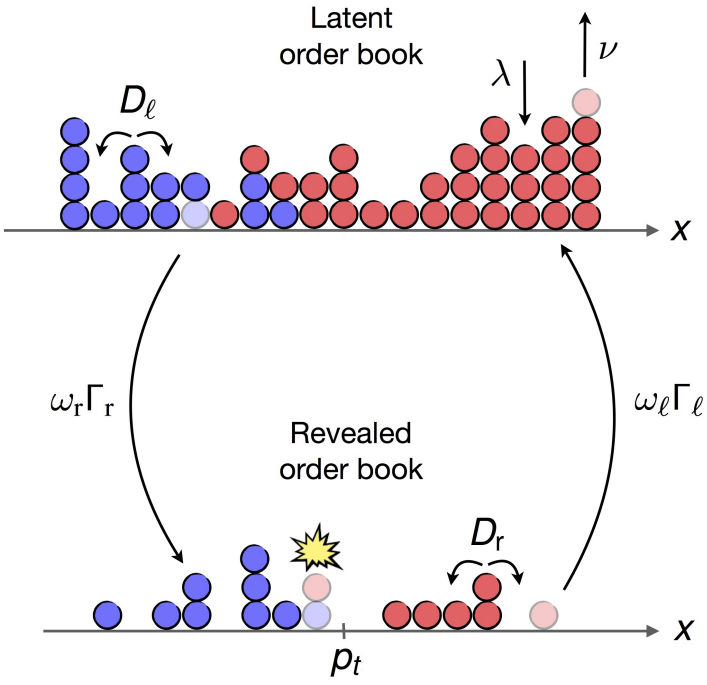

Figure 5.1: *Schematics of the latent and revealed order books. Depositions, cancellations, diffusion and liquidity flow between the two books is signified with arrows (see Sect. 5.2).*

$\xi = x - p_t > 0$.[1] The parameter $\mathcal{L}$ was coined the **latent liquidity**. Here we choose to work in such an infinite memory limit. For an analysis of finite memory effects $\nu, \lambda \neq 0$ see [48].

With the intention of building a mechanism for latent liquidity revealing we define the revealed and latent order books (see Fig. 5.1), together with the revealed and latent limit order densities for the bid and ask sides of the book $\rho^{(\mathrm{r})}_{\mathrm{A/B}}(x,t)$ and $\rho^{(\ell)}_{\mathrm{A/B}}(x,t)$. We denote D_ℓ and D_r the diffusion coefficients in the latent and revealed order books respectively. While diffusion in the latent book signifies heterogeneous reassessments of agents intentions [46], the idea of diffusion in the revealed order book certainly deserves a discussion. Once a limit order is placed in the revealed order book, if one wants to change its position before it gets executed, one has to cancel it and place it somewhere else. So one may argue that there should be no diffusion in the revealed book such that revealed order reassessments must go through the latent book before they can be posted again. However, we believe that (*i*) unrevealing one's order because one is no longer confident about one's reservation price and waiting for an arbitrary amount of time (of order $(\Gamma\omega_\mathrm{r})^{-1}$, see below) to reveal it back, and (*ii*) canceling an order knowing that it will immediately be posted back at a revised price, are in fact two distinct processes. We thus leave the possibility for a nonzero diffusivity D_r in the revealed order book. In addition, note that trading fees and priority queues discourage traders from changing posted orders. Indeed, when canceling a revealed order traders lose their position in the priority queue which may result in harmful delays in the execution. One is thus tempted to surmise that $D_\mathrm{r} < D_\ell$ in the general case, but one might as well argue that the presence of HFT can considerably increase the value of D_r thereby inverting such an inequality. Be as it may, the limit $D_\mathrm{r} \to 0$ will very likely be an interesting one to address.

[1] Following [46] we are setting in the reference frame of the informational price component $\hat{p}_t = \int_0^t ds\, V_s$, where V_t is an exogenous term responsible for the price moves related to common information.

Furthermore we posit that latent orders are revealed at a position dependent rate $\omega_{\rm r}\Gamma_{\rm r}(k\xi)$ and unrevealed at rate $\omega_\ell\Gamma_\ell(k\xi)$, where $\xi = x - p_{\rm t}$ denotes the distance from the trade price, k^{-1} is a characteristic price scale, and $\Gamma_{\rm r}$ and Γ_ℓ are functions taking values in $[0,1]$.[2] Naturally, buy/sell order matching $A+B \to \varnothing$ (with rate κ) only takes place in the revealed order book. Assuming $\Gamma_{{\rm r}/\ell}$ to be continuous and sufficiently regular on $\mathbb{R}^*$, one may write for the ask side:

$$\partial_t \rho_{\rm A}^{({\rm r})} = D_{\rm r}\partial_{xx}\rho_{\rm A}^{({\rm r})} + \omega_{\rm r}\Gamma_{\rm r}(k\xi)\rho_{\rm A}^{(\ell)} - \omega_\ell\Gamma_\ell(k\xi)\rho_{\rm A}^{({\rm r})} - \kappa\rho_{\rm A}^{({\rm r})}\rho_{\rm B}^{({\rm r})} \tag{5.1a}$$

$$\partial_t \rho_{\rm A}^{(\ell)} = D_\ell\partial_{xx}\rho_{\rm A}^{(\ell)} - \omega_{\rm r}\Gamma_{\rm r}(k\xi)\rho_{\rm A}^{(\ell)} + \omega_\ell\Gamma_\ell(k\xi)\rho_{\rm A}^{({\rm r})} \ , \tag{5.1b}$$

and for the bid side:

$$\partial_t \rho_{\rm B}^{({\rm r})} = D_{\rm r}\partial_{xx}\rho_{\rm B}^{({\rm r})} + \omega_{\rm r}\Gamma_{\rm r}(-k\xi)\rho_{\rm B}^{(\ell)} - \omega_\ell\Gamma_\ell(-k\xi)\rho_{\rm B}^{({\rm r})} - \kappa\rho_{\rm A}^{({\rm r})}\rho_{\rm B}^{({\rm r})} \tag{5.2a}$$

$$\partial_t \rho_{\rm B}^{(\ell)} = D_\ell\partial_{xx}\rho_{\rm B}^{(\ell)} - \omega_{\rm r}\Gamma_{\rm r}(-k\xi)\rho_{\rm B}^{(\ell)} + \omega_\ell\Gamma_\ell(-k\xi)\rho_{\rm B}^{({\rm r})} \ . \tag{5.2b}$$

In the limit $\kappa \to \infty$, $\rho_{\rm A}^{({\rm r})}(x,t)$ and $\rho_{\rm B}^{({\rm r})}(x,t)$ do not overlap such that one may instead consider the difference function $\phi_{\rm r}(x,t) := \rho_{\rm B}^{({\rm r})}(x,t) - \rho_{\rm A}^{({\rm r})}(x,t)$ and absorb the reaction terms without loss of information. Note however that the bid and ask sides of the latent order book are perfectly allowed to overlap. The trade price $p_{\rm t}$ is defined as the sign changing point of $\phi_{\rm r}$:

$$\lim_{\epsilon\to 0}\left[\phi_{\rm r}(p_{\rm t}+\epsilon,t)\phi_{\rm r}(p_{\rm t}-\epsilon,t)\right] < 0 \ . \tag{5.3}$$

For the sake of simplicity we shall set $\omega_{\rm r} = \omega_\ell = \omega$.[3] We also set $\Gamma_{\rm r} = 1 - \Gamma_\ell := \Gamma$ where Γ is the conversion probability distribution function for which we impose $\Gamma(y \le 0) = 1$. This implies that latent orders falling on the "wrong side" reveal themselves with rate ω. One may rightfully argue that such orders should then be executed against the best quote, consistent with real market rules for which the real order book cannot be crossed. However this would prevent analytical progress. We ran numerical simulations (see section 5.3) in which such revealed orders are properly located at the best quote and did not observe any significant impact on our main results.

Subtracting Eq. (5.1a) to Eq. (5.2a) and injecting $\rho_{\rm B}^{({\rm r})} = \phi_{\rm r}\mathbb{1}_{\{x<p_{\rm t}\}}$, $\rho_{\rm A}^{({\rm r})} = -\phi_{\rm r}\mathbb{1}_{\{x>p_{\rm t}\}}$, one obtains the following set of equations, central to our study:

$$\partial_t \rho_{\rm B}^{(\ell)} = D_\ell\partial_{xx}\rho_{\rm B}^{(\ell)} - \omega\left\{\Gamma(-k\xi)\rho_{\rm B}^{(\ell)} - \left[1-\Gamma(-k\xi)\right]\mathbb{1}_{\{x<p_{\rm t}\}}\phi_{\rm r}\right\} \tag{5.4a}$$

$$\partial_t \rho_{\rm A}^{(\ell)} = D_\ell\partial_{xx}\rho_{\rm A}^{(\ell)} - \omega\left\{\Gamma(k\xi)\rho_{\rm A}^{(\ell)} + \left[1-\Gamma(k\xi)\right]\mathbb{1}_{\{x>p_{\rm t}\}}\phi_{\rm r}\right\} \tag{5.4b}$$

$$\partial_t \phi_{\rm r} = D_{\rm r}\partial_{xx}\phi_{\rm r} + \omega\left\{\Gamma(-k\xi)\rho_{\rm B}^{(\ell)} - \Gamma(k\xi)\rho_{\rm A}^{(\ell)} - \left[1-\Gamma(k|\xi|)\right]\phi_{\rm r}\right\} \ . \tag{5.4c}$$

Equations (5.4) must be complemented with a set of boundary conditions. In particular we impose that $\lim_{x\to\infty}\partial_x\rho_{\rm A}^{(\ell)} = -\lim_{x\to-\infty}\partial_x\rho_{\rm B}^{(\ell)} = \mathcal{L}$ (see [46]), and that $\rho_{\rm A}^{(\ell)}$ when $x \to -\infty$, respectively $\rho_{\rm B}^{(\ell)}$ when $x \to \infty$, do not diverge. In addition, whenever $D_{\rm r} \neq 0$,[4] one must impose that $\phi_{\rm r}(0) = 0$ and $\phi_{\rm r}(x)$ does not diverge when $|x| \to \infty$.

[2] While it may be reasonable that, when unrevealed, orders don't land on the same price x they took off from (by that moving away the earlier decision, say $(x)_{\rm r} \to (x+\Delta x)_\ell$, with $\mathrm{sign}(\Delta x) = \mathrm{sign}(x - p_{\rm t})$), we shall not consider such a possibility in the present study for reasons of analytical tractability (restrict to $\Delta x = 0$).

[3] Note that relaxing this hypothesis is possible (see e.g. Sec. 5.3 for the case $D_{\rm r} = 0$) but at the cost of additional complexity. We checked that this point was without effect on our main qualitative results.

[4] While $D_{\rm r} = 0$ is an interesting limit, $D_\ell = 0$ does not seem to be particularly appealing on modelling grounds. In section 5.3 we give a more solid theoretical argument to support this claim.

5.3 Stationary order books

In this section we compute analytically and numerically the stationary order books as function of the different parameters, and discuss interesting limit cases. Setting $\partial_t \rho_{\rm B}^{(\ell)} = \partial_t \rho_{\rm A}^{(\ell)} = \partial_t \phi_{\rm r} = 0$ in Eqs. (5.4) one obtains for all $\xi \in \mathbb{R}^*$, $\rho_{\rm B}^{(\ell)}(\xi) = \rho_{\rm A}^{(\ell)}(-\xi)$ and $\phi_{\rm r}(\xi) = -\phi_{\rm r}(-\xi)$. This allows one to solve the problem on $\mathbb{R}^{+*}$, with boundary conditions $\rho_{\rm B}^{(\ell)}(0^+) = \rho_{\rm A}^{(\ell)}(0^+), \partial_\xi \rho_{\rm B}^{(\ell)}(0^+) = -\partial_\xi \rho_{\rm A}^{(\ell)}(0^+)$. The system one must solve for $\xi > 0$ reduces to:

$$
\begin{aligned}
0 &= D_\ell \partial_{\xi\xi} \rho_{\rm B}^{(\ell)} - \omega \rho_{\rm B}^{(\ell)} && \text{(5.5a)} \\
0 &= D_\ell \partial_{\xi\xi} \rho_{\rm A}^{(\ell)} - \omega \left\{ \Gamma(k\xi) \rho_{\rm A}^{(\ell)} + [1 - \Gamma(k\xi)] \phi_{\rm r} \right\} && \text{(5.5b)} \\
0 &= D_{\rm r} \partial_{\xi\xi} \phi_{\rm r} - \omega \left\{ \Gamma(k\xi) \rho_{\rm A}^{(\ell)} + [1 - \Gamma(k\xi)] \phi_{\rm r} - \rho_{\rm B}^{(\ell)} \right\} . && \text{(5.5c)}
\end{aligned}
$$

Analytical and numerical solutions

Here we provide a solution of Eqs. (5.5) for three distinct cases of interest $D_{\rm r} = 0$, $D_{\rm r} = D_\ell$, and $D_{\rm r} \neq D_\ell$. Note that for $D_\ell = 0$, one can show that $\rho_{\rm B}^{(\ell)}(\xi > 0) = 0$, while $\phi_{\rm r}(\xi > 0) = a\xi + b$ with a and b two constants, and $\rho_{\rm A}^{(\ell)} = \phi_{\rm r}[\Gamma(k\xi) - 1]/\Gamma(k\xi) \approx -\phi_{\rm r}/\Gamma(k\xi)$ for $\xi \to \infty$, by assuming Γ to vanish at infinity. Such solutions are not compatible with the boundary conditions at infinity and will therefore not be further inspected.

The limit case $D_{\rm r} = 0$

Setting $D_{\rm r} = 0$ in Eqs. (5.5) and introducing $\ell_\ell := \sqrt{D_\ell/\omega}$, on finds that the stationary order book densities are given by (see Fig. 5.2(a)):

$$
\begin{aligned}
\rho_{\rm B}^{(\ell)}(\xi) &= \frac{\mathcal{L}\ell_\ell}{2} e^{-\xi/\ell_\ell} && \text{(5.6a)} \\
\rho_{\rm A}^{(\ell)}(\xi) &= \mathcal{L}\xi + \frac{\mathcal{L}\ell_\ell}{2} e^{-\xi/\ell_\ell} && \text{(5.6b)} \\
\phi_{\rm r}(\xi) &= \frac{\mathcal{L}\ell_\ell}{2} e^{-\xi/\ell_\ell} - \frac{\mathcal{L}\xi\Gamma(k\xi)}{1 - \Gamma(k\xi)} . && \text{(5.6c)}
\end{aligned}
$$

Let us stress that the solution $\phi_{\rm r}(\xi)$ is discontinuous in $\xi = 0$, consistent with no diffusion in the revealed order book. More precisely, provided $\Gamma'(0^+) \neq 0$, one has $\phi_{\rm r}(0^-) - \phi_{\rm r}(0^+) = -\mathcal{L}\left[\ell_\ell + 2/(\Gamma'(0^+)k)\right]$. While the solution for the case $D_{\rm r} = 0$ can be expressed for an arbitrary function $\Gamma(y > 0)$, this is not the case for $D_{\rm r} \neq 0$ and one must specify its shape. In the following we choose to work with:

$$
\Gamma(y) = \begin{cases} 1 & \forall y \leq 0 \\ e^{-y} & \forall y > 0 . \end{cases} \qquad \text{(5.7)}
$$

Note that studying the effect of a scale-invariant power law decaying Γ could also yield interesting results.[5]

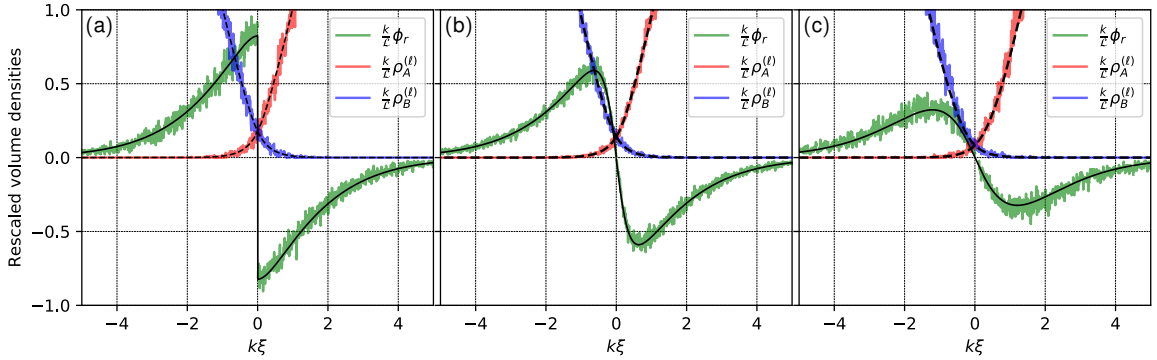

Figure 5.2: *Rescaled stationary order books as function of rescaled price for (a) $D_r = 0$, (b) $D_r \neq D_\ell$ ($D_r < D_\ell$), and (c) $D_r = D_\ell$. Solid black lines indicate the rescaled theoretical revealed order density $k\phi_r/\mathcal{L}$ while dashed black lines signify the theoretical latent order densities $k\rho^{(\ell)}_{A/B}/\mathcal{L}$. The results of the numerical simulation presented in Sect. 5.3 are plotted with color lines on top of the analytical curves, with $k\ell_\ell = 0.35$ for (a) and (c), and $\ell_r/\ell_\ell = 0.32$ for (b).*

The limit case $D_\mathrm{r} = D_\ell$

For $D_\mathrm{r} = D_\ell$ and provided $k\ell_\ell \neq 1$ the stationary books are given by (see Fig. 5.2(c)):

$$\rho^{(\ell)}_\mathrm{B}(\xi) = \frac{\mathcal{L}}{k} g(k\ell_\ell) e^{-\xi/\ell_\ell} \tag{5.8a}$$

$$\rho^{(\ell)}_\mathrm{A}(\xi) = \mathcal{L}\xi + \frac{\mathcal{L}}{k} g(k\ell_\ell) e^{-\xi/\ell_\ell} + \phi_\mathrm{r}(\xi) \tag{5.8b}$$

$$\begin{aligned}\phi_\mathrm{r}(\xi) = \mathcal{L}\Bigg(&\frac{1}{(k\ell_\ell)^2-1}\left[\xi + \frac{2k\ell_\ell^2}{(k\ell_\ell)^2-1}\right] e^{-k\xi} + \frac{g(k\ell_\ell)}{k^2\ell_\ell(k\ell_\ell+2)} e^{-(1/\ell_\ell+k)\xi} \\ &+ \left[\frac{g(k\ell_\ell)}{2k\ell_\ell}\xi - \frac{2k\ell_\ell^2}{[(k\ell_\ell)^2-1]^2} - \frac{g(k\ell_\ell)}{k^2\ell_\ell(k\ell_\ell+2)}\right] e^{-\xi/\ell_\ell}\Bigg) \ ,\end{aligned} \tag{5.8c}$$

where we introduced $g(\zeta) = 2\zeta^2(2+\zeta)^2/[(1+\zeta)^2(8+3\zeta)]$. For $k\ell_\ell = 1$ the result can be obtained by Taylor expanding Eqs. (5.8) about $k\ell_\ell = 1$. Note that in this case the function $\phi_\mathrm{r}(\xi)$ is continuous in $\xi = 0$, consistent with nonzero diffusivity in the revealed order book.

The general case $D_\mathrm{r} \neq D_\ell$

For $D_\mathrm{r} \neq D_\ell$ the set of Eqs. (5.5) must be solved numerically. Figure 5.2(b) displays a plot of the stationary order books computed using a finite difference method for $D_\mathrm{r}/D_\ell \approx 0.1$, that is $\ell_\ell/\ell_\mathrm{r} \approx 3$ where we introduced $\ell_\mathrm{r} := \sqrt{D_\mathrm{r}/\omega}$. As one can see, in the situation $D_\mathrm{r} < D_\ell$ the revealed order book's shape is somewhat in between the cases $D_\mathrm{r} = 0$ and $D_\mathrm{r} = D_\ell$, that is continuous but with a steeper slope at $\xi = 0$. As expected, a little amount of diffusion in the revealed order book suffices to regularize the singularity at the trade price.

As it can be seen from Eq. (5.5a) (or from Eqs. (5.6a) and (5.8a) in the particular cases $D_\mathrm{r} = 0$ and $D_\mathrm{r} = D_\ell$), in all cases ℓ_ℓ denotes the typical scale over which the latent books

[5] Also note that in this particular case, the solution for $\omega_\ell \neq \omega_\mathrm{r}$ can be easily expressed by substituting ℓ_ℓ by $\ell^{(\mathrm{r})}_\ell = \sqrt{D_\ell/\omega_\mathrm{r}}$ into Eqs. (5.6a) and (5.6b), and replacing Eq. (5.6c) by:

$$\phi_\mathrm{r}(\xi) = \frac{\omega_\mathrm{r}}{\omega_\ell}\left[\frac{\mathcal{L}\ell^{(\mathrm{r})}_\ell}{2} e^{-\xi/\ell^{(\mathrm{r})}_\ell} - \frac{\mathcal{L}\xi e^{-k\xi}}{1-e^{-k\xi}}\right] .$$

overlap. This is consistent with the idea that ℓ_ℓ is the typical displacement by diffusion of a latent order in the vicinity of the trade price during a time interval ω^{-1}, that is before it gets revealed. Also, it can be seen from Eqs. (5.6c) and (5.8c) in the particular cases $D_\mathrm{r} = 0$ and $D_\mathrm{r} = D_\ell$ that the typical horizontal extension of the revealed order book, commonly called **order book depth**, is given by $\max(k^{-1}, \ell_\ell)$, consistent with the decay of the conversion probability function Γ and the horizontal extension of the latent books. Note however that, as shall be argued in Sect. 5.4, k^{-1} must always be of order or larger than ℓ_ℓ for stability reasons, and therefore $\max(k^{-1}, \ell_\ell) \sim k^{-1}$. In the following we shall thus call k^{-1} the order book depth. Finally note that when ℓ_r (equivalently D_r) is decreased while keeping all other parameters constant, the slope of the revealed order book around the origin increases, by that concentrating further the available liquidity around the trade price.

The LLOB limit

Our model being built upon the locally linear order book model (LLOB) by Donier *et al.* [46], we should be able to recover such a limit for certain values of the parameters. Since there is only one diffusion coefficient in the LLOB model, the latter should correspond to the $D_\mathrm{r} = D_\ell$ case. Then, the LLOB model assumes no lag effect, i.e. latent orders are immediately executed when at the trade price. This translates into $\omega \to \infty$ or equivalently $\ell_\ell \to 0$, that is no overlap of the latent books. More rigorously, nondimensionalizing Eqs. (5.8) as $\{\tilde{\phi}_\mathrm{r}, \tilde{\rho}^{(\ell)}\} = \{k\phi_\mathrm{r}/\mathcal{L}, k\rho^{(\ell)}/\mathcal{L}\}$ and $\tilde{\xi} = k\xi$, one can see that taking the limit $k\ell_\ell \to 0$ yields for all $\tilde{\xi} > 0$, $\tilde{\rho}^{(\ell)}_\mathrm{B}(\tilde{\xi}) \to 0$, and $\tilde{\rho}^{(\ell)}_\mathrm{A}(\tilde{\xi}) + \tilde{\rho}^{(\mathrm{r})}_\mathrm{A}(\tilde{\xi}) = \tilde{\xi} := \tilde{\rho}^{\mathrm{LLOB}}_\mathrm{A}(\tilde{\xi})$ that is precisely the LLOB result. To summarize, provided the latent order book of Donier *et al.* is defined as the sum of the latent and revealed books, the LLOB limit is recovered for $k\ell_\ell \ll 1$. The latter condition indicates that the typical displacement ℓ_ℓ of latent orders in the vicinity of the price must remain small compared to the order book depth k^{-1}. Note that, despite what a first intuition might suggest, the condition $k \to \infty$, that is no incentive to give away information until absolutely necessary, is not required to recover the LLOB limit.

Numerical simulation

In order to test our results, we performed a numerical simulation of our model (see Fig. 5.2) which proceeds as follows. We define four vectors $\rho^{(\ell)}_\mathrm{A}, \rho^{(\mathrm{r})}_\mathrm{A}, \rho^{(\ell)}_\mathrm{B}, \rho^{(\mathrm{r})}_\mathrm{B}$ of size 2000 on the price axis (a good trade-off between the continuous approximation of the model and computational time cost). Each component of vectors stores the number of orders contained at that price at a given time. At each cycle we draw the orders that shall diffuse from a binomial distribution of parameter $p_{\ell/\mathrm{r}}$, directly related to the diffusion constant in the respective book by the relation $D_{\ell/\mathrm{r}} = p_{\ell/\mathrm{r}}/(2\tau)$ where τ denotes the time step. Some of the orders (drawn from a binomial of parameter 1/2) will move to the left and the remaining to the right. Reflecting boundary conditions are imposed for revealed orders; the slope of the latent book at the boundaries is ensured by an incoming current of particles $J = D_\ell\mathcal{L}$. Then, some orders in the latent book are drawn from a binomial distribution of parameter $\omega\tau\Gamma(k\xi)$ for the ask side (resp. $\Gamma(-k\xi)$ for the bid side)) and moved to the revealed book. Here p_t denotes the mid-price. Equivalently revealed orders are moved to the latent book, only with parameter $\omega\tau(1 - \Gamma(\cdot))$. Whenever bid and ask orders are found at the same price, they are cleared from the book. Figure 5.2 shows that the results of the numerical simulations are in very good agreement with the analytical solutions.

5.4 Market stability and calibration to real data

In this section, we address the important question of market stability, as given by the amount of liquidity in the revealed order book. Clearly, when the conversion rate ω is low,

the revealed liquidity is thin and prices can be prone to liquidity crises, even when the latent liquidity is large. We calibrate our model to real order book data and discuss the results in the light of the stability map provided by our model.

Market stability

Imposing that the order densities $\rho_{\rm A}^{(\ell)}, \rho_{\rm A}^{(\rm r)}, \rho_{\rm B}^{(\ell)}, \rho_{\rm B}^{(\rm r)}$ must be non negative, consistent with a physically meaningful solution, restricts the possible values of $\ell_\ell := \sqrt{D_\ell/\omega}$ for a given order book depth k^{-1}.

In the $D_{\rm r} = 0$ case, combining Eq. (5.6c) with Eq. (5.7) yields $\phi_{\rm r}(0^+) = \mathcal{L}\left[\ell_\ell/2 - 1/k\right]$. Restricting to $\phi_{\rm r}(0^+) \leq 0$ (which is tantamount to $\rho_{\rm A}^{(\rm r)}(0^+), \rho_{\rm B}^{(\rm r)}(0^+) \geq 0$) gives $k\ell_\ell \leq 2$. Note however that this condition is not sufficient to say that the order densities are everywhere positive, but that they are only positive around the origin. The necessary and sufficient condition to ensure full positiveness reads $k\ell_\ell \leq 1$. For $1 \leq k\ell_\ell \leq 2$ the order book displays a "hole" along the price axis, but is well defined around the origin. Since we are most interested in the revealed liquidity in the vicinity of the trade price we will choose $k\ell_\ell \leq 2$ (or, in terms of ω, $\omega \geq D_\ell k^2/4$) as our **stability condition**, with no qualitative and only little quantitative effect on our main conclusions. The maximum amplitude of the real order book density scales as:

$$\max_\xi \left|\phi_{\rm r}(\xi)\right| = -\phi_{\rm r}(0^+) = \frac{\mathcal{L}}{k}\left(1 - \frac{k\ell_\ell}{\zeta_{\rm c}}\right), \quad \zeta_{\rm c} = 2\ . \tag{5.9}$$

For $D_\ell = D_{\rm r}$ the stability condition is imposed by the sign of the slope at $\xi = 0$. One finds that the critical value of $k\ell_\ell$ for which the liquidity around the origin vanishes is given by $\zeta_{\rm c} = [-2 + (73 - 6\sqrt{87})^{1/3} + (73 + 6\sqrt{87})^{1/3}]/3 \approx 1.875$.[6] Arguing that in this case the maximum of the density can be approximated by $\max_\xi \left|\phi_{\rm r}'(0^+)\xi e^{-k\xi}\right| = |\phi_{\rm r}'(0^+)|/(ek)$ yields:

$$\max_\xi \left|\phi_{\rm r}(\xi)\right| \sim \frac{\mathcal{L}}{ek}\frac{\zeta_{\rm c}(3\zeta_{\rm c}^2 + 4\zeta_{\rm c} - 3)}{(1+\zeta_{\rm c})^2(8+3\zeta_{\rm c})}\left(1 - \frac{k\ell_\ell}{\zeta_{\rm c}}\right), \quad \zeta_{\rm c} \approx 1.875\ . \tag{5.10}$$

Figure 5.3(a) displays $-k\phi_{\rm r}'(0^+)/\mathcal{L}$ as function of the dimensionless parameters $k\ell_\ell$ and $k\ell_{\rm r}$. The dash-dotted line corresponding to $\phi_{\rm r}'(0) = 0$ splits the parameter space into a stable region (green) and an unstable region (red). We naturally checked that the analytical values of $\zeta_{\rm c}$ obtained above for $\ell_\ell = \ell_{\rm r}$ and $\ell_{\rm r} \to 0$ are recovered. As one can see, while the role played by $\ell_{\rm r}$ with respect to the position of the critical line $\zeta_{\rm c}$ is quite marginal (quasi-vertical dash dotted line), the slope of the order book around $\xi = 0$ increases with decreasing $\ell_{\rm r}/\ell_\ell$. More precisely, Fig. 5.3(c) displays the slope of the revealed book in the vicinity of the transition and shows that, at given $\ell_{\rm r}/\ell_\ell$, the slope indeed scales linearly with $|k\ell_\ell - \zeta_{\rm c}|$. In addition the top right inset shows that the slope also scales as $\ell_\ell/\ell_{\rm r}$, which finally leads to $|\phi_{\rm r}'(0^+)| \sim |k\ell_\ell - \zeta_{\rm c}|(\ell_\ell/\ell_{\rm r})$. The other insets show $\zeta_{\rm c}$ as function of $\ell_{\rm r}/\ell_\ell$, and the total revealed volume. For the sake of completeness, Fig. 5.3(b) displays a proxy of the overlap between the latent bid and ask books in the parameter space $(k\ell_\ell, k\ell_{\rm r})$. While vanishing in the region $k\ell_\ell \ll \zeta_{\rm c}$, the overlap is quite large (of the order of k^{-1}) in the vicinity of the critical line $k\ell_\ell \lesssim \zeta_{\rm c}$ indicating a large volume of latent orders in the vicinity of the price. Interestingly, combined with a vanishing level of liquidity, the increased level of activity around the origin induces important fluctuations of the trade price. To illustrate this, Fig. 5.3(d) displays the numerically determined squared volatility of the trade price p_t

[6] Note that in this case the solution, provided $k\ell_\ell > 1$, is also asymptotically unstable: $\lim_{\xi\to\infty}\phi_{\rm r}(\xi) = \mathcal{L}g(k\ell_\ell)\xi e^{-\xi/\ell_\ell}/(2k\ell_\ell) > 0$, while for $k\ell_\ell = 1$, $\lim_{\xi\to\infty}\phi_{\rm r} < 0$.

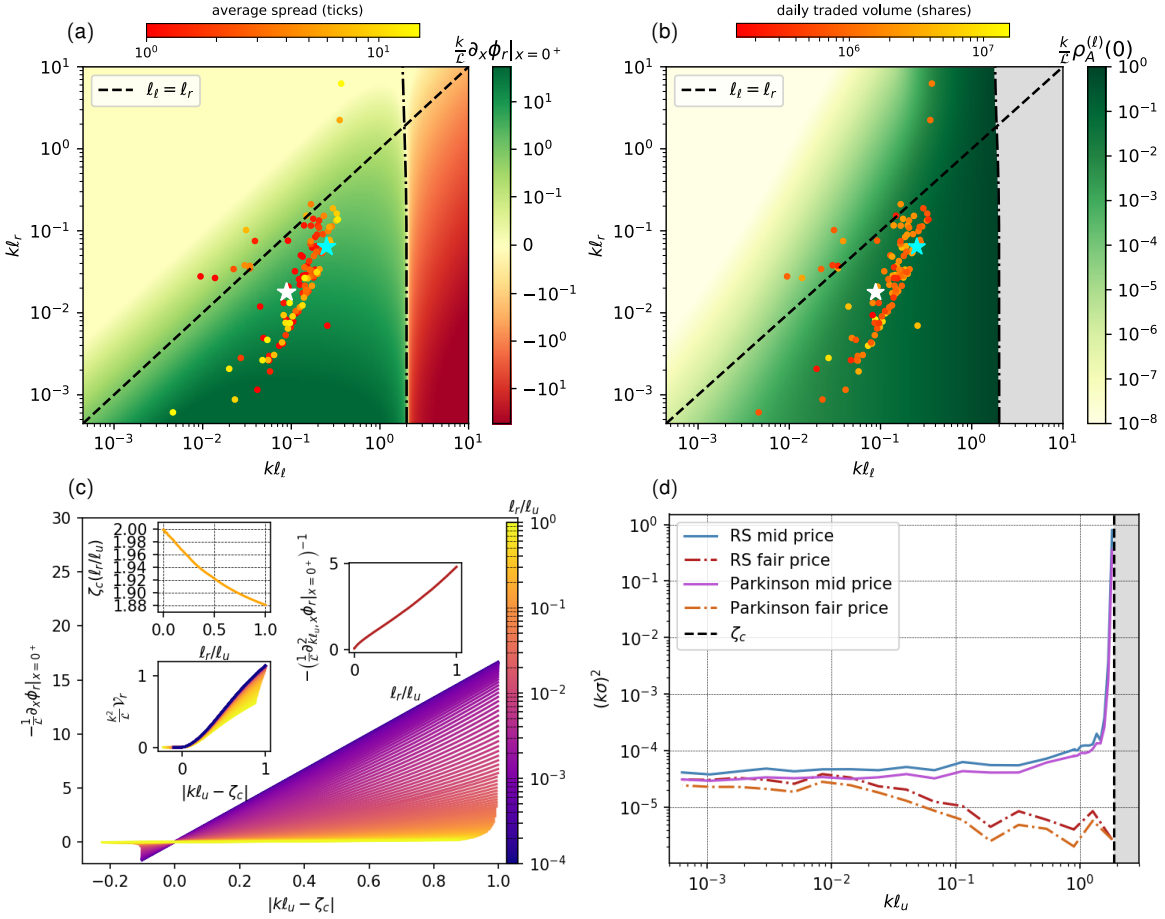

Figure 5.3: *Parametric study of stationary order books. (a) Stability map. Density plot (symlog scale) of the rescaled slope of the revealed order density at the origin, as function of $k\ell_\ell$ and $k\ell_r$. The dashed line indicates $\ell_r = \ell_\ell$, the dash-dotted line indicates the critical line $\phi_r'(0) = 0$. (b) Overlap of the latent order books. Density plot (log scale) of the y-intercept of the latent order book densities at the origin. Note that such a quantity is a direct measure of the overlap. The empirical order book data (US stocks, see Tab. A.3, and Euro Stoxx, white star) are reported with a colormap scaling with their average spread value (see (a)) and with their average daily traded volume (see (b)). (c) Plot of the slope of the revealed order book at the origin as function of $\zeta_c - k\ell_\ell$, for different values of ℓ_r/ℓ_ℓ. The top inset shows ζ_c as function of ℓ_r/ℓ_ℓ, and the center left inset displays the total volume in the revealed order book $\mathcal{V}_r = \left|\int_0^\infty d\xi\, \phi_r(\xi)\mathbb{1}_{\phi_r(\xi)<0}\right|$, as function of $\zeta_c - k\ell_\ell$. The right inset shows the angular coefficient of the slope of the main plot at the origin. (d) Numerical volatility. Plot of rescaled numerical squared volatility of the trade price and the fair price (see Eq. (5.11)) in the $\ell_r = \ell_\ell$ case. We display two different estimations: Rogers-Satchell, $\sigma^2_{RS} = \mathbb{E}\left[(p_H - p_O)(p_H - p_C) + (p_L - p_O)(p_L - p_C)\right]$, and Parkinson, $\sigma^2_p = \frac{1}{4\ln(2)}\mathbb{E}\left[(p_H - p_L)^2\right]$ where p_H, p_L, p_O, p_C denote the high, low, open and close prices respectively [87, 11].*

as function of $k\ell_\ell$ in the $\ell_r = \ell_\ell$ limit. For comparison, we also plotted the volatility of the **fair price** $p_t^{\rm f}$, here defined as the value that equilibrates total (revealed and latent) supply and demand:

$$\int_0^{p_t^{\rm f}} {\rm d}\xi \left[\rho_{\rm A}^{({\rm r})}(\xi,t) + \rho_{\rm A}^{(\ell)}(\xi,t)\right] = \int_{p_t^{\rm f}}^{\infty} {\rm d}\xi \left[\rho_{\rm B}^{({\rm r})}(\xi,t) + \rho_{\rm B}^{(\ell)}(\xi,t)\right] \ . \tag{5.11}$$

As one can see, for $\omega \gg \omega_{\rm c} := D_\ell k^2/\zeta_{\rm c}^2$ the volatility of the trade price coincides with its

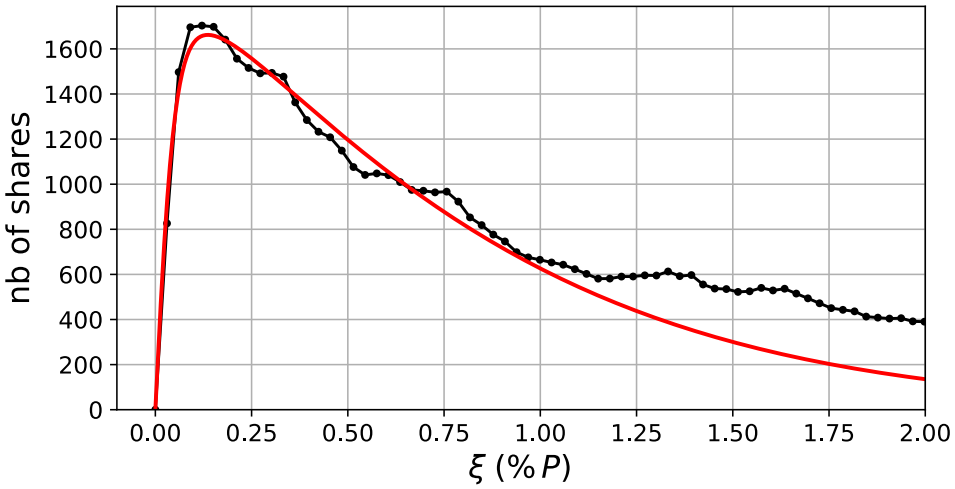

Figure 5.4: *Fit of the stationary revealed order book ϕ_r to the average Euro Stoxx futures contract order book. The calibration yields $\mathcal{L} = 4599$, $k = 2.12$, $\ell_\ell = 0.042$ and $\ell_r = 0.0084$.*

fair price counterpart, consistent with the idea that for high conversion rates the coupling between the revealed and latent books is almost instantaneous and therefore the mid-price tends to follow the fair price. In the vicinity of the critical line the volatility of the fair price slightly decreases. However, the volatility of the trade price strongly diverges as the vanishing liquidity limit is approached, i.e. when the conversion rate ω decreases to ω_c. Note that while the trade price can no longer be defined when a liquidity crisis arises, the fair price as defined in Eq. (5.11) remains well behaved. We also investigated the volatility in the $\ell_r = 0$ limit and obtained similar qualitative results, only with weaker overall volatility levels consistent with liquidity concentration around the trade price.

At this point, let us summarise our results. The market is most stable when the conversion rate is large and/or the latent orders diffusivity is small. In these cases, there is a good level of revealed liquidity and the trade price follows the fair price. However, when lag effects become important, and more particularly when the conversion time ω^{-1} becomes longer than the typical diffusion time of a latent order across the revealed order book depth k^{-1}, the order book empties out and the trade price undergoes large excursions away from the fair price. As for the effect of diffusion in the real order book, a small ℓ_r concentrates the liquidity around the origin, therefore providing a wall to price fluctuations, while a large ℓ_r induces a weaker revealed order book slope around the origin, facilitating larger price excursions. Thus, our framework in the vicinity of the critical line could provide an interesting scenario to understand the nature of liquidity crises in financial markets. One indeed expects that in the presence of increased uncertainty, the conversion rate will decrease (as investors remain on the sidelines) and latent orders diffusivity will increase, both effects driving the market towards a liquidity crisis.

Order book data

To illustrate how our model allows one to calibrate latent parameters using visible order book data, we calibrate it to the real order book of the Euro Stoxx futures contract and of a set of over 100 large cap US stocks extracted from their primary market on the period August 2017 to April 2018, see Table A.3. For each asset, we take a snapshot of the order book every ten minutes (every minute for the Euro Stoxx contract), on regular trading hours. We then fold the bid side onto the ask side, the origin being taken at the opposite best [6], we average over the whole sample and rescale the x-axis by the average price taken over the

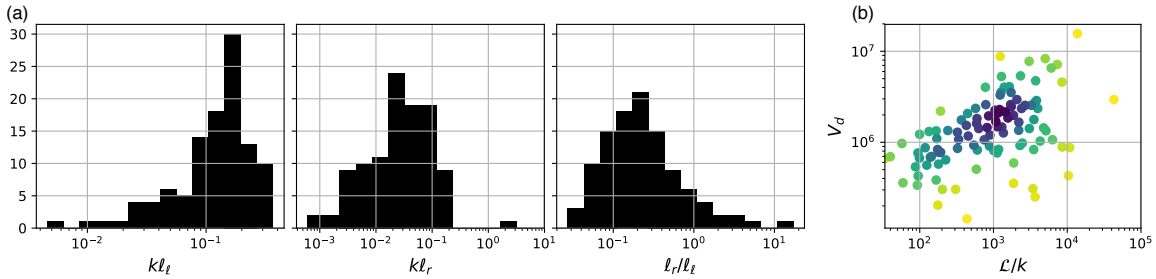

Figure 5.5: *(a) Histograms of the fitted parameters $k\ell_\ell$, $k\ell_r$ and ℓ_r/ℓ_ℓ for the US stocks presented in Table A.3. (b) Average daily traded volume V_d as function of the liquidity parameter $\mathcal{L}/k$. The data points are colored by density (from yellow to dark blue).*

sample period. Finally, fitting the stationary order book $\phi_{\rm r}$ (see Figs. 5.4, A.4, A.5 and A.6) outputs four parameters: $\mathcal{L}$, k, ℓ_ℓ and $\ell_{\rm r}$ (see Table A.3). Note that k^{-1}, ℓ_ℓ and $\ell_{\rm r}$ have units of %p, and $\mathcal{L}$ is in shares per %p.

The fitted values of $k\ell_\ell$ and $k\ell_{\rm r}$ for the Euro Stoxx contract and the US stocks presented in Table A.3 are reported in Figs. 5.3(a) and (b). Figure 5.5(a) displays the statistics of $k\ell_\ell$, $k\ell_{\rm r}$ and $\ell_{\rm r}/\ell_\ell$ for the stocks. As one can see the values of $k\ell_\ell$ stand below the critical line by typically one order of magnitude. Also most of the data is consistent with $\ell_{\rm r} < \ell_\ell$. More precisely, the ratio $\ell_{\rm r}/\ell_\ell$ is typically $\approx 3-10$, which is $D_{\rm r}/D_\ell$ typically $\approx 0.01-0.1$, consistent with our initial intuition that diffusivity is much smaller in the revealed order book than in its latent counterpart. While not a strong effect, the $\ell_{\rm r}/\ell_\ell$ ratios are on average slightly smaller for the small tick assets (Fig. 5.3(a)). The daily traded volume $V_{\rm d}$ does not seem to play a notable role in the distribution of the data in the $(k\ell_{\rm r}, k\ell_\ell)$ map (Fig. 5.3(b)). However, $\mathcal{L}/k$ shows positive correlation with $V_{\rm d}$ (see Fig 5.5(b)), consistent with the interpretation given to the liquidity parameter $\mathcal{L}$ in the latent order book models [46].

5.5 Price impact

In this section we study how liquidity reacts, in our model, to the presence of a metaorder, namely a large trading order split into small orders executed incrementally. Following Donier *et al.* [46] we introduce a metaorder as an additional current of buy/sell particles falling precisely at the trade price. The system of equations governing the system in the presence of a metaorder is left unchanged for the latent order book (Eqs. (5.4a) and (5.4b)), while the RHS of Eq. (5.4c) must be complemented with the extra additive term $+\, m_t\delta(x-p_t)$ representing the metaorder, where m_t denotes the execution rate. In the following we restrict to buy metaorders with constant execution rates $m_t = m_0 > 0$, without loss of generality since the sell metaorder $m_0 < 0$ is perfectly symmetric. In order to extract the dimensionless parameters governing the dynamic system, we introduce $\tilde\xi = k\xi, \tilde t = \omega t, \tilde\rho = k\rho/\mathcal{L}, \tilde\phi_{\rm r} = k\phi_{\rm r}/\mathcal{L}$ and write the equations in a dimensionless form:

$$\partial_{\tilde t}\tilde\rho^{(\ell)}_{\rm B} = (k\ell_\ell)^2\partial_{\tilde x\tilde x}\tilde\rho^{(\ell)}_{\rm B} - \Big\{\Gamma(-\tilde\xi)\tilde\rho^{(\ell)}_{\rm B} - [1-\Gamma(-\tilde\xi)]\mathbb{1}_{\{\tilde x<\tilde p_{\tilde t}\}}\tilde\phi_{\rm r}\Big\} \tag{5.12a}$$

$$\partial_{\tilde t}\tilde\rho^{(\ell)}_{\rm A} = (k\ell_\ell)^2\partial_{\tilde x\tilde x}\tilde\rho^{(\ell)}_{\rm A} - \Big\{\Gamma(\tilde\xi)\tilde\rho^{(\ell)}_{\rm A} + [1-\Gamma(\tilde\xi)]\mathbb{1}_{\{\tilde x>\tilde p_{\tilde t}\}}\tilde\phi_{\rm r}\Big\} \tag{5.12b}$$

$$\partial_{\tilde t}\tilde\phi_{\rm r} = (k\ell_{\rm r})^2\partial_{\tilde x\tilde x}\tilde\phi_{\rm r} - \Big\{\Gamma(\tilde\xi)\tilde\rho^{(\ell)}_{\rm A} - \Gamma(-\tilde\xi)\tilde\rho^{(\ell)}_{\rm B} + [1-\Gamma(|\tilde\xi|)]\tilde\phi_{\rm r}\Big\} + (m_0/\mathcal{J})\delta(\tilde\xi) \tag{5.12c}$$

with $\mathcal{J} = \mathcal{L}\omega/k^2$ the typical scale of the rate at which latent orders are revealed (recall that $\mathcal{L}/k^2$ is the typical available volume in the latent order book that have a substantial

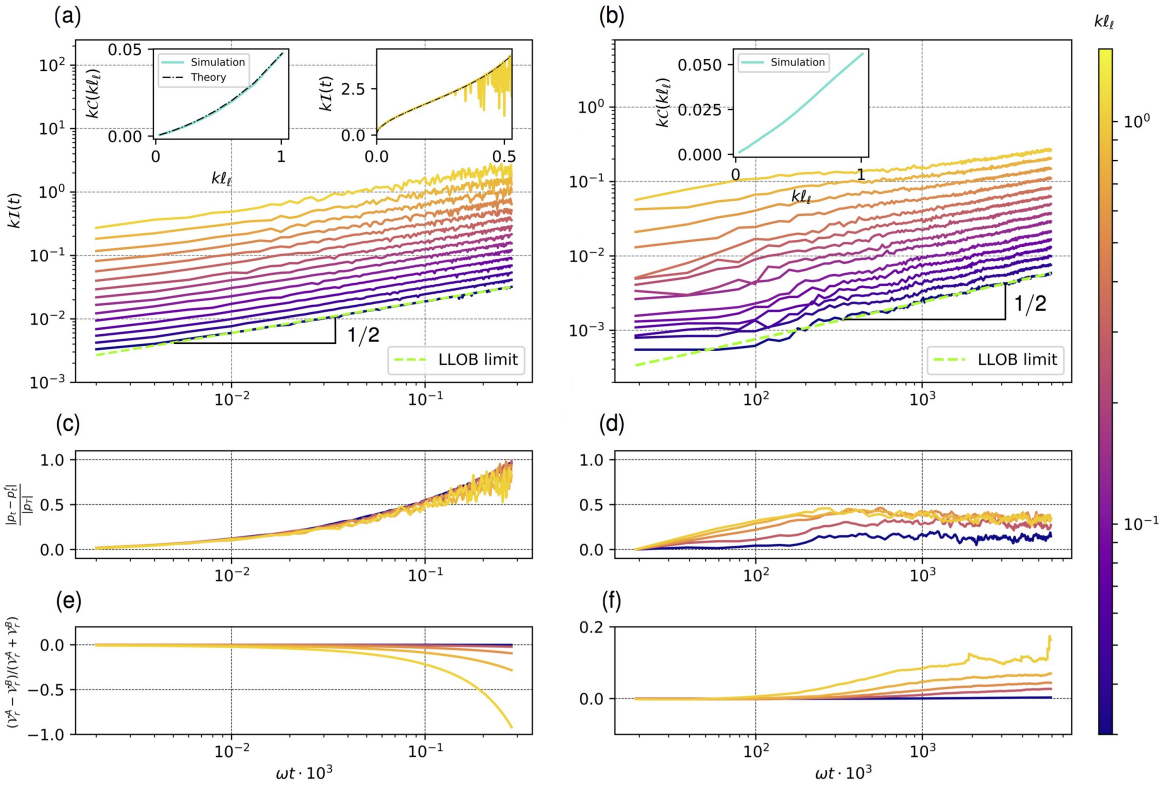

Figure 5.6: *Price impact for $\ell_r = \ell_\ell$. (a) $m_0 \gg J_r$ (b) $m_0 \ll J_r$. The dashed green lines indicate the LLOB limits, $I_{LLOB}(t) = \sqrt{\alpha Q_t/(\pi\mathcal{L})}$ with $\alpha = m_0/J_u$ for the slow regime and $I_{LLOB}(t) = \sqrt{2Q_t/\mathcal{L}}$ for the fast regime. The top left insets on each plot indicate the factor c as function of $k\ell_\ell$ defined as $I(t) = c\, I_{LLOB}(t)$. The top right inset of subplot (a) shows an extreme regime with very high execution rate, the dash-dotted line indicates the theoretical prediction as given by the numerical inversion of Eq. (5.14). Subplots (c) and (d) display relative price difference between the trade price and the fair price (see Eq. (5.11)). Subplots (e) and (f) display the relative revealed volume imbalance.*

probability to be revealed). Matching the first and third terms on the right hand side of Eq. (5.12c) yields a relevant dimensionless number $(m_0/\mathcal{J})/(k\ell_\mathrm{r})^2 = m_0/J_\mathrm{r}$ with $J_\mathrm{r} = D_\mathrm{r}\mathcal{L}$. In the case $\ell_\mathrm{r} = 0$ the relevant dimensionless number is simply given by $m_0/\mathcal{J}$.

In order to compute the price impact $I(Q_t) = \mathbb{E}[p_t - p_0 | Q_t = m_0 t]$, we performed numerical simulations of our model in the presence of a metaorder in several limit cases. We explored in particular $\ell_\mathrm{r} = \ell_\ell$ and $\ell_\mathrm{r} = 0$, in both high and low participation rate regimes, for different values of $k\ell_\ell$ (see Figs. 5.6 and 5.7).

Before presenting the results of the numerical simulations, note that there exists a regime where the calculations can be brought a little bit further analytically, that is when we can give a geometrical interpretation to the problem. When the book is almost static on the time scale of the metaorder execution *i.e.* $m_0 \gg J_\mathrm{r}$ (resp. $m_0 \gg \mathcal{J}$ for $\ell_\mathrm{r} = 0$). One has $\int_0^t \mathrm{d}s\, m_0 = -\int_0^{p_\mathrm{t}} \mathrm{d}\xi \phi_\mathrm{r}^{\mathrm{st}}(\xi)$ with $\xi = x - p_0$. In particular for $\ell_\mathrm{r} = 0$ one obtains:

$$Q_t = -\frac{\mathcal{L}\ell_\ell^2}{2}\left(1 - e^{-p_\mathrm{t}/\ell_\ell}\right) + \frac{\mathcal{L}p_\mathrm{t}}{k}\log\left(1 - e^{-kp_\mathrm{t}}\right) - \frac{\mathcal{L}}{k^2}\left[\mathrm{Li}_2(e^{-kp_\mathrm{t}}) - \mathrm{Li}_2(1)\right] , \quad (5.13)$$

where $\mathrm{Li}_2(y) = \sum_{k=1}^{\infty} y^k/k^2$ stands for the polylogarithm of order 2, and can be inverted

numerically to obtain the price trajectory p_t. Similarly, for $\ell_r = \ell_\ell$ one has:

$$\begin{aligned} Q_t &= \frac{\mathcal{L}\alpha}{k^2}\left\{[k(p_t+\beta)+1]e^{-kp_t} - (k\beta+1)\right\} - \frac{\mathcal{L}\ell_\ell\gamma}{1+k\ell_\ell}\left(1-e^{-(k+1/\ell_\ell)p_t}\right) \\ &+ \mathcal{L}\ell_\ell\delta p_t e^{-p_t/\ell_\ell} - \mathcal{L}[\delta\ell_\ell^2 - \ell_\ell(\alpha\beta+\gamma)]\left(1-e^{-p_t/\ell_\ell}\right) , \end{aligned} \tag{5.14}$$

where $\alpha = [(k\ell_\ell)^2-1]^{-1}$, $\beta = 2\alpha k\ell_\ell^2$, $\gamma = g(k\ell_\ell)[k^2\ell_\ell(k\ell_\ell+2)]^{-1}$, $\delta = g(k\ell_\ell)[2k\ell_\ell]^{-1}$. In the following we discuss the more general numerical results for both limit cases $\ell_\ell = \ell_r$ and $\ell_r = 0$.

The case $\ell_\ell = \ell_r$

The main plots in Figs. 5.6(a) and (b) display robust square root price trajectories, regardless of the values of $k\ell_\ell$. For $m_0 \gg J_r$ the price trajectory matches the theoretical prediction given above inverting Eq. (5.14). As expected from the exponentially vanishing liquidity when $x - p_0 > k^{-1}$, impact eventually diverges for very extreme regimes, see top right inset in Fig. 5.6(a). For $k\ell_\ell \ll 1$, one recovers the LLOB limit in both fast and slow regimes, also as expected. For non vanishing values of $k\ell_\ell$, the impact increases with increasing $k\ell_\ell$. In particular for $m_0 \gg J_r$ one obtains at short times (equivalently small volumes):

$$p_t = \sqrt{\frac{2Q_t}{|\partial_x\phi_r(0^+)|}} \sim \sqrt{2Q_t}\left(1-\frac{k\ell_\ell}{\zeta_c}\right)^{-1/2} . \tag{5.15}$$

As expected, impact diverges when at the incipient liquidity crisis point. Figures 5.6(c) and (d) display the relative distance between the trade price and the fair price as function of time. In the fast execution regime all curves fall on top of each other and $|p_t - p_t^f| \approx |p_t|$, consistent with the idea that the book (in particular latent) does not have time to reassess during the execution, and as a consequence the fair price varies at a much slower rate than the trade price. A different scenario takes place in the small execution rate regime. We observe that the relative distance between trade and fair prices stabilizes. In other terms, the latent order book evolves at a speed that is comparable to that of the metaorder and the fair price follows the trade price quite accurately.

The evolution of relative volume imbalance (see Figs. 5.6(e) and (f)) allows one to draw similar conclusions. In the fast execution limit, the imbalance diverges as the latent order book has no time to refill the revealed order book (this effect is all the more evident as we approach the vanishing liquidity limit $k\ell_\ell \to \zeta_c$), while in the slow execution limit the imbalance is much smaller. Most importantly, note that in this limit the imbalance becomes positive. This is consistent with the fact that when the trade price moves slowly, the conversion probability Γ is shifted with it and new orders reveal on top of the existing ones to supply the metaorder, while the orders left behind progressively unreveal.

The case $\ell_r = 0$

The limit $\ell_r \to 0$ corresponds to $m_0/J_r \to \infty$, so in some sense one could say that we are always in a high participation rate regime. However the absence of diffusion means that the system can only evolve through the revealing and unrevealing currents. As mentioned above, in this case the relevant dimensionless number becomes $m_0/\mathcal{J}$, that shall be referred to as participation rate in the following.

Figure 5.7(a) displays price trajectories in the fast execution regime, here $m_0 \gg \mathcal{J}$. The metaorder is faster than the revealing current and the price trajectory is given by inverting

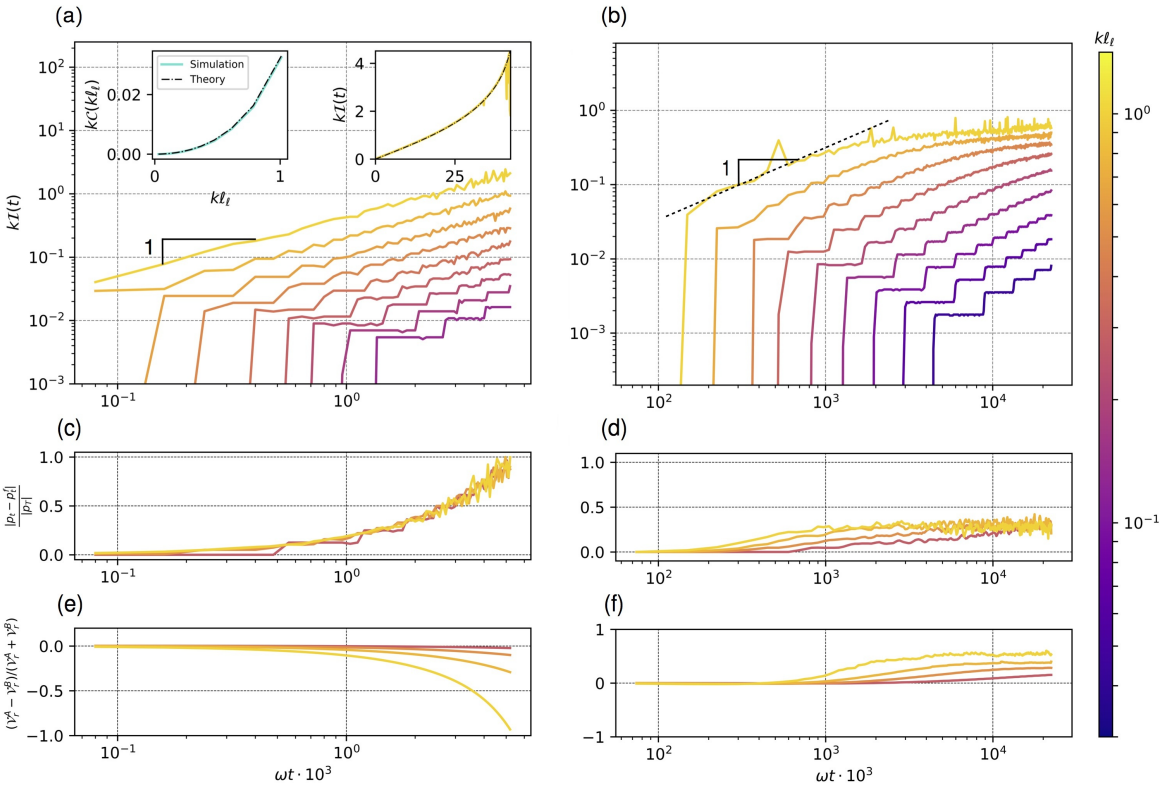

Figure 5.7: *Price impact for $\ell_r = 0$. (a) and $m_0 \gg \mathcal{J}$ (b) $m_0 \ll \mathcal{J}$. The top left insets on subplot (a) indicates the factor c as function of $k\ell_\ell$ here defined as $I(t) = ct$ for $\ell_r = 0$. The top right insets show an extreme regime with very high execution rate for which the impact diverges. Subplots (c) and (d) display relative price difference between the trade price and the fair price, see Eq.* (5.11)*. Subplots (e) and (f) display the relative revealed volume imbalance.*

Eq. (5.13). At short times, one obtains (see Eq. (5.9)):

$$p_{\mathrm{t}} = \frac{kQ_t}{\mathcal{L}} \left(1 - \frac{k\ell_\ell}{\zeta_{\mathrm{c}}}\right)^{-1} , \tag{5.16}$$

which is linear impact, consistent with $\phi_{\mathrm{r}}(0) \neq 0$. Analogous to the case $\ell_\ell = \ell_{\mathrm{r}}$, in extreme regimes the impact eventually diverges (see top right inset of Fig. 5.7(a)). Regarding the imbalance and the relative distance between the trade price and the fair price, the interpretation is analogous to the $\ell_{\mathrm{r}} = \ell_\ell$ case.

Figure 5.7(b) displays the price trajectories in the low participation rate regime $m_0 \ll \mathcal{J}$. Here the impact is genuinely linear at short times but crossovers to concave after a typical time $t^\star \sim \mathcal{V}_{\mathrm{r}}/m_0$ with $\mathcal{V}_{\mathrm{r}}$ the typical volume available in the revealed order book. This interesting regime can be easily understood as follows. At short times the metaorder is executed against the orders present in the stationary locally constant revealed order book (linear impact), but after a while liquidity revealing from the linear latent order book takes over (implying concave impact).[7] More precisely, as $k\ell_\ell$ is increased, $t^\star$ is decreased consistent with the idea that: the larger $k\ell_\ell$, the smaller the revealed liquidity $\mathcal{V}_{\mathrm{r}}$ and thus the sooner it gets consumed. Note that linear impact at short times (equiv. small volumes) has been

[7] Note that recovering precisely the square root law in this regime is quite challenging because the numerical simulation, by essence discontinuous, induces artificial spread effects: the spread widens and does not get refilled as fast as it should, due to limited resolution and vanishing liquidity in the price region. Obtaining smooth results requires a lot of averaging.

reported empirically in the literature [88]. An alternative theoretical framework to understand linear impact at short times is provided in [48] with the introduction of two types of agents, fast and slow. Our model, in its final version, should also include the possibility for agents with different timescales, possibly with different conversion rates ω. In Fig. 5.7(d), we observe that the relative distance between trade and fair prices stabilizes after the typical time $t^\star$. In other terms, for $t > t^\star$ the latent order book evolves at a rate comparable to that of the metaorder, and the fair price follows the trade price with some constant lag. Figure 5.7(f) displays similar conclusions.

5.6 Concluding remarks

We have proposed a simple, consistent model describing how latent liquidity gets revealed in the real order book. As a first step in the rapprochement of latent order book models and real order book data, our study upgrades the former from a **toy model** status to an observable setup that can be quantitatively calibrated on real data. Although probably too simple in its present form, our main contribution is to show how the latent order book could be inferred from its revealed counterpart. One of our key theoretical result is the existence of a market instability threshold, where the conversion of the trading intentions of market participants into *bona fide* limit orders becomes too slow, inducing **liquidity crises**. Furthermore, from a regulatory perspective, our model indicates how assets can be sorted according to their position in the stability map, a proxy for their propensity to liquidity dry-ups and large price jumps. In particular, our setup could constitute an insightful alternative to relate stability and tick size, a subject that has raised the attention of many in the recent past (see e.g. [89]).

While providing quite satisfactory results on several grounds, our model lacks a number of features that must be addressed in future work. In particular, being an inheritance of the LLOB model [46], our model does not solve the so-called diffusivity puzzle (even persistent order flow lead to mean-reverting prices – see [36, 90, 48]). An interesting extension is suggested by the stocks data presented in Figs A.4, A.5 and A.6. Indeed, some of the order books display a bimodal shape indicating that they would be better fitted with a model involving two conversion timescales (equivalently two price scales). The recent multi-timescale liquidity setup (see [48]) allows for both a **fast** liquidity of high frequency market makers, and a **slow** liquidity of directional traders, while resolving several difficulties of latent order book models. Such a framework should output bimodal distributions and yield even better fits of the real order book, allowing one to infer different liquidity timescales.

Take home message of Chapter 5

1. Revealing liquidity. This mechanism is introduced in the LLOB framework via an interaction between the real order book and the latent order book. It is based on the following simple idea: an agent reveals its orders only if the corresponding price is close to the mid-price.

2. Market stability. There is a stability condition that ensures that the order books are not empty. Beyond this condition, lag effects are responsible for a liquidity crisis.

3. Calibration. The stationary solutions are calibrated on the order book data and the parameters displayed on a stability map.

4. Market Impact. This model numerically reproduces the square root law.

Conclusion and future research

In this thesis we have studied liquidity crises utilizing various theoretical tools and empirical evidence. Then, we were able to discuss the possible reasons which give rise to this sort of systemic financial crises. Properly modeling liquidity crises is challenging, but it is nevertheless critical in order to better understand its roots so that we can improve our financial systems by preventing, or at least mitigating, such events.

The first step in modeling liquidity crises lies in understanding price volatility, and the use of Q-Hawkes process to model such price dynamics served us well. In **Chapter 2**, we introduced the generalized quadratic Hawkes processes and applied them to study order book dynamics. The power of such models consists in encoding the feedback of past price changes on order book events (limit order deposition, cancelations, market orders). Using tick-by-tick data from four liquid futures contracts, we have started an empirical analysis in a minimal framework, limiting ourselves to the best quotes. The results conclude on the existence of a Zumbach-like effect: past price trends diminish future liquidity. Developing our study further, we have set up a full calibration procedure of the GQ-Hawkes processes. This calibration returns kernels which encode the weight of past price changes in the feedback. We followed by applying it on empirical data of the Eurostoxx future data and by displaying the obtained kernels we proved the existence of the Zumbach-like effect once again, that can be interpreted as the microfoundation of the Zumbach effect. Furthermore, we have seen that the kernels are power laws with critical exponents and that the total activity of the market exhibits a high ratio of endogeneity. This accumulation of clues indicates that markets are constantly close, but below, an instable phase. In other words, financial markets are on the very edge of instability. Since we so far solely focused on best quotes, we turn to a variable that accounts for the liquidity dynamics: the effective spread. Computing empirical covariances with the squared past trend reveals that the Zumbach-like effect exists not only at the best quotes, but that it also exists across the entire order book. The effective spread also appears to be fat-tailed distributed, which is another piece of evidence of critical markets.

In **Chapter's 3** modelling section, we coupled GQ-Hawkes process with the Santa Fe Model, thus, creating the Quadratic Santa Fe Model. Using rigorous numerical analysis, we proved the existence of a second order phase transition. Then, using a finite size scaling procedure, we computed the exponents and found a transition of a new universality class. This scenario is very appealing as the power law kernels found in chapter 2 are in agreement with a phase transition scenario. Adding qualitative arguments of Self Organized Criticality, which state that the critical point is an attractor of the system, gives a convincing explanation for markets' criticality.

In order to circumvent analytical issues arising from the Quadratic Santa Fe Model, we set aside the microstructure of the order book and introduced spread models in **Chapter 4**. We only focus on events that changes the spread. Then, the dynamics consists in modeling the rate of spread opening events and spread closing events. We provided many possible scenarios that model spread opening events, such as a linear Hawkes process, a quadratic Hawkes process and a non-linear Hawkes process. The first couple of the aforementioned models hold in cases when the rate of spread closing events is constant but the spread is opening. The two models have three phases, which we analyzed from a theoretical point of view. The non-linear Hawkes process has a meta-stable behavior, when the non-linear feedback is small enough, the spread is apparently stable. However, if we wait long enough

it explodes and results in a liquidity crisis. From a physicist's perspective, this meta-stable property can be interpreted as a particle trapped in a local minimum of potential energy that than crosses an energy barrier. Having done this parallel with Physics, we derived the average time of the first liquidity crisis and we than compared it to numerical results. Nevertheless, this convincing scenario is not in agreement with empirical results, which support phase transition. We also provided a scenario where the rate of spread closing events is proportional to the spread. Combined with a linear Hawkes process for spread opening events, we showed that the two phases exist. The main advantage of the linear Hawkes model lies in its analytical solutions. Using it and Laplace transforms, we were able to fully characterize the spread dynamics.

In **Chapter 5**, we proposed a mechanism for revealing liquidity in the order book, as an extension of the Latent Limit Order Book Model. Based on a reaction-diffusion framework, we analytically solved the shape of the stationary order book in some particular cases. In the general case, we used a numerical scheme to compute these shapes. We have shown that a condition for market stability exits, and that it is a condition which we can numerically quantify. Furthermore, we proposed a stability map as a function of the model's parameters. One key advantage of our model is the possibility to calibrate stationary order book shapes on empirical data. We calibrated the model on more than one hundred US stocks and have compared the obtained fits with the original shapes. We later plotted the stocks on the aforementioned stability map and confirmed that the "distance" to criticality varies according to the particular stock. We than quantified market impact within this framework. Impossible to solve analytically, we proposed a numerical approach, showing that the square root law holds.

The results, while very gratifying, lead to several open-ended questions that need to be resolved. On the empirical side, further research could be dedicated to calibrate GQ-Hawkes processes on more assets. Indeed, we focused on only a few liquid future contracts in **Chapter 2** and it would be interesting to look at equities, FX, commodities, cryptocurrencies and options as well. Nonetheless, this follow up research would require to adapt our calibration recipe to small tick assets. The reason for that is that on large tick assets (such as the future contracts presented in this work) the main activity is concentrated on the best quotes, but this premise does not hold for small tick assets. We could bypass a possible curse of dimentionality by considering a region around the best quotes, of a typical size of the average spread, and calibrate a GQ-Hawkes process on it. Since our calibrated kernels are power laws, we would like to do this calibration on longer time scales that cannot be done without dealing with overnight price changes. Concerning the effective spread, studying its dynamics in more detail should provide interesting results. Indeed, its behavior will be special around a liquidity crisis and will depend if this crisis is exogenous or endogenous. Understanding the behavior of effective spread, volatility and square price trends around the liquidity crisis point has not been tackled to date, and will give more results on the origins and causes for liquidity crises. Such results could be of particular interest to regulators, as well as for practitioners.

Introduced in **Chapter 3**, the Quadratic Santa Fe model opens many fields of research. First, we have had limited success in deriving the exponents we found. A simple mean-field approach did not provide the right ones, meaning that a deeper investigation into the dynamics is required. Further research should be devoted to computing them and it can also give rise to more theoretical reasonings for our numerical results. To match this transition with the near critical behavior of markets, we have briefly mentioned self-organized criticality without any theoretical justications. We believe that we can construct a model that mixes the Quadratic Santa Fe model, or at least in a simpler setting, and a game that will give self-organized criticality. Previous works have shown that introducing the appropriate dynamics can lead to SOC in certain phase transition. We believe that this result can be generalized

to our scenario. Further research should be devoted to this subject as there is a significant amount of empirical evidence pointing to the criticality of the market. On the empirical side, studies have shown that liquidity crises can arise simultaneously on different assets. For example, during the Flash Crash of May 6th 2010, many stocks suffered from a huge drop of price with very few orders on the bid side. We could think of several multi-dimensional extensions of the Quadratic Santa Fe Model that, by introducing the correct feedback, will help explain how this happens.

Concerning the simpler class model introduced in **Chapter 4**, while Hawkes-based model for price dynamics have been deeply investigated, coupling it with spread dynamics has not yet been tackled to our knowledge. Unfortunately, we have not been able to solve all the dynamics that we introduced above. Indeed, it seems that the asymptotic spread distribution is geometric in the case of constant rate of spread closing events and a linear Hawkes for spread opening events. We were not able to show it analytically, yet the numerical evidence leads us to believe that it can be proved. More generally, deriving this distribution in all cases will be very interesting. Another subject of interest would be to investigate the asymptotic dynamics when the market tends to criticality. We hope that the asymptotic spread distribution displays a non-trivial dynamics.

In **Chapter 5**, such development of latent limit order book models can lead to many possible extensions. From a theoretical point of view, one hypothesis of this model consists in a revealing an equal rate for all market participants, while in reality they are highly heterogeneous. Hence, an enhancement of this model would consider a distribution of revealing rates to account for high frequency traders and for long term investors. We believe that it will provide better fit of empirical order books. Concerning market impact, we have not achieved an analytical proof of the square root law but numerical findings suggest that it can be done. Further research could be dedicated to prove it analytically. One could also introduce quadratic price coupled with the revealing rate, in the manner of the Quadratic Santa Fe model, and then study the dynamics ofhow the market order flows impact liquidity. This model is not only interesting from an academic point of view but also from a practical one. We believe that it will provide interesting answers to liquidity forecasting and help with estimating trading costs.

We believe that all of these questions are both highly interesting as well as relevant. I truly hope that these questions will be all answered. I also hope that this thesis will lead to a better understanding of liquidity crises and perhaps even pave the way to reducing them and their intensity in the future.

APPENDICES

A

Technical details and additional results

We explain some technical details of Chapter 2, 3, 4 and 5. Concerning Chapter 2, we provide additional tricks to data analysis as well as the "raw" kernels of the GQ-Hawkes calibration. For Chapter 3, we explain the numerical procedure of the finite size scaling. Then we switch to the derivation of the probability density function of orders far from the mid-price and give some conditions of stationarity in the lack of market orders. We also detail all the computations of the analytical results of Chapter 4. We end by presenting calibration results of Chapter 5.

La différence entre l'amour et l'argent, c'est que si on partage son argent, il diminue, tandis que si on partage son amour, il augmente. L'idéal étant d'arriver à partager son amour avec quelqu'un qui a du pognon.

Philippe Geluck

A.1 Appendix of Chapter 2

Empirical Data and minimal setting calibration

We used tick-by-tick (or event-by-event) data for 4 futures contracts (EUROSTOXX, BUND, BOBL & SCHATZ) over around 160 trading days provided by CFM. We have chosen these assets because of their high liquidity and because they are all large tick (the spread is equal to its minimal value of 1 tick more than 99% of the time). Before doing any specific inference on the data, we preprocess it in the following way:

- We load data from 9am to 4pm.
- Separate events displaying the same timestamps are shuffled within the microsecond without breaking causality.
- We restrict to the best queues only.
- We use the mid-price changes in tick units.

The number of events after cleaning is of the order of one million per day for the most liquid asset, and 50 000 for the least liquid. First, we perform a non-parametric Hawkes calibration that gives the parameters $\tilde{\boldsymbol{\alpha}}_0$ and $\boldsymbol{\phi}$, as defined in Chapter 2.Then, we turn to the contribution of the trend and the volatility. To do so, we compute $\beta' F^{\mathrm{b+a}}_{\beta'}$, $\beta' H^{\mathrm{b+a}}_{\beta'}$, $\beta' F^{\mathrm{b-a}}_{\beta'}$, $\beta' H^{\mathrm{b-a}}_{\beta'}$, R_β and Σ^2_β, as defined in Section 2.2. For practical reasons, we approximate the kernels with a sum of three exponentials, in the spirit of [91], which allows for a fast algorithm thanks to the recursivity of the exponentially weighted moving averages. We associate a weight to each of these quantities that is the fraction of inter-event time, and bin the data in $100\times100\times100$-sized windows for $F^{\mathrm{b+a}}_{\beta'}$ with $H^{\mathrm{b+a}}_{\beta'}$, R_β, Σ^2_β and $F^{\mathrm{b-a}}_{\beta'}$ with $H^{\mathrm{b-a}}_{\beta'}$, R_β, Σ^2_β. We aggregate the weights to get a weight for each bin, and perform the regressions given in Eqs. (2.3) and (2.4) using a very standard generalised least square method [92]. We take the values of β and β' that maximise the absolute correlation $\mathrm{Cor}(F^{b+a}_{\beta'}, R^2_\beta)$.

GQ-Hawkes Estimation procedure

Here we show how to practically estimate the kernels presented in section 2.3 from empirical data. First, we detail the empirical estimators for averages and covariances, then focus on the time grids used for estimation, and finally discuss the numerical discretisation of Eqs. (2.6).

Covariance estimators We assume that we have a sample of events of type i that happen at times $\left(T^i_n\right)_n$, with $i = P$ for the price process. Calling T the total length of observation, the estimators of the average intensities read:

$$\Lambda^i \approx \frac{N^i_T}{T} \tag{A.1a}$$

$$\Delta_k \approx \frac{1}{T}\sum_n \left(\Delta_{T^P_n}\right)^k. \tag{A.1b}$$

For the covariance estimators, we use a classical approach for asynchronous data. Denoting Δt, Δx the time steps associated with times t and x, one has:

$$\chi^{ij}_{NN}(t) \approx \frac{1}{T\Delta t}\sum_{n,p} \mathbb{1}_{\{T^i_n - T^j_p \in [t-\Delta t/2, t+\Delta t/2]\}} - \Lambda^i\Lambda^j \tag{A.2a}$$

$$\chi^{i}_{NP}(t) \approx \frac{1}{T\Delta t}\sum_{n} \Delta_{T^P_p} \mathbb{1}_{\{T^i_n - T^P_p \in [t-\Delta t/2, t+\Delta t/2]\}} \tag{A.2b}$$

$$\chi^{i}_{NP^2}(t) \approx \frac{1}{T\Delta t}\sum_{n,p} \left(\Delta_{T^P_p}\right)^2 \mathbb{1}_{\{T^i_n - T^P_p \in [t-\Delta t/2, t+\Delta t/2]\}} - \Lambda^i\Delta_2 \tag{A.2c}$$

$$\chi^{i}_{NPP}(t,x) \approx \frac{1}{T^2\Delta t\Delta x}\sum_{n,p,q} \Delta_{T^P_p}\Delta_{T^P_q} \mathbb{1}_{\{T^i_n - T^P_p \in [t-\Delta t/2, t+\Delta t/2],\ T^i_n - T^P_q \in [x-\Delta x/2, x+\Delta x/2]\}} \tag{A.2d}$$

$$\chi_{P^2P^2}(t) \approx \frac{1}{T\Delta t}\sum_{n,p} \left(\Delta_{T^P_n}\right)^2 \left(\Delta_{T^P_p}\right)^2 \mathbb{1}_{\{T^P_n - T^P_p \in [t-\Delta t/2, t+\Delta t/2]\}} - \Delta_2^2. \tag{A.2e}$$

Note that, as mentioned above, one can choose different time grids for the Hawkes and price contributions. Symmetry properties of the covariances enable us to estimate them only for positive times:

- $\chi^{ij}_{NN}(-t) = \chi^{ji}_{NN}(t)$
- $\chi^{i}_{NP}(t) = 0$ and $\chi^{i}_{NP^2}(t) = 0$ for $t < 0$
- $\chi^{i}_{NPP}(t,x) = 0$ for $\min(t,x) < 0$
- $\chi_{P^2P^2}(-t) = \chi_{P^2P^2}(t)$.

One can reasonably assume that the covariances are $\mathcal{C}^1$ except in zero.

Choice of time grids A good choice of time grid to estimate the kernels is provided in [16]. Indeed, quadrature points in log-scale are well suited to accurately account for long range behaviour in the norm of the kernels. Consistently, it is advised to have time intervals increasing at the same rate as the grid of points we use. On the other hand, taking disjoint intervals $[t - \Delta t/2, t + \Delta t/2]$ enables fast computations of the covariances. To enforce all of this, we compute the differences between the quadrature points, sort them and take the cumulative sum. This gives the disjoint time intervals suited for fast computations. Then, with linear interpolation, we obtain the final values on the quadrature points.

Discretisation Equations (2.6) can be discretised in two different ways, using properties of the covariances and time grids. To show how to approximate the integrals, we provide an example of discretisation of $\int_{\mathbb{R}^+} f(s)ds$ for an arbitrary function f using the time grid (t_n). The two possibilities are:

- The quadrature technique: $\int_{\mathbb{R}^+} f(s)ds \approx \sum_n f(t_n)\, w_n$.
- The piece-wise $\mathcal{C}^1$ approximation: $\int_{\mathbb{R}^+} f(s)ds \approx \sum_n \frac{t_{n+1}-t_n}{2}\left[f(t_n^+) + f\left(t_{n+1}^-\right)\right]$, with $f(x^+) = \lim_{\substack{y\to x \\ y>x}} f(y)$ and $f(x^-) = \lim_{\substack{y\to x \\ y<x}} f(y)$.

The first approximation is very efficient to compute $\operatorname{Tr} K$ or $||\boldsymbol{\phi}||$ using (t^h_n) and (w^h_n). The second handles very well the behavior around zero and can be useful to solve Eq. (2.7).

Low rank approximation

The Zumbach approximation consists in a rank one symmetric contribution of the off-diagonal part of a symmetric kernel. But if we estimate such kernels on data, we cannot obtain a rank one kernel because of noise. So we present a method that cleans the quadratic kernel by taking a low rank approximation. First we explain a theoretical result for the best low rank approximation and then we discuss its numerical implementation.

A theoretical result

We choose a continuous symmetric kernel K such that $\int_{\mathbb{R}^2} K(t,s)dtds < +\infty$. We would like to find the best low rank symmetric function g such that $\int_{\mathbb{R}^2} \left(K(t,s) - g(t,s)\right)^2 dtds$ is minimum. For us, g is low rank symmetric if we can find k, $(\alpha_i)_{1\leq i\leq k}$ and $(g_i)_{1\leq i\leq k}$ linearly independent functions such that $g(t,s) = \sum_{i=1}^{k} \alpha_i g_i(t) g_i(s)$, $\int g_i(s)^2 ds = 1$ and $\alpha_i \neq 0$. In that case the rank of g is k. Thanks to linear algebra theory, we can provide a solution to this best low rank symmetric approximation.

We introduce the auto-adjoint operator $\mathcal{L}_K$ defined as $\mathcal{L}_K(f)(t) = \int_{\mathbb{R}} K(t,s)f(s)ds$ for a continuous function f such that $\int_{\mathbb{R}} f(s)^2 ds < +\infty$. In this appendix, we will restrict ourselves to this set of functions. The spectral theory tells us that there exists a family of eigenvalues and eigenvectors $(\mathcal{E}_n, Z_n)_{n\in\mathbb{N}}$ such that $\mathcal{L}_K(Z_n) = \mathcal{E}_n Z_n$, $\left|\left|Z_n^2\right|\right| = 1$ and that for any function f we can write $f = \sum_n c(f)_n Z_n$ with $c(f)_n = \int_{\mathbb{R}} f(s)Z_n(s)ds$. For simplicity, we assume that the eigenvalues are sorted such that $|\mathcal{E}_1| \geq |\mathcal{E}_2| \geq \ldots \geq |\mathcal{E}_n| \geq \ldots$. From this, we deduce that:

$$\forall t,s \quad K(t,s) = \sum_n \mathcal{E}_n Z_n(t) Z_n(s) \tag{A.3}$$

We consider a symmetric rank k function g. Using the above considerations, we have g_i linearly independent functions such that $g(t,s) = \sum_{i=1}^{k} \alpha_i g_i(t) g_i(s)$ and then:

$$\forall t,s \quad g(t,s) = \sum_{n,m} \left(\sum_{i=1}^{k} \alpha_i c(g_i)_n c(g_i)_m \right) Z_n(t) Z_m(s) \tag{A.4}$$

We call $a_{nm} = \sum_{i=1}^{k} \alpha_i c(g_i)_n c(g_i)_m$. As the $\alpha_i \neq 0$ and (g_i) linearly independent, we have k coefficients a_{nn} that are not equal to zero. A simple computation gives:

$$\int_{\mathbb{R}^2} \left(K(t,s) - g(t,s)\right)^2 dtds = \sum_n \left(a_{nn} - \mathcal{E}_n\right)^2 + \sum_{n\neq m} a_{nm}^2 \tag{A.5}$$

This quantity is minimal when $\forall n \neq m$, $a_{nm} = 0$ and $\forall n > k$, $a_{nn} = 0$, which corresponds to $g(t,s) = \sum_{i=1}^{k} \mathcal{E}_i Z_i(t) Z_i(s)$.

How do we use it in practice?

We have an estimator of the symmetric kernel K and we would like to clean it by taking a low rank approximation. To keep the same notation as before, (t_i) is the grid of time and (w_i) are the weights used to discretise the integral. Then, we have several possibilities that we can choose:

- Minimize $\sum_{i,j} \left(K(t_i,t_j) - g(t_i,t_j)\right)^2$, this consists, as before, by taking the first k eigenvalues and eigenvectors of the matrix $\left(K(t_i,t_j)\right)_{i,j}$.

- As $\int_{\mathbb{R}^2} (K(t,s) - g(t,s))^2 \, dtds \approx \sum_{i \neq j} (K(t_i, t_j) - g(t_i, t_j))^2 \, w_i w_j$ we minimize this to get the low rank approximation. Srebro *et al*[69] provides an algorithm that answers this problem.

The second option captures well slowly decreasing kernels. Nevertheless, when the tails of the kernels are noisy, it will give an important weight to noise and lead to incorrect results. To avoid this issue, we use the first option.

Additional plots and tables

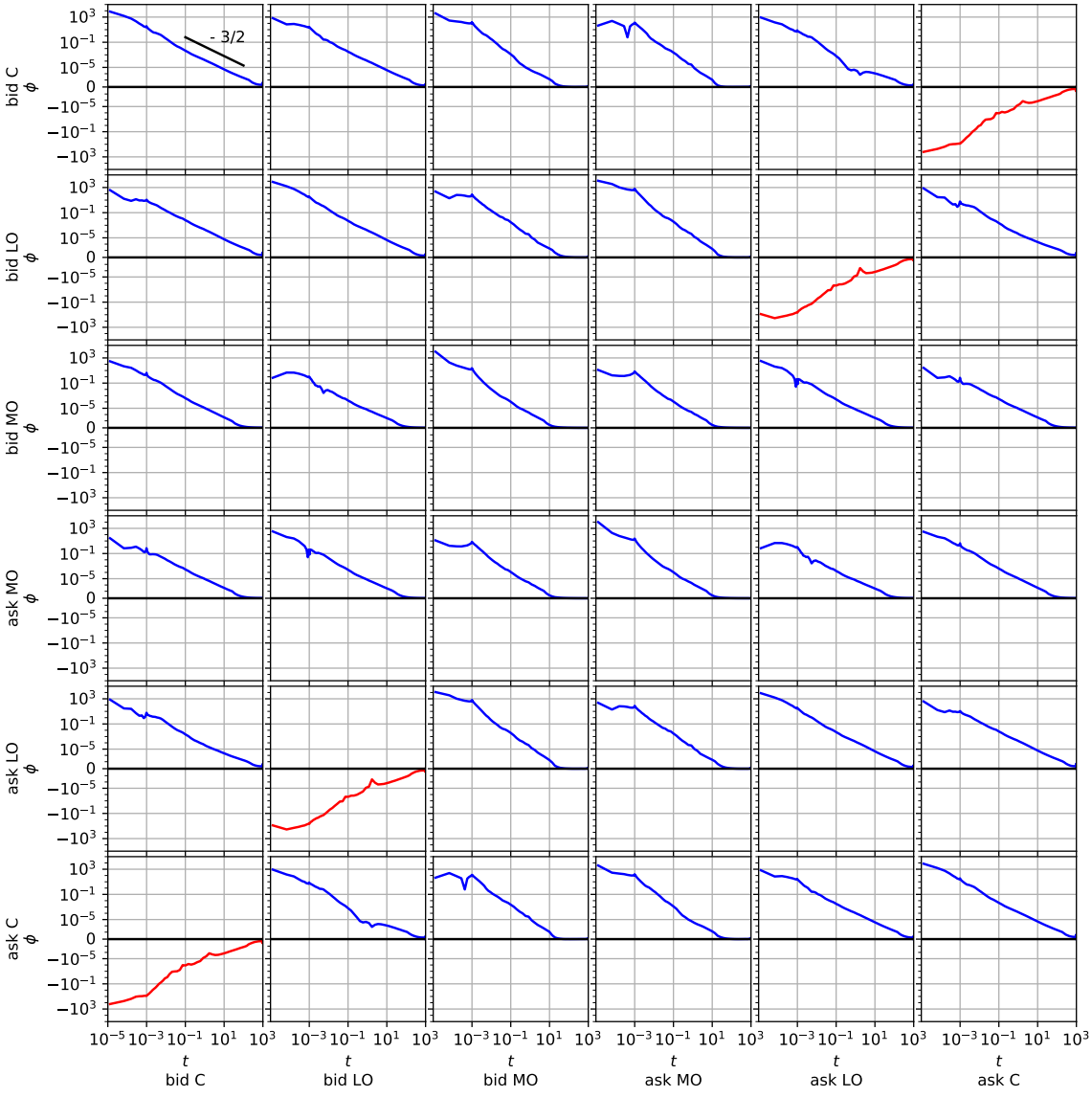

Figure A.1: Hawkes kernels for the EURO STOXX futures contract between 2016/09/12 and 2020/02/07 (t in seconds).

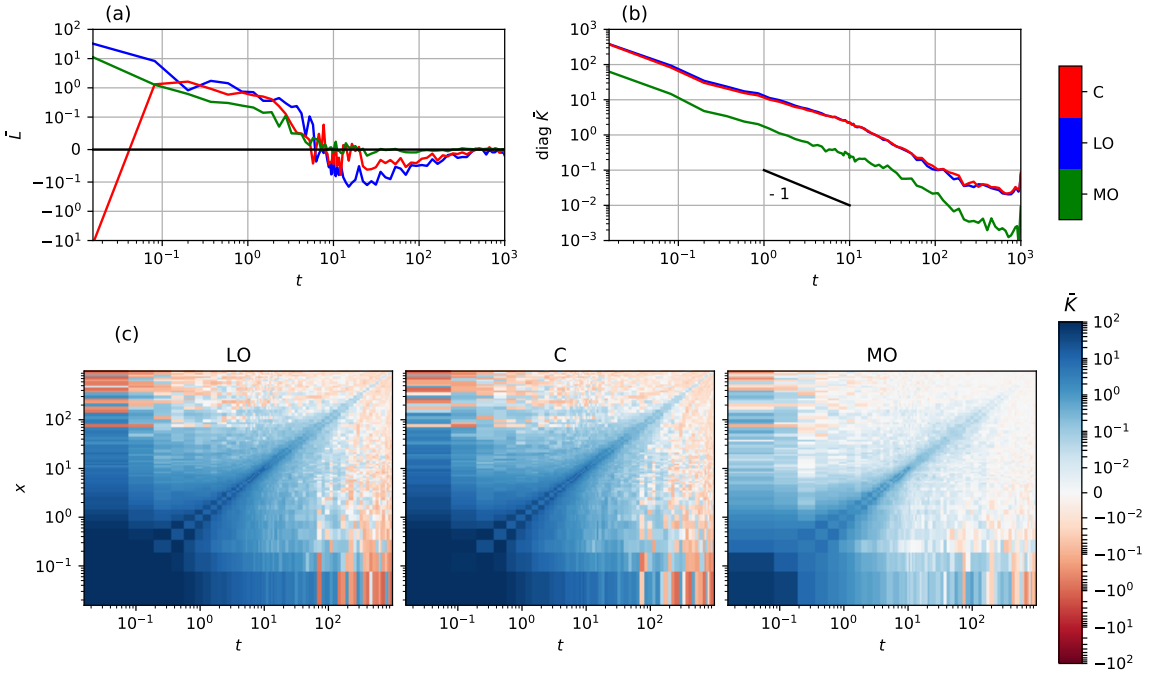

Figure A.2: *Raw effective kernels resulting from the calibration on the EURO STOXX futures contract between* 2016/09/12 *and* 2020/02/07*, without any smoothing procedure – compare with Fig. 2.7. (a) Linear kernels* $\bar{\boldsymbol{L}}$*. (b) Diagonal of quadratic kernels* $\bar{\boldsymbol{K}}_{\mathrm{d}}$*. (c) Full quadratic kernels* $\bar{\boldsymbol{K}}(t,x)$*.*

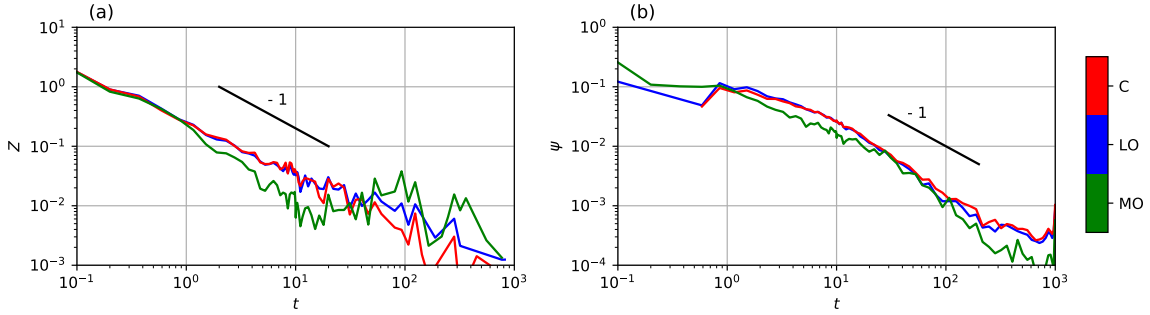

Figure A.3: *Zumbach approximation of the effective kernel* $\bar{\boldsymbol{K}}$ *on the EURO STOXX futures contract between* 2016/09/12 *and* 2020/02/07 *– without any smoothing procedure – compare with Fig. 2.8. (a) Zumbach kernel* $\boldsymbol{Z}$*, (b) Volatility kernel* $\boldsymbol{\psi}$*. Both kernels are normalised such that* $||\boldsymbol{\psi}|| = ||\boldsymbol{Z}^2|| = 1$*, with a cut-off in the time integrals at 1000 secs.*

A.2 Appendix of Chapter 3

Finite Size Scaling Method

Here, we discuss the method used to do the finite size scaling in Section 3.3. First, let's recall the framework. The susceptibility writes:

$$\chi(\alpha_K, T, N) = T^{\gamma} G\left(T(\alpha_K - \alpha_m(T,N))^{\zeta}\right) = T^{\gamma}\mathcal{G}\left(NT^{-1/\eta}, T^{1/\zeta}(\alpha_K - \alpha^*)\right) , \quad \text{(A.6)}$$

where the function $\mathcal{G}$ satisfies:

- $\lim_{|y|\to+\infty} \mathcal{G}(x,y) = 0$
- $\forall x, \quad y \mapsto \mathcal{G}(x,y)$ has a unique maximum, denoted $y^*(x)$.

First, we determine γ. We introduce $\alpha_m(T,N) =_{\alpha_K} \chi(\alpha_K, T, N)$ and we assume that $\lim_{T,N\to\infty} \alpha_m(T,N) = \alpha^*$. The idea is to look at $\max_{\alpha_K} \chi(\alpha_K, T, N) = \chi(\alpha_m(T,N), T, N)$:

$$\chi(\alpha_m(T,N),T,N) = T^{\gamma} \max_y \mathcal{G}(NT^{-1/\eta}, y) \underset{N\to+\infty}{\longrightarrow} T^{\gamma} \lim_{x\to+\infty} \max_y \mathcal{G}(x,y) \ . \quad \text{(A.7)}$$

If $N_{max}^{\eta} \gg T$, then $\chi(\alpha_m(T,N_{max}),T,N_{max}) \approx T^{\gamma} \lim_{x\to+\infty} \max_y \mathcal{G}(x,y)$ on our range of T. Note that the validity of such a hypothesis depends on the value of η, which we shall determine and self-consistently validate below. Then we compute the value of $\gamma \approx 2$ from a linear regression of $\log \chi(\alpha_m(T,N_{max}),T,N_{max})$ vs. $\log T$.

Then we determine ζ. If T, N_{max} are large enough that $N_{max}^{\eta} \gg T$, then $T^{1/\zeta}(\alpha_K - \alpha_m(T,N_{max})) \approx T^{1/\zeta}(\alpha_K - \alpha^*)$ and $\chi(\alpha_K, T, N_{max}) \approx T^{\gamma} \lim_{x\to+\infty} \mathcal{G}(x, T^{1/\zeta}(\alpha_K - \alpha^*))$. So we plot $\chi(\alpha_K, T, N_{max})$ as a function of $T^{1/\zeta}(\alpha_K - \alpha_m(T,N_{max}))$ for different values of T and α and we tune the exponent ζ to make all the curves collapse together, see Fig. 3.4. We can do this experiment numerically by minimising the distance between the curves as a function of ζ. Adding the fact that we expect regular rational values we deduce the most likely exponent, $\zeta = 3$, see right inset of Fig. 3.4.

Finally, we compute α^* and η. By definition of $\alpha_m(T,N)$, one has $T^{1/\zeta}(\alpha_m(T,N) - \alpha^*) = y^*(NT^{-1/\eta})$. Thus, if one plots $T^{1/\zeta}(\alpha_m(T,N) - \alpha^*)$ as a function of $NT^{-1/\eta}$ for different values of T and N, one should find a set of parameters η and α^* such that all the curves collapse together. This leads to $\alpha^* \approx 6.3 \times 10^{-2}$ and $\eta \approx 3$, which is compatible with the direct result on the spread dynamics shown in Fig. 3.2, where one observes that $S(t) \sim t^{1/3}$. But since the finite size-finite time crossover should occur when $S(T) \sim N$, one finds that $T^{1/3} \sim N$, again leading to $\eta \approx 3$.

		C	LO	MO
$V \operatorname{Tr} \bar{K}\Delta_2$	EUROSTOXX	20.4	18.8	2.1
	BUND	5.7	6.6	1.7
$V\bar{K}_1\Delta_2$	EUROSTOXX	9.7	8.6	0.5
	BUND	3.5	4.6	0.7
$V\bar{K}_{\mathrm{d}}\Delta_2$	EUROSTOXX	10.7	10.1	1.6
	BUND	2.2	2.1	1.0

Table A.1: Quadratic, Zumbach and volatility contributions to the liquidity rate of events (in shares per second).

	t (s)	C	LO	MO
α_0^i/Λ^i	10	0.25	0.14	0.29
	100	0.24	0.14	0.27
	1000	0.23	0.13	0.27
$\Delta_2 \operatorname{Tr} K^i/\Lambda^i$	10	0.04	0.03	0.03
	100	0.05	0.03	0.04
	1000	0.06	0.04	0.05
$\Delta_2 \operatorname{Tr} \bar{K}^i/\Lambda^i$	10	0.15	0.16	0.14
	100	0.23	0.23	0.21
	1000	0.28	0.28	0.24
$\alpha_0^i/\sum_j \|\|\phi_{ij}\|\|\Lambda^j$	10	0.35	0.17	0.42
	100	0.34	0.17	0.40
	1000	0.32	0.16	0.40
$\Delta_2 K_1^i/\sum_j \|\|\phi_{ij}\|\|\Lambda^j$	10	0.06	0.05	-0.01
	100	0.06	0.05	-0.01
	1000	0.06	0.05	-0.01
$\Delta_2 K_{\mathrm{d}}^i/\sum_j \|\|\phi_{ij}\|\|\Lambda^j$	10	-0.01	-0.01	0.06
	100	0.0	-0.01	0.08
	1000	0.02	0.0	0.08
$\Delta_2 \bar{K}_1^i/\Lambda^i$	10	0.13	0.13	0.05
	100	0.13	0.13	0.05
	1000	0.13	0.13	0.05
$\Delta_2 \bar{K}_{\mathrm{d}}^i/\Lambda^i$	10	0.02	0.03	0.09
	100	0.10	0.11	0.16
	1000	0.15	0.15	0.19

Table A.2: Different ratios between the quadratic contributions, base rates and Hawkes contributions, truncated at different time scales $t(s)$ for the EURO STOXX futures contract between 2016/09/12 and 2020/02/07. The top three entries are the most important ones. For sake of simplicity, we have here approximated $\boldsymbol{K}_1$ as $(1 - ||\boldsymbol{\phi}||)\,\bar{\boldsymbol{K}}_1$ and $\boldsymbol{K}_{\mathrm{d}}$ as $(1 - ||\boldsymbol{\phi}||)\,\bar{\boldsymbol{K}}_{\mathrm{d}}$.

Asymptotic properties of the Quadratic Santa Fe Model

We look at the distribution of number of orders far from the mid-price, as well as the gap between two occupied price levels. Due to the past price coupling, conditioning on the price information is the only way to have some tractable computations.

Law of $v_t(\infty)|\mathcal{F}_t^{\mathrm{P}}$

We derive Eq. (3.5) using the master equation:

$$\begin{aligned}
\rho_v(t+dt,n) &= \mathbb{P}\left[v_{t+dt}(\infty) = n \middle| \mathcal{F}_{t+dt}^{\mathrm{P}}\right] \qquad \text{(A.8)}\\
&= \mathbb{P}\left[dv_t(\infty) = 1 \middle| \mathcal{F}_t^{\mathrm{P}}, v_t(\infty) = n-1\right] \mathbb{P}\left[v_t(\infty) = n-1 \middle| \mathcal{F}_{t+dt}^{\mathrm{P}}\right]\\
&\quad + \mathbb{P}\left[dv_t(\infty) = -1 \middle| \mathcal{F}_t^{\mathrm{P}}, v_t(\infty) = n+1\right] \mathbb{P}\left[v_t(\infty) = n+1 \middle| \mathcal{F}_{t+dt}^{\mathrm{P}}\right]\\
&\quad + \mathbb{P}\left[dv_t(\infty) = 0 \middle| \mathcal{F}_t^{\mathrm{P}}, v_t(\infty) = n\right] \mathbb{P}\left[v_t(\infty) = n \middle| \mathcal{F}_{t+dt}^{\mathrm{P}}\right] + o(dt)\\
&= \lambda dt \rho_v(t,n-1) + \nu_t(n+1)\rho_v(t,n+1) + (1 - \lambda dt - \nu_t n dt)\rho_v(t,n) + o(dt)
\end{aligned}$$

we take the limit $dt \to 0$ and get Eq. (3.5).

We can solve it by injecting the solution given in Eq.(3.5) and verifying that it works. Here we are going to present a more general method that solves this equation for any initial

solution. First we consider the generating function $\hat{\rho}_v(t,z) = \sum_{n\geq 0} z^n \rho_v(t,n)$. By multiplying Eq.(3.5) by z^n and summing over n we get the following PDE:

$$\partial_t \hat{\rho}_v = \lambda(z-1)\hat{\rho}_v - \nu_t(z-1)\partial_z \hat{\rho}_v \tag{A.9}$$

We do a change of variable $u = \log(z-1)$ and get:

$$\partial_t \hat{\rho}_v = \lambda e^u \hat{\rho}_v - \nu_t \partial_u \hat{\rho}_v \tag{A.10}$$

Now we can apply the characteristic method: we look for a solution $\hat{\rho}_v(t,u(t))$. In order to get rid of the term in ∂_u we take $u(t) = u_0 + \int_0^t \nu_s ds$ and get:

$$\hat{\rho}_v(t,u(t)) = f(u_0)\exp\left(\lambda e^{u_0}\int_0^t e^{\int_0^s \nu_x dx} ds\right) \tag{A.11}$$

where f is a function. We can rewrite it as:

$$\hat{\rho}_v(t,u) = f\left(u - \int_0^t \nu_s ds\right)\exp\left(\lambda e^u \int_0^t e^{-\int_s^t \nu_x dx} ds\right) \tag{A.12}$$

And switching back to the variable z:

$$\hat{\rho}_v(t,z) = f\left(\log(z-1) - \int_0^t \nu_s ds\right)\exp\left(\lambda(z-1)\int_0^t e^{-\int_s^t \nu_x dx} ds\right) \tag{A.13}$$

By taking $t = 0$, we get the function f as a function of the initial condition. It reads:

$$\hat{\rho}_v(t,z) = \hat{\rho}_v\left(0, 1 + (z-1)e^{-\int_0^t \nu_s ds}\right)\exp\left(\lambda(z-1)\int_0^t e^{-\int_s^t \nu_x dx} ds\right) \tag{A.14}$$

When the initial condition is a Poisson distribution of parameter V^*, it gives $\hat{\rho}_v(0,z) = e^{V^*(z-1)}$ and so $\hat{\rho}_v(t,z) = e^{V_t^*(z-1)}$.

Law of the gap between two occupied price level

We compute the law of the gap ΔG_t far from the mid price and conditioned to $\mathcal{F}_t^{\mathrm{P}}$. Let's consider an occupied price level. The probability of having a gap greater or equal than n is the probability that the next $n-1$ level are empty. As those levels are mutually independent and follow a Poisson distribution of parameter V_t^*, we get that this probability is $e^{-(n-1)V_t^*}$. We immediately get that the gap is geometrically distributed with parameter $1 - e^{-V_t^*}$, shifted by one:

$$\mathbb{P}\left[\Delta G_t = n \middle| \mathcal{F}_t^{\mathrm{P}}\right] = \left(1 - e^{-V_t^*}\right)e^{-(n-1)V_t^*}, \quad n \geq 1 \tag{A.15}$$

A condition of transition when $\mu = 0$

We decide not to take into account market orders ($\mu = 0$) for simplicity. If we neglect memory effects coming from spread insertions, the distribution of the gap holds for the whole order book. In order to remain general, we assume that:

$$\nu_t = \nu_0 + \int_0^t \int_0^t K(t-s, t-u) dP_s dP_u \tag{A.16}$$

We can easily compute the probability that the spread changes and get:

$$\mathbb{P}\left[dS_t = n \middle| \mathcal{F}_t^{\mathrm{P}}\right] = \left(1 - e^{-V_t^*}\right) e^{-(n-1)V_t^*} \times \nu_t e^{-V_t^*} dt \tag{A.17a}$$

$$\mathbb{P}\left[dS_t = -1 \middle| \mathcal{F}_t^{\mathrm{P}}\right] = \lambda\, \mathbb{P}\left[S_t > 1 \middle| \mathcal{F}_t^{\mathrm{P}}\right] dt \tag{A.17b}$$

Then we deduce:

$$\mathbb{P}\left[dS_t \middle| \mathcal{F}_t^{\mathrm{P}}\right] = \frac{\nu_t}{e^{V_t^*} - 1} - \lambda\, \mathbb{P}\left[S_t > 1 \middle| \mathcal{F}_t^{\mathrm{P}}\right] \tag{A.18a}$$

$$\mathbb{E}\left[d[S]_t \middle| \mathcal{F}_t^{\mathrm{P}}\right] = \frac{\nu_t \left(1 + e^{-V_t^*}\right)}{e^{V_t^*} - 1} + \lambda\, \mathbb{P}\left[S_t > 1 \middle| \mathcal{F}_t^{\mathrm{P}}\right] \tag{A.18b}$$

where $[S]$ is the quadratic variation of S *i.e.* $d[S]_t = (dS_t)^2$. A condition for equilibrium is that, when $t \to \infty$, the spread is stable *i.e.* $\mathbb{E}[dS_t] = 0$. It gives:

$$\lambda \mathbb{P}\left[S > 1\right] = \lim_{t \to +\infty} \mathbb{E}\left[\frac{\nu_t}{e^{V_t^*} - 1}\right] \tag{A.19}$$

The transition occurs when $\mathbb{P}\left[S > 1\right] = 1$.

Let's turn to the dynamics of ν_t. Thanks to the bid/ask symmetry, we have that the price is a $\mathcal{F}^{\mathrm{P}}$-martingale. On the other hand, we have $[S]_t = 2[P]_t$. Then it reads that:

$$\mathbb{E}[\nu_t] = \nu_0 + \frac{1}{2} \int_0^t K(t-s, t-s) \left(\mathbb{E}\left[\frac{\nu_s \left(1 + e^{-V_s^*}\right)}{e^{V_s^*} - 1}\right] + \lambda \mathbb{P}\left[S_s > 1\right] \right) ds \tag{A.20}$$

Assuming equilibrium and calling $\alpha_K = \operatorname{Tr} K$, we have:

$$\lim_{t \to +\infty} \mathbb{E}[\nu_t] = \nu_0 + \frac{\alpha_K}{2} \left(\lim_{t \to +\infty} \mathbb{E}\left[\frac{\nu_t \left(1 + e^{-V_t^*}\right)}{e^{V_t^*} - 1}\right] + \lambda \mathbb{P}\left[S > 1\right] \right) \tag{A.21}$$

While using a mean-field approach seems to be natural, it will not give the good exponents. A more rigorous approach of those equations is required to compute them.

A.3 Appendix of Chapter 4

More on the Linear Spread Model

Here, we focus on the linear case ($\epsilon = 0$), see Eq. (4.15). In order to remain very general we rewrite the equation as $\lambda_t^+ = \lambda_0^+ + (\phi * dS^+)_t = \lambda_0^+ + \int_0^t \phi(t-s) dS_s^+$. Point process theory teaches us that there exists two independent martingales M_t^- and M_t^+ such that $S_t^\pm = \lambda_t^\pm dt + dM_t^\pm$. One can write:

$$\lambda_t^+ = \lambda_0^+ + \left(\phi * \lambda^+\right)_t + \left(\phi * dM^+\right)_t \ . \tag{A.22}$$

Assuming that $||\phi|| < 1$ one can define the resolvent $\mathcal{R} = \sum_{n \geq 1} \phi^{*n}$, with $\phi^{*(n+1)} = \phi * \phi^{*n}$. Note that $(\delta + \mathcal{R}) * \phi = \mathcal{R}$ with δ the Dirac function. This enables to invert the above equation and obtain:

$$\lambda_t^+ = \left(1 + \int_0^t \mathcal{R}(s) ds\right) \lambda_0^+ + \left(\psi * dM^+\right)_t \ . \tag{A.23}$$

Combining the previous equations and introducing the martingale M_t with $dM_t = dM_t^+ - dM_t^- + (\mathcal{R} * dM^+)_t dt$, one gets:

$$S_t = S_0 + \int_0^t \left[\left(1 + \int_0^s \mathcal{R}(u) du \right) \lambda_0^+ - \mathbb{1}_{\{S_s \geq 2\}} \lambda_0^- \right] ds + M_t \ . \tag{A.24}$$

Equation (4.2) is the particular case with $\phi(t) = \alpha\beta e^{-\beta t}$. Choosing such a kernel one can derive the Fokker-Planck equation for the joint distribution of the variables $(S_t, X_t = \beta \int_0^t e^{-\beta(t-s)} dS_t^+)$ given in Eq. (4.3). While we did not manage to solve this equation, we can compute the Laplace transform of the variable X_t at equilibrium:

$$\mathbb{E}\left[e^{-uX}\right] = \int_{\mathbb{R}^+} \rho_X^{st}(x) e^{-ux} dx = \exp\left(\int_0^u \frac{\lambda_0^+ \left(1 - e^{-\beta v}\right)}{\alpha\left(1 - e^{-\beta v}\right) - \beta v} dv \right) \ , \tag{A.25}$$

from which we can get the cumulants. In particular, one has: $\mathbb{E}[X] = \lambda_0^+/(1-\alpha)$ and $\mathbb{V}[X] = \beta\lambda_0^+/(2(1-\alpha)^2)$. Interestingly, we can get the full stationary solution ρ^{st} in two simple limit:

- $\alpha = 0$: $\rho^{st}(S, x) = (1-r) r^S \rho_X^{st}(x)$ with $r = \lambda_0^+/\lambda_0^-$.
- $\beta \to 0$: $\rho^{st}(S, x) = \delta\left(x - \frac{\lambda_0^+}{1-\alpha}\right)(1-r) r^S$ with $r = \frac{1-\alpha_c}{1-\alpha}$.

Note that the spread is geometrically distributed in both cases.

More on the Stabilizing Mechanism

Derivation of spread moments

We remain very general and follow the hypotheses of model in Appendix A.3 for λ_t^+. Keeping the same definition of resolvent, it leads to Eq. (A.23). Noticing that λ_t^- follows a first order ODE:

$$\lambda_t^- = \lambda_0^-(S_t^+ - M_t^-)dt - \lambda_0^- \int_0^t \lambda_s^- ds \tag{A.26}$$

we can solve it easily. By combining it with Eq. (A.23), we get:

$$\begin{aligned} S_t =& 1 + e^{-\lambda_0^- t}(S_0 - 1) + \lambda_0^+ \int_0^t ds e^{-\lambda_0^-(t-s)} \left[1 + \int_0^s \mathcal{R}(u) du \right] ds \\ &+ \int_0^t ds e^{-\lambda_0^-(t-s)} \left[1 + \int_0^{t-s} \mathcal{R}(u) e^{\lambda_0^- u} du \right] dM_s^+ - \int_0^t ds e^{-\lambda_0^-(t-s)} dM_s^- \end{aligned} \tag{A.27}$$

Computing the average spread at equilibrium is straight forward and the variance uses the following properties $\mathbb{E}\left[\left(\int_0^t f(s) dM_s^\pm\right)^2\right] = \int_0^t f(s)^2 \mathbb{E}\left[\lambda_s^\pm\right] ds$ for some regular enough function f and $\mathbb{E}\left[\int_0^t \int_0^t dM_s^+ dM_s^-\right] = 0$.

Derivation of Laplace transform of (S_t^+, S_t^-)

We split the proof in two parts: first we deal with the heterogeneous Poisson case and then we tackle the general case.

The heterogeneous Poisson case In this subsection only, we assume that S^+ is a heterogeneous Poisson process of intensity $\tilde{\lambda}(t)$. Then, we have:

$$de^{-xS_t^+ - yS_t^-} = e^{-xS_t^+ - yS_t^-}(e^{-x}-1)dS_t^+ + e^{-xS_t^+ - yS_t^-}(e^{-y}-1)dS_t^- \tag{A.28}$$

Then:

$$\mathbb{E}\left[de^{-xS_t^+ - yS_t^-}\right] = \mathbb{E}\left[e^{-xS_t^+ - yS_t^-}(e^{-x}-1)\tilde{\lambda}(t)dt + \lambda_0^- e^{-xS_t^+ - yS_t^-}(e^{-y}-1)(S_t^+ - S_t^-)dt\right] \tag{A.29}$$

And so we get, by calling $\mathcal{D}^0_{\tilde{\lambda}}(x,y,t) = \mathbb{E}\left[e^{-xS_t^+ - yS_t^-}\right]$, the following PDE:

$$\partial_t \mathcal{D}^0_{\tilde{\lambda}} = \tilde{\lambda}(t)(e^{-x}-1)\mathcal{D}^0_{\tilde{\lambda}} + \lambda_0^-(e^{-y}-1)\left(\partial_y \mathcal{D}^0_{\tilde{\lambda}} - \partial_x \mathcal{D}^0_{\tilde{\lambda}}\right) \tag{A.30}$$

with initial condition $\mathcal{D}^0_{\tilde{\lambda}}(x,y,0) = 1$. Note that we have chosen to write in index the base rate of the Poisson process. With a change of variable $u = x+y,\ v = ln\,(e^y - 1)$ and using the characteristic method we can solve this PDE and find:

$$\mathcal{D}^0_{\tilde{\lambda}}(x,y,t) = \exp\left(\left[e^{-(x+y)}-1\right]\int_0^t \tilde{\lambda}(s)ds + e^{-(x+y)}\left[e^y - 1\right]\int_0^t \tilde{\lambda}(s)e^{-\lambda_0^-(t-s)}ds\right) \tag{A.31}$$

The general case The setup is much more complex because of the Hawkes process: the paper of El Euch *et al*[82] tells us how to deal with it. The Hawkes process can be seen as a migrant process: each event gives birth to a heterogeneous poisson process of rate $\phi(t)$. Calling $S_t^{+,0}$ the heterogeneous poisson process of rate $\lambda_0^+(t)$ and $T_1, \ldots, T_n, \ldots$ its time of events, we introduce $S_t^{+,n}$ the number of child events from the $n-$th event of $S_t^{+,0}$. We have the following equality in law:

$$S_t^+ = S_t^{+,0} + \sum_{n=1}^{S_t^{+,0}} S_t^{+,n} = S_t^{+,0} + \sum_{n=1}^{S_t^{+,0}} \overline{S}^{+,n}_{t-T_n} \tag{A.32}$$

where $\overline{S}^{+,n}$ are iid processes, independent of $S^{+,0}$. Note that the processes $\overline{S}^{+,n}$ are Hawkes processes of base intensity $\phi(t)$ and kernel ϕ.

We apply the same idea on the joint process (S^+, S^-), we can write the following equality in law:

$$S_t^- = S_t^{-,0} + \sum_{n=1}^{S_t^{+,0}} S_t^{-,n} = S_t^{-,0} + \sum_{n=1}^{S_t^{+,0}} \overline{S}^{-,n}_{t-T_n} \tag{A.33}$$

where the processes $S_t^{-,n}$ have for stochastic intensity $\lambda_0^-\left(S_t^{+,n} - S_t^{-,n}\right)$. And we have that $\left(\overline{S}^{+,n}, \overline{S}^{-,n}\right)$ are iid processes, independent of $\left(S^{+,0}, S^{-,0}\right)$. Then we have:

$$\mathbb{E}\left[e^{-xS_t^+ - yS_t^-}\middle| S^{+,0}, S^{-,0}\right] = e^{-xS_t^{+,0} - yS_t^{-,0}} \prod_{n=1}^{S^{+,0}} \overline{\mathcal{L}}\,(x,y,t-T_n) \tag{A.34}$$

with $\overline{\mathcal{D}}(x,y,t) = \mathbb{E}\left[e^{x\overline{S_t}^{+,1} + y\overline{S_t}^{-,1}}\right]$. Now, conditionally to $S_t^{+,0}$, the variables $(T_1, ..., T_{S_t^{+,0}})$ have the same law as $(X_(1), ..., X_{(S_t^{+,0})})$ the order statistics built from iid variables $(X_1, .., X_{S_t^{+,0}})$ with density $\lambda_0^+(s)/\int_0^t \lambda_0^+(s)ds$. We get then:

$$\mathbb{E}\left[e^{-xS_t^+ - yS_t^-}\middle| S_t^{+,0}, S_t^{-,0}\right] = e^{-xS_t^{+,0} - yS_t^{-,0}}\left(\int_0^t \overline{\mathcal{D}}\,(x,y,t-s)\,\frac{\lambda_0^+(s)}{\int_0^t \lambda_0^+(u)du}\right)^{S_t^{+,0}} \tag{A.35}$$

And now we have:

$$\mathcal{D}(x,y,t) = \mathcal{D}^0_{\lambda_0^+}\left(x - \ln\left(\int_0^t \overline{\mathcal{D}}\left(x,y,t-s\right)\frac{\lambda_0^+(s)}{\int_0^t \lambda_0^+(u)du}ds\right), y, t\right) \tag{A.36}$$

We can do this analysis again to compute $\overline{\mathcal{D}}$ using the decomposition of Eq.(4.1) and Eq.(A.33) applied on $\left(\overline{S}^{+,1}, \overline{S}^{-,1}\right)$. What changes between those processes is the base rate. Indeed, the base rate of $S^{+,0}$ is λ_0^+ while the base rate of $\overline{S}^{+,1}$ is ϕ. So we deduce:

$$\overline{\mathcal{D}}(x,y,t) = \mathcal{D}^0_{\phi}\left(x - \ln\left(\int_0^t \overline{\mathcal{D}}\left(x,y,t-s\right)\frac{\phi(s)}{\int_0^t \phi(u)du}ds\right), y, t\right) \tag{A.37}$$

We can rewrite those equations using Eq.(A.31):

$$\begin{aligned}
\mathcal{D}(x,y,t) &= \exp\left(\lambda_0^+\left[e^{-(x+y)}\int_0^t \overline{\mathcal{D}}(x,y,s)ds - t\right]\right) && \text{(A.38a)}\\
&\quad\times\exp\left(\frac{\lambda_0^+}{\lambda_0^-}e^{-x}\left[1-e^{-y}\right]\left[\frac{1-e^{-\lambda_0^- t}}{t}\right]\int_0^t \overline{\mathcal{D}}(x,y,s)ds\right)\\
\overline{\mathcal{D}}(x,y,t) &= \exp\left(\int_0^t \phi(s)\left[e^{-(x+y)}\overline{\mathcal{D}}(x,y,t-s) - 1\right]ds\right) && \text{(A.38b)}\\
&\quad\times\exp\left(e^{-x}\left[1-e^{-y}\right]\int_0^t \overline{\mathcal{D}}(x,y,t-s)\phi(s)ds\frac{\int_0^t e^{-\lambda_0^-(t-s)}\phi(s)ds}{\int_0^t \phi(s)ds}\right)
\end{aligned}$$

that ends the proof.

More on the Model with Price Feedback on the Spread

The proof of such results uses the same techniques as in the previous appendix but is slightly more complex. First of all, there exits four martingales $M_t^{-,b}$, $M_t^{+,b}$, $M_t^{-,a}$ and $M_t^{+,a}$ such that:

$$db_t^{\pm} = \lambda_t^{\pm}dt/2 + dM_t^{\pm,b},\ da_t^{\pm} = \lambda_t^{\pm}dt/2 + dM_t^{\pm,a} \tag{A.39}$$

Note that we have:

$$\begin{aligned}
dS_t &= da_t^+ + db_t^+ - da_t^- + db_t^-\\
dP_t &= \left(da_t^+ - da_t^- + db_t^- - db_t^+\right)/2 && \text{(A.40)}\\
d[P]_t &= (dP_t)^2 = \left(da_t^+ + da_t^- + db_t^- + db_t^+\right)/4\ .
\end{aligned}$$

We then use Eq. (4.14) in a more general framework:

$$\lambda_t^+ = \lambda_0^+ + \int_0^t\int_0^t K(t-s,t-u)dP_s dP_u\ , \tag{A.41}$$

where K is symmetric. Calling $\alpha = \operatorname{Tr} K = \int_0^{+\infty} K(t,t)dt$, one can rewrite:

$$\lambda^+ = \lambda_0^+ + \int_0^t K(t-s,t-s)d[P]_s + M_t^P = \lambda_0^+ + \left(\phi * (\lambda^+ + \lambda^-)\right)_t + \frac{1}{2}\left(\phi * (M^+ + M^-)\right)_t + M_t^P\ , \tag{A.42}$$

where $\phi(t) = K(t,t)/2$, $M_t^{\pm} = M_t^{\pm,a} + M_t^{\pm,b}$ and $M_t^P = \int_0^t \left(\int_0^{s-} K(t-s,t-u)dP_u\right)dP_s$, that is a martingale. Introducing the resolvent $\mathcal{R} = \sum_{n\geq 1}\phi^{*n}$ and the martingale:

$$dM_t = \left[\left(\mathcal{R} * (M^+ + M^-)\right)_t/2 + \left((\delta + \mathcal{R}) * M^P\right)_t\right]dt,$$

we solve the equation:

$$\lambda_t^+ = \left(1 + \int_0^t \mathcal{R}(s)ds\right)\lambda_0^+ + \left(\mathcal{R} * \lambda^-\right)_t + dM_t \ , \tag{A.43}$$

and deduce the dynamics of the spread:

$$S_t = S_0 + \int_0^t \left[\lambda_0^+\left(1 + \int_0^s \mathcal{R}(u)du\right) - \lambda_0^- \mathbb{1}_{\{S_s \geq 2\}}\left(1 - \int_0^{t-s}\mathcal{R}(u)du\right)\right]ds + M_t \ . \tag{A.44}$$

This gives the condition of stability: if $\alpha < \alpha_c$ then $\mathbb{P}[S \geq 2] = (1-\alpha_c)/(1-\alpha)$. Then we get the diffusivity of the price:

$$\lim_{t\to+\infty}\frac{1}{t}\mathbb{E}[[P]_t] = \lim_{t\to+\infty}\frac{1}{2}\left(\mathbb{E}[\lambda_t^+ + \lambda_t^-]\right) = \frac{\lambda_0^+ + \lambda_0^-\mathbb{P}[S\geq 2]}{2(1-||\phi||)}$$

One can check that $||\phi|| = \alpha/2$.

Metastability – some analytical results

In the "slow limit", the intensity is approximately constant and thus the point process can be locally approximated by a poisson process. The time continuous version of it is the CIR like process given in Eq. (4.18). The associated Fokker-Planck equation is:

$$\partial_t\rho = \partial_x\left(-\mathcal{V}'\rho\right) + \partial_{xx}(D\rho)$$

Proof of Eq.(4.20)

We derive this expression using the formalism explained in [83]. ρ does not reach a stationary solution because of the expressions of $\mathcal{V}$ and D. The idea of this computation consists in solving the stationarized equation:

$$-J^* - \mathcal{V}'\rho^{st} + \partial_x(D\rho^{st}) = 0 \tag{A.45}$$

where J^* is such that $\int \rho^{st} = 1$. Let's interpret the dynamics of the system to understand why we solve Eq. (A.46). The potential interpretation of this dynamics tells us that the particle is trapped in a local minimum X_{eq} and if we wait long enough it will escape it by crossing an energy barrier $\mathcal{V}(X^*) - \mathcal{V}(X_{\text{eq}})$. So, we can interpret J^* as the flux of particles that loops from X^* to X_{eq} in order to make the dynamics stable.

The only stable solution of Eq. (A.46) is:

$$\rho^{st}(X) = \frac{J^*}{D(X)}\int_0^X \exp\left(\int_x^X \frac{\mathcal{V}'(y)}{D(y)}dy\right)dx \tag{A.46}$$

The average time to cross this energy barrier is given from the flux J^*:

$$\mathbb{E}[\tau_c] = J^{*-1} = \int_0^{+\infty}\frac{1}{D(X)}\int_0^X \exp\left(\int_x^X \frac{\mathcal{V}'(y)}{D(y)}dy\right)dxdX \tag{A.47}$$

Eq.(A.47) is tractable only in very special cases and unfortunately not in ours. Nevertheless, we can do an expansion when the energy barrier is high using a saddle-point method. It

reads that:

$$\int_0^X \exp\left(-\int_0^x \frac{\mathcal{V}'(y)}{D(y)}dy\right)dx \approx \mathbb{1}_{\{x>X_{\rm eq}\}} \exp\left(-\int_0^{X_{\rm eq}} \frac{\mathcal{V}'(y)}{D(y)}dy\right)\sqrt{\frac{2\pi D(X_{\rm eq})}{\mathcal{V}''(X_{\rm eq})}} + \mathbb{1}_{\{x>X^*\}} \exp\left(-\int_0^{X^*} \frac{\mathcal{V}'(y)}{D(y)}dy\right)\sqrt{\frac{2\pi D(X^*)}{\mathcal{V}''(X^*)}} \tag{A.48}$$

Using it a second time gives:

$$\begin{aligned}\mathbb{E}[\tau_c] &\approx \exp\left(-\int_0^{X_{\rm eq}} \frac{\mathcal{V}'(y)}{D(y)}dy\right)\sqrt{\frac{2\pi D(X_{\rm eq})}{\mathcal{V}''(X_{\rm eq})}}\int_0^{+\infty}\frac{1}{D(X)}\exp\left(\int_0^X \frac{\mathcal{V}'(y)}{D(y)}dy\right)\mathbb{1}_{\{x>X_{\rm eq}\}}dX \\ &\approx 2\pi\left(\frac{D(X_{\rm eq})}{D(X^*)|\mathcal{V}''(X^*)\mathcal{V}''(X_{\rm eq})|}\right)^{1/2}\times\exp\left(\int_{X_{\rm eq}}^{X^*} {\rm d}x\frac{\mathcal{V}'(x)}{D(x)}\right)\end{aligned} \tag{A.49}$$

That proves Eq. (4.20).

Expansion of Eq.(4.20) **in** ϵ

Let's turn to the development with the coefficients. First we can compute X^* and $X_{\rm eq}$:

$$X^* = \frac{1-\alpha+\sqrt{(1-\alpha)^2-4\epsilon\lambda_0^+}}{2\epsilon}, \quad X_{\rm eq} = \frac{1-\alpha-\sqrt{(1-\alpha)^2-4\epsilon\lambda_0^+}}{2\epsilon}$$

Then:

$$\int_{X_{\rm eq}}^{X^*}\frac{\mathcal{V}'(x)}{D(x)}dx = \frac{2}{\beta}\left[X_{\rm eq}-X^*+\int_{X_{\rm eq}}^{X^*}\frac{x}{\lambda_0^+ + \alpha x+\epsilon x^2}dx\right]$$

The second part of the above equation is tractable, but its value depends on the values of the parameters:

- If $\alpha^2 - 4\lambda_0^+\epsilon < 0$:

$$\begin{aligned}\int_{X_{\rm eq}}^{X^*}\frac{x}{\lambda_0^+ + \alpha x+\epsilon x^2}dx =& \frac{1}{2\epsilon}\log\left(\frac{X^*}{X_{\rm eq}}\right) - \frac{\alpha}{2\epsilon^2 C(\alpha,\epsilon)}\arctan\left(C(\alpha,\epsilon)^{-1}\left(X_{\rm eq}+\frac{\alpha}{2\epsilon}\right)\right) \\ &+ \frac{\alpha}{2\epsilon^2 C(\alpha,\epsilon)}\arctan\left(C(\alpha,\epsilon)^{-1}\left(X^*+\frac{\alpha}{2\epsilon}\right)\right)\end{aligned}$$

  with $C(\alpha,\epsilon) = \sqrt{\epsilon^{-1}\left(\lambda_0^+ - \alpha^2/2\epsilon\right)}$.

- If $\alpha^2 - 4\lambda_0^+\epsilon = 0$:

$$\int_{X_{\rm eq}}^{X^*}\frac{x}{\lambda_0^+ + \alpha x+\epsilon x^2}dx = \frac{1}{2\epsilon}\log\left(\frac{X^*}{X_{\rm eq}}\right) - \sqrt{\frac{\lambda_0^+}{\epsilon}}\left[\frac{1}{X^*-\sqrt{\lambda_0^+/\epsilon}} - \frac{1}{X_{\rm eq}-\sqrt{\lambda_0^+/\epsilon}}\right]$$

- If $\alpha^2 - 4\lambda_0^+\epsilon > 0$:

$$\int_{X_{\rm eq}}^{X^*} \frac{x}{\lambda_0^+ + \alpha x + \epsilon x^2} dx = \frac{1}{2\epsilon}\left(1 - \frac{\alpha}{\sqrt{\alpha^2 - 4\lambda_0^+\epsilon}}\right)\log\left(\frac{X^* - X_+}{X_{\rm eq} - X_+}\right) \\ \frac{1}{2\epsilon}\left(1 + \frac{\alpha}{\sqrt{\alpha^2 - 4\lambda_0^+\epsilon}}\right)\log\left(\frac{X^* - X_-}{X_{\rm eq} - X_-}\right)$$

with $X_\pm = \left(-\alpha \pm \sqrt{\alpha^2 - 4\lambda_0^+\epsilon}\right)/2\epsilon$.

Using the equations, we can develop in ϵ for fixed α and we get:

- If $\alpha = 0$:

$$\int_{X_{\rm eq}}^{X^*} \frac{\mathcal{V}'(x)}{D(x)} dx \approx \frac{2}{\beta}\left[\frac{1}{2\epsilon}\left(\log\frac{1}{\epsilon\lambda_0^+} - 2\right) + \lambda_0^+\right]$$

.

- If $\alpha > 0$:

$$\int_{X_{\rm eq}}^{X^*} \frac{\mathcal{V}'(x)}{D(x)} dx \approx \frac{2}{\beta}\left[\frac{\lambda_0^+}{\alpha^2}\log\left(\frac{\lambda_0^+\epsilon}{\alpha^2(1-\alpha)^2}\right) + \frac{1}{\epsilon}\log\left(\frac{1}{\alpha}\right) - \frac{1-\alpha}{\epsilon} + \frac{\lambda_0^+(1-2\alpha)}{\alpha^2}\right]$$

We now have to develop the logarithm of the prefactor. Noticing that $D(X_{\rm eq})/D(X^*) = X_{\rm eq}/X^*$, we have:

$$\log\left(2\pi\sqrt{\frac{D(X_{\rm eq})}{D(X^*)}}\sqrt{\frac{1}{|\mathcal{V}''(X^*)\mathcal{V}''(X_{\rm eq})|}}\right) \approx \frac{1}{2}\log\epsilon + \frac{1}{2}\log\lambda_0^+ + \log(2\pi) - 2\log(1-\alpha)$$

Putting all together gives Eq. (4.21).

A.4 Appendix of Chapter 5

A trick for computing stationary order books

We recall the equations we need to solve numerically from section 5.3. The system one must solve for $\xi > 0$ is:

$$0 = D_\ell \partial_{\xi\xi}\rho_{\rm B}^{(\ell)} - \omega\rho_{\rm B}^{(\ell)} \tag{A.50a}$$

$$0 = D_\ell \partial_{\xi\xi}\rho_{\rm A}^{(\ell)} - \omega\left\{\Gamma(k\xi)\rho_{\rm A}^{(\ell)} + [1-\Gamma(k\xi)]\phi_{\rm r}\right\} \tag{A.50b}$$

$$0 = D_{\rm r}\partial_{\xi\xi}\phi_{\rm r} - \omega\left\{\Gamma(k\xi)\rho_{\rm A}^{(\ell)} + [1-\Gamma(k\xi)]\phi_{\rm r} - \rho_{\rm B}^{(\ell)}\right\}. \tag{A.50c}$$

with boundary conditions $\rho_{\rm B}^{(\ell)}(0^+) = \rho_{\rm A}^{(\ell)}(0^+), \partial_\xi\rho_{\rm B}^{(\ell)}(0^+) = -\partial_\xi\rho_{\rm A}^{(\ell)}(0^+), \lim_{\xi\to+\infty}\rho_{\rm B}^{(\ell)}(\xi) = \lim_{\xi\to+\infty}\phi_{\rm r}(\xi) = 0, \lim_{\xi\to+\infty}\partial_\xi\rho_{\rm A}^{(\ell)}(\xi) = \mathcal{L}$. We provide a smarter numerical scheme that solve

those equations. Using linear combination of Eq.(A.50), one gets:

$$\rho_{\mathrm{B}}^{(\ell)}(\xi) = \rho_{\mathrm{B}}^{(\ell)}(0+)e^{-\xi/\ell_\ell} \tag{A.51a}$$

$$\mathrm{B}^{(\ell)}(\xi) - \mathrm{A}^{(\ell)}(\xi) + \frac{\ell_{\mathrm{r}}^2}{\ell_\ell^2}\phi_{\mathrm{r}} = -\mathcal{L}\xi \tag{A.51b}$$

Then plugging it into Eq.(A.50c) and the boundary conditions, we get:

$$0 = \frac{2}{\ell_\ell}\rho_{\mathrm{B}}^{(\ell)}(0+) - 1 - \frac{\ell_{\mathrm{r}}^2}{\ell_\ell^2}\partial_\xi\phi_{\mathrm{r}}(0+) \tag{A.52a}$$

$$\begin{aligned}\partial_{\xi\xi}\phi_{\mathrm{r}} = {} & \frac{1}{\ell_{\mathrm{r}}^2}\left(\left[1+\Gamma(k\xi)\left(\frac{\ell_{\mathrm{r}}^2}{\ell_\ell^2}-1\right)\right]\phi_{\mathrm{r}} + \Gamma(k\xi)\mathcal{L}\xi\right) \\ & + \frac{1}{\ell_{\mathrm{r}}^2}\rho_{\mathrm{B}}^{(\ell)}(0+)e^{-\xi/\ell_\ell}\left(\Gamma(k\xi)-1\right)\end{aligned} \tag{A.52b}$$

that is a linear system in the variables $(\rho_{\mathrm{B}}^{(\ell)}(0+), \phi_{\mathrm{r}})$. Unfortunately, we have not been able to analytically solve these equations, but we can discretize it and numerically solve it to get the solutions of Eq.(A.50). Note that such trick diminishes the time of computations by a factor roughly equal to three.

Plots and fits of US stocks

We display on Fig.A.4,A.4,A.4 the empirical average order books over one hundred US stocks with the according fit of ϕ_{r} that were displayed on Fig.5.3(a).

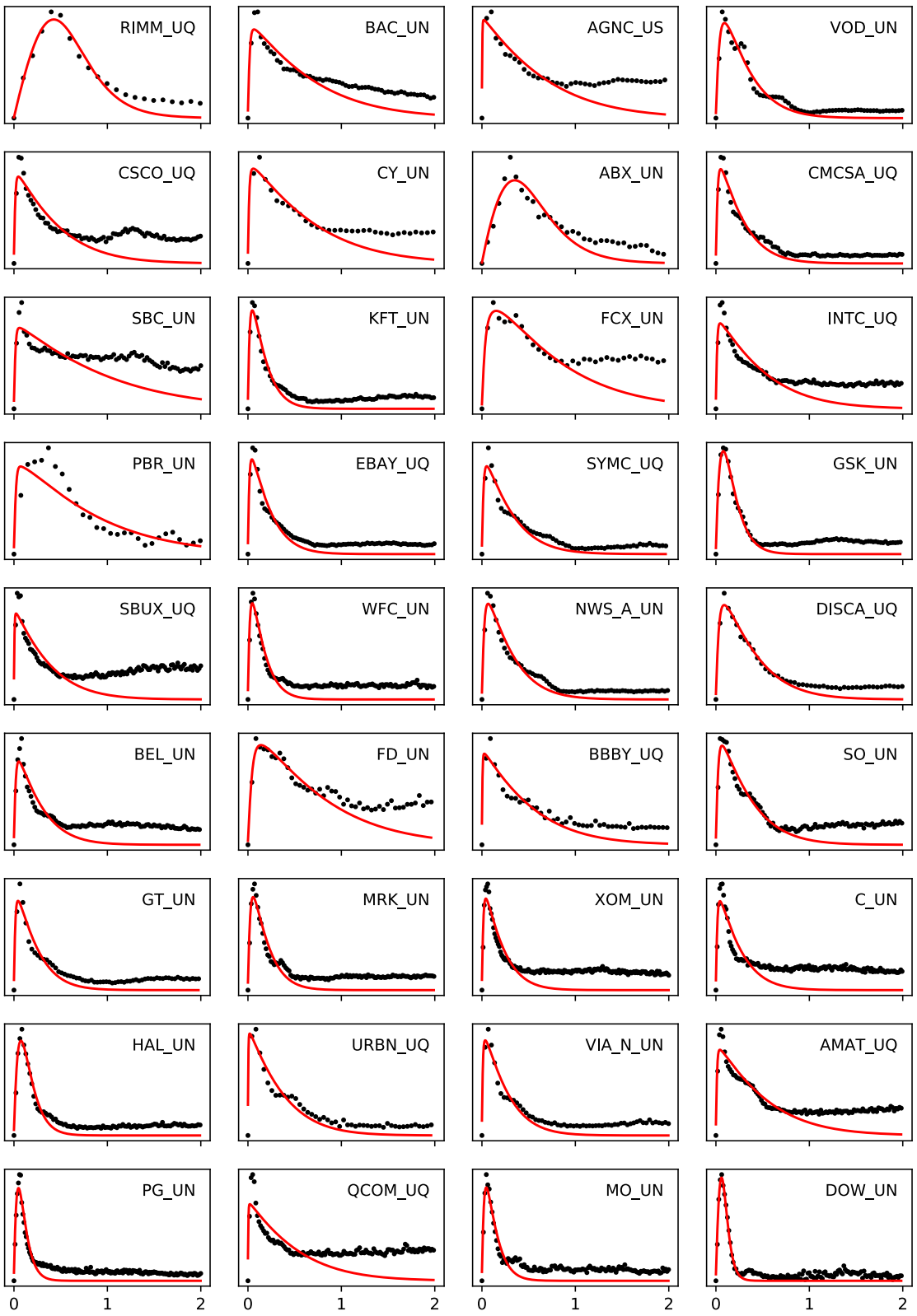

Figure A.4: *Fit of the stationary revealed order book ϕ_r to the average order books of over one hundred US stocks, see Table A.3.*

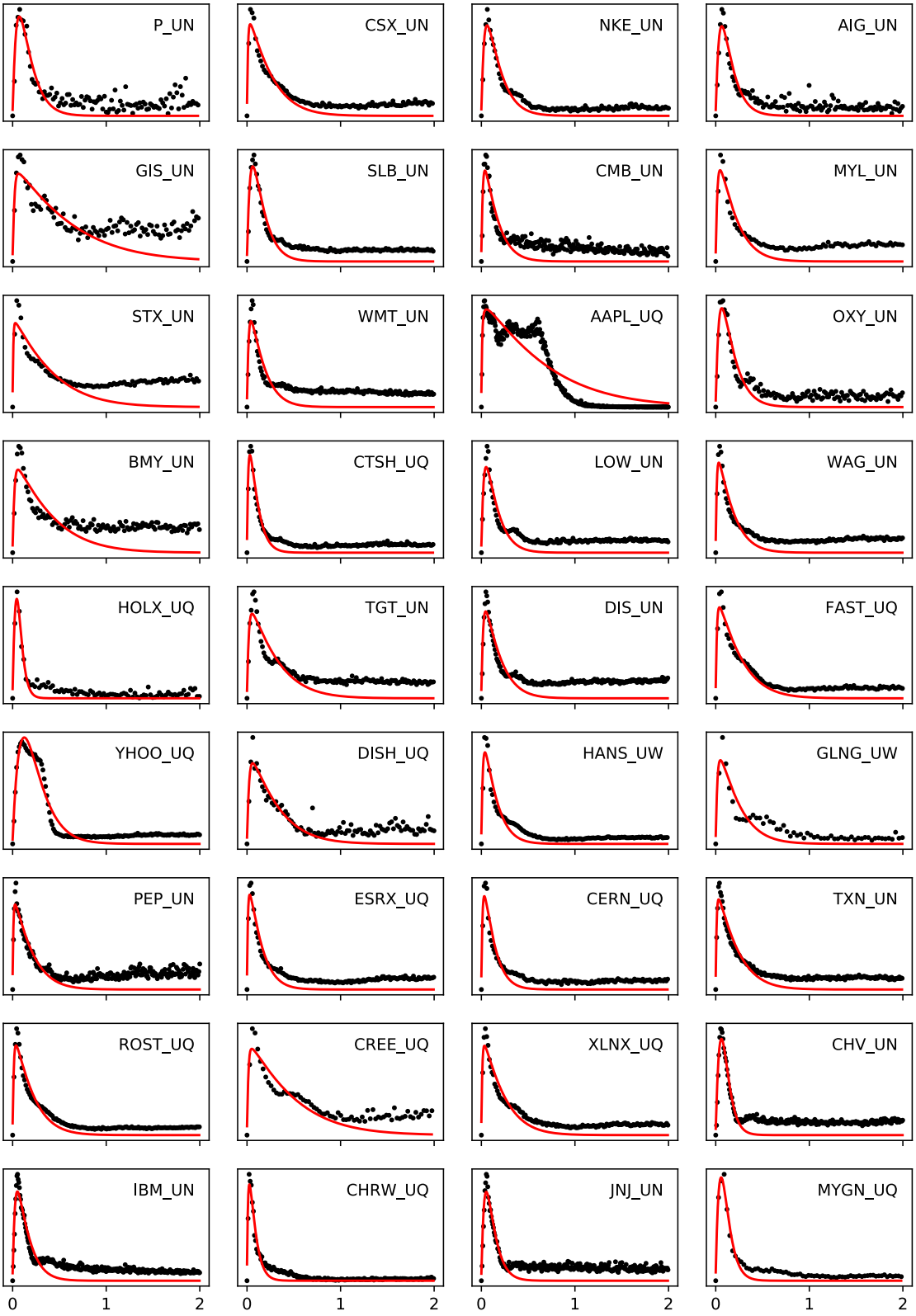

Figure A.5: *Fit of the stationary revealed order book ϕ_r to the average order books of over one hundred US stocks, see Table A.3.*

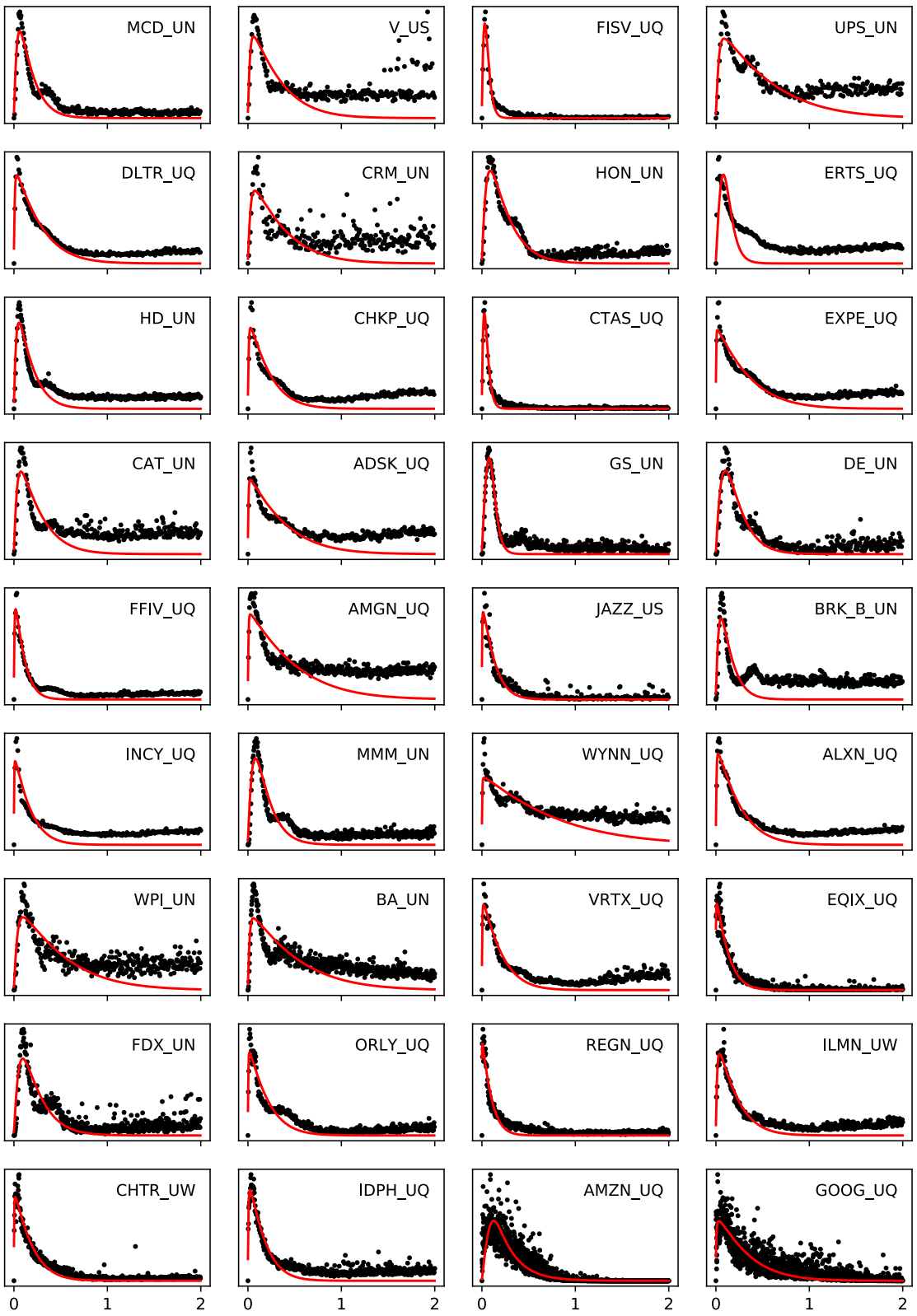

Figure A.6: *Fit of the stationary revealed order book ϕ_r to the average order books of over one hundred US stocks, see Table A.3.*

Table A.3: US stocks (large cap.) used for the empirical analysis of Sec. 5.4 (see also Figs. A.4, A.5 and A.6). The average spread S has tick units, V_{d} denotes the average daily traded volume (in shares), k^{-1}, ℓ_ℓ and ℓ_{r} are expressed in %price, and $\mathcal{L}$ is shares per unit %price.

Stock	price \$	S	$10^{-6}V_{\mathrm{d}}$	$10^{-3}\mathcal{L}$	k	ℓ_ℓ	ℓ_{r}
RIMM	10.03	1.003	0.87	602.0	4.71	0.0020	0.0059
BAC	28.66	1.007	15.62	34.3	2.50	0.0350	0.0033
AGNC	19.92	1.009	1.03	10.8	2.51	0.0165	0.0005
VOD	29.62	1.011	0.89	47.6	5.58	0.0230	0.0090
CSCO	38.57	1.012	7.17	26.7	3.64	0.0309	0.0027
CY	16.14	1.018	1.44	11.9	2.49	0.0195	0.0020
ABX	16.46	1.023	2.95	191.1	4.45	0.0031	0.0060
CMCSA	37.65	1.023	6.54	38.3	6.31	0.0230	0.0046
SBC	36.51	1.029	7.76	5.3	1.75	0.0417	0.0023
KFT	42.25	1.036	2.88	39.1	10.22	0.0131	0.0047
FCX	16.45	1.040	4.74	8.3	2.22	0.0201	0.0054
INTC	44.87	1.042	8.31	16.7	3.31	0.0318	0.0024
PBR	13.54	1.044	4.59	16.9	1.99	0.1284	0.0035
EBAY	39.12	1.052	2.73	28.1	7.71	0.0176	0.0037
SYMC	28.96	1.072	1.78	19.4	5.50	0.0227	0.0040
GSK	37.99	1.074	0.83	38.4	10.94	0.0084	0.0069
SBUX	57.01	1.076	2.95	9.4	4.53	0.0178	0.0009
WFC	56.31	1.082	5.37	25.6	11.02	0.0156	0.0057
NWS	33.21	1.100	2.55	18.7	5.74	0.0262	0.0065
DISCA	22.57	1.101	1.42	13.7	4.46	0.0247	0.0072
BEL	49.35	1.104	4.09	10.0	6.11	0.0278	0.0048
FD	23.44	1.117	2.46	3.9	2.26	0.0411	0.0093
BBBY	22.20	1.118	1.35	7.0	3.17	0.0178	0.0008
SO	44.21	1.143	1.69	5.2	4.87	0.0323	0.0060
GT	31.36	1.191	0.98	17.8	7.24	0.0169	0.0035
MRK	56.76	1.210	3.54	11.5	9.16	0.0209	0.0071
XOM	80.51	1.219	4.03	11.2	8.03	0.0231	0.0042
C	73.26	1.225	5.28	8.8	6.83	0.0261	0.0040
HAL	47.17	1.254	2.35	28.7	11.94	0.0117	0.0097
URBN	23.44	1.257	0.92	10.5	4.57	0.0123	0.0007
VIA	29.54	1.264	1.66	14.2	6.45	0.0127	0.0020
AMAT	53.43	1.315	3.53	5.6	3.23	0.0305	0.0021
PG	84.03	1.401	2.60	30.7	17.95	0.0098	0.0078
QCOM	59.38	1.416	3.30	4.0	3.25	0.0177	0.0006
MO	64.07	1.428	2.09	14.9	13.02	0.0143	0.0064
DOW	64.99	1.439	2.35	100.6	25.26	0.0015	0.0030
P	52.99	1.439	1.85	17.5	11.15	0.0149	0.0104
CSX	54.49	1.561	2.16	9.8	6.77	0.0199	0.0026
NKE	63.01	1.586	2.29	12.4	10.24	0.0191	0.0088
AIG	61.12	1.592	1.48	15.9	12.27	0.0168	0.0109
GIS	49.88	1.645	1.17	1.3	2.79	0.0431	0.0037
SLB	67.36	1.661	2.20	14.9	11.92	0.0167	0.0097
CMB	106.81	1.667	4.03	8.6	11.14	0.0199	0.0048
MYL	39.10	1.748	1.98	16.1	8.65	0.0184	0.0049
STX	45.28	1.822	1.48	4.6	4.09	0.0212	0.0013
WMT	90.73	1.884	2.59	8.3	10.61	0.0211	0.0055
AAPL	168.14	1.922	8.78	3.1	2.51	0.0107	0.0011
OXY	64.65	1.971	1.20	9.6	10.77	0.0191	0.0101
BMY	61.12	2.032	1.76	1.5	4.21	0.0372	0.0044
CTSH	75.94	2.129	1.27	23.7	17.41	0.0095	0.0040
LOW	81.69	2.204	1.61	6.9	11.71	0.0194	0.0078

Stock	price \$	S	$10^{-6}V_{\mathrm{d}}$	$10^{-3}\mathcal{L}$	k	ℓ_ℓ	ℓ_{r}
WAG	71.64	2.298	2.25	10.3	9.79	0.0176	0.0032
HOLX	42.09	2.314	0.88	317.2	29.35	0.0008	0.0012
TGT	66.76	2.409	1.53	2.4	5.62	0.0320	0.0050
DIS	103.38	2.440	2.36	5.4	9.51	0.0236	0.0057
FAST	50.13	2.495	0.91	5.9	6.68	0.0213	0.0032
YHOO	71.07	2.649	2.55	21.6	8.05	0.0042	0.0043
DISH	48.54	2.671	0.82	3.3	5.53	0.0309	0.0059
HANS	59.37	2.751	0.84	13.8	11.79	0.0163	0.0047
GLNG	27.57	2.925	0.35	14.1	7.52	0.0187	0.0048

Stock	price \$	S	$10^{-6}V_{\mathrm{d}}$	$10^{-3}\mathcal{L}$	k	ℓ_ℓ	ℓ_{r}
PEP	112.52	3.009	1.42	5.3	8.42	0.0174	0.0020
ESRX	69.15	3.032	1.45	9.6	11.69	0.0137	0.0029
CERN	67.81	3.100	0.81	13.6	13.42	0.0134	0.0037
TXN	99.90	3.131	1.82	4.6	7.61	0.0200	0.0025
ROST	70.66	3.149	1.06	6.2	8.32	0.0198	0.0033
CREE	34.92	3.165	0.51	2.0	3.48	0.0322	0.0030
XLNX	70.21	3.199	0.93	4.0	7.34	0.0200	0.0026
CHV	116.12	3.867	1.95	16.8	19.58	0.0085	0.0108
IBM	152.11	3.917	1.29	3.9	11.96	0.0218	0.0083
CHRW	87.75	3.980	0.59	41.7	22.18	0.0075	0.0034
JNJ	131.86	4.007	2.07	6.9	15.56	0.0149	0.0098
MYGN	33.28	4.032	0.31	61.1	17.84	0.0019	0.0021
MCD	156.99	4.131	1.07	3.5	10.38	0.0276	0.0109
V	121.14	4.170	2.20	1.0	5.21	0.0381	0.0058
FISV	106.11	4.408	0.43	377.8	36.42	0.0008	0.0010
UPS	107.88	5.055	0.87	0.4	3.02	0.0566	0.0071
DLTR	97.27	5.124	0.86	2.0	6.07	0.0206	0.0019
CRM	116.98	5.563	1.22	0.5	4.61	0.0452	0.0074
HON	148.04	5.754	0.78	1.4	7.36	0.0365	0.0151
ERTS	116.94	5.872	1.07	220.6	34.96	0.0101	0.0641
HD	175.53	5.944	1.35	2.4	9.83	0.0275	0.0079
CHKP	104.95	6.161	0.38	1.3	7.57	0.0183	0.0020
CTAS	161.47	6.443	0.25	141.6	38.58	0.0038	0.0040
EXPE	124.49	6.716	0.83	0.8	4.82	0.0114	0.0006
CAT	153.78	6.934	1.10	1.2	6.78	0.0408	0.0106
ADSK	118.11	6.967	0.77	0.8	4.34	0.0181	0.0010
GS	230.09	6.976	0.76	30.5	27.22	0.0011	0.0038
DE	154.44	6.985	0.58	1.6	8.70	0.0338	0.0216
FFIV	128.76	7.457	0.30	4.9	15.98	0.0095	0.0016
AMGN	179.67	7.504	1.31	0.5	3.42	0.0187	0.0009
JAZZ	146.67	8.266	0.14	5.6	12.72	0.0064	0.0007
BRK	202.45	8.669	1.34	2.1	12.53	0.0257	0.0107
INCY	97.51	8.723	0.64	2.2	9.68	0.0095	0.0007
MMM	222.45	8.976	0.70	1.4	9.74	0.0334	0.0167
WYNN	162.67	9.496	0.76	0.2	2.17	0.0106	0.0004
ALXN	122.92	9.738	0.69	0.9	6.73	0.0154	0.0013
WPI	176.75	10.580	0.70	0.1	3.37	0.0575	0.0093
BA	297.60	10.630	0.97	0.2	3.31	0.0404	0.0037
VRTX	155.65	11.509	0.56	1.0	8.18	0.0105	0.0009

B

By Force of Habit: Self-Trapping in a Dynamical Utility Landscape

Historically, rational choice theory has focused on the utility maximization principle to describe how individuals make choices. In reality, there is a computational cost related to exploring the universe of available choices and it is often not clear whether we are truly maximizing an underlying utility function. In particular, memory effects and habit formation may dominate over utility maximisation. We propose a stylized model with a history-dependent utility function where the utility associated to each choice is increased when that choice has been made in the past, with a certain decaying memory kernel. We show that self-reinforcing effects can cause the agent to get stuck with a choice by sheer force of habit. We discuss the special nature of the transition between free exploration of the space of choice and self-trapping. We find in particular that the trapping time distribution is precisely a Zipf law at the transition, and that the self-trapped phase exhibits super-aging behaviour.

From:
By force of habit: Self-trapping in a dynamical utility landscape
J. Moran, **A. Fosset**, D. Luzzati, J. P. Bouchaud, M. Benzaquen

Contents

I would like to thanks Davide Luzzati whom I initiated the project, Pierre Lecointre for its contribution during the early stages of this project. And finally, I warmly thank José Moran who reshaped this project and made major breakthroughts.

L'homme est une chose imparfaite qui tend sans cesse à quelque chose de meilleur et de plus grand qu'elle-même.

Descartes

In modelling the behaviour of agents, the common view in standard economics is that their actions are guided by the maximization of an utility function. For convenience, the utility for each agent is often thought of as independent of the actions of others, as well as static in time. A myriad of results in economic theory actually rest upon this assumption. Complexity economics has recently begun to tackle the issue of interactions between agents with analytical and numerical tools, and we address here the possibility of reinforcement mechanisms that make an agent's utility depend on his past. This simple toy model leads to non-ergodic dynamics, where the agent's actions depend crucially on past decisions.

B.1 Introduction

A key assumption in rational choice theory is that individuals set their preferences according to an utility maximization principle. Each choice an individual can make is assigned a certain "utility", i.e. a quantity measuring the satisfaction it provides to the agent and frequently related to the dispassionate forecast of a related payoff. This framework is often accompanied by the assumption that the agent considers *all* available choices present to her/him, weighs their utilities against one another, and then makes her/his choice taking into account possible constraints, such as a finite budget.

A number of criticisms to this view of human behaviour have emerged, with e.g. Simon [93] as a key figure highlighting that individuals may be "satisfiers" rather than pure optimisers, in the sense that there is both a computational cost and a cognitive bias related to considering the universe of available choices. Sometimes finding the optimum of the utility function can itself be such a computationally hard problem that even the most powerful computers would not be able to find it in a reasonable amount of time. This led to the idea of bounded rationality as a way to model real agents [94, 95, 96, 97]. More recently, Kahneman [98, 99] pointed at what he considers to be significant divergences between economics and psychology in their assumptions of human behaviour, with a special emphasis on the empirical evidence of the cognitive biases, and therefore the irrationality, that guides individual behaviour. A pervasive effect, for example, is that the utility of a certain choice strongly depends on the choice made by others. These so called "externalities" can lead to interesting collective effects, where choices made by agents synchronise and condense on a small subset of choices, or lead to confidence crises – see for example [100, 101, 102, 103, 104].

An interesting idea developed in [105] is the fact that the utility associated to a certain decision may depend also on our memory if it has already been made in the past. Here we propose a simple model that encapsulates this idea, and show that this too can lead to choices that do not necessarily conform to their "objective" utilities, but are rather dominated by past choices alone. This is related to what economists call "habit formation" [106, 107, 108, 109, 110, 111]. Memory effects chisel the utility landscape in a way that may render objectively sub-optimal choices subjectively optimal. In the case of sufficiently long range memory, agents may, in a self-fulfilling kind of way, become "trapped" forever in a certain choice and stop exploring alternative choices.

As a practical example, one may imagine a situation where one must choose where to have lunch every day. Standard rational theory dictates that we ought to scrutinize every restaurant, eatery and cafeteria, taking into account our personal tastes and the costs associated with going to any of these places. In contrast, we want to model the fact that habit

may take over: instead of seeking to maximize a certain objective cost function, we are likely to persist in going to a specific place just because we are used to it. Anecdotal evidence shows that this is indeed what often happens in practice!

Our model assumes that the utility landscape is affected by past choices, with a memory kernel that decays with time. Agents can change their decision using a logit (or Metropolis) rule, parameterised by an "intensity of choice" β that plays the role of the inverse temperature in statistical physics. This type of model belongs to a wide class of so-called "reinforcement" models, which contains Polya Urns, Reinforced Random Walks, Elephant Walks, etc. – for a review see [112] and references therein.[1] Such models have also gained traction in the economics literature, where positive reinforcement of certain choices made by agents are shown to impact the emergence of certain macro outcomes and structures [115, 116].

After properly defining our model, we provide analytical arguments to confirm the intuition that sufficiently strong memory effects, coupled with the optimization of the subjective memory-induced utility, can lead to "self-trapping", i.e. the agent sticks to a choice whose objective utility is not necessarily maximal, simply by force of habit. We confirm our result *via* numerical simulations that explore different topologies for the space of different choices. We discover a particularly interesting dynamical transition when the memory kernel decays as the inverse of time, with rather unusual scaling and super-aging properties. We finally propose possible extensions.

B.2 A Simple model

Consider a set of N discrete choices, labeled $(x_i)_{1\leq i\leq N}$, to which we assign an utility – a measure of the value an individual assigns a given choice. The perceived utility of site x_i and time t is postulated to be:

$$U(x_i,t) = U_0(x_i)\left(1+\sum_{t'=0}^{t}\phi(t-t')\mathbf{1}_{x(t')=x_i}\right), \tag{B.1}$$

where the first term on the right-hand side is the intrinsic, or objective utility of the choice, while the second accounts for memory effects, affecting the utility of that choice for the only reason that the individual has picked it in the past.[2] The decaying memory kernel ϕ encodes that more recent choices have a stronger effect, and $x(t)$ denotes the choice of the individual at time t. Hence, past history "chisels" the utility landscape, in a way similar to ants leaving a pheromone trace that guide other ants along the same path, or rivers creating their own bed through erosion. Note that in most reinforcement random walk models reviewed in [112], infinite memory span is assumed, i.e. $\phi(t) =$ constant, while we will be mostly concerned here with decaying memory kernels.

The sign of the kernel ϕ separates two different cases: $\phi < 0$ indicates a situation where an individual grows weary of his past choices, while $\phi > 0$ corresponds to the case where an individual becomes increasingly endeared with them. In agreement with intuition, the former case leads to an exploration of all the choices unless the optimal choice has an utility too far apart from the rest to be sufficiently affected by the kernel. In all that follows we focus on the more interesting case $\phi \geq 0$. The reason behind studying such utility reinforcement lies in the behavioural idea that people tend to prefer what they already know, thus paving the way for "habit formation" as in [117], see also [107, 108, 109, 110, 111] and [103]. We then consider the following dynamics. An individual, standing by choice x_i at time t, draws an

[1] For recent developments, see also [113, 114].

[2] One may also think, in the physicist's language, of an energy landscape (akin to minus the utility) where the energy of a given site or configuration increases or decreases if the system has already visited that site.

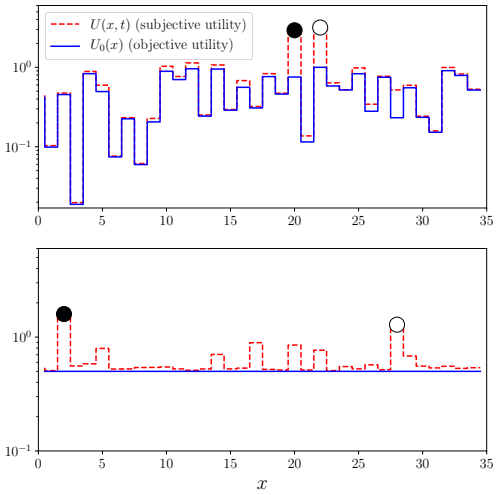

Figure B.1: *Schematic representation of our problem at a given time t. The plot on the top depicts the case of random "objective" utilities $U_0(x)$, while the one on the bottom shows the situation where they are uniform $U_0(x) = U_0$. In both plots, the solid black ball represents the choice made at time t, while the empty ball represents the choice made at time $t-1$. Both correspond to a simulation run with a power-law kernel $\phi(t) \propto (1+t)^{-\gamma}$ with $\gamma = 1.5$ and $\beta = 0.2$, on a fully connected graph.*

alternative x_j from a certain ensemble of "nearby choices" ∂_i, e.g. the set of neighbors of i in a graph $\mathcal{G}$, with probability:

$$\mathcal{T}_{x_i \to x_j} = \frac{\mathbf{1}_{x_j \in \partial_i}}{\mathcal{N}_i}, \quad \mathcal{N}_i := \sum_j \mathbf{1}_{x_j \in \partial_i}, \tag{B.2}$$

where $\mathcal{N}_i$ is the number of neighbours of i. Restricting to nearby choices is a parsimonious way to model adaptation costs, that penalize large decision changes. However, our framework is quite versatile since the topology of the graph $\mathcal{G}$ is arbitrary, and we will consider different cases below.

The target choice x_j is then adopted with the logit probability, standard in Choice Theory [118]:[3]

$$p(x_i \to x_j) = \frac{1}{1 + e^{\beta[U(x_i,t) - U(x_j,t)]}}, \tag{B.3}$$

where β is called the "intensity of choice" and accounts for the degree of rationality (it is the analogue of the inverse temperature in statistical mechanics). Indeed, as long as $0 < \beta < \infty$, the agent is more likely to switch whenever $U(x_j,t) > U(x_i,t)$ (optimizing behaviour), but the probability to pick a choice with a lower utility is non-zero, which encodes for bounded-rationality (or uncertainty about the true utility) in the economics literature. In the $\beta \to 0$ limit (equivalent to the infinite temperature limit in physics) the agent explores the whole space of possible choices without taking their utility into account. In the opposite limit $\beta \to \infty$ (or zero temperature) the agent has a greedy behaviour and only switches to choices with a higher utility, but this also implies that he/she may stay in a local maximum instead of taking the chance to explore all available possibilities. An illustration of these dynamics is given in Fig. B.1.

[3] For non-trivial trapping to emerge, we consider graphs without singletons, that is to say that all sites have a non-empty set of neighbours that are different to itself.

When $\phi = 0$, the dynamics is that of the Metropolis-Hastings algorithm used to sample the Boltzmann-Gibbs distribution [119, 120]. The stationary state of the dynamics is such that the probability to pick choice x_i is proportional to $\mathcal{N}_i e^{\beta U_0(x_i)}$. This can by itself lead to interesting phenomena depending on the statistics of U_0. For example the study of the Random Energy Model [121, 122], for a finite value of N and for Gaussian utilities of variance σ^2, shows that for $\beta > \beta_c = \sqrt{2 \ln N}/\sigma$, the probability measure condenses on a small number of choices, much smaller than N.

B.3 Non-Ergodicity & Condensation of Choices

Adding the kernel introduces the possibility that the agent gets stuck in a non-optimal choice exclusively through memory effects: staying a long time in a given choice self-reinforces its utility, thereby increasing the likelihood to stay there and leading to non-ergodic dynamics. To study the possible condensation or trapping induced by memory alone, we restrict ourselves to the case where $U_0(x_i) = 1$, $\forall i$ henceforth. (Any other value of U_0 can be reabsorbed in β). The interplay between memory-induced trapping and utility heterogeneity is quite interesting in itself, but we leave it to future investigations.

We consider an agent starting from a given choice x_0 at time $t = 0$ and follow his/her evolution for times $t = 1, \dots, T$ with T sufficiently large. We then compute the empirical state histogram $p_i = \sum_t \mathbf{1}_{x(t)=x_i}/T$ and define the order parameter h, in a similar way to the inverse participation ratio used in condensed matter physics [123, 124] or to the Herfindahl index in economics [125], as:

$$h := \sum_{i=1}^{N} p_i^2. \tag{B.4}$$

This parameter indicates how the agent has explored the space of possible choices: if all choices were visited with equal probability then one has immediately $p_i = 1/N$ and thus $h = \sum_i 1/N^2 = 1/N$. On the other hand if the agent was stuck in a single choice j, then $p_i = \delta_{i,j}$ and so $h = 1$. Therefore $1/h$ gives an order of magnitude of the number of different choices picked by the agent during time T. In practice, we average h over a large number of trajectories and starting sites x_0, to obtain an average parameter h. For a set of simulations on a graph $\mathcal{G}$ with N choices and lasting a time T, we therefore define the critical value β_c, defining the crossover between $h = \mathcal{O}(1/N)$ and $h = \mathcal{O}(1)$ as the value for β that maximizes the variance of h over different trajectories.

An important question is whether β_c corresponds to a true transition or to a mere crossover. This depends on the L^1 norm of the memory kernel, $\phi = \sum_{t=0}^{\infty} \phi(t)$. Suppose that this norm is finite. Then if the agent has been stuck in a given site i for a time $t \gg 1$, we can approximate its utility by $(1 + \phi)$. The difference in utility with the neighbouring choices thus remains finite. For any finite value of β, the probability to leave that site is non-zero, and therefore the individual will eventually pick a different choice. The time for this to happen is however of the order of $\exp(\beta\phi)$. If this time is much longer than T, we will in fact measure $h \sim 1$, even though running the trajectory for a longer time would result in $h = \mathcal{O}(1/N)$. Hence in this case β_c is a crossover that depends on T as $\ln(T)/(\phi)$.

A more interesting situation (at least from a theoretical point of view) is when $\phi = \infty$. As we will show below, there exists cases where β_c corresponds to a true phase transition and is independent of T (when T is large).

B.4 Mean Field Approximation

In order to draw further analytical features, we start by looking at a mean-field approximation. This means that we take the graph $\mathcal{G}$ to be fully connected with $\mathcal{T}_{x_i \to x_j} = 1/(N-1)$ and in the limit $N \to \infty$.

We now formalize the argument previously sketched. If the individual started first at a given choice corresponding to node i, then the probability $P_>(\tau)$ that he/she remains there up to a time τ is given by the product over $t \in 0, \tau - 1$ of the probabilities not to leave the site between times t and $t+1$, $p_{\rm stay}(t)$. Now, $p_{\rm stay}(t) = 1 - p_{\rm leave}(t)$ with:

$$p_{\rm leave}(t) = \sum_{j \in \partial_i} \mathcal{T}_{x_i \to x_j} \frac{1}{1 + e^{\beta[U(x_i,t) - U(x_j,t)]}}. \tag{B.5}$$

For the fully connected graph, this expression simplifies to[4] $p_{\rm stay}(t) = \left[1 + e^{-\beta\Phi(t)}\right]^{-1}$, with $\Phi(t) = sum_0^t \phi(s)$. It follows that:

$$P_>(\tau) = \prod_{t=0}^{\tau} \left[1 + e^{-\beta\Phi(t)}\right]^{-1} \approx e^{-I(\tau)}, \tag{B.6}$$

with $I(\tau) := \int_0^\tau {\rm d}t \, \ln\left[1 + e^{-\beta\Phi(t)}\right]$, where we have replaced discrete sums by integrals. Equation (B.6) determines the distribution of the "trapping" time τ that the agent spends stuck on a certain choice. Its nature will entirely depend on the behaviour of the integral $I(\tau)$ when $\tau \to \infty$.

Short Term Memory

Consider first the case where $\lim_{t\to\infty} \Phi(t) = \phi < +\infty$. Then $I(\tau) \approx \lambda\tau$ for $\tau \to \infty$, with

$$\lambda := \ln\left[1 + e^{-\beta\phi}\right]. \tag{B.7}$$

This means that the trapping time distribution decays exponentially fast for large τ, with an average trapping time $\langle\tau\rangle$ approximately given by $1/\lambda$. For sufficiently small λ, we recover the qualitative criterion of the previous section by setting $T\lambda \sim 1$. But the dynamics remains ergodic when $T \to \infty$.

Long Term Memory

Suppose now that $\phi(t)$ decays sufficiently slowly for large t for ϕ to diverge. For definiteness, we will focus on power-law kernels:

$$\phi(t) = \frac{C}{(1+t)^\gamma}. \tag{B.8}$$

When $\gamma > 1$, ϕ is finite and we are back to the previous case. Hence we restrict to $\gamma \leq 1$. When $\gamma < 1$, one finds that $\Phi(t) \propto t^{1-\gamma}$ for large t. Hence $I(\tau)$ converges to a finite limit I_∞ for large τ. This means that there is a finite probability $P_\infty = e^{-I_\infty}$ that the choice is made *forever*. When $\gamma = 1$, $\Phi(t) \approx C \ln t$ for large t. This leads to three further sub-cases:

1. When $\beta C > 1$, $I(\tau)$ again converges to a finite limit when $\tau \to \infty$, i.e. decisions self-trap forever.

2. At the transition point, defined as $\beta_c^\star = C^{-1}$, one finds that $P_>(\tau)$ decays as τ^{-1}, i.e. the trapping time distribution is a Zipf law, τ^{-2}. This is the marginal case that appears in several models of aging in the literature [126, 127]. For a finite observation time T, the average trapping time grows like $\ln T$.

[4] In the general case in which the agent started in a "site" different from i and then got stuck in i, one wants to replace the right-hand side by an average of the logit rule over the utility gaps $U(x_i,t) - U(x_j,t)$. However, as $N \to \infty$ it is very unlikely that a site that was previously picked is chosen again. We can thus safely replace the average gap by the gap with the base level $U_0 = 1$.

3. When $\beta C < 1$, $I(\tau)$ behaves for large τ as τ^b/b, where $b = 1 - \beta C > 0$. The average trapping time $\langle\tau\rangle$ is thus finite. A careful analysis[5] shows that $\langle\tau\rangle$ diverges as b^{-1} when $b \to 0$, but higher moments $\langle\tau^k\rangle$ with $k > 1$ diverge much faster, as $\exp((k-1)/b)$, i.e. according to the so-called Vogel-Tamman-Fulcher law, see e.g. [128].

Let us summarize the above results. When the kernel ϕ decays fast enough, there is a crossover regime in β between free exploration of the space of choice and trapping. The crossover value of β depends on the observation time T and is given, using Eq. (B.7) for T large, by

$$\beta_c = \frac{\ln T}{\phi}. \tag{B.9}$$

When memory is long ranged, and described by a power-law kernel with decay exponent γ, there exists a genuine transition when $\gamma = 1$ between a free exploration regime and a (non-ergodic) trapped regime at a T independent value of β that we shall henceforth call $\beta_c^\star$. When $\beta > \beta_c^\star$ or $\gamma < 1$, there is a non-zero probability to get trapped in the same decision forever. The characteristic time for changing decision is of the same order of magnitude as T itself, a phenomenon called "aging", see e.g. [129, 127], on which we will comment further below, see Fig. B.4. Note finally that for $\gamma = 1$, our mean-field analysis predicts that while the average trapping time diverges as $(\beta_c^\star - \beta)^{-1}$, all higher moments diverge much faster, as $\sim \exp(A/(\beta_c^\star - \beta))$.

B.5 Numerical results

We have conducted simulations using a long-range memory kernel given by Eq. (B.8) with $\gamma \in [1; \infty[$. For numerical convenience, we represent $\phi(t)$ as a superposition of exponentials as done in [130]. We have considered a variety of different graph topologies $\mathcal{G}$: fully connected graphs, one-dimensional chains, and finally Watts-Strogatz small world networks. Without loss of generality, we set again $U_0 = 1$ as this simply corresponds to a rescaling of β.

Figure B.2 (Left) shows the value of β_c, determined as the maximum of the variance of h, as a function of T for two different topologies (one-dimensional and fully connected) and two different values of $\gamma \in \{1, 1.5\}$. Our results show excellent qualitative agreement with the theoretical prediction for the two topologies, in particular Eq. (B.9) in the $\gamma > 1$ case, although there is an overall factor needed to account for the one-dimensional data.

One can actually interpolate between the two situations by considering Watts-Strogatz small-world networks [131], with a rewiring parameter p such that $p = 0$ corresponds to one-dimension chains and $p = 1$ to the fully connected graph. Figure B.2 (Right) shows the value of $\beta_c^\star$ as a function of the rewiring parameter p of interpolating between one-dimensional chains for $p = 0$ and the fully connected graph for $p = 1$. The parameter p therefore allows to interpolate between a situation where one may only do local jumps to a situation where one can go anywhere. As expected, $\beta_c^\star$ increases with p, as it is easier to get trapped in less connected graphs, where the same choice is revisited more often.

We now study more carefully the behaviour of the order parameter h close to the transition point $\beta_c^\star$, when $\gamma = 1$, both for one-dimensional chains and for the fully connected graph. We choose $N = 10^5$ henceforth, such that finite size effects are negligible in the range of T that we explore. Figure B.3 suggests that as $T \to \infty$, $\langle h\rangle(\beta)$ appears to slowly converge to a step function that is zero for $\beta < \beta_c^\star$ and unity when $\beta > \beta_c^\star$, at least in the fully connected case where the speed of convergence is found to be $\sim T^{-1/3}$. In the one-dimensional case,

[5] Indeed, a direct integration of the kernel yields $P_>(\tau) = \exp\left[1 - (1+\tau)^b/b\right]$. As $b \to 0$ this function can be approximated by $P_>(\tau) = (1+\tau)^{-1}$ up to a cutoff at $\tau \sim e^{1/b}$. Direct integration then gives $\int_0^{e^{1/b}} \mathrm{d}\tau\ \tau^{k-1}/(1+\tau) \approx \exp((k-1)/b)$ for $k > 1$ and $\sim 1/b$ for $k = 1$.

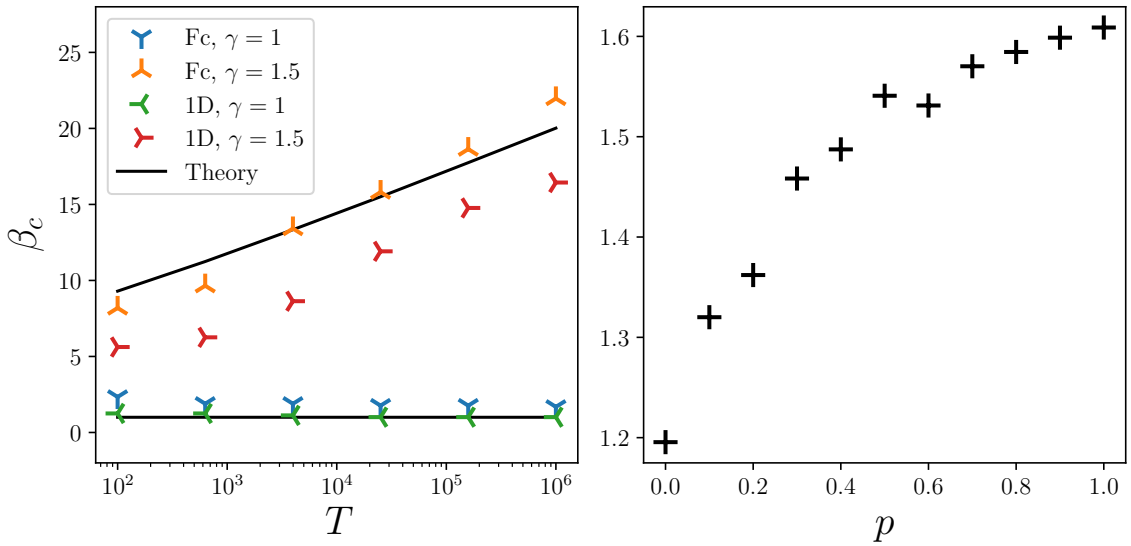

Figure B.2: *Left: critical β_c as a function of $\ln T$ for $\gamma = 1$ and 1.5, $N = 10^5$ and different topologies. (Fc stands for fully connected, while 1D is the one-dimensional chain). Black lines correspond to the prediction of mean-field theory. Right: dependence of the critical intensity of choice $\beta_c^\star$ on the parameter p of Watts-Strogatz networks, for $T = 5 \cdot 10^3$ and $N = 2 \cdot 10^3$.*

one cannot exclude with the available data that this limiting function remains continuous when $T \to \infty$.

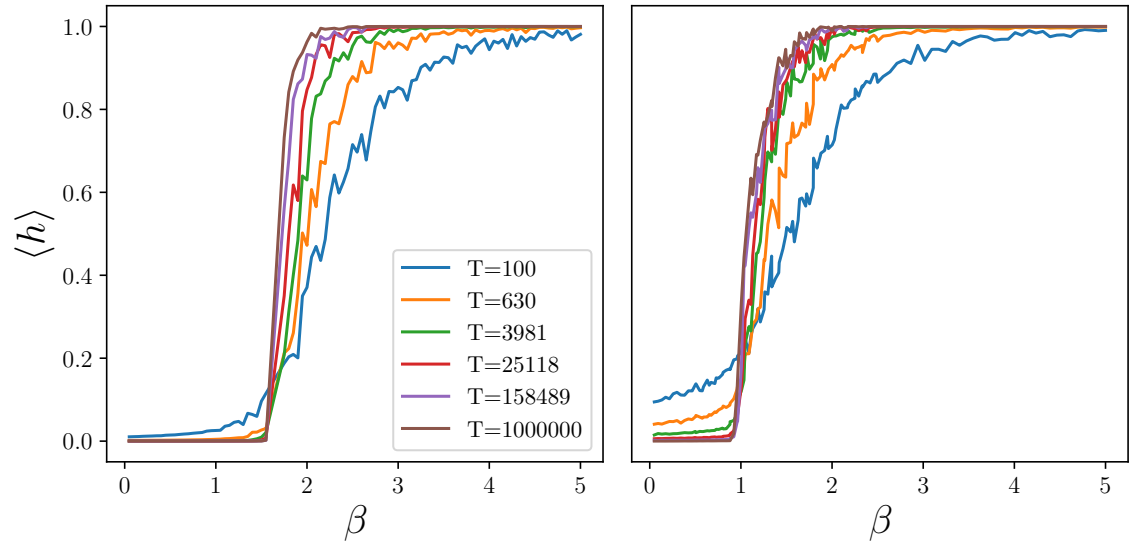

Figure B.3: *Order parameter h as a function β for $N = 10^5$, $\gamma = 1$ and different values of T. Left: Fully connected graph, for which a step function is approached as $T^{-1/3}$. Right: One-dimensional chain geometry, for which we cannot exclude that h remains a continuous function of β when $T \to \infty$.*

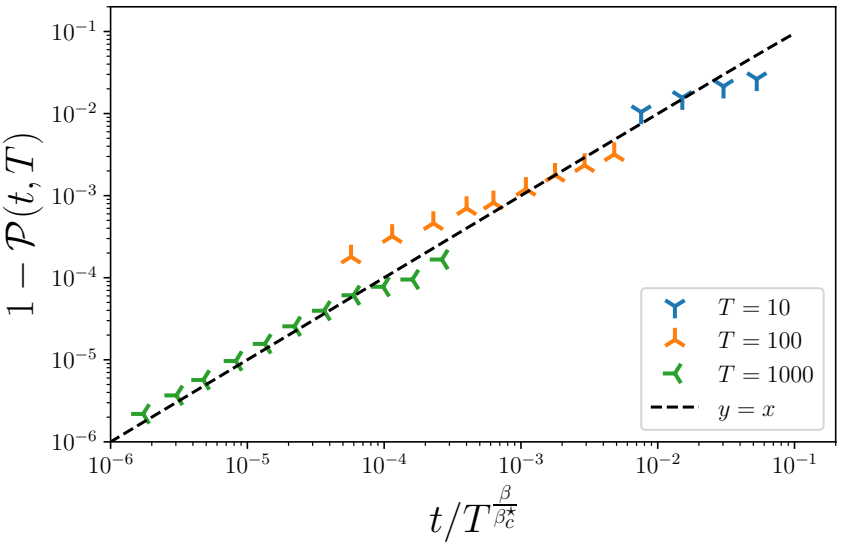

Figure B.4: *Aging function* $1-\mathcal{P}(t,T)$ *as a function of* $t/T^{\beta/\beta_c^\star}$ *in a fully connected graph with* $N=10000$*, with* $\beta_c^\star \approx 1.5$ *and* $\beta = 3.5$*. Eq.* (B.10) *predicts that* $\mathcal{P}(t,T) \approx 1 - t/T^{\beta/\beta_c^\star}$ *when* $t \ll T$ *(dashed line).*

B.6 Aging

Finally, let us be a little more specific about the meaning of self-trapping for finite T when $\beta > \beta_c^\star$. The correct statement is that the system *ages*, in the following sense [129, 132]: assume that the agent's choice at time T is a certain x_i and ask: What is the probability $\mathcal{P}(t,T)$ that the agent has never changed his/her mind between T and a later time $T+t$? In the free exploration phase $\beta < \beta_c^\star$, this probability is, for large T, independent of T: the process is time-translation invariant. In the trapped phase $\beta > \beta_c^\star$, $\mathcal{P}(t,T)$ can be estimated by appropriately generalizing Eq. (B.6). The result takes the following aging form (see Fig B.4):[6]

$$\mathcal{P}(t,T) \approx \exp\left(\frac{1}{a(T+t)^a} - \frac{1}{aT^a}\right), \quad a = \frac{\beta}{\beta_c^\star} - 1 > 0, \tag{B.10}$$

where the exponent a is equal to minus the exponent b characterizing the stretched exponential distribution in the phase $\beta < \beta_c^\star$ (see Section B.4). Note that in the regime $t \ll T$, $\mathcal{P}(t,T)$ is a function of t/T^{1+a} (precisely $\mathcal{P}(t,T) \approx 1 - t/T^{1+a}$, see dashed line in Fig. B.4), a regime called *super-aging* [134] since the effective time for changing one's mind grows faster than the age T itself. This is quite interesting since we are not aware of simple models leading to such a super-linear aging behaviour. Hence, memory effects of the type discussed here might very well be an interesting lead to interpret experiments that show such a super-aging behaviour, such as those reported in [135].

Right at the transition point $\beta = \beta_c^\star$, one finds simple aging, i.e. a scaling function of t/T:

$$\mathcal{P}(t,T) \approx \frac{1}{1+\frac{t}{T}}, \qquad \beta = \beta_c^\star. \tag{B.11}$$

When the kernel has a finite norm and leads to a crossover rather than a true transition, aging will take place whenever $T \ll e^{\beta\phi}$ but revert to a normal time translation dynamics when $T \gg e^{\beta\phi}$ (see [132] for a similar situation). When $\gamma < 1$, on the contrary, relaxation is quasi-frozen for large T, in the sense that $\mathcal{P}(t,T) \approx 1 - t\exp(-\beta C T^{1-\gamma})$ when $t \ll T^\gamma$.

[6] Note that $\mathcal{P}(t,T)$ can be written in the general form advocated by Cugliandolo and Kurchan [133]: $\mathcal{P}(t,T) = F(h(T)/h(T+t))$, where $F(u) = 1/u$ and $h(x)$ is an effective clock.

Asymptotics of $\sum_{t=0}^{T}\phi(t)$	$\phi<\infty$	$\ln(T)$	$T^{1-\gamma}$, $\gamma<1$
Asymptotics of $P_{>}(\tau)$	$e^{-\lambda\tau}$ with $\lambda=\ln\left[1+e^{-\beta\phi}\right]$	$\beta>\beta_c^\star$ (trapped regime): $P_\infty>0$ $\beta=\beta_c^\star$ (critical regime): τ^{-1} $\beta<\beta_c^\star$ (ergodic regime): $\exp(-\tau^b/b)$ with $b=1-\beta/\beta_c^\star$	$P_\infty>0$ (trapped)
Aging $\mathcal{P}(t,T)$	Trapping & aging for $T\ll e^{\beta\lvert\phi\rvert}$	$\beta>\beta_c^\star$ super-aging $t\sim T^{\beta/\beta_c^\star}$ $\beta=\beta_c^\star$ normal-aging $t\sim T$ $\beta<\beta_c^\star$ equivalent to $\phi<\infty$	Quasi-frozen relaxation

Table B.1: Summary of the different dynamical regimes.

B.7 Conclusion

Although quite simple, our model shows that non-trivial choice distortion effects can emerge through memory or self-reinforcing mechanisms. Our main result is that the addition of memory effects can hinder the full exploration of all choices by the agent, and it may even cause him/her to leave a substantial number of possible options totally unexplored. The emergence of aging properties also shows that including memory effects in agents' preferences can lead to non-ergodic dynamics, when ergodicity is a crucial assumption to many models in economics. Table B.1 summarises our results.

Several extensions can be thought of, and would be a sensible way to incorporate more realism into the model. As we mentioned, we have explored here the case where the objective utility landscape $U_0(x)$ is totally flat, in a way to highlight the effects induced by memory alone. Reintroducing some heterogeneities in $U_0(x)$ would allow one to study the competition between "landscape trapping" and "memory trapping", with possibly interesting transitions between the two. One could also imagine, along the lines of Ref. [136], a situation where an agent is only sensitive to past extreme values of his/her utility.

Another direction is to introduce many agents with interactions between them, meaning that the subjective utility may also depend on what others are doing. Here again, one expects some interesting competition between herding induced condensation of choices and memory effects. Steps in this direction, with agents interacting through a market and learning through past experience, have already been taken in [137, 138]. In particular, the combined effect of imitation of the past and imitation of peers may generate *collective self-fulfilling prophecies*.

One could also explore the case where the graph $\mathcal{G}$ defining the topology of the space of choices is itself time dependent – see [139] for a step in this direction. For example, the neighbourhood of each choice could be itself affected by past choices, or some new choices, not present initially, could present themselves later in time (for example, the opening of a new restaurant).

In all these cases, the basic question is whether memory effects, habit formation, or herding completely distort the choices dictated by their objective utilities or not. Such distortions may have very significant economic consequences at the macro level.

From a purely theoretical point of view, revisiting reinforcement models considered in the literature [112] with a power-law decaying memory kernel could lead to new interesting transitions of the type discussed above. In particular, the super-aging behaviour reported in the trapped phase might have applications much beyond the present setting.

C

Schrödinger's ants: A continuous description of Kirman's recruitment model

We show how the approach to equilibrium in Kirman's ants model can be fully characterized in terms of the spectrum of a Schrödinger equation with a Pöschl-Teller ($\tan^2$) potential. Among other interesting properties, we have found that in the bimodal phase where ants visit mostly one food site at a time, the switch time between the two sources only depends on the "spontaneous conversion" rate and not on the recruitment rate. More complicated correlation functions can be computed exactly, and involve higher and higher eigenvalues and eigenfunctions of the Schrödinger operator, which can be expressed in terms of hypergeometric functions.

From:
Schrödinger's ants: A continuous description of Kirman's recruitment model
J. Moran, **A. Fosset**, M. Benzaquen, J. P. Bouchaud

Contents

I warmly thank José Moran who had the idea of this project and worked on the parallel with quantum mechanics.

Science sans conscience n'est que ruine de l'âme.

François Rabelais

C.1 Introduction

Kirman's **ant model** [140] undoubtedly stands among some of the most inspiring toy models in the behavioural economics literature. While initially inspired by the experiment described below, its conclusions have implications much beyond collective animal behaviour, and has been used to model shifts in sentiment of economic agents, trend reversal in financial markets, herding and social influence, etc. Kirman's model is also akin to another famous model in population dynamics with competing species: the Moran model [141].

Several decades ago entomologists were puzzled by the following observation [142, 143]. Ants, faced with two identical and inexhaustible food sources A and B, tend to concentrate on one of them for a while, but occasionally switch to the other. Such intermittent herding behaviour is also observed in humans choosing between equivalent restaurants [144], or in financial markets [145, 146, 147] consistent with large endogenous fluctuations. Clearly the asymmetric exploitation observed in ants does not seem to correspond to the equilibrium state of an isolated representative ant with rational expectations. The phenomenon is rather to be explained in terms of interactions between individual ants, or, as put by biologists, recruitment dynamics. To account for such intricate behaviour, Kirman proposed a simple and insightful model [140] based on tandem recruitment that we now recall.

Consider N ants and denote by $k(t) \in [0, N]$ the number of ants feeding on source A at time t. When two ants meet, one of them converts the other with probability μ/N, but each ant may in addition change its own mind spontaneously with probability ϵ. Within such a simple setting, Kirman was able to show that, in the large N limit, the stationary state depends only on a parameter $\alpha := \epsilon/\mu$. When $\alpha > 1$ the distribution is unimodal, with a maximum at $k = N/2$, whereas for $\alpha < 1$ the stationary distribution of k is bimodal, with maximum probability for $k = 0$ and $k = N$ (corresponding to the situation observed in the experiments). It is remarkable that the interesting $\alpha < 1$ regime can be obtained even for weakly persuasive agents (μ small) provided self-conversion ϵ is itself low enough.

The most important point is that in the $\alpha < 1$ regime no one of the k states is, in itself, an equilibrium. Although the system can spend a long time at $k = 0, N$ (local stationarity) these states cannot be considered as such: all the states are always revisited and there is no convergence to any particular state, discarding also the notion of multiple equilibria. Rather, there is perpetual change, and the system's natural endogenous dynamics is only in a **statistical equilibrium**. Most economic models focus on finding the equilibrium to which the system will finally converge, and the system may only be knocked off its path by large exogenous shocks.

Yet financial markets, and even larger economic and social systems, display a number of regular large switches (correlations, mood of investors etc.) which do not seem to be always driven by exogenous shocks. In Kirman's stylised setting such switches can be understood endogenously. Several extensions of the model have been proposed [147, 148, 149], and the basic dynamics of imitation coupled with random switching can also be used to describe agents making political choices – say voting to the left or to the right – while being influenced by their peers, as described in the so-called voter model, see e.g. [150]. In particular, the original version of Kirman's model does take into account the heterogeneity in encounter probabilities induced by the topology of the social network; but one can easily (at least

numerically!) modulate the probability of encounters according to their distance along such a network, for example restricting recruitments to nearest neighbours only.

In the present paper we present a continuous description of Kirman's ant model which notably allows us to derive the typical switching time, using classical methods from statistical physics and quantum mechanics.

C.2 Master Equation

As mentioned above the original model describes N ants faced with two identical food sources, with the relevant dynamical variable being k, the number of ants feeding on – say – source A. Each time step allows an ant to either switch randomly to the other food source with probability proportional to ϵ, or get recruited by another ant from the other food source with probability proportional to μ.

Defining the unit of time as the time required for all the ants to make a decision, leads to $\mathrm{d}t = 1/N$ as the infinitesimal time step. It is also clear that, to remain intensive in the large N limit, the probability to interact with another ant should be proportional to $1/N$. Altogether, we may write a Master equation for the evolution of the probability $\mathbf{P}(k,t)$ that there are k ants feeding at source A at time t:

$$\begin{aligned}\mathbf{P}\left(k, t+\frac{1}{N}\right) - \mathbf{P}(k,t) &= \frac{1}{N}\Big\{W(k+1\to k)\mathbf{P}(k+1,t) + W(k-1\to k)P(k-1,t) \\ &\quad -\big[W(k\to k-1) - W(k\to k+1)\big]\mathbf{P}(k,t)\Big\}, \end{aligned} \tag{C.1}$$

where the transition rates are given by:

$$W(k\to k+1) = \left(1-\frac{k}{N}\right)\left(\epsilon + \frac{\mu}{N}\frac{k}{N-1}\right) \tag{C.2a}$$

$$W(k\to k-1) = \frac{k}{N}\left(\varepsilon + \frac{\mu}{N}\frac{N-k}{N-1}\right). \tag{C.2b}$$

Note that this specification only differs from Kirman's original one in the rescaling of the recruitment rate by N. With the notations of [140], $1-\delta = \mu/N$.

C.3 Continuous description and Fokker-Planck equation

Here we follow Kirman's original paper [140] and derive a proper continuous-time Fokker-Planck equation in the limit $N\to\infty$.

We define the variable $x = \frac{k}{N} \in [0;1]$ together with its probability density function $f(x,t)$. Taking the continuous limit $N\to\infty$ of Eq. (C.1) leads to the following Fokker-Planck equation [151]:

$$\partial_t f = \partial_x J^f, \quad \text{with} \quad J^f(x,t) = -\varepsilon(1-2x)f(x,t) + \mu\partial_x\left[x(1-x)f(x,t)\right], \tag{C.3}$$

the probability flux, see Appendix C.A for the details of the calculations and the first $1/N$ corrections. The conservation of the number of ants in the model is ensured by the condition $J^f(x,t) = 0$ at the boundaries $x = 0$ and $x = 1$ at all times. Equation (C.3) corresponds to the following stochastic process for x:

$$\dot{x} = \varepsilon(1-2x) + \sqrt{2\mu x(1-x)}\eta(t), \tag{C.4}$$

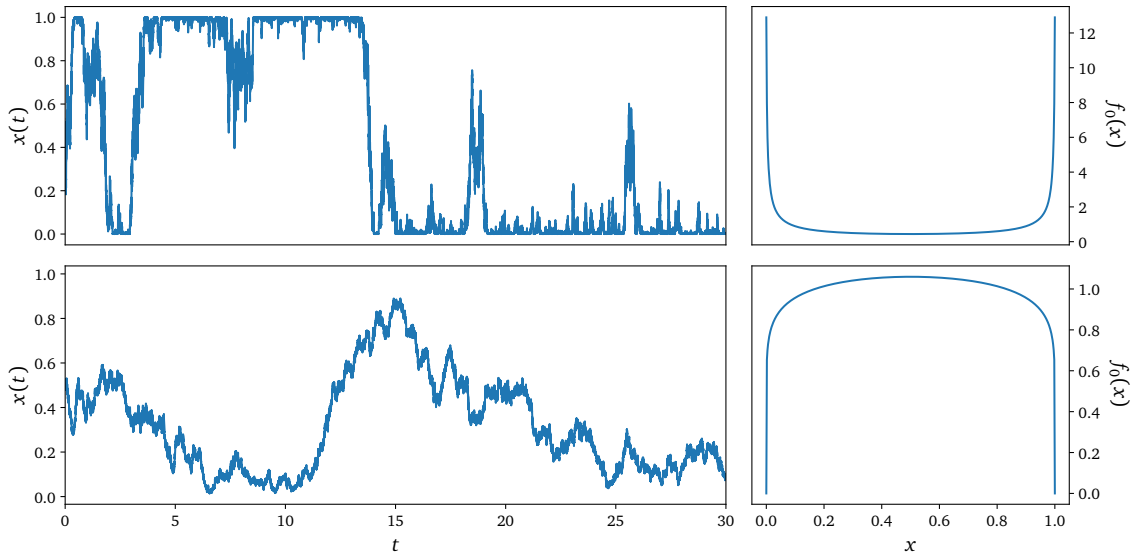

Figure C.1: *Simulations of the model in the continuous limit. The top plots correspond to* $\alpha = 0.1 < 1$ *while the bottom ones to* $\alpha = 2 > 1$*. Both simulations were run with* $\epsilon = 0.1$*. The left panels display the evolution of* $x(t)$ *as defined in Eq.* (C.4)*. The right panels display the corresponding stationary probability densities, as given by Eq.* (C.5)*.*

with η a Gaussian white noise with unit variance. One can note that while the drift term $\varepsilon(1-2x)$ is maximal at the boundaries and tends to pull x towards $1/2$, the noise term has the opposite effect. The diffusion constant is proportional to $\sqrt{2\mu x(1-x)}$ and is maximal at $x = 1/2$ and so tends to push the system away from $x = 1/2$.

Note that this stochastic process is very similar to the Moran model of genetic population dynamics [141] – with the same diffusion term $\propto \sqrt{x(1-x)}$ – where the analogue of the number of ants at each food source is the proportion of genes from two competing alleles (A or B) [152]. The ε term corresponds to spontaneous mutations. When $\epsilon = 0$, there is a non zero probability that the whole population becomes of type A or B after a finite time, corresponding to $\delta(x)$ or $\delta(1-x)$ contributions to $f(x,t)$ with a time dependent weight, see [153], and [154] for a recent thorough discussion. It is also equivalent to a model describing noise-induced bistability transitions in chemical reactions [155], as shown in [156], where the equation describing the process is equivalent to Eq. (C.3). The same diffusion term $\propto \sqrt{x(1-x)}$ also emerges naturally within the so-called voter model, that describes the opinion dynamics of peer-influenced voters [150].

When $\varepsilon > 0$, one can check that the normalised stationary distribution $f_0(x)$, obtained by setting $J^f(x,t) = 0$, writes:

$$f_0(x) = \frac{\Gamma(2\alpha)}{\Gamma^2(\alpha)}\big[x(1-x)\big]^{\alpha-1}, \quad \text{with} \quad \alpha := \frac{\varepsilon}{\mu}. \tag{C.5}$$

This result is the same as that obtained by Föllmer and Kirman in [140].

Upon looking at the behaviour of the solution, shown in Fig. C.1, one can see that there is a clear transition in the behaviour of the model at $\alpha_c = 1$. For $\alpha > \alpha_c$, the stationary density in Eq. (C.5) is maximal at $x = 1/2$, and the dynamics shows that $x(t)$ fluctuates around $1/2$, corresponding to a situation where the ants are, on average, evenly distributed across both food sources. For $\alpha < \alpha_c$ the density f_0 diverges at the boundaries. The

top left panel in Fig. C.1 shows that this corresponds to a very different picture, in which nearly all of the ants choose either one of the sources for a certain amount of time, until a noise-induced "avalanche" causes a switch over to the other source. It is also easy to check that in the absence of noise (and $\alpha \to 0$) the long-time stationary density is given by $f_0(x) = \frac{1}{2}\left[\delta(x) + \delta\left(x-1\right)\right]$, a situation discussed at length in [154].

Having this in mind, a natural question to ask is: Given a certain initial condition $f(x,0) = \delta(x - x_0)$, how long does it take for the system to converge to the stationary state, or equivalently, how long does it take for the ants to switch from one source to the other in the $\alpha < 1$ regime?

C.4 Schrödinger's equation and general solution

Here we obtain a full dynamical solution in terms of the eigenvalues and eigenfunctions of a certain quantum mechanical Hamiltonian.

Using the Itô rule [157], one can see that introducing a change of variables $\varphi(x)$ in Eq. (C.4) yields a noise term proportional to $\sqrt{x(1-x)}\varphi'(x)$, and so motivates a choice satisfying $\varphi'(x) = 1/\sqrt{x(1-x)}$. We therefore define a new, more convenient, variable $\varphi \in [-\pi/2, \pi/2]$ as:

$$\sin\varphi = 2x - 1. \tag{C.6}$$

The corresponding Fokker-Planck equation for its probability density $g(\varphi, t)$ writes:

$$\partial_t g = \mu\partial_\varphi J^g, \quad \text{with} \quad J^g(\varphi,t) = 2\beta\tan\varphi g(\varphi,t) + \partial_\varphi g(\varphi,t)\,, \quad \text{and} \quad \beta := \alpha - \frac{1}{2}\,, \tag{C.7}$$

where the probability flux must now verify $J^g(\pm\pi/2, t) = 0$ at all times. Setting again $J^g = 0$ everywhere, one finds the normalized stationary solution:

$$g_0(\varphi) = \frac{\Gamma\left(\alpha+\frac{1}{2}\right)}{\sqrt{\pi}\Gamma(\alpha)}(\cos\varphi)^{2\alpha-1}. \tag{C.8}$$

The advantage of this formulation in φ is that, in contrast with the former, the second order derivative term $\partial_{\varphi\varphi}$ in Eq. (C.7) only depends on φ through $g(\varphi, t)$. Standard techniques for the resolution of Fokker-Plank equations, see e.g. [151], motivate the introduction of a function Ψ such that:

$$g(\varphi,t) := \sqrt{g_0(\varphi)}\Psi(\varphi,t)\,, \tag{C.9}$$

and $\Psi(\varphi, t) \to \sqrt{g_0(\varphi)}$ when $t \to \infty$.

Combining Eqs. (C.7) and (C.9) one obtains a Schrödinger-like equation of the form [158]:

$$-\frac{1}{\mu}\partial_t\Psi = \mathbf{H}\Psi, \tag{C.10}$$

where the Hamiltonian $\mathbf{H}$ is defined as:

$$\mathbf{H} := -\partial_{\varphi\varphi} + V(\varphi), \quad V(\varphi) := -\beta + \beta(\beta-1)\tan^2\varphi, \tag{C.11}$$

and with boundary conditions given by:

$$\Big[\cos^\beta\varphi\big(\beta\tan\varphi\Psi(\varphi,t) + \partial_\varphi\Psi(\varphi,t)\big)\Big]_{\varphi=\pm\pi/2} = 0\,. \tag{C.12}$$

We have left the μ parameter out of the Hamiltonian $\mathbf{H}$ in order to ease the comparison to the canonical form presented in [159, 160]. The $\tan^2$ term in Eq. (C.10) is known as

the Pöschl-Teller potential [159], and appears in a similar context of social dynamics within a version of the voter model in Ref [161]. The potential we have here was fully solved in the case $\beta > 0$ with boundary conditions $\Psi(\pm\pi/2, t) = 0$ in [160]. To be applicable to our framework, we shall verify that their solutions also satisfy Eq. (C.12) in the general case $\beta > -1/2$. The Hamiltonian $\mathbf{H}$ is Hermitian (contrarily to the Fokker-Planck operator) and has a discrete set of orthogonal eigenfunctions and eigenvalues, given by:

$$\mathbf{H}\Psi_n = \mathcal{E}_n \Psi_n \,, \tag{C.13}$$

where, splitting into even ($n = 2k$) and odd ($n = 2k+1$) states:

$$\begin{aligned}
\mathcal{E}_n &= n(2\alpha + n - 1)\,, && \text{(C.14a)}\\
\Psi_{2k}(\varphi) &= A_{2k}(\beta)\ {}_2F_1\left(-k, \beta + k; \beta + \tfrac{1}{2}, \cos^2\varphi\right) \cos^\beta \varphi, && \text{(C.14b)}\\
\Psi_{2k+1}(\varphi) &= A_{2k+1}(\beta)\ {}_2F_1\left(-k, \beta + k + 1; \beta + \tfrac{1}{2}, \cos^2\varphi\right) \sin\varphi\ \cos^\beta \varphi, && \text{(C.14c)}
\end{aligned}$$

with ${}_2F_1$ the ordinary hypergeometric function.[1] The coefficients A_n are set such as to ensure normalisation, $\int_{[-\pi/2,\pi/2]} \Psi_n \Psi_m = \delta_{n,m}$, and can be expressed as integrals of hypergeometric functions. Note that the parity of n also defines the parity of the function Ψ_n with respect to the y-axis. One can then easily check that for all n (both even and odd):

$$\cos^\beta\varphi \left[\beta \tan\varphi \Psi_n(\varphi) + \Psi_n'(\varphi)\right] \underset{\varphi\to\pm\pi/2}{\sim} \left(\frac{\pi}{2} \mp \varphi\right)^{1+2\beta}, \tag{C.15}$$

which, since $\beta > -1/2$, ensure that the boundary conditions given by Eq. (C.12) are satisfied. Noting that $\Psi_0 = \sqrt{g_0}$, the general solution of Eq. (C.10) then reads:

$$\Psi(\varphi, t) = \lambda_0 \sqrt{g_0(\varphi)} + \sum_{n>1} \lambda_n \Psi_n(\varphi) e^{-\mu \mathcal{E}_n t}, \tag{C.16}$$

with λ_n given by the projections of the initial conditions on each mode n, namely $\lambda_n = \int_{-\pi/2}^{\pi/2} \mathrm{d}\varphi\ \Psi_n(\varphi)\Psi(\varphi, 0)$.

Back to the physical variable x, the initial condition $f(x, 0) = \delta(x - x_0)$ becomes $g(\varphi, 0) = \delta(\varphi - \varphi_0)$ with $\varphi_0 = \arcsin(2x_0 - 1)$. Further using Eq. (C.9), it is easy to see that the initial condition in turn translates into $\Psi(\varphi, 0) = \delta(\varphi - \varphi_0)/\sqrt{g_0(\varphi)}$. The full solution for $g(\varphi, t)$ follows:

$$g(\varphi, t) = g_0(\varphi) + \sum_{n>1} e^{-\mu \mathcal{E}_n t} \Psi_n(\varphi_0) \sqrt{g_0(\varphi)} \Psi_n(\varphi)\,, \tag{C.17}$$

with the orthogonality between $\Psi_0 = \sqrt{g_0}$ and Ψ_n for $n > 1$ ensuring that $\int_{-\pi/2}^{\pi/2} \mathrm{d}\varphi\ g(\varphi, t) = \int_{-\pi/2}^{\pi/2} \mathrm{d}\varphi\ g_0(\varphi) = 1$, or equivalently for $f(x, t)$:

$$f(x, t) = f_0(x) + \sum_{n>1} e^{-\mu \mathcal{E}_n t} \Psi_n(\varphi_0) f_n(x)\,, \tag{C.18}$$

with:

$$f_n(x) = \frac{\sqrt{g_0(\varphi(x))}\, \Psi_n(\varphi(x))}{2\sqrt{x(1-x)}}\,, \tag{C.19}$$

(see Appendix C.D for an explicit expression). Equation (C.18) is the central result of the present communication.

[1] Here, the function ${}_2F_1$ takes the form of a polynomial: ${}_2F_1(-k, a; b, u) = \sum_{l=0}^{k} \binom{k}{\ell} (-1)^\ell \frac{\Gamma(a+\ell)}{\Gamma(a)} \frac{\Gamma(b)}{\Gamma(b+\ell)} u^\ell$ for any integer k.

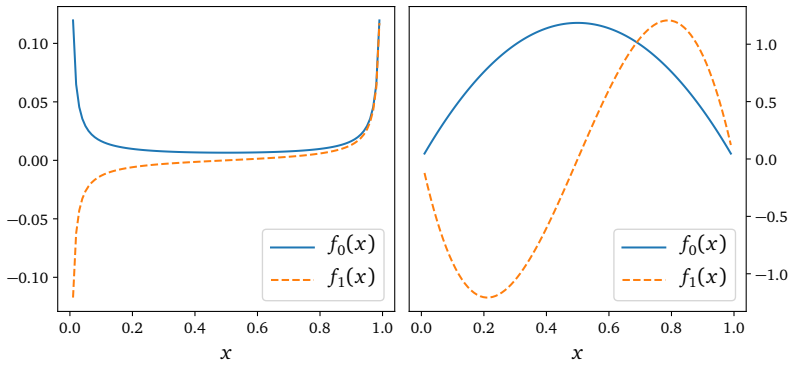

Figure C.2: *A plot showing the shape of the first two modes $f_0(x)$ and $f_1(x)$. The top panel corresponds to $\alpha = 0.1$, while the one on the bottom corresponds to $\alpha = 2$. $f_0(x)$ is the stationary state, whereas $f_1(x)$ is the slowest decaying mode, that corresponds to hopping between the two food sources.*

C.5 Relaxation towards the stationary state

With the full dynamical solution of Eq. (C.18) at hand, one can see how long a system initially prepared at an initial value $x_0 \approx 0$, for example, takes to explore the whole space. In other words, one can ask how much time τ is required to reach, say, $x(\tau) \approx 1$ with a reasonable probability.

Since the stationary distribution f_0 has weight on the whole interval $[0; 1]$, this time τ is none other than the relaxation time (or ergodic time) τ_{R} required to converge to stationarity. Owing to the form of Eq. (C.18) this convergence is asymptotically exponential, with the slowest mode given by $n = 1$. Hence, we find:

$$\tau_{\mathrm{R}} := \frac{1}{\mu \mathcal{E}_1} \equiv \frac{1}{2\epsilon}. \tag{C.20}$$

Perhaps surprisingly, this relaxation time depends only on the noise intensity ε, but not on the recruitment intensity μ. Since $n = 1$ corresponds to the slowest mode of the system, it also governs the collective "switch time" between the two food sources, A and B – see Fig. C.2.

We have checked our prediction for the switching time numerically by running trajectories starting at $x_0 = \Delta x \ll 1$ and computing the probability $\mathbb{P}(x(t) > 1 - \Delta x)$. This quantity should converge to $\int_{[1-\Delta x;1]} f_0$ at an exponential rate $\propto e^{-\mu \mathcal{E}_1 t}$, which is in perfect agreement with our simulations, see Figure C.3.

Similarly, given an initial condition $x_0 = 1/2$ where the ants are initially distributed evenly between the two sources, one may ask how long it takes for all the ants to "decide" on concentrating on one of them. Since this condition is equivalent to $\varphi_0 = 0$, and since Ψ_1 is an odd function of φ, it follows that $\Psi_1(\varphi_0) = 0$ in this case. The convergence to the stationary distribution is then controlled by the second mode, with a much shorter relaxation time given by:

$$\tau'_{\mathrm{R}} := \frac{1}{\mu \mathcal{E}_2} \equiv \frac{1}{4\varepsilon + 2\mu}. \tag{C.21}$$

Directly applying tools from stochastic calculus on Eq. (C.4), one can obtain the following correlation functions (see Appendix C.E):

$$\mathrm{Cov}\left[\sigma_n(x(T+t)), \sigma_n(x(T))\right] \propto e^{-\mu \mathcal{E}_n t}, \tag{C.22}$$

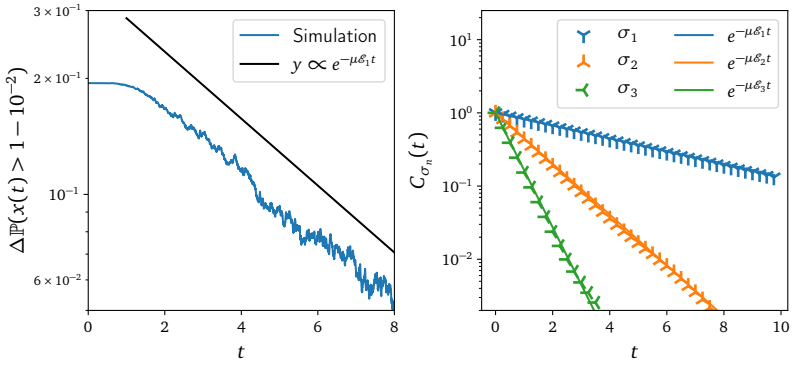

Figure C.3: *Left: plot of* $\Delta\mathbb{P}(x(t) > 1 - 10^{-2})$*, defined as the difference between* $\mathbb{P}(x(t) > 1 - 10^{-2})$ *and its stationary value, for* $\varepsilon = 0.1$ *and* $\mu = 0.5$*. The initial condition is* $x_0 = 10^{-2}$*. Right: plots of the covariances* $C_{\sigma_n}(t) = Cov[\sigma_n(x(T+t)), \sigma_n(x(T))]$*, computed over simulations with* $\varepsilon = 0.1$ *and* $\mu = 0.2$*. The agreement with theoretical predictions is excellent.*

where $\sigma_n(x)$ are polynomials of degree n that allow one to "diagonalize" the evolution of the correlations:

$$\begin{aligned} \sigma_1(x) &= x, \\ \sigma_2(x) &= x(1-x), \\ \sigma_3(x) &= (2x-1)\left[\left(1+\frac{2\alpha}{3}\right)(2x-1)^2 - 1\right]. \end{aligned} \tag{C.23}$$

See Appendix C.E for further details and Figure C.3 for a comparison with numerical results.

This result actually hides a deeper interpretation of the different modes f_n. In the case described above, one can surmise that the dynamics of the moments $\mathbb{E}[x]$, $\mathbb{E}[x^2]$ and $\mathbb{E}[x^3]$ are determined exclusively by the modes f_1,f_2 and f_3. In fact, focusing on any moment $\mathbb{E}[x^m]$, it is possible to prove that:

$$\forall n > m, \quad B_{n,m} = \int_0^1 \mathrm{d}x \; f_n(x) x^m = 0\,, \tag{C.24}$$

as well as for all values n that do not have the same parity as m. This implies in fact that the dynamics of the moments $\mathbb{E}[x^m]$ are fully described by the modes $(f_1, \ldots, f_m)$, with only even values of n contributing to even moments m and vice-versa. For example, for $m = 3$ with the initial condition $x(0) = x_0$ we can compute:

$$\mathbb{E}[x^3(t)] = B_{1,3}\Psi_1(\varphi_0)e^{-2\epsilon t} + B_{3,3}\Psi_3(\varphi_0)e^{-3(2\epsilon+2\mu)t}, \tag{C.25}$$

where the exact expression of $B_{n,m}$ is given in Appendix C.D, Eqs. (C.61) and (C.62). Mind that $B_{0,m}$ is the stationary value of moment $\mathbb{E}[x^m(t)]$ for all moments.

C.6 Conclusion

In this work, we have shown how that the approach to equilibrium in Kirman's ants model can be fully characterized in terms of the spectrum of relaxation times, itself computable as the eigenvalues of a Schrödinger equation with a Pöschl-Teller ($\tan^2$) potential. Note that similar techniques have been recently applied to discuss the dynamics of wealth inequality in Ref. [162]. Among other interesting properties, we have found that in the bimodal phase where ants visit mostly one food site at a time, the switch time between the two sources only depends on the "spontaneous conversion" rate ϵ and *not* on the recruitment rate μ. This

means that a single ant deciding on its own to explore an alternative food source can trigger an "avalanche" where the whole colony follows suit. More complicated correlation functions can be computed exactly, and involve higher and higher eigenvalues and eigenfunctions of the Schrödinger operator.

The possibility to solve exactly the dynamics of Kirman's model is of course intellectually satisfying. It is also important in view of the number of possible applications of such a model, recalled in the introduction, and which has reappeared recently in the context of self-fulfilling prophecies in a simple economic model [163] and in the empirical study of the dynamics of fishers seeking to exploit fishing zones with finite resources [164]. Our analytical approach, while similar to the techniques used in [161], can also be easily generalized to other models of genetic population or social dynamics, such as the general setting discussed in [154], as the change of variable we introduce always leads to a Schrödinger equation with a trigonometric potential provided the drift is linear in x. These equations may then be solved using known analytical tools [165].

Appendix C.A Derivation of the Fokker-Planck equation and stationary solution

We define the continuous distribution $f(x,t)$ as:

$$f(x,t) = \lim_{N\to\infty} \sum_{k=0}^{N} \delta\left(x - \frac{k}{N}\right) \mathbf{P}(k,t)\,, \tag{C.26}$$

which amounts to replacing $\frac{k}{N}$ by x in Eqs. (C.1) and (C.2). In this case, and to leading order in $\frac{1}{N}$, the term e.g. $W(k+1\to k)\mathbf{P}(k+1,t)$ reads:

$$\left(1 - \left(x + \frac{1}{N}\right)\right)\left(\varepsilon + \frac{\mu}{N}\left(x + \frac{1}{N}\right)\right) f\left(x + \frac{1}{N}, t\right). \tag{C.27}$$

We proceed similarly for all terms in the right-hand side of Eq. (C.1), and Taylor-expand the left-hand side to leading order in the time variable, to obtain:

$$\begin{aligned}\partial_t f(x,t) =& \tfrac{\varepsilon}{\Delta}\left[(x+\Delta)f(x+\Delta,t) - xf(x,t) - (1-x)f(x,t) + (1-(x-\Delta))\,f(x-\Delta,t)\right] \\ &+ \tfrac{\mu}{\Delta^2}\left[(x+\Delta)\,(1-(x+\Delta))\,f(x+\Delta,t) + (x-\Delta)\,(1-(x-\Delta))\,f(x-\Delta,t)\right. \\ &\left. - 2x(1-x)f(x,t)\right],\end{aligned} \tag{C.28}$$

where $\Delta = \frac{1}{N}$ for simplicity. We next Taylor-expand the right-hand side terms, such as e.g. $(x+\Delta)f(x+\Delta,t) \approx xf(x,t) + \Delta\partial_x\left[xf(x,t)\right] + \mathcal{O}(\Delta^2)$, to order Δ for the terms with prefactor ϵ/Δ and to order Δ^2 for the terms with prefactor μ/Δ^2. Gathering everything, we obtain the Fokker-Planck equation:

$$\partial_t f(x,t) = -\epsilon\partial_x\left[(1-2x)f(x,t)\right] + \mu\partial_{xx}\left[x(1-x)f(x,t)\right], \tag{C.29}$$

the same as given in Eq. (C.3). This equation can be written as $\partial_t f(x,t) = \partial_x J^f(x,t)$, where J^f is the probability flux, a function such that $J^f(x)\Delta$ corresponds to the probability mass flowing from $x+\Delta$ to x. To ensure the conservation of probability in $[0;1]$, we impose $J^f = 0$ at the boundaries, meaning that no probability mass comes in or goes out during the dynamic evolution of the process.

In other words, writing $I_f(t) = \int_0^1 \mathrm{d}x\ f(x,t)$, direct integration of Eq. (C.29) leads to $\dot{I}_f(t) = J^f(1,t) - J^f(0,t) = 0$, ensuring that $I_f(t) = 1$ at all times. Keeping the next term of order Δ only slightly alters the equation:

$$\partial_t f(x,t) = -\epsilon\partial_x\left[(1-2x)f(x,t)\right] + \partial_{xx}\left[(\mu x(1-x) + \epsilon\Delta)\,f(x,t)\right]. \tag{C.30}$$

Recalling now that a Fokker-Planck equation of the form

$$\partial_t p(y,t) = -\partial_y\left[a(y,t)p(y,t)\right] + \partial_{yy}\left[b(y,t)p(y,t)\right] \tag{C.31}$$

corresponds to the Itô stochastic differential equation

$$\dot{y} = a(y,t) + \sqrt{b(y,t)}\eta(t) \tag{C.32}$$

where η is a brownian white noise, one readily recovers Eq. (C.4). Physically, the 0-flux boundary condition corresponds to a reflecting boundary condition: a "wall" that prevents x from getting out of $[0;1]$.

Determining the stationary solution

Looking for a stationary solution, one sets the right-hand side of Eq. (C.29) to 0, looking to solve

$$\frac{f_0'(x)}{f_0(x)} = (\alpha - 1)\,\frac{1-2x}{x(1-x)} \quad \text{with} \quad \alpha := \frac{\varepsilon}{\mu} \tag{C.33}$$

which, after direct integration, yields $f_0(x) \propto (x(1-x))^{\alpha-1}$. Integrating for $x \in [0;1]$ allows one to find the normalisation constant in terms of the Beta function, or equivalently as a ratio of Gamma functions, to get Eq. (C.5).

Appendix C.B Change of variables under an SDE

Obtaining Eq. (C.7) and understanding the rationale behind the change of variables of Eq. (C.6) is easier by starting from Eq. (C.4).

Imposing a change of variables $x \to \varphi(x)$ leads to a new stochastic differential equation for φ, which after applying the Itô rule for differentiation reads

$$\frac{\mathrm{d}\varphi(x)}{\mathrm{d}t} = \varepsilon(1-2x)\varphi'(x) + \mu x(1-x)\varphi''(x) + \sqrt{2\mu x(1-x)}\varphi'(x)\eta(t), \tag{C.34}$$

which is still difficult to interpret because of the dependence on x of the term in front of the white noise η.

Picking however $\varphi'(x) = \frac{1}{\sqrt{x(1-x)}}$ amounts to $\varphi(x) = \arcsin(2x-1)$ and rids us of this dependence. Computing the derivatives $\varphi' = 2/\cos\varphi$ and $\varphi'' = -4\tan\varphi/\cos^2\varphi$ and replacing in Eq. (C.34):

$$\dot{\varphi} = -\,(2\epsilon - \mu)\tan\varphi + \sqrt{2\mu}\eta(t), \tag{C.35}$$

which because of the equivalence between stochastic differential equations and Fokker-Planck equations discussed in Appendix C.29 leads to Eq. (C.7). As before, imposing the reflecting boundary conditions $J^g(\pm\pi/2, t) = 0$ ensures conservation of probability.

Keeping instead the term of order Δ given in Eq. (C.30) leads first to the Langevin equation

$$\dot{x} = \varepsilon(1-2x) + \sqrt{2\mu x(1-x) + 2\varepsilon\Delta}\eta(t), \tag{C.36}$$

which leads to the change of variables

$$\phi = \arctan\left(\frac{2x-1}{2\sqrt{x(1-x)+\alpha\Delta}}\right), \tag{C.37}$$

where now $\phi \leq \arctan\left(1/\sqrt{2\alpha\Delta}\right) \approx \frac{\pi}{2} - 2\sqrt{\alpha\Delta}$, and naturally one can check that the definition of ϕ corresponds to φ as $\Delta \to 0$, with $\phi \approx \varphi - 2\alpha\Delta\tan(\varphi)$ to leading order in Δ. The analysis in the limit $N \to \infty$ therefore holds only in the limit $\tan(\varphi) \ll \frac{N}{2\alpha}$.

This new variable actually verifies the very same SDE, Eq. (C.34), but with a different boundary.

Appendix C.C Schrödinger from Fokker-Planck

The following is a common "trick" to transform a non-hermitian dynamic evolution coming from a Fokker-Planck equation with drift into a hermitian evolution determined by a Schrödinger equation. We start from a generic Fokker-Planck equation such as the one defined in Eq. (C.31), but with constant $b(y,t) = 1$ and time-independent drift, which we

represent with the derivative of some function A, $a(y,t) = -A'(y)$. The resulting Fokker-Planck equation reads

$$\partial_t p(y,t) = \partial_y \left[A'(y)p(y,t)\right] + \partial_{yy} p(y,t) \tag{C.38}$$

and has a stationary solution that can be written as a Boltzmann distribution $p_0(y) = e^{-A(y)}/Z$, where Z is a constant ensuring normalisation.

We next introduce a function Ψ verifying $p(y,t) = e^{-A(y)/2}/\sqrt{Z}\Psi(y,t)$. We can compute derivatives to find

$$\begin{aligned}\partial_y \left[A'(y)p(y,t)\right] &= e^{-A(y)/2}/\sqrt{Z}\left[\left(A''(y) - \frac{A'(y)^2}{2}\right)\Psi(y,t) + A'(y)\partial_y\Psi(y,t)\right] \\ \partial_{yy} p(y,t) &= e^{-A(y)/2}/\sqrt{Z}\left[-\frac{1}{2}\left(A''(y) - \frac{A'(y)^2}{2}\right)\Psi(y,t) - A'(y)\partial_y\Psi(y,t) + \partial_{yy}\Psi(y,t)\right].\end{aligned} \tag{C.39}$$

Adding these terms and simplifing, we find the following Schrödinger's equation for Ψ:

$$-\partial_t \Psi(y,t) = \mathbf{H}\Psi, \tag{C.40}$$

where the Hamiltonian is here defined as

$$\mathbf{H} = -\partial_{yy} + V(y), \quad V(y) = -\frac{1}{2}\left(A''(y) - \frac{A'(y)^2}{2}\right). \tag{C.41}$$

Equation (C.10) simply uses this substituion, with $\int \mathrm{d}\varphi\ \tan\varphi = \log\cos\varphi$ playing the role of $A(y)$ (up to a multiplicative constant).

Appendix C.D Properties of the solution

We take the solutions in Eq. (C.14) as those given in [160]. We first check that they satisfy the boundary condition.

Checking the boundary condition

We recall that

$${}_2F_1\left(-k, a; b, u\right) = \sum_{l=0}^{k} \binom{k}{\ell} (-1)^\ell \frac{\Gamma(a+\ell)}{\Gamma(a)} \frac{\Gamma(b)}{\Gamma(b+\ell)} u^\ell. \tag{C.42}$$

In this case, direct differentiation in Eq. (C.14) for e.g. even modes $n = 2k$ in the limit $\varphi \to \pm\frac{\pi}{2}$leads to

$$\begin{aligned}\frac{\mathrm{d}}{\mathrm{d}\varphi}\left({}_2F_1\left(-k, \beta+k; \beta+\frac{1}{2}, \cos^2\varphi\right)\right) &= 2\sin\varphi\cos\varphi\frac{k(\beta+k)}{\beta+1/2} + \mathcal{O}(\cos\varphi) \\ &\approx \pm 2\left(\frac{\pi}{2} \mp \varphi\right)\frac{k(\beta+k)}{\beta+1/2}.\end{aligned} \tag{C.43}$$

With this one can directly compute, with ${}_2F_1\left(-k, \beta+k; \beta+\frac{1}{2}, 1\right) := c_1$ and for $\varphi \to \pm\frac{\pi}{2}$:

$$\begin{aligned}\beta\tan\varphi\Psi_{2k}(\varphi) + \Psi'_{2k}(\varphi) &\approx \beta\tan\varphi\cos^\beta\varphi\ c_1 - \beta\tan\varphi\cos^\beta\varphi\ c_1 \pm 2\cos^\beta\varphi\ \left(\frac{\pi}{2} \mp \varphi\right)\frac{k(\beta+k)}{\beta+1/2} \\ &\approx \pm 2\frac{k(\beta+k)}{\beta+1/2}\left(\frac{\pi}{2} \mp \varphi\right)^{1+\beta},\end{aligned} \tag{C.44}$$

which after multiplication with $\cos^\beta\varphi \approx \left(\frac{\pi}{2} \mp \varphi\right)^\beta$ proves Eq. (C.15) for $n = 2k$. The proof for odd $n = 2k+1$ is strictly equivalent. It therefore follows that the solutions of [160], although found initially for vanishing boundary conditions, also satisfy the boundary condition given in Eq. (C.12).

Explicit expressions

In this section we discuss the explicit expressions of the functions f_n and the constants A_n.

The constants A_n are set so that $\int_{-\pi/2}^{\pi/2} \Psi_n \Psi_m = \delta_{n,m}$, and therefore implies, in terms of the variable α,

$$\begin{aligned} A_{2k}(\alpha) &= \left(\int_{-\frac{\pi}{2}}^{\frac{\pi}{2}} \mathrm{d}\varphi \ \cos^{2\alpha-1}\varphi \ {}_2F_1\left(-k, \alpha+k-\frac{1}{2}; \alpha, \cos^2\varphi\right)^2 \right)^{-1/2} \\ A_{2k+1}(\alpha) &= \left(\int_{-\frac{\pi}{2}}^{\frac{\pi}{2}} \mathrm{d}\varphi \ \cos^{2\alpha-1}\varphi \ \sin^2\varphi \ {}_2F_1\left(-k, \alpha+k+\frac{1}{2}; \alpha, \cos^2\varphi\right)^2 \right)^{-1/2}. \end{aligned} \tag{C.45}$$

To substitute and find the expressions of $f_n(x)$, we recall that

$$\sin\varphi = 2x-1, \quad \cos\varphi = 2\sqrt{x(1-x)} \tag{C.46}$$

and get, using Eq. (C.14) and replacing into $f_n(x) = \frac{\sqrt{g_0(\varphi(x))}\Psi_n(\varphi(x))}{2\sqrt{x(1-x)}}$, the explicit expression

$$f_{2k}(x) = A_{2k}(\alpha)\sqrt{\frac{\Gamma(\alpha+1/2)}{\sqrt{\pi}\Gamma(\alpha)}} \ {}_2F_1\left(-k, \alpha+k-\frac{1}{2}; \alpha, 4x(1-x)\right)(4x(1-x))^{\alpha-1} \tag{C.47}$$

$$f_{2k+1}(x) = A_{2k+1}(\alpha)\sqrt{\frac{\Gamma(\alpha+1/2)}{\sqrt{\pi}\Gamma(\alpha)}} \ {}_2F_1\left(-k, \alpha+k+\frac{1}{2}; \alpha, 4x(1-x)\right)(4x(1-x))^{\alpha-1}(2x-1). \tag{C.48}$$

Computing the moments of the distribution

To understand the dynamics of the moments of the distribution

$$\mathbb{E}\left[x^m(t)\right] = \int_0^1 \mathrm{d}x \ f(x,t)x^m \tag{C.49}$$

it is necessary to understand the behaviour of $B_{n,m} = \int_0^1 \mathrm{d}x \ f_n(x)x^m$. Owing to the parity of $f_n(x)$ with respect to $x = 1/2$ it is clear that for even moments $m = 2p$ only even modes $n = 2k$ will be non zero, and vice versa for odd moments and modes.

We therefore develop the computation of even moments only, as the extension to odd moments is direct. We wish to evaluate the integral $\int_0^1 \mathrm{d}x \ f_{2k}(x)x^{2p} = 2\int_0^{1/2} \mathrm{d}x \ f_{2k}(x)x^{2p}$, after changing variables as $t = 4x(1-x)$, it is clear that this integral is proportional to

$$I_{2p,2m} = \int_0^1 \mathrm{d}t \ {}_2F_1\left(-k, \alpha+k-\frac{1}{2}; \alpha, t\right) t^{\alpha-1}(1-t)^{p-1/2}. \tag{C.50}$$

After expanding the hypergeometric function and integrating explicitly, we find

$$I_{2k,2p} = \frac{\Gamma(\alpha)\Gamma(1/2+p)}{\Gamma(\beta+k)} \sum_{l=0}^{k} \binom{k}{l} (-1)^l \frac{\Gamma(\beta+k+l)}{\Gamma(\beta+1+l+p)} = \frac{\Gamma(\alpha)\Gamma(1/2+p)}{\Gamma(\beta+k)} S_{2k,2p} \tag{C.51}$$

requiring then the explicit computation of the sum $S_{2k,2p}$.

Mind that for $m = 2p+1$ the only modes that contribute are $n = 2k+1$, and the equivalent of the previous integral is

$$I_{2k+1,2p+1} = \frac{\Gamma(\alpha)\Gamma(3/2+p)}{\Gamma(\beta+k+1)} \sum_{l=0}^{k} \binom{k}{l} (-1)^l \frac{\Gamma(\beta+1+k+l)}{\Gamma(\beta+2+l+p)} = \frac{\Gamma(\alpha)\Gamma(3/2+p)}{\Gamma(\beta+k+1)} S_{2k+1,2p+1} \tag{C.52}$$

We discuss this for $k \geq 1$ in two situations, $k > m$ and $k \leq m$.

First case: $k > m$

We can then write the sum $S_{2k,2p}$ as

$$\sum_{l=0}^{k} \binom{k}{l} (-1)^l \prod_{i=p+1}^{k-1} (\beta+l+i), \tag{C.53}$$

which, written as such, leads us to introduce the function

$$P(X) = \sum_{l=0}^{k} \binom{k}{l} (-1)^l X^{\beta+l+k-1} = X^{\beta+k-1}(1-X)^k. \tag{C.54}$$

Applying the generalized Leibniz rule to compute the $k-p-1$-th derivative of this function, we obtain directly that $S_{2k,2p} = P^{(k-p-1)}(1) = 0$ in this case. A similar calculation can be done for $S_{2k+1,2p+1}$, and it follows therefore that

$$\int_0^1 \mathrm{d}x \; f_n(x) x^m = 0 \quad \text{for } n > m. \tag{C.55}$$

Second case: $k \leq m$

In this case, we now write the sum as

$$\sum_{l=0}^{k} \binom{k}{l} (-1)^l \prod_{i=k}^{p} \frac{1}{\beta+l+i}, \tag{C.56}$$

which can instead be seen as the result of successive integrations on the function defined in Eq. (C.54).

To compute it, we define the functions ${}_0(t;a,b) = t^{a-1}(1-t)^{b-1}$ and ${}_{n+1}(t;a,b) = \int_0^t \mathrm{d}u \; {}_n(u;a,b)$, with ${}_1$ corresponding to the standard incomplete Beta function. With this definition, the sum reads

$$S_{2k,2p} = \int_0^1 \mathrm{d}u \; {}_{p-k}(u;\beta+k+1,k+1), \tag{C.57}$$

while on the other hand successive integration by parts gives

$$\begin{aligned} {}_n(1;a,b) &= \left[\sum_{j=0}^{n-1} (-1)^{j+1} \frac{(t-1)^{j+1}}{\Gamma(j+2)} \, {}_{n-j}(u;a,b) \right]_0^1 + (-1)^n \int_0^1 \mathrm{d}u \; \frac{(t-1)^n}{\Gamma(n+1)} \, {}_0(u;a,b) \\ &= \frac{{}_1(n+a,b)}{\Gamma(n+1)}. \end{aligned} \tag{C.58}$$

Finally, gathering everything we get

$$S_{2k,2p} = \frac{\Gamma(p+\beta+1)\Gamma(k+1)}{\Gamma(p+\beta+k+2)\Gamma(p-k+1)}, \tag{C.59}$$

while replacing $\beta \to \beta+1$ gives the similar expression

$$S_{2k+1,2p+1} = \frac{\Gamma(p+\beta+2)\Gamma(k+1)}{\Gamma(p+\beta+k+3)\Gamma(p-k+1)}. \tag{C.60}$$

The final result follows,

$$B_{n,m} = \int_0^1 \mathrm{d}x\ f_n(x)x^m = A_n(\alpha)\sqrt{\frac{\Gamma(\alpha+1/2)}{\sqrt{\pi}\Gamma(\alpha)}} I_{n,m}\mathbf{1}\,(n \leq m) \tag{C.61}$$

with

$$\begin{aligned} I_{2k,2p+1} &= 0 \\ I_{2k,2p} &= \frac{\Gamma(\alpha)\Gamma(1/2+p)\Gamma(p+\beta+1)\Gamma(k+1)}{\Gamma(\beta+k)\Gamma(p+\beta+k+2)\Gamma(p-k+1)} \\ I_{2k+1,2p+1} &= \frac{\Gamma(\alpha)\Gamma(3/2+p)\Gamma(p+\beta+2)\Gamma(k+1)}{\Gamma(\beta+k+1)\Gamma(p+\beta+k+3)\Gamma(p-k+1)}, \end{aligned} \tag{C.62}$$

allowing then for explicit computation of the dynamics of $\mathbb{E}\left[x^m(t)\right]$.

Appendix C.E Stochastic calculus techniques

In this Appendix, we shall directly integrate stochastic differential equations describing the model to obtain information on the covariances of moments $x^n(t)$. We begin by looking at the covariance $\mathrm{Cov}(x(t+T),x(T))$.

A direct integration of Eq. (C.4) leads to

$$x(t+T) = x(T) + \varepsilon t - 2\varepsilon\int_T^{t+T}\mathrm{d}s\ x(s) + \int_T^{t+T}\mathrm{d}s\ \sqrt{2\mu x(s)(1-x(s))}\eta(s). \tag{C.63}$$

Taking now the covariance with $x(t)$ and using linearity,

$$\begin{aligned} \mathrm{Cov}(x(t+T),x(T)) =& \mathrm{Cov}(x(T),x(T)) - 2\varepsilon\int_T^{t+T}\mathrm{d}s\ \mathrm{Cov}(x(s),x(T)) \\ &+ \int_T^{t+T}\mathrm{d}s\ \mathbb{E}\left[\sqrt{2\mu x(s)(1-x(s))}x(T)\eta(s)\right] \end{aligned} \tag{C.64}$$

with the last integral being equal to 0, as

$$\mathbb{E}\left[\sqrt{2\mu x(s)(1-x(s))}x(T)\eta(s)\right] = \mathbb{E}\left[\sqrt{2\mu x(s)(1-x(s))}x(T)\right]\mathbb{E}\left[\eta(s)\right] = 0. \tag{C.65}$$

Taking finally the derivative with respect to t and solving the resulting differential equation we find

$$\begin{aligned} &\frac{\mathrm{d}}{\mathrm{d}s}\mathrm{Cov}(x(T+s),x(T)) = -2\varepsilon\mathrm{Cov}(x(T+s),x(T)) \\ &\mathrm{Cov}(x(t+T),x(T)) \propto e^{-2\varepsilon t}. \end{aligned} \tag{C.66}$$

Similarly, one can derive the stochastic differential equation followed by $\sigma_2(x) = x(1-x)$

using the differentiation rule exemplified in Eq. (C.34), namely

$$\frac{\mathrm{d}[x(1-x)]}{\mathrm{d}t} = \varepsilon - (4\varepsilon + 2\mu)x(1-x) + \sqrt{2\mu x(1-x)}(1-2x)\eta(t), \tag{C.67}$$

and as before, we can take the covariance $\mathrm{Cov}(\sigma_2(x(t+T)), \sigma_2(x(T)))$, differentiate with respect to t and find that it satisfies a differential equation, which after integrating reads

$$\mathrm{Cov}(\sigma_2(x(t+T)), \sigma_2(x(T))) \propto e^{-(4\varepsilon+2\mu)t}. \tag{C.68}$$

This method can be extended to computing $C_{n,k}(t+T,T) = \mathrm{Cov}\left(x(t+T)^n, x(T)^k\right)$. Applying Itô calculus as before, one can show that these functions satisfy the following ODE system:

$$\frac{\mathrm{d}}{\mathrm{d}s}\left[C_{n,k}(T+s,T)\right] = -\mu\mathcal{E}_n C_{n,k}(T+s,T) + \mu n(n-1+\alpha)C_{n-2,k}(T+s,T). \tag{C.69}$$

Owing to its triangular structure, it can be diagonalized iteratively to find functions σ_n, such that $\sigma_n(x)$ is a polynomial of degree n and that the covariances $C_{\sigma_n}(T+s,T) = \mathrm{Cov}\left[\sigma_n(x(T+s)), \sigma_n(x(T))\right]$ satisfy

$$\frac{\mathrm{d}}{\mathrm{d}s}C_{\sigma_n}(T+s,T) = -\mu\mathcal{E}_n C_{\sigma_n}(T+s,T). \tag{C.70}$$

Knowing that $\sigma_1(x) = x$ and $\sigma_2(x) = x(1-x)$, it is possible to find the third combination $\sigma_3(x) = (2x-1)\left[\left(1+\frac{2\alpha}{3}\right)(2x-1)^2 - 1\right]$. Integrating the equations in Eq. (C.70), one finds then that

$$C_{\sigma_n}(t+T,T) \propto e^{-\mu\mathcal{E}_n t}. \tag{C.71}$$

These results can also be obtained directly from the eigenvalues and eigenfunctions of the Schrödinger problem.

D

From Ants to Fishing Vessels: A Simple Model for Herding and Exploitation of Finite Resources

Empirical data reveals that the fraction of fishermen fishing in the zone they are based in is well approximated by a Beta distribution. Furthermore its auto-correlation appears to be exponential, similar to the famous Kirman's ants recruitment model. This piece of evidence has led us to extend such model to two asymmetric zones with finite resources. We show that, in the mean-field regime, our model exhibits the same properties that the empirical data: asymmetric Beta distribution for the fraction of fishermen fishing in their zone and exponential auto-correlations. From those results, we draw a phase diagram that separates high and low herding but also fish extinction.

From:
From Ants to Fishing Vessels: A Simple Model for Herding and Exploitation of Finite Resources
J. Moran, **A. Fosset**, A. Kirman, M. Benzaquen

Contents

I truly thank Alan Kirman for his insights on fish markets, herding dynamics as well as his help for setting up this project, giving us access to fisheries data. I also warmly thank José Moran for his work on this article.

Eschyle

D.1 Introduction

A problem of general interest is that of the individual and collective exploitation of a resource. Depending on the particular context, the dynamics can be very different. A crucial factor is the effect of the behaviour of individuals on the collective outcome. In financial markets for example, the decision to buy may enhance the value of the resource for others as the price of an asset may increase as the demand for it grows. This positive feedback can lead to "herd behaviour" and to creation of "bubbles". If, on the other hand, the resource is in fixed supply or can only generate a limited flow, as in the case of agricultural production, over exploitation can lead to its exhaustion when individuals do not take account of the overall consequences of their actions. This leads to what has been called "The Tragedy of the Commons" [166].

In this paper we will use a version of a model which was developed in the context of financial markets, but we modify it to look at a problem of exhaustible resources, in particular that of fisheries. There is a substantial literature on fishing management which analyses the causes of over exploitation and the behaviour that leads to this. Much of that literature was based on understanding the strategies that individual boats use to decide when and where to fish. The simplest idea is that the individuals base their decisions on Catch per Unit Effort (CPUE), see [167]. This suggests that boats fish until their catch falls below a certain threshold and then move on. This is a purely individualistic model and argues that past individual experience is an adequate basis for decision making. Two questions arise here. Firstly, can one deduce the behaviour from the observed behaviour of individual vessels and secondly does the behaviour of other vessels influence the choices of a particular boat? The answer to the first question is that with the development of satellite technology individual vessels can be identified and followed, and this provides a basis for analysing the individual and collective behaviour of fishing fleets. It was, of course, known that vessels do not act in total isolation and a model using tracking data for New Zealand fisheries was, for example, studied in Ref. [168]. This came to the conclusion that âthere is evidence that vessels make decisions about where to fish based on both their own recent catch history and on observation about the location and aggregation of other vessels. There is no evidence that there is enough information transfer for vessels to make decisions on the basis of catch rates of the other vessels in the fleetâ. While the influence of other players is taken into account, it is not the major driving influence for collective behaviour.

However, a more radical approach, abandoning a simple optimization approach had been developed earlier by Allen and McGlade [169]. They developed models in part based on the Lotka-Volterra equations which already incorporated recent advances in the understanding of the evolution of complex systems. They studied herd behaviour and simulations a dynamic model of a Nova Scotia fishery. Their analysis revealed that human responses amplified rapid random fluctuations in recruitment and excite strong Lotka-Volterra type oscillations in a system that would normally settle to a stable stationary state. Their dynamic, multi-species, multi-fleet spatial model was calibrated to the Nova Scotian groundfish fisheries. They examined the role of "exploration" and "exploitation". They identified two types of hunters, "stochasts" or high-risk takers, and "cartesian" followers, or low risk takers. The result of the interaction between the two reveals, as they say, "the 'out of phase' relationship between abundance and the ease with which fishermen locate a highly sought species and its converse". They emphasize, contrary to more conventional analysis, "the importance of information exchange in defining the attractivity of a particular fishing zone to different fleets and the ability of the model to take into account coded information, misinformation, spying

and lying; and the fact that models based on global principles, such as 'optimal efficiency' or 'maximum profit', are clearly of dubious relevance to the real world. "

Our approach is in this spirit and is based on a model in which agents are "recruited" to a source of profit by those already benefiting from that source. The actors follow simple rules, but their interaction can produce interesting dynamics. A related approach by computer scientists [170] suggested that the result might be that of a uniform distribution across the space in which the resource is found. We show that vessels can typically operate near to their home port with excursions to another area, but that changing the parameters of the model can lead to a persistent mixing of the two fleets recalling a result of Allen and McGlade in which the survival of the fishery was dependent on the existence of some vessels which chose the place to fish at random.

D.2 Empirical fishing data

As mentioned above, while applicable to a wider range of situations, our work was originally inspired by imitation and herding effects in fishing areas. Here we present the data we use together with some stylized facts, both quantitative and qualitative.

Description of the data

We use the Fishing Vessels Dataset from Global Fishing Watch [171] from Octobre 2012 to December 2016. Since our aim is to analyse the behaviour of fishermen seeking to exploit clearly distinguishable fishing areas, we geographically focus on the Adriatic Sea and specifically on the area encompassing the Italian cities of Ancona and Pescara in which two of the largest fishing harbours and fish markets are set (see for example [172] for a detailed study and description of the Ancona fishing market). The two cities are separated by a reasonable distance of about 150 km, meaning that boats based in one city can easily find themselves fishing close to the other. Further, the existence of large and comparable fish markets in both cities hints the possibility of matching fishing activity to market data, provided of course one has access to the latter. Note that while another city, San Benedetto del Tronto, lies between Ancona and Pescara, it is responsible for a rather negligible amount of the activity in the area.

We have also restricted our analysis to the behaviour of trawlers. These boats have a low cruise speed and fish in shallow waters close to the coast. A reasonable hypothesis, which we've confirmed with the local market authorities, is that trawlers fishing in the area are based in either one of the two cities and go out for a short amount of time before coming back to sell their catch on the local market. In particular we were told that, due to the policy of the market to sell fresh local fish, vessels (almost) always get back to the port after 24 hours. We were also told that while there is no ban for a boat registered in a given port to land his fish elsewhere, this seldom happens.[1] In other words, one expects trawlers based in, say, Pescara to leave port, fish for at most a day or two and then come back to sell their catch.

The reduced data set consists of daily tracking of these trawlers, identified by their 9-digit Maritime Mobile Service Identity (MMSI) number. Each vessel is tracked on a latitude-longitude grid with resolution 0.1.1 squared degrees. At Ancona and Pescara's latitude ($\approx 43^\circ$ North), this implies a spatial resolution of $\approx 11 \times 8$ km^2 (latitude by longitude). Finally, a preliminary study of the data shows that there is a significative reduction of fishing activity from Friday to Sunday, consistent with markets being open Monday through

[1] According to the director of the Ancona fish market, there are no relationships with nearby wholesale markets (Pescara and San Benedetto del Tronto)and two or three times a year, it happens that a boat based in the nearby port in the north (Fano or Cattolica) comes to sell.

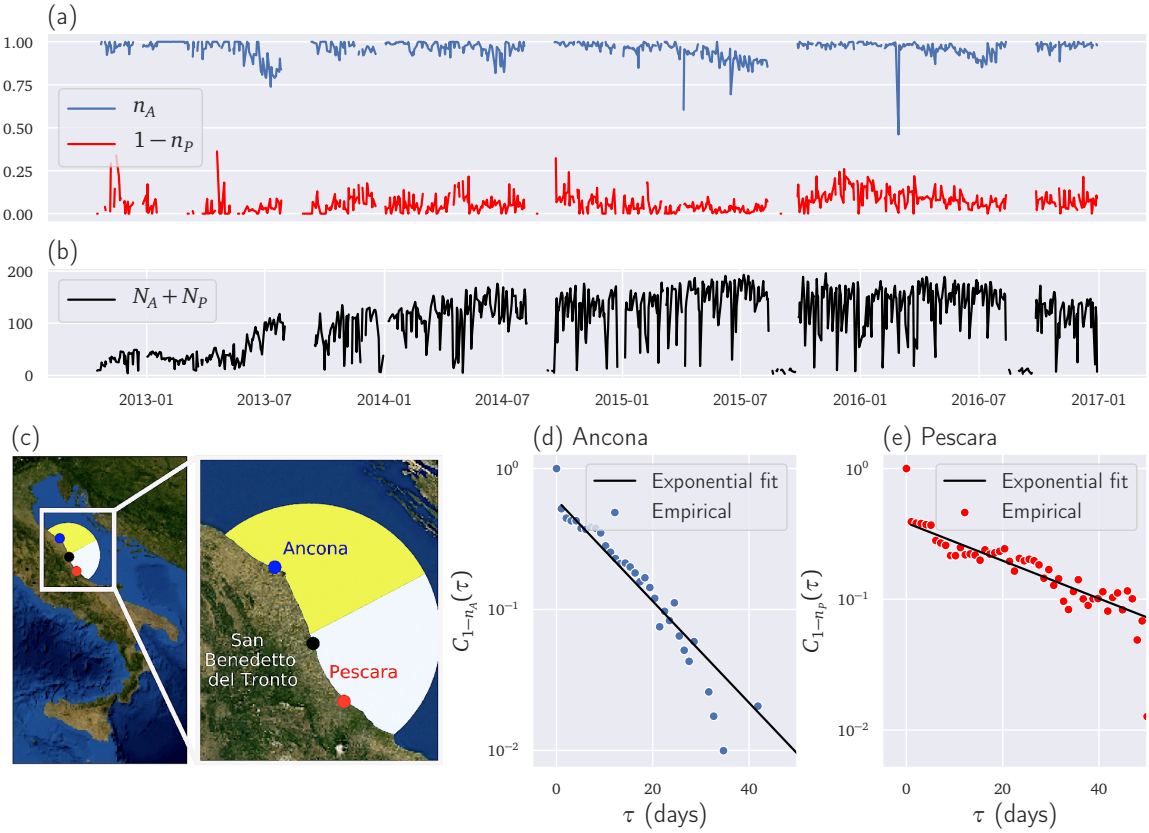

Figure D.1: *Various Figures depicting the data. Blue curves and markers correspond to data related to the area of Ancona, while red curves and markers correspond to Pescara. (a) Plot of the fraction $n_i(t)$ as defined in Eq.* (D.2) *(b) Plot of the total number of active boats through time $N_A + N_P$. (c) Satellite view of the Adriatic Sea along with the areas $\mathcal{D}_\mathrm{A}$ and $\mathcal{D}_\mathrm{P}$ defined in Eq.* (D.1)*. (d) and (e) Autocorrelation plots $C_{1-n_i}(\tau)$ defined in Eq.* (D.3) *for both zones. For Ancona we find an exponential fit with a decay rate of ≈ 11 days, while for Pescara we find a decay of ≈ 33 days.*

Thursday only. We have thus dropped the former from our data set, keeping only trading days to ensure significant fishing activity.

Defining fishing areas

To assign each trawler with its base port (Ancona or Pescara), we use the following heuristic procedure, which we then cross-validate with MMSI data provided by the Ancona market authorities. We introduce the notations:

- $h^i(x,t)$ the time spent by trawler i fishing at grid-point x on day t,
- $w^i(x) := \sum_t h^i(x,t) / \sum_{y,s} h^i(y,s)$, for the average fraction of time spent by trawler i fishing at point x,
- $d_\mathrm{A}(x)$ the distance between point x and Ancona, and d the distance between the two cities,
- $d^i_\mathrm{A} := \sum_x w^i(x) d_\mathrm{A}(x)$, the average distance separating trawler i and Ancona when it is fishing,

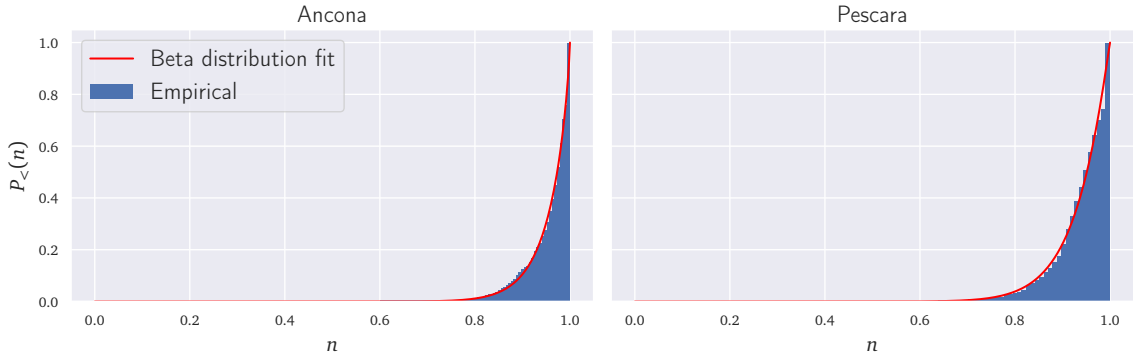

Figure D.2: *Cumulative distribution function (cdf) of the fractions* n_{A} *and* n_{P} *as defined in Eq.* (D.2). *The solid red curves correspond to a fit with a generalized Beta distribution, which has a cdf given by* $P_>(n) = C \int_0^n \mathrm{d}x\, x^{\gamma_0 - 1}(1-x)^{\gamma_1 - 1}$ *with* C *a normalization constant. The parameters for Ancona are* $\gamma_0 = 18.48$ *and* $\gamma_1 = 0.82$, *while those for Pescara read* $\gamma_0 = 17.73$ *and* $\gamma_1 = 1.27$.

- $D^i_{\mathrm{A}} := \sum_x w^i(x)[d_{\mathrm{A}}(x)]^2$, the average square distance between trawler i and Ancona.

and of course symmetrically for Pescara with index P. We then define the neighborhood of Ancona and Pescara as the pseudo-ellipsoid with focal points the two ports, i.e. the set $\{x \mid d_{\mathrm{A}}(x)^2 + d_{\mathrm{P}}(x)^2 \leq 2d^2\}$, of course excluding land, see Fig. D.1(c). We restrict our analysis to trawlers evolving within this area, namely $\{i \mid D^i_{\mathrm{A}} + D^i_{\mathrm{P}} \leq 2d^2\}$. We then assign the trawlers to one of the two ports according to their average distance to each of them. Defining two distinct areas as:

$$\mathcal{D}_{\mathrm{A}} = \left\{x \mid d_{\mathrm{A}}(x) \leq d_{\mathrm{P}}(x) \quad \text{and} \quad d_{\mathrm{A}}(x)^2 + d_{\mathrm{P}}(x)^2 \leq 2d^2\right\} \tag{D.1a}$$

$$\mathcal{D}_{\mathrm{P}} = \left\{x \mid d_{\mathrm{P}}(x) < d_{\mathrm{A}}(x) \quad \text{and} \quad d_{\mathrm{A}}(x)^2 + d_{\mathrm{P}}(x)^2 \leq 2d^2\right\}, \tag{D.1b}$$

a given trawler is assigned to, say, Pescara if its fishing time-weighted average position lies in $\mathcal{D}_{\mathrm{P}}$. In other words $i \in$ Pescara (resp. Ancona) if $d^i_{\mathrm{P}} \leq d^i_{\mathrm{A}}$ (resp. $d^i_{\mathrm{A}} < d^i_{\mathrm{P}}$). To validate our method of home port identification, we were able to confront our classification to the list of the Ancona-based trawlers, kindly provided by the Ancona fish market authorities. Up to a few minor errors, notably related to having identified as Ancona-based a few vessels based in the much smaller San Benedetto del Tronto, the cross-check was successful. Over the whole period we counted $N_{\mathrm{A}} = 108$ Ancona-based and $N_{\mathrm{P}} = 118$ Pescara-based trawlers.

Stylized facts

Having tagged each boat to either Ancona or Pescara, we now turn to studying the dynamics of fishing within the two areas $\mathcal{D}_{\mathrm{A}}$ and $\mathcal{D}_{\mathrm{P}}$. We define the fraction $n_{\mathrm{A}}(t)$ of time spent by Ancona-based vessels fishing in $\mathcal{D}_{\mathrm{A}}$ namely:

$$n_{\mathrm{A}}(t) = \frac{\sum_{x \in \mathcal{D}_{\mathrm{A}}, i \in \text{Ancona}} h^i(x,t)}{\sum_{y, i \in \text{Ancona}} h^i(y,t)}, \tag{D.2}$$

and vice-versa $n_{\mathrm{P}}(t)$ for Pescara. Figure D.1(b) displays the evolution of $n_{\mathrm{A}}(t)$ and $n_{\mathrm{B}}(t)$ throughout the period of interest. While these fractions are most often very close to 1, indicating as one would intuitively expect that trawlers spend most of their time fishing near their home port, one can see that they regularly undergo persistent excursions, revealing that a sizeable fraction of the vessels in each area decide collectively to go elsewhere.

To evaluate the typical length of such excursions, Figs. D.1(d) and (e) display the auto-

correlation functions:

$$C_{1-n}(\tau) := \mathrm{Cor}\left(1 - n(t+\tau), 1 - n(t)\right), \tag{D.3}$$

for both $n_{\mathrm{A}}(t)$ and $n_{\mathrm{P}}(t)$. These are well fitted by the sum of a delta-peak at 0, which can be attributed to measurement noise and other exogenous factors such as the weather,and an exponentially decaying function with typical timescale ranging from ≈ 11 to ≈ 30 days. Interestingly enough, Fig. D.2 reveals that the empirical distributions of n_{A} and n_{P} are remarkably well fitted by a Beta distribution.This is exactly what one obtains in Kirman's ant recruitment model [140, 173], in which the Beta distribution emerges as the stationary distribution describing a colony of ants preying on two distinct food sources. Such a distribution also emerges as the stationary distribution describing genetic populations between two competing alleles[141, 152]. The key ingredient in these models is the competition between two different entities, be they food sources or genetic alleles. In Kirman's ant model however, the two food sources are strictly equivalent and the resulting Beta distribution describing the fraction of ants at each source necessarily symmetric, at odds with the results obtained in the present setting. This motivates the asymmetric zones model introduced below. Another significant difference with Kirman's original model is that the "food sources" here are not inexhaustible, as fishes do not have the ability to reproduce at an infinite rate.

These empirical results and observations motivate us to introduce a model extending Kirman's original ant recruitment model to our context. In essence, one can think of the two cities as two distinct ant colonies that can prey on any of the two zones. For each colony, the further fishing area is necessarily less attractive, allowing for the asymmetric character of the distribution. In addition, at odds with Kirman's model, we are not in a setting with unlimited resources, and our model should take into account the fact that over-fishing may deplete the sea.

D.3 A Simple Model

Kirman's original ant-recruitment model [140] was successful at explaining a rather puzzling fact well known to entomologists [142, 143]. Ants, faced with two identical and inexhaustible food sources tend to concentrate on one of them and occasionally switch to the other. Such intermittent herding behaviour is observed in a variety of settings including choosing between equivalent restaurants [144], or financial markets [145, 146, 147] consistent with large endogenous fluctuations. In Kirman's model, at each time step a given ant may either (i) encounter another ant from the other inexhaustible food source and decide to switch to her peer's source (be recruited), or (ii) spontaneously decide to switch food sources without interacting. The driving mechanism of the dynamics results from the trade-off between the intensity of the noise-term ε (spontaneous switching), and that of the interaction term μ, see also Appendix C.

Here we present an extension of Kirman's original model to account for **non-inexhaustible** and asymmetric sources, notably aimed at accounting for some of the stylized facts presented in the previous section for fishing areas. Seeking to model fishermen exploiting a set of fishing areas, we imagine that boats follow the same basic dynamics as the ants: if they initially fish within a certain zone, they may decide to move elsewhere either because they see their peers fishing there, deciding to imitate them because they assume that their yield is good or spontaneously decide to move elsewhere randomly for the sake of exploration.

Our model has two major differences that depart from the original ant-recruitment model. First, we consider that a fishing area has finite resources: fish reproduce until reaching a certain finite capacity but they are also depleted by fishermen in the area (as in e.g. MacArthur's models [174, 175]). As a consequence, we decide for the random switching rate at which fishermen decide to depart from a given area depends on the fish population of

that area. Note that this is very close in spirit to the modelling done in Ref. [169], albeit our model takes into account imitative behaviour in fishermen. The second difference with the ant model is that we imagine two "colonies" instead of just one, corresponding to vessels based at the two different fishing ports of Ancona and Pescara. Guided by the idea that fishermen prefer to go to areas close to their own home port, we introduce an asymmetry between the fishing areas for each food source.

The two ports, labelled A and P, have two distinct populations of fishermen, which may decide to exploit two fishing areas, S_1 and S_2, with the fishermen from A preferring to fish at S_1 and vice versa. One may of course reasonably argue that this view is far too coarse-grained, and that there may be, for example, many different fishing areas that are available close to each port. It is however possible to show under mild hypotheses that the two zones S_1 and S_2 in the model can be seen as the aggregation of a large number of smaller areas, with the same dynamics, see Appendix D.B for details. For clarity, we shall define the model in discrete time, before moving into continuous time for analytical convenience.

Without loss of generality, we focus only on the dynamics of fishing vessels at one of the two ports, say Ancona, as we assume that fishermen only interact with boats coming from the same city[2]. We define now N_A and N_P as the number of boats based at Ancona and Pescara respectively, and let each of them decide to go to any of the two areas S_1 and S_2. We denote $m_i(t)$, with $i = 1, 2$, their respective fish populations at time t, and further assume that:

- Boats only fish in one area each day (consistent with discussions with port authorities) and come back to that area if they don't decide to switch to another one for the next day.
- A vessel's daily catch $c_i(t)$ is proportional to the amount of fish available in the area: $c_i(t) = \frac{\beta}{N_A} m_i(t)$ with $\beta/N_A \in [0; 1]$.[3]
- Fish reproduce at a multiplicative rate ν_i, which we will take to be equal to ν for both areas.
- As a first approximation, fish do not travel from one area to the other.[4]
- The fish population within any area cannot exceed a carrying capacity K_i, which is the maximal population that can be present within an area in the absence of fishing. This carrying capacity is the same for all areas, as we have taken all of them to be equivalent. Without loss of generality, we take $K_1 = K_2 = 1$ in all that follows.

Note that these definitions, which also amount to thinking of the fish population as consisting of the same species in both areas, are partially justified by our considering only trawlers, that therefore fish only very specific, shallow water dwelling species.f

We further define $N_{A,i}(t)$ the number of vessels from port A fishing at zone i at time t (and $N_{P,i}(t)$ respectively). The number of fishing vessels in each port is fixed, implying for

[2] Anecdotal evidence suggests indeed that the main interaction between people working in different boats happens at port in the fishing market or during informal conversation.

[3] Without changing our main conclusions, one could also allow for noise by drawing $c_i(t)$ from a given distribution centred about $\beta m_i(t)/N$. This would allow introducing randomness into the fishing efficiency of each trawler, an interesting extension that we leave to further work.

[4] This constraint can be easily relaxed by e.g. adding a migration term where fishes from 2 move to 1 at a certain rate and vice-versa. In practice, this would only tend to prevent the difference between the two fish populations from fluctuating too wildly.

all t: $N_{A,1}(t) + N_{A,2}(t) = N_A$. Our assumptions translate into following evolution for the fish population:

$$m_i(t+1) - m_i(t) = m_i(t)\left[\nu g(m_i(t)) - \beta\left(N_{A,i}(t) + N_{P,i}(t)\right)\right], \tag{D.4}$$

where the function g must satisfy $g(0) = 1$ and $g(1) = 0$. The simplest assumption one can make is that of logistic growth, leading to $g(m_i(t)) = 1 - m_i(t)$. It follows that $m_i(t) \in [0;1]$, $\forall t$, where $m = 1$ corresponds to a fishing area at full capacity and $m = 0$ corresponds to a depleted area. Under these assumptions, the evolution of the fish population is of the Lotka-Volterra type, as advocated in [169][5].

Furthermore, we assume that a fishing vessel based at A fishing at i can randomly decide to go elsewhere with probability $\varepsilon_{A,i} f(m_i(t))$, where the function f satisfies $f(1) = 1$ and $f(0) = 1 + \kappa$. Here, $\varepsilon_{A,i}$ controls the base intensity of the noise, that can take a maximal value $\varepsilon_{A,i}(1+\kappa)$ when the zone is depleted. Fishermen have then a higher incentive to go elsewhere as their fishing yield decreases, and we highlight the preference of fishermen from A for zone 1 by setting $\varepsilon := \varepsilon_{A,1} = \varepsilon_{A,2}/C_d$ with $C_d > 1$ a parameter controlling the degree of asymmetry between zones S_1 and S_2 for a fisher from A. This allows us to have a larger spontaneous switching rate $S_2 \to S_1$ for fishermen from A.

Besides this random switching rate, we add in the crucial element in our model, which is that agents imitate each other. Each day, a fisher randomly picks one of his peers at random and decides to imitate him/her with probability μ/N, so that μ is the fraction of boats deciding to take an imitation strategy at each step. In this case, the probability that a boat from A initially at zone S_i decides to move to zone S_j is given by:

$$P_A(S_i \to S_j) = \varepsilon_{A,i} f(m_i(t)) + \frac{\mu}{N_A}\frac{N_{A,j}(t)}{N_A - 1}. \tag{D.5}$$

Writing then $n_{A,i} = N_{A,i}/N_A$ and taking the limit $N_A, N_P \to \infty$ with $N_P/N_A = C_N$ fixed, it is possible to write the following Fokker-Planck equation for the probability density $\rho(\mathbf{n}_A, \mathbf{n}_P, \mathbf{m})$, where $\mathbf{n}_A = (n_{A,1}, n_{A,2})$ and $\mathbf{m} = (m_1, m_2)$,

$$\begin{aligned}
\partial_t \rho = &- \varepsilon \partial_{n_{A,1}}\left[C_d f(m_2) - n_{A,1}\left[C_d f(m_2) + f(m_1)\right]\right]\rho + \mu \partial^2_{n_{A,1},n_{A,1}}\left[n_{A,1}(1-n_{A,1})\right]\rho \\
&+ \left[(n_{A,1}, m_1) \leftrightarrow (n_{P,2}, m_2)\right] \\
&- \partial_{m_1}\left[\nu(1-m_1) - \beta\left(n_{A,1} + C_N(1-n_{P,2})\right)\right] m_1 \rho \\
&+ \left[(m_1, n_{A,1}, n_{P,2}) \leftrightarrow (m_2, 1-n_{A,1}, 1-n_{P,2})\right],
\end{aligned} \tag{D.6}$$

where the bracket $[x \leftrightarrow y]$ is shorthand for the same expression where one replaces x by y.

These equations fully close the model, which in our view represent the simplest setting for a system with limited resources exploited by entities with a myopic exploration/imitation strategy. As they stand, however, they cannot be solved analytically. We shall now resort to a mean-field approximation to find a solution.

[5] As an interesting anecdote, we learned in [176] that "Vito Volterra was born in the Jewish ghetto of Ancona in 1860, shortly before the unification of Italy, when the city still belonged to the Papal States", and that "in 1925, at age 65, Volterra became interested in a study by the zoologist Umberto DâAncona, who would later become his son-in-law, on the proportion of cartilaginous fish (such as sharks and rays) landed in the fishery during the years 1905â1923 in three harbours of the Adriatic Sea: Trieste, Fiume and Venice. DâAncona had noticed that the proportion of these fish had increased during the First World War, when the fishing effort had been reduced". This led him to take interest in models that Alfred Lotka had first used to model very general population dynamics, and that we now apply, without knowing any of this at first, to the fish population dynamics at the ports of Ancona and Pescara.

D.4 Mean-field approximation

The mean-field approximation in our setting amounts to replacing the behaviour of the fish populations m_i with their long-term averages. The evolution of the fish population of, e.g., zone 1 follows:

$$\frac{\mathrm{d}m_1}{\mathrm{d}t} = m_1(t)\left(\nu(1-m_1(t)) - \beta\left(n_{A,1} + C_N\left(1-n_{P,2}\right)\right)\right). \tag{D.7}$$

Taking the average of this equation and setting $\frac{\mathrm{d}m_1}{\mathrm{d}t} = 0$ yields:

$$m_1 = \left[1 - \frac{\beta}{\nu}\left(n_{A,1} + C_N\left(1-n_{P,2}\right)\right)\right]_+, \tag{D.8}$$

where $[x]_+ = x\mathbf{1}_{x>0}$ denotes the positive part of x. In particular, one can see that there exists an extinction line for the fish population for:

$$\nu = \beta\left[n_{A,1} + C_N\left(1-n_{P,2}\right)\right], \tag{D.9}$$

corresponding to the case where the reproductive rate of fish corresponds exactly to the rate at which they are fished.

We then insert Eq. (D.8) into the vessels' dynamics by replacing the argument of $f(m_i)$ by the average, as $f(m_i) := f_i$. Choosing, for the sake of definiteness, a linear function for f, i.e. $f(x) = 1 + \kappa(1-x)$, the average $n_{A,1}$ can now be easily computed from Eq. (D.6) by setting the drift term to 0, as:

$$n_{A,1} = \frac{C_d f_2}{C_d f_2 + f_1} = \frac{C_d\left(1+\kappa(1-m_2)\right)}{2 + \kappa\left[1 - m_1 + C_d\left(1-m_2\right)\right]}. \tag{D.10}$$

Stationary solutions

Consistent with our mean-field approximation, we set $m_1 = m_1$ (resp. $m_2 = m_2$) in Eq. (D.6) to obtain a single Fokker-Planck equation where we have decoupled the two variables n_A and n_P, as:

$$\partial_t \rho = \partial_{n_{A,1}} J_1 + \partial_{n_{P,2}} J_2, \tag{D.11}$$

where:

$$J_1 = -\varepsilon\left[C_d f_2 - n_{A,1}\left[C_d f_2 + f_1\right]\right]\rho + \mu\partial_{n_{A,1}}\left[n_{A,1}(1-n_{A,1})\right]\rho, \tag{D.12}$$

and where the transposition to find the definition of J_2 is transparent. The stationary state is found by setting $J_1 = 0$ and $J_2 = 0$ and solving for ρ. The decoupling of the two variables allows one to write:

$$\rho(n_{A,1}, n_{P,2}) = \rho_1\left(n_{A,1}\right)\rho_2\left(n_{P,2}\right), \tag{D.13}$$

with:

$$\rho_1(n_{A,1}) = C_1 n_{A,1}^{\gamma_{A,0}-1}\left(1-n_{A,1}\right)^{\gamma_{A,1}-1}, \quad \rho_2\left(n_{P,2}\right) = C_2 n_{P,2}^{\gamma_{P,0}-1}\left(1-n_{P,2}\right)^{\gamma_{P,1}-1}, \tag{D.14}$$

where C_1 and C_2 are normalisation constants and the γ parameters for the ρ_1 distribution (the parameters for ρ_2 can be easily deduced) read:

$$\gamma_{A,0} = \frac{\varepsilon}{\mu} C_d f_2, \quad \gamma_{A,1} = \frac{\varepsilon}{\mu} f_1. \tag{D.15}$$

Note also that full dynamical solutions $\rho(n_{A,1}, t)$, $\rho(n_{P,2}, t)$ can be obtained in terms of hypergeometric functions, in the same spirit of [173], see Appendix D.A.

Our model thus successfully replicates the observed distributions shown in Figure D.2, and captures the qualitative behaviour from Figure D.1. An example of simulation from the

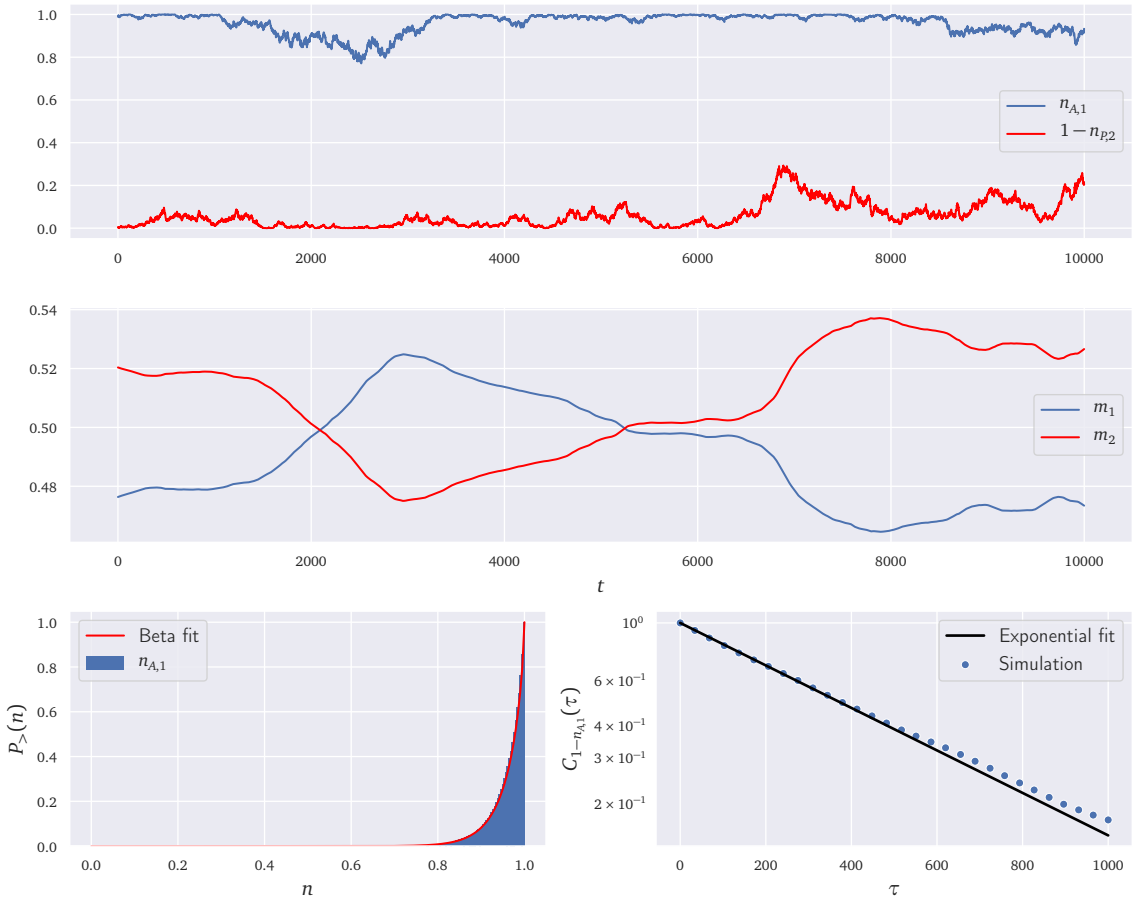

Figure D.3: *A simulation of our model. We have chosen the different parameters as to obtain the same stationary Beta distribution as observed in Fig. D.2. Note also the similarity of the Figure on the left with plot (a) in Figure D.1. We have used the parameters* $\varepsilon = 0.69$, $\nu = 10$, $\beta = 5$, $C_N = 1$, $C_d = 26.5$ *for Ancona and* 15.7 *for Pescara and* $\kappa = 0.1$. *The upper panel shows the two trajectories* $n_{A,1}(t)$ *and* $n_{P,2}(t)$ *and the middle panel shows the fish populations* $m_1(t)$ *and* $m_2(t)$, *while the bottom left panel shows the cumulative density function for* $n_{A,1}$ *along with a Beta distribution fit, and the bottom right panel shows the empirical correlation function as defined by Eq.* (D.17) *along with an exponential fit. Note that the fish populations oscillate around the theoretical mean-field value* $m = 0.5$, *and that large oscillations coincide with large collective movements of the fishermen in both areas.*

model is provided in Figure D.3. For this Figure, we have set $\mu = 1$ as it only amounts to a certain choice of the time-scale, while picking a small value $\kappa = 0.1$ to keep $f_2, f_1 \approx 1$ and we have then picked ε and C_d as to obtain the values for γ_0 and γ_1 from Figure D.2.

Dynamics and correlation functions

Within the mean-field model above, it is straightforward to show (see the appendices in Ref [173]) that the variable $n_{A,1}$ follows the following stochastic evolution:

$$\frac{\mathrm{d}n_{A,1}}{\mathrm{d}t} = \mu\left(\gamma_{A,0} - (\gamma_{A,0} + \gamma_{A,1})\, n_{A,1}\right) + \sqrt{2\mu n_{A,1}\,(1 - n_{A,1})}\eta(t), \tag{D.16}$$

with η a gaussian white noise of unit variance. Using standard tools from stochastic calculus it is then possible to compute the auto-correlation of $1 - n_{A,1}$, defined as in Eq. (D.3), to

find

$$C_{1-n_{A,1}}(\tau) = \exp\left(-\mu\left(\gamma_{A,0} + \gamma_{A,1}\right)\tau\right), \tag{D.17}$$

which is exactly what one sees from the data in Fig. D.1 (d) and (e), provided one interprets the delta-peak at $\tau = 0$ as the result of exogenous noise, e.g. weather conditions.

Indeed, if one considers that the measured signal is in fact a noisy signal,

$$\tilde{n}(t) = (1-\sigma)n(t) + \sigma\xi(t), \tag{D.18}$$

where $n(t)$ is the "true" process and $\xi(t)$ is a gaussian white noise of unit one, then one can show directly that the measured correlation function reads

$$C_{1-\tilde{n}}(\tau) = \delta\left(\tau\right) + \frac{(1-\sigma)^2}{\sigma^2} C_{1-n}(\tau). \tag{D.19}$$

We have checked for this in our simulations as well, with the results shown in the bottom right panel in Figure D.3. Again, the agreement is excellent both with the theory and the data, meaning that our model can correctly replicate the main dynamical features of real data from fishing dynamics.

Furthermore, one can deduce the value of μ from the values of γ_0, γ_1 and the decay factor in the exponential, that should match $\mu\left(\gamma_0 + \gamma_1\right)$. Using this formula, we find $\mu = 4.3 \cdot 10^{-3}$ day^{-1} for Ancona and $\mu = 1.7 \cdot 10^{-3}$ day^{-1} for Pescara.

More complicated correlation functions can also be computed, along the lines of [173], although they are more prone to statistical noise. For example, using stochastic calculus techniques described in detail in Appendices B and E of Ref. [173], one can show that the polynomial defined by

$$\sigma_A(n_{A,1}) = n_{A,1}^2 - \frac{2(\gamma_{A,0}+1)}{\gamma_{A,0}+\gamma_{A,1}+2} n_{A,1} \tag{D.20}$$

has an autocorrelation function that is exponential, meaning that $C_{\sigma_A}(\tau)$ defined by

$$C_{\sigma_A}(\tau) = \mathrm{Cor}\left(\sigma_A\left(n_{A,1}(t+\tau)\right), \sigma_A\left(n_{A,1}(t+\tau)\right)\right) \tag{D.21}$$

verifies

$$C_{\sigma_A}(\tau) = \exp\left(-2\mu(1+\gamma_{A,0}+\gamma_{A,0})\tau\right), \tag{D.22}$$

and the same definition can of course be transposed to the variables indexed by P.

We have tested this prediction, with the results shown in Fig. D.4. This correlator is necessarily more affected by noise, because it is of order two in the n variables and because it depends on a reliable estimation of the γ and μ variables. Despite these limitations, the theoretical prediction is satisfactory when compared with the data, especially in the case of Pescara.

D.5 The Symmetric Limit

In general, the fixed-point equations defined at the beginning of Section D.4 linking the averages m_i with the averages n_1 cannot be solved directly. Nonetheless, if one takes $C_N = 1$ to have completely symmetric fishing areas, then the equations simplify considerably as this immediately implies $f_1 = f_2$, with then Eq. (D.10) becoming

$$n_{A,1} = n_{P,2} = \frac{C_d}{C_d + 1}. \tag{D.23}$$

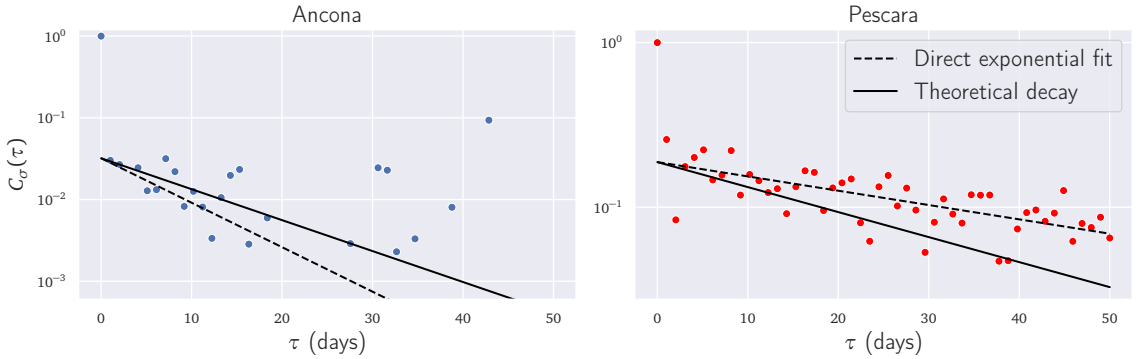

Figure D.4: *Empirical correlation function $C_\sigma(\tau)$ as defined in Eqs.* (D.20) *and* (D.22). *The solid black line is the theoretical prediction given the estimations of γ_0 and γ_1 from the empirical probability distribution in Figure D.2 and from the subsequent estimation of μ using the exponential decay factor from Figure D.1. The reliable computation of σ depends of course on the proper estimation of these parameters, and we expect them to be noisy. Nonetheless, the agreement with theory, especially in the case of Pescara, is good.*

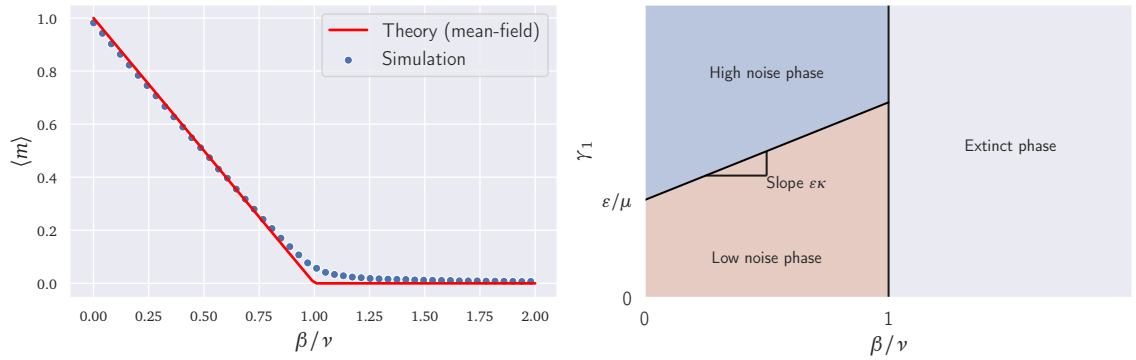

Figure D.5: *Left: simulation results with the same parameters as previously. The simulation was run for $T = 10^5$ steps and with $\nu = 10$. Note that the convergence of the simulation to the mean-field results from Eq.* (D.24) *is better as T or ν grow larger. Right: phase diagram of the model.*

One can then write Eq. (D.8) more explicitly, to obtain the following extinction line,

$$m_1 = m_2 = \begin{cases} 1 - \frac{\beta}{\nu} & \text{if} \quad \beta < \nu \\ 0 & \text{if} \quad \beta \geq \nu \end{cases}, \tag{D.24}$$

which has the intuitive interpretation that the population within a given area goes extinct if the fishing rate is larger than the reproduction rate of the fish there. We have shown in Figure D.5 that the agreement of simulations with our mean-field analysis is excellent. One should note however that this convergence may be slow as $\nu \to 0$, as this parameter controls the global time-scale of the fishes.

Note also that in this case, one can directly compute $f_1 = f_2 = 1 + \frac{\kappa\beta}{\nu}$. In this case, the parameters in Eq. (D.15) simplify to yield

$$\gamma_0 = \frac{\tilde{\varepsilon}}{\mu} C_d, \quad \gamma_1 = \frac{\tilde{\varepsilon}}{\mu}. \tag{D.25}$$

where we've dropped the A index as the parameters for both areas A and P are identical, and where we've set $\tilde{\varepsilon} = \varepsilon \left(1 + \frac{\kappa\beta}{\nu}\right)$.

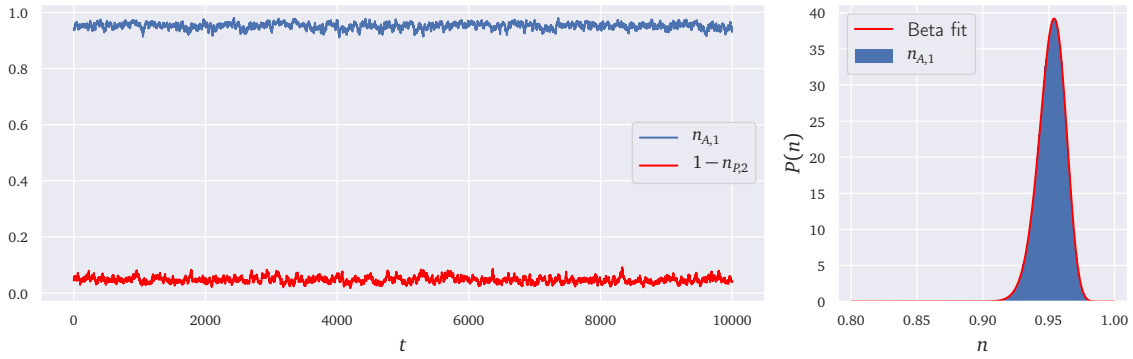

Figure D.6: *Plot of our simulations in the case $\gamma_1 > 1$. The parameters are the same as that of Figure D.3, but with $\kappa = 10$ instead. The fit gives $\gamma_0 = 220$ and $\gamma_1 = 20$, while the predicted theoretical values from Eq. D.25 are $\gamma_0 = 220$ and $\gamma_1 = 11$. Note that, contrary to Figure D.2, we show the density directly instead of the cumulative density function.*

In this limit it is then clear that our mean-field model amounts to a modification of the original ant model [140], where the noise ε is augmented because of the sensitivity of the fishermen to the local fish population by the factor given above, and where we have introduced an asymmetry between the two areas/food-sources through the parameter C_d.

One would then typically expect that $\gamma_0 > 1$ always because of the strong preference for the fishing area closest to one's port. However, if ε or κ are strong, one can have a crossover at $\gamma_1 = 1$. The simulations on Figure D.3 correspond both to $\gamma < 1$, the empirical data shown in Figures D.1 and D.2 has $\gamma_1 < 1$ for Ancona, and $\gamma_1 \lessapprox 1$ for Pescara. When $\gamma_1 > 1$ the behaviour is qualitatively different: instead of having the majority of the boats nearly always fish at the closest area, with occasional "jumps" to go to the neighbouring zone, there is always a degree of "mixing", as at any given time there is always a fraction $\approx 1 - n_{A,0}$ of fishermen from Ancona fishing near Pescara. We show a simulation of this case, with γ_1 well above 1, in Figure D.6.

D.6 Conclusion

In this paper, we have empirically analysed fishing vessels in the two areas nearby Ancona and Pescara. By detecting to which area a vessel belongs, we have computed the fraction of fishermen fishing in their own zone and looked at their statistical properties. It reads that the empirical distribution functions are well approximated by asymmetric Beta distributions and their auto-correlations look exponentials. Inspired by such evidence, we have extended the famous Kirman's ants recruitment model to finite and asymmetric resources. Thanks to a numerical and theoretical analysis, we have derived the auto-correlations and the stationary distribution of the fraction of fishermen that appears to be respectively exponential and Beta distributed. Then we have drawn the phase diagram that separates a high herding phase with a low one but also fish extinction.

We have tested our dynamics by looking at higher order correlations that can be empirically computed. This signal appears to be very noisy and of low intensity but compatible with an exponential decay. Its time scale is of the same order of magnitude than the one predicted by our model. On the other hand, there could exist other models that can reproduce the stylized facts we have exposed. Thus, we should design a test that could discriminate whether fishermen follow the dynamics of our model or not. Nevertheless, we have been very surprised to see how well such a simple model reproduces the stylized facts we have highlighted.

One major drawback of our model relies on the fact that it does not take into account essential parameters that rule vessels activity such as weather. We believe that a full model for fishermen's behavior should consider this point. Indeed, we should understand its impact on herding and exploration and incorporate it in the model. Having access to weather data could also have helped us in the cleaning procedure and hopefully given us cleaner results, especially for higher correlations.

Appendix D.A Full dynamical solution

The goal of this section is to sketch a full dynamical solution for the dynamics of Eq.(D.16). We drop indices A or P for clarity, obtaining:

$$\frac{\mathrm{d}n}{\mathrm{d}t} = \mu\left(\gamma_0 - (\gamma_0+\gamma_1)\, n\right) + \sqrt{2\mu n(1-n)}\eta(t), \tag{D.26}$$

a stochastic differential equation that corresponds to the following Fokker-Planck equation [151],

$$\partial_t \rho = \mu\partial_{nn}\left(n(1-n)\rho\right) - \mu\partial_n\left(\left(\gamma_0 - (\gamma_0+\gamma_1)\, n\right)\rho\right), \tag{D.27}$$

with reflecting boundary conditions in $n = 0$ and $n = 1$.

As in Ref. [173], we can "diagonalize" this equation. Indeed, writing it as

$$\partial_t \rho = \mathcal{A}\rho, \tag{D.28}$$

with $\mathcal{A}$ a Fokker-Planck operator that gives the right-hand side of Eq. (D.27) when applied to ρ. It is in principle possible to apply the same techniques as in Ref. [173] to obtain a Schrödinger's equation for an alternative function Ψ, that one could then use to compute ρ explicitly.

On the other hand, we can directly solve the eigenvalue problem

$$\mathcal{A}\rho_{\mathcal{E}} = \mathcal{E}\rho_{\mathcal{E}}, \tag{D.29}$$

so that the general solution reads

$$\rho(n,t) = \sum_{\mathcal{E}} \lambda_{\mathcal{E}}\rho_{\mathcal{E}}(n)e^{-\mathcal{E}t}. \tag{D.30}$$

In this setting, $\mathcal{E}$ and $\rho_{\mathcal{E}}$ are respectively the eigenvalues and eigenvectors of the operator $\mathcal{A}$. These eigenvectors should also be normalized so that their integral is equal to 1.

Therefore, the problem translates into finding functions $\rho_{\mathcal{E}}$ and numbers (or "energies") $\mathcal{E}$ that satisfy

$$\begin{aligned}
\mu\mathcal{E}\rho_{\mathcal{E}} &= \mu\partial_{nn}\left(n(1-n)\rho_{\mathcal{E}}\right) - \mu\partial_n\left(\left(\gamma_0 - (\gamma_0+\gamma_1)\, n\right)\rho_{\mathcal{E}}\right) && \text{(D.31a)}\\
J_{\mathcal{E}}(0) &= J_{\mathcal{E}}(1) = 0 && \text{(D.31b)}\\
\int_0^1 \mathrm{d}n\ \rho_{\mathcal{E}}(n) &= 1, && \text{(D.31c)}
\end{aligned}$$

with $J_{\mathcal{E}}(n) = \mu\partial_n\left(n(1-n)\rho_{\mathcal{E}}\right) - \mu\left(\gamma_0 - (\gamma_0+\gamma_1)\, n\right)\rho_{\mathcal{E}}$.

In order to solve Eq.(D.31a), we rewrite it as.

$$n(1-n)\rho''_{\mathcal{E}} + \left(2 - \gamma_0 - (4-\gamma_0-\gamma_1)\, n\right)\rho'_{\mathcal{E}} - \left(2 + \mathcal{E} - \gamma_0 - \gamma_1\right)\rho_{\mathcal{E}} = 0 \tag{D.32}$$

The solutions of this differential equation are given in terms of the hypergeometric function,

$$ {}_2F_1(a,b;c;n) = \sum_k \frac{(a)_k (b)_k}{(c)_k} \frac{n^k}{k!}, \quad (a)_k = \prod_{i=0}^{k-1} (a+i) \tag{D.33} $$

Here the two linear independent solutions well defined around zero, see e.g.[177], are ${}_2F_1(a,b;2-\gamma_0;n)$ and $n_2^{\gamma_0-1}F_1(a+\gamma_0-1, b+\gamma_0-1; \gamma_0; n)$, where a, b are the solutions of:

$$ a+b = 3-\gamma_0-\gamma_1 \tag{D.34a} $$
$$ ab = 2+\mathcal{E}-\gamma_0-\gamma_1. \tag{D.34b} $$

Only the second solution cited above verifies the boundary condition at $n=0$. Applying then an Euler transformation[6] on this solution leads to

$$ \rho_{\mathcal{E}}(n) = C_{\mathcal{E}} n^{\gamma_0-1}(1-n)^{\gamma_1-1} {}_2F_1(1-a, 1-b; \gamma_0; n), \tag{D.35} $$

which is well defined at $n=1$ and also verifies the boundary condition. Note that $C_{\mathcal{E}}$ is a constant. We now need to check the integrability condition. We can compute explicitly

$$ \int_0^1 \mathrm{d}n \; \rho_{\mathcal{E}}(n) = C_{\mathcal{E}} \sum_k \frac{(1-a)_k (1-b)_k \Gamma(\gamma_0+k)\Gamma(\gamma_1)}{(\gamma_0)_k \Gamma(\gamma_0+\gamma_1+k) k!}, \tag{D.36} $$

with Γ the Gamma function. If $1-a$ is a non-negative integer[7] all the terms in the series are non-zero. Using then $(x)_k \propto \Gamma(x+k)$ together with the Stirling formula $\Gamma(x+1) \underset{x\gg 1}{\approx} \sqrt{2\pi} x^{x+1/2} e^{-x}$, we find that the general term of the series converges to a constant when $k \to +\infty$ and therefore that $\int_0^1 \mathrm{d}n \; \rho_{\mathcal{E}}(n) = +\infty$.

This entails that there exists a positive integer k such that $1-a=-k$, and so also that $b = 2-k-\gamma_0-\gamma_1$ and $\mathcal{E} = -k(\gamma_0+\gamma_1+k-1)$.

In conclusion, the eigenvectors ρ_k and eigenvalues $\mathcal{E}_k$ are discrete and given by

$$ \mathcal{E}_k = -k(\gamma_0+\gamma_1+k-1) \tag{D.37} $$
$$ \rho_k(n) = C_k n^{\gamma_0-1}(1-n)^{\gamma_1-1} {}_2F_1(-k, \gamma_0+\gamma_1+k-1; \gamma_0; n), \tag{D.38} $$

which allows then for a solution of the form given in Eq. (D.30). The only remaining part is to find the coefficients $\lambda_{\mathcal{E}}$ that depend on the initial condition. This can be done by transforming the Fokker-Planck equation into a Schrödinger's equation as in Ref. [173], noticing that the solutions to said Schrödinger equation can be found in terms of the eigenvalues and eigenvectors ρ_k, and one can therefore find the coefficients $\lambda_{\mathcal{E}}$ by projecting the initial condition on the orthogonal set of eigenvectors of the Schrödinger operators, see the Appendices in Ref. [173] for a detailed technical explanation.

Appendix D.B A symmetric multizones extension

We now present a very natural extension of our model to the general case of M symmetric zones with finite resources. Without loss of generality we set $C_d = 1$ to have lighter notations, but this doesn't change our main message. We also introduce the vector notations $\mathbf{n}(t) = (n_1(t), \ldots, n_M(t))$ and $\mathbf{m}(t) = (m_1(t) \ldots, m_M(t))$, where the index accounts for the zone, and call $p_{j\to i}(\mathbf{n}(t), \mathbf{m}(t))$ the infinitesimal probability that an agent initially present in zone

[6] The Euler transformation states that ${}_2F_1(a,b;c;n) = (1-n)_2^{c-a-b} F_1(c-a, c-b; c; n)$.

[7] As the hypergeometric function is symmetric with respect to its two first arguments, we restrict our analysis to the first one only.

j at time t moves to zone i at $t+dt$. It follows that the evolution of $\mathbf{n}$ and $\mathbf{m}$ is given by

$$dm_i(t) = m_i(t)(\nu(1-m_i(t)) - \beta n_i(t))\mathrm{d}t \tag{D.39}$$

$$p_{j\to i}(\mathbf{n}(t),\mathbf{m}(t)) = \frac{n_j(t)N}{M-1}\left[\varepsilon f\left(m_j(t)\right)\right] + \mu N^2 n_i(t) n_j(t). \tag{D.40}$$

Introducing for simplicity $h(n,m) = m(\nu(1-m)-\beta n)$, the joint density ρ of the variables$(\mathbf{n}(t),\mathbf{m}(t))$ evolves according to the following Fokker-Planck equation,

$$\begin{aligned}\partial_t \rho(\mathbf{n},\mathbf{m}) = &-\sum_i \partial_{m_i}\left(h(n_i,m_i)\rho\right) + \sum_{i\neq j}\left(\partial_{n_i} - \partial_{n_j}\right)\left(\frac{\varepsilon f\left(m_j\right)}{M-1} n_j \rho\right) \\ &+ \mu \sum_{i\neq j}\left(\partial_{n_i n_i} - \partial_{n_j n_i}\right)\left(n_i n_j \rho\right).\end{aligned} \tag{D.41}$$

Owing to the symmetry of the problem, one may generalize the argument used in Section D.4 to obtain the stationary averages

$$n_i = \frac{1}{M}, \quad m_i = \left(1 - \frac{\beta}{M\nu}\right)_+ \tag{D.42}$$

with $(x)_+$ the positive part of x. This again shows the existence of an extinction regime whenever $\beta = M\nu$. In what follows we assume that $\beta/\nu < 1/M$, to study the behaviour of the system outside of extinction.

When $\kappa = 0$ the density of $\boldsymbol{n}$ is a Dirichlet distribution with all parameters equal to (ϵ/δ), namely:

$$\rho_{\boldsymbol{n}}(n_1,\ldots,n_M) = \left(\prod_{i=1}^M n_i^{\epsilon/\mu}\right)\mathbf{1}_{\left\{\sum_{i=1}^M n_i = 1\right\}}. \tag{D.43}$$

As argued previously, whenever the noise-level is coupled to the fish population with $\kappa > 0$, we postulate that the solution can be approximated by a Dirichlet distribution with all parameters set to $(\tilde{\varepsilon}/\mu)$ with $\tilde{\epsilon} = f(1-\frac{\beta}{M\nu})\epsilon$.

The Dirichlet distribution has one key property: $\sum_{i\geq k} n_i$ follows a Beta distribution with parameters $(k\tilde{\varepsilon}/\mu, (M-k)\tilde{\varepsilon}/\mu)$, corresponding to the stationary state of our two-zone model. We have also checked that the mean-field approximation of Eq.D.39 follows the same type of property: the variable $\sum_{i\geq k} n_i(t)$ is ruled by the mean-field approximation of D.6. This result gives solid micro-foundations to our approach and justifies our looking at two aggregated zones for empirical analysis. This may explain the agreement between empirical results and our model.

References

[1] https://en.wikipedia.org/wiki/Panic_of_1907.

[2] Sasha Stoikov. The micro-price: a high-frequency estimator of future prices. *Quantitative Finance*, 18(12):1959–1966, 2018.

[3] Martin D Gould and Julius Bonart. Queue imbalance as a one-tick-ahead price predictor in a limit order book. *Market Microstructure and Liquidity*, 2(02):1650006, 2016.

[4] Andrei Kirilenko, Albert S Kyle, Mehrdad Samadi, and Tugkan Tuzun. The flash crash: High-frequency trading in an electronic market. *The Journal of Finance*, 72(3):967–998, 2017.

[5] Jason Zweig. Back to the future: lessons from the forgoten "flash crash" of 1962. *Intell Invest*, 2010.

[6] Jean-Philippe Bouchaud, Julius Bonart, Jonathan Donier, and Martin Gould. *Trades, quotes and prices: financial markets under the microscope.* Cambridge University Press, 2018.

[7] Louis Bachelier. Théorie de la spéculation. In *Annales scientifiques de l'École normale supérieure*, volume 17, pages 21–86, 1900.

[8] Burton G Malkiel and Eugene F Fama. Efficient capital markets: A review of theory and empirical work. *The journal of Finance*, 25(2):383–417, 1970.

[9] Robert J Shiller. Do stock prices move too much to be justified by subsequent changes in dividends? Technical report, National Bureau of Economic Research, 1980.

[10] Armand Joulin, Augustin Lefevre, Daniel Grunberg, and Jean-Philippe Bouchaud. Stock price jumps: news and volume play a minor role. *Wilmott Magazine*, September/October:1–7, 2008.

[11] Michael Parkinson. The extreme value method for estimating the variance of the rate of return. *Journal of business*, pages 61–65, 1980.

[12] Jim Gatheral, Thibault Jaisson, and Mathieu Rosenbaum. Volatility is rough. *Quantitative Finance*, 18(6):933–949, 2018.

[13] Alan G Hawkes. Spectra of some self-exciting and mutually exciting point processes. *Biometrika*, 58(1):83–90, 1971.

[14] Emmanuel Bacry, Sylvain Delattre, Marc Hoffmann, and Jean-Francois Muzy. Some limit theorems for hawkes processes and application to financial statistics. *Stochastic Processes and their Applications*, 123(7):2475–2499, 2013.

[15] Emmanuel Bacry, Khalil Dayri, and Jean-François Muzy. Non-parametric kernel estimation for symmetric hawkes processes. application to high frequency financial data. *The European Physical Journal B*, 85(5):157, 2012.

[16] Emmanuel Bacry, Thibault Jaisson, and Jean-François Muzy. Estimation of slowly decreasing hawkes kernels: application to high-frequency order book dynamics. *Quantitative Finance*, 16(8):1179–1201, 2016.

[17] Emmanuel Bacry and Jean-François Muzy. First-and second-order statistics characterization of hawkes processes and non-parametric estimation. *IEEE Transactions on Information Theory*, 62(4):2184–2202, 2016.

[18] Stephen J Hardiman, Nicolas Bercot, and Jean-Philippe Bouchaud. Critical reflexivity in financial markets: a hawkes process analysis. *The European Physical Journal B*, 86(10):442, 2013.

[19] Stephen J Hardiman and Jean-Philippe Bouchaud. Branching-ratio approximation for the self-exciting hawkes process. *Physical Review E*, 90(6):062807, 2014.

[20] Vladimir Filimonov and Didier Sornette. Quantifying reflexivity in financial markets: Toward a prediction of flash crashes. *Physical Review E*, 85(5):056108, 2012.

[21] Thibault Jaisson, Mathieu Rosenbaum, et al. Limit theorems for nearly unstable hawkes processes. *The annals of applied probability*, 25(2):600–631, 2015.

[22] Thibault Jaisson, Mathieu Rosenbaum, et al. Rough fractional diffusions as scaling limits of nearly unstable heavy tailed hawkes processes. *The Annals of Applied Probability*, 26(5):2860–2882, 2016.

[23] John C Cox, Jonathan E Ingersoll Jr, and Stephen A Ross. A theory of the term structure of interest rates. In *Theory of valuation*, pages 129–164. World Scientific, 2005.

[24] Jean-Philippe Bouchaud, Andrew Matacz, and Marc Potters. Leverage effect in financial markets: The retarded volatility model. *Physical review letters*, 87(22):228701, 2001.

[25] Gilles Zumbach. Time reversal invariance in finance. *Quantitative Finance*, 9(5):505–515, 2009.

[26] Gilles Zumbach. Volatility conditional on price trends. *Quantitative Finance*, 10(4):431–442, 2010.

[27] Rémy Chicheportiche and Jean-Philippe Bouchaud. The fine-structure of volatility feedback i: Multi-scale self-reflexivity. *Physica A: Statistical Mechanics and its Applications*, 410:174–195, 2014.

[28] Omar El Euch, Jim Gatheral, Radoš Radoičić, and Mathieu Rosenbaum. The zumbach effect under rough heston. *Quantitative Finance*, 20(2):235–241, 2020.

[29] Enrique Sentana. Quadratic arch models. *The Review of Economic Studies*, 62(4):639–661, 1995.

[30] Pierre Blanc, Jonathan Donier, and J-P Bouchaud. Quadratic hawkes processes for financial prices. *Quantitative Finance*, 17(2):171–188, 2017.

[31] Aditi Dandapani, Paul Jusselin, and Mathieu Rosenbaum. From quadratic hawkes processes to super-heston rough volatility models with zumbach effect. *arXiv preprint arXiv:1907.06151*, 2019.

[32] Bence Tóth, Yves Lemperiere, Cyril Deremble, Joachim De Lataillade, Julien Kockelkoren, and J-P Bouchaud. Anomalous price impact and the critical nature of liquidity in financial markets. *Physical Review X*, 1(2):021006, 2011.

[33] Nicolo Torre. Barra market impact model handbook. *BARRA Inc., Berkeley*, 1997.

[34] Robert Almgren, Chee Thum, Emmanuel Hauptmann, and Hong Li. Direct estimation of equity market impact. *Risk*, 18(7):58–62, 2005.

[35] Engle Robert, Ferstenberg Robert, and Russell Jeffrey. Measuring and modeling execution cost and risk. *The Journal of Portfolio Management*, 38(2):14–28, 2012.

[36] Iacopo Mastromatteo, Bence Toth, and Jean-Philippe Bouchaud. Agent-based models for latent liquidity and concave price impact. *Physical Review E*, 89(4):042805, 2014.

[37] Xavier Brokmann, Emmanuel Serie, Julien Kockelkoren, and J-P Bouchaud. Slow decay of impact in equity markets. *Market Microstructure and Liquidity*, 1(02):1550007, 2015.

[38] Emmanuel Bacry, Adrian Iuga, Matthieu Lasnier, and Charles-Albert Lehalle. Market impacts and the life cycle of investors orders. *Market Microstructure and Liquidity*, 1(02):1550009, 2015.

[39] Nataliya Bershova and Dmitry Rakhlin. The non-linear market impact of large trades: Evidence from buy-side order flow. *Quantitative finance*, 13(11):1759–1778, 2013.

[40] Jonathan Donier and Julius Bonart. A million metaorder analysis of market impact on the bitcoin. *Market Microstructure and Liquidity*, 1(02):1550008, 2015.

[41] Emilio Said, Ahmed Bel Hadj Ayed, Alexandre Husson, and Frédéric Abergel. Market impact: A systematic study of limit orders. *Market Microstructure and Liquidity*, 3(03n04):1850008, 2017.

[42] Bence Tóth, Zoltán Eisler, and J-P Bouchaud. The square-root impace law also holds for option markets. *Wilmott*, 2016(85):70–73, 2016.

[43] Marcus G Daniels, J Doyne Farmer, László Gillemot, Giulia Iori, and Eric Smith. Quantitative model of price diffusion and market friction based on trading as a mechanistic random process. *Physical review letters*, 90(10):108102, 2003.

[44] Eric Smith, J Doyne Farmer, L Gillemot, Supriya Krishnamurthy, et al. Statistical theory of the continuous double auction. *Quantitative finance*, 3(6):481–514, 2003.

[45] Weibing Huang, Charles-Albert Lehalle, and Mathieu Rosenbaum. Simulating and analyzing order book data: The queue-reactive model. *Journal of the American Statistical Association*, 110(509):107–122, 2015.

[46] Jonathan Donier, Julius Bonart, Iacopo Mastromatteo, and J-P Bouchaud. A fully consistent, minimal model for non-linear market impact. *Quantitative finance*, 15(7):1109–1121, 2015.

[47] Jean-Philippe Bouchaud, Yuval Gefen, Marc Potters, and Matthieu Wyart. Fluctuations and response in financial markets: the subtle nature of ârandomâprice changes. *Quantitative finance*, 4(2):176–190, 2004.

[48] Michael Benzaquen and J-P Bouchaud. Market impact with multi-timescale liquidity. *Quantitative Finance*, 18(11):1781–1790, 2018.

[49] D M Cutler, J M Poterba, and L H Summers. What moves stock prices? *Journal of Portfolio Management*, 15(3):4–12, 1989.

[50] Ray Fair. Events that shook the market. *The Journal of Business*, 75(4):713–732, 2002.

[51] Jean-Philippe Bouchaud. The endogenous dynamics of markets: price impact and feedback loops. *arXiv preprint arXiv:1009.2928*, 2010.

[52] Antoine Fosset, Jean-Philippe Bouchaud, and Michael Benzaquen. Endogenous liquidity crises. *Available at SSRN 3496148*, 2019.

[53] Alan G Hawkes. Spectra of some self-exciting and mutually exciting point processes. *Biometrika*, 58(1):83–90, 1971.

[54] Ioane Muni Toke. An introduction to hawkes processes with applications to finance. *Lectures Notes from Ecole Centrale Paris, BNP Paribas Chair of Quantitative Finance*, 193, 2011.

[55] Emmanuel Bacry, Iacopo Mastromatteo, and Jean-François Muzy. Hawkes processes in finance. *Market Microstructure and Liquidity*, 1(01):1550005, 2015.

[56] Maxime Morariu-Patrichi and Mikko S Pakkanen. State-dependent hawkes processes and their application to limit order book modelling. *arXiv preprint arXiv:1809.08060*, 2018.

[57] Marcello Rambaldi, Emmanuel Bacry, and Fabrizio Lillo. The role of volume in order book dynamics: a multivariate hawkes process analysis. *Quantitative Finance*, 17(7):999–1020, 2017.

[58] Giacomo Bormetti, Lucio Maria Calcagnile, Michele Treccani, Fulvio Corsi, Stefano Marmi, and Fabrizio Lillo. Modelling systemic price cojumps with hawkes factor models. *Quantitative Finance*, 15(7):1137–1156, 2015.

[59] Peng Wu, Marcello Rambaldi, Jean-François Muzy, and Emmanuel Bacry. Queue-reactive hawkes models for the order flow. *arXiv preprint arXiv:1901.08938*, 2019.

[60] Emmanuel Bacry and Jean-François Muzy. Hawkes model for price and trades high-frequency dynamics. *Quantitative Finance*, 14(7):1147–1166, 2014.

[61] Emmanuel Bacry, Sylvain Delattre, Marc Hoffmann, and Jean-François Muzy. Modelling microstructure noise with mutually exciting point processes. *Quantitative finance*, 13(1):65–77, 2013.

[62] Marcello Rambaldi, Paris Pennesi, and Fabrizio Lillo. Modeling foreign exchange market activity around macroeconomic news: Hawkes-process approach. *Phys. Rev. E*, 91:012819, Jan 2015.

[63] Aurélien Alfonsi and Pierre Blanc. Extension and calibration of a hawkes-based optimal execution model. *Market Microstructure and Liquidity*, 2(02):1650005, 2016.

[64] Aurélien Alfonsi and Pierre Blanc. Dynamic optimal execution in a mixed-market-impact hawkes price model. *Finance and Stochastics*, 20(1):183–218, 2016.

[65] Massil Achab, Emmanuel Bacry, Jean-François Muzy, and Marcello Rambaldi. Analysis of order book flows using a non-parametric estimation of the branching ratio matrix. *Quantitative Finance*, 18(2):199–212, 2018.

[66] Lucio Maria Calcagnile, Giacomo Bormetti, Michele Treccani, Stefano Marmi, and Fabrizio Lillo. Collective synchronization and high frequency systemic instabilities in financial markets. *Quantitative Finance*, 18(2):237–247, 2018.

[67] Shinsuke Koyama and Shigeru Shinomoto. The statistical physics of discovering exogenous and endogenous factors in a chain of events. *arXiv preprint arXiv:2003.00659*, 2020.

[68] David S Bates. How crashes develop: intradaily volatility and crash evolution. *The Journal of Finance*, 74(1):193–238, 2019.

[69] Nathan Srebro and Tommi Jaakkola. Weighted low-rank approximations. In *Proceedings of the 20th International Conference on Machine Learning (ICML-03)*, pages 720–727, 2003.

[70] P. Jusselin and M. Rosenbaum. No-arbitrage implies power-law market impact and rough volatility. *Available at SSRN 3180582*, 2018.

[71] J Doyne Farmer, Paolo Patelli, and Ilija I Zovko. The predictive power of zero intelligence in financial markets. *Proceedings of the National Academy of Sciences*, 102(6):2254–2259, 2005.

[72] Rama Cont and Adrien De Larrard. Order book dynamics in liquid markets: limit theorems and diffusion approximations. *Available at SSRN 1757861*, 2012.

[73] Ananth Madhavan, Matthew Richardson, and Mark Roomans. Why do security prices change? a transaction-level analysis of nyse stocks. *The Review of Financial Studies*, 10(4):1035–1064, 1997.

[74] Matthieu Wyart, Jean-Philippe Bouchaud, Julien Kockelkoren, Marc Potters, and Michele Vettorazzo. Relation between bid–ask spread, impact and volatility in order-driven markets. *Quantitative Finance*, 8(1):41–57, 2008.

[75] P Bak, C Tang, and K Wiesenfeld. Self-organized criticality: an explanation of 1/f noise, 1987. *Phys. Rev. Lett*, 59:381.

[76] Damien Challet and Yi-Cheng Zhang. On the minority game: Analytical and numerical studies. *Physica A: Statistical Mechanics and its applications*, 256(3-4):514–532, 1998.

[77] Irene Giardina and J-P Bouchaud. Bubbles, crashes and intermittency in agent based market models. *The European Physical Journal B-Condensed Matter and Complex Systems*, 31(3):421–437, 2003.

[78] V Alfi, Matthieu Cristelli, L Pietronero, and A Zaccaria. Minimal agent based model for financial markets i. *The European Physical Journal B*, 67(3):385–397, 2009.

[79] Alessio Emanuele Biondo, Alessandro Pluchino, and Andrea Rapisarda. Modeling financial markets by self-organized criticality. *Physical Review E*, 92(4):042814, 2015.

[80] Victor Buendía, Serena di Santo, Juan A Bonachela, and Miguel A Muñoz. Feedback mechanisms for self-organization to the edge of a phase transition. *arXiv preprint arXiv:2006.03020*, 2020.

[81] Sidney Redner. *A guide to first-passage processes*. Cambridge University Press, 2001.

[82] Omar El Euch and Mathieu Rosenbaum. The characteristic function of rough heston models. *Mathematical Finance*, 29(1):3–38, 2019.

[83] Peter Hänggi, Peter Talkner, and Michal Borkovec. Reaction-rate theory: fifty years after kramers. *Reviews of modern physics*, 62(2).

[84] C Godreche, JP Bouchaud, and M Mézard. Entropy barriers and slow relaxation in some random walk models. *Journal of Physics A: Mathematical and General*, 28(23):L603, 1995.

[85] Charles-Albert Lehalle, Olivier Guéant, and Julien Razafinimanana. High-frequency simulations of an order book: a two-scale approach. In *Econophysics of Order-driven Markets*, pages 73–92. Springer, 2011.

[86] Per Bak, Maya Paczuski, and Martin Shubik. Price variations in a stock market with many agents. *Physica A: Statistical Mechanics and its Applications*, 246(3-4):430–453, 1997.

[87] Leonard CG Rogers, Stephen E Satchell, and Y Yoon. Estimating the volatility of stock prices: a comparison of methods that use high and low prices. *Applied Financial Economics*, 4(3):241–247, 1994.

[88] Elia Zarinelli, Michele Treccani, J Doyne Farmer, and Fabrizio Lillo. Beyond the square root: Evidence for logarithmic dependence of market impact on size and participation rate. *Market Microstructure and Liquidity*, 1(02):1550004, 2015.

[89] Khalil Dayri and Mathieu Rosenbaum. Large tick assets: implicit spread and optimal tick size. *Market Microstructure and Liquidity*, 1(01):1550003, 2015.

[90] Michael Benzaquen and Jean-Philippe Bouchaud. A fractional reaction–diffusion description of supply and demand. *The European Physical Journal B*, 91(2):23, 2018.

[91] Thierry Bochud and Damien Challet. Optimal approximations of power laws with exponentials: application to volatility models with long *Quantitative Finance*, 7(6):585–589, 2007.

[92] KV Mardia, JT Kent, and JM Bibby. Multivariate analysis. 1979. *Probability and mathematical statistics. Academic Press Inc.*

[93] Herbert A. Simon. A behavioral model of rational choice. *The Quarterly Journal of Economics*, 69(1):99–118, 1955.

[94] Herbert A Simon. Theories of bounded rationality. *Decision and organization*, 1(1):161–176, 1972.

[95] Reinhard Selten. Bounded rationality. *Journal of Institutional and Theoretical Economics (JITE) / Zeitschrift fÃ̃¼r die gesamte Staatswissenschaft*, 146(4):649–658, 1990.

[96] W. Brian Arthur. Inductive reasoning and bounded rationality. *The American Economic Review*, 84(2):406–411, 1994.

[97] Gerd Gigerenzer and Reinhard Selten. *Bounded rationality: The adaptive toolbox*. MIT press, 2002.

[98] Daniel Kahneman. A psychological perspective on economics. *American Economic Review*, 93(2):162–168, April 2003.

[99] Daniel Kahneman and Richard H. Thaler. Anomalies: Utility maximization and experienced utility. *Journal of Economic Perspectives*, 20(1):221–234, March 2006.

[100] William A. Brock and Steven N. Durlauf. Discrete choice with social interactions. *The Review of Economic Studies*, 68(2):235–260, 2001.

[101] Steven N Durlauf and H Peyton Young. *Social dynamics*, volume 4. Mit Press, 2004.

[102] Christian Borghesi and Jean-Philippe Bouchaud. Of songs and men: a model for multiple choice with herding. *Quality & Quantity*, 41(4):557–568, March 2007.

[103] Jean-Philippe Bouchaud. Crises and collective socio-economic phenomena: Simple models and challenges. *Journal of Statistical Physics*, 151(3-4):567–606, January 2013.

[104] Federico Guglielmo Morelli, Michael Benzaquen, Marco Tarzia, and Jean-Philippe Bouchaud. Confidence collapse in a multi-household, self-reflexive dsge model. 2019.

[105] Daniel Kahneman. Experienced utility and objective happiness: A moment-based approach. In *Choices, Values, and Frames*, pages 673–692. Cambridge University Press, September 2000.

[106] John Y. Campbell and John H. Cochrane. By force of habit: A consumptionâbased explanation of aggregate stock market behavior. *Journal of Political Economy*, 107(2):205–251, 1999.

[107] Andrew Abel. Asset prices under habit formation and catching up with the joneses. Technical report, March 1990.

[108] George M. Constantinides. Habit formation: A resolution of the equity premium puzzle. *Journal of Political Economy*, 98(3):519–543, 1990.

[109] Christopher D. Carroll, Jody Overland, and David N. Weil. Saving and growth with habit formation. *American Economic Review*, 90(3):341–355, June 2000.

[110] Jeffrey C. Fuhrer. Habit formation in consumption and its implications for monetary-policy models. *American Economic Review*, 90(3):367–390, June 2000.

[111] Robert A. Pollak. Habit formation and dynamic demand functions. *Journal of Political Economy*, 78(4):745–763, 1970.

[112] Robin Pemantle. A survey of random processes with reinforcement. *Probab. Surveys*, 4:1–79, 2007.

[113] Denis Boyer, Andrea Falcón-Cortés, Luca Giuggioli, and Satya N Majumdar. Anderson-like localization transition of random walks with resetting. *Journal of Statistical Mechanics: Theory and Experiment*, 2019(5):053204, may 2019.

[114] Robert L. Jack and Rosemary J. Harris. Giant leaps and long excursions: fluctuation mechanisms in systems with long-range memory, 2020.

[115] W. Brian Arthur, Yu.M. Ermoliev, and Yu.M. Kaniovski. Path-dependent processes and the emergence of macro-structure. *European Journal of Operational Research*, 30(3):294–303, June 1987.

[116] W. Brian Arthur. Positive feedbacks in the economy. *Scientific American*, 262(2):92–99, 1990.

[117] Alan P. Kirman and Nicolaas J. Vriend. Evolving market structure: An ACE model of price dispersion and loyalty. *Journal of Economic Dynamics and Control*, 25(3-4):459–502, March 2001.

[118] Simon P. Anderson, Andre de Palma, and Jacques-Francois Thisse. *Discrete Choice Theory of Product Differentiation (The MIT Press)*. The MIT Press, 1992.

[119] Nicholas Metropolis and S. Ulam. The Monte Carlo method. *Journal of the American Statistical Association*, 44(247):335–341, September 1949.

[120] W. K. Hastings. Monte carlo sampling methods using markov chains and their applications. *Biometrika*, 57(1):97–109, April 1970.

[121] Bernard Derrida. Random-energy model: An exactly solvable model of disordered systems. *Phys. Rev. B*, 24:2613–2626, Sep 1981.

[122] Jean-Philippe Bouchaud and Marc Mézard. Universality classes for extreme-value statistics. *Journal of Physics A: Mathematical and General*, 30(23):7997–8015, dec 1997.

[123] F. Wegner. Inverse participation ratio in $2 + \varepsilon$ dimensions. *Zeitschrift für Physik B Condensed Matter and Quanta*, 36(3):209–214, September 1980.

[124] R. J. Bell and P. Dean. Atomic vibrations in vitreous silica. *Discussions of the Faraday Society*, 50:55, 1970.

[125] Marshall Hall and Nicolaus Tideman. Measures of concentration. *Journal of the American Statistical Association*, 62(317):162–168, March 1967.

[126] E Bertin and J-P Bouchaud. Dynamical ultrametricity in the critical trap model. *Journal of Physics A: Mathematical and General*, 35(13):3039–3051, mar 2002.

[127] Ariel Amir, Yuval Oreg, and Yoseph Imry. On relaxations and aging of various glasses. *Proceedings of the National Academy of Sciences*, 109(6):1850–1855, 2012.

[128] Pablo G. Debenedetti and Frank H. Stillinger. Supercooled liquids and the glass transition. *Nature*, 410(6825):259–267, March 2001.

[129] J. P. Bouchaud. Weak ergodicity breaking and aging in disordered systems. *Journal de Physique I*, 2(9):1705–1713, September 1992.

[130] Thierry Bochud and Damien Challet. Optimal approximations of power-laws with exponentials. 2006.

[131] Duncan J. Watts and Steven H. Strogatz. Collective dynamics of 'small-world' networks. *Nature*, 393(6684):440–442, June 1998.

[132] Cécile Monthus and Jean-Philippe Bouchaud. Models of traps and glass phenomenology. *Journal of Physics A: Mathematical and General*, 29(14):3847–3869, jul 1996.

[133] L F Cugliandolo and J Kurchan. On the out-of-equilibrium relaxation of the sherrington-kirkpatrick model. *Journal of Physics A: Mathematical and General*, 27(17):5749–5772.

[134] J-Ph Bouchaud. Aging in glassy systems: new experiments, simple models, and open questions. *Soft and Fragile Matter: Nonequilibrium Dynamics, Metastability and Flow*, pages 285–304, 2000.

[135] Luca Cipelletti, S. Manley, R. C. Ball, and D. A. Weitz. Universal aging features in the restructuring of fractal colloidal gels. *Phys. Rev. Lett.*, 84:2275–2278, Mar 2000.

[136] Rosemary J Harris. Random walkers with extreme value memory: modelling the peak-end rule. *New Journal of Physics*, 17(5):053049, may 2015.

[137] Aleksandra Alorić, Peter Sollich, and Peter McBurney. Spontaneous segregation of agents across double auction markets. In *Lecture Notes in Economics and Mathematical Systems*, pages 79–90. Springer International Publishing, October 2014.

[138] Aleksandra Alorić and Peter Sollich. Market fragmentation and market consolidation: Multiple steady states in systems of adaptive traders choosing where to trade. *Physical Review E*, 99(6), June 2019.

[139] Codina Cotar and Vlada Limic. Attraction time for strongly reinforced walks. *The Annals of Applied Probability*, 19(5):1972–2007, October 2009.

[140] Alan Kirman. Ants, rationality, and recruitment. *The Quarterly Journal of Economics*, 108(1):137–156, 1993.

[141] P. A. P. Moran. Random processes in genetics. *Mathematical Proceedings of the Cambridge Philosophical Society*, 54(1):60–71, 1958.

[142] J. L. Deneubourg, S. Aron, S. Goss, and J. M. Pasteels. The self-organizing exploratory pattern of the argentine ant. *Journal of Insect Behavior*, 3(2):159–168, March 1990.

[143] R. Beckers, J. L. Deneubourg, S. Goss, and J. M. Pasteels. Collective decision making through food recruitment. *Insectes Sociaux*, 37(3):258–267, September 1990.

[144] Gary S Becker. A note on restaurant pricing and other examples of social influences on price. *Journal of political economy*, 99(5):1109–1116, 1991.

[145] David S Scharfstein and Jeremy C Stein. Herd behavior and investment. *The American economic review*, pages 465–479, 1990.

[146] Robert J Shiller and John Pound. Survey evidence on diffusion of investment among institutional investors. Technical report, National Bureau of Economic Research, 1986.

[147] Thomas Lux. Herd behaviour, bubbles and crashes. *The economic journal*, 105(431):881–896, 1995.

[148] Alan Kirman and Gilles Teyssiere. Microeconomic models for long memory in the volatility of financial time series. *Studies in Nonlinear Dynamics & Econometrics*, 5(4), 2002.

[149] Manfred Gilli and Peter Winker. A global optimization heuristic for estimating agent based models. *Computational Statistics & Data Analysis*, 42(3):299–312, 2003.

[150] R. Lambiotte and S. Redner. Dynamics of vacillating voters. *Journal of Statistical Mechanics: Theory and Experiment*, 2007(10):L10001–L10001, Oct 2007. arXiv: 0710.0914.

[151] Hannes Risken. Fokker-planck equation. In *The Fokker-Planck Equation*, pages 63–95. Springer, 1996.

[152] Sewall Wright. Statistical genetics and evolution. *Bull. Amer. Math. Soc.*, 48(4):223–246, 04 1942.

[153] M. Kimura. Stochastic processes and distribution of gene frequencies under natural selection. *Cold Spring Harbor Symposia on Quantitative Biology*, 20(0):33–53, January 1955.

[154] A.J. McKane and D. Waxman. Singular solutions of the diffusion equation of population genetics. *Journal of Theoretical Biology*, 247(4):849–858, August 2007.

[155] Kristen Fichthorn, Erdogan Gulari, and Robert Ziff. Noise-induced bistability in a monte carlo surface-reaction model. *Physical Review Letters*, 63(14):1527–1530, Oct 1989.

[156] D. Considine, S. Redner, and H. Takayasu. Comment on "noise-induced bistability in a monte carlo surface-reaction model". *Physical Review Letters*, 63(26):2857–2857, Dec 1989.

[157] Kiyosi Itô. *On stochastic differential equations*. Number 4. American Mathematical Soc., 1951.

[158] Claude Cohen-Tannoudji, Bernard Diu, and Frank Laloe. *Quantum Mechanics*. Wiley, Jan 1991.

[159] Michael Martin Nieto and L. M. Simmons. Coherent states for general potentials. ii. confining one-dimensional examples. *Phys. Rev. D*, 20:1332–1341, Sep 1979.

[160] H. Taşeli. Exact analytical solutions of the hamiltonian with a squared tangent potential. *Journal of Mathematical Chemistry*, 34(3/4):243–251, November 2003.

[161] F. Vazquez and S. Redner. Ultimate fate of constrained voters. *Journal of Physics A: Mathematical and General*, 37(35):8479–8494, Sep 2004. arXiv: cond-mat/0405652.

[162] Xavier Gabaix, Jean-Michel Lasry, Pierre-Louis Lions, and Benjamin Moll. The dynamics of inequality. *Econometrica*, 84(6):2071–2111, 2016.

[163] Jean-Philippe Bouchaud and Roger Farmer. in preparation.

[164] José Moran, Antoine Fosset, Alan Kirman, and Michael Benzaquen. in preparation.

[165] Hakan Ciftci, Richard Hall, and Nasser Saad. Exact and approximate solutions of schrödinger's equation for a class of trigonometric potentials. *Open Physics*, 11(1), January 2013.

[166] Garrett Hardin. The tragedy of the commons. *Science*, 162(3859):1243–1248, 1968.

[167] Stratis Gavaris. Use of a multiplicative model to estimate catch rate and effort from commercial data. *Canadian Journal of Fisheries and Aquatic Sciences*, 37(12):2272–2275, 1980.

[168] Marianne Vignaux. Analysis of vessel movements and strategies using commercial catch and effort data from the new zealand hoki fishery. *Canadian Journal of Fisheries and Aquatic Sciences*, 53(9):2126–2136, 1996.

[169] Peter M Allen and Jacqueline M McGlade. Dynamics of discovery and exploitation: the case of the scotian shelf groundfish fisheries. *Canadian Journal of Fisheries and Aquatic Sciences*, 43(6):1187–1200, 1986.

[170] Sorin Dascalu, Tudor Scurtu, Andreea Urzica, Mihai Trascau, and Adina Magda Florea. Using norm emergence in addressing the tragedy of the commons. In *International conference on computational collective intelligence*, pages 165–174. Springer, 2013.

[171] Global Fishing Watch, Fishing Vessels Dataset, `https://globalfishingwatch.org/datasets-and-code/vessel-identity`, 2020.

[172] Mauro Gallegati, Gianfranco Giulioni, Alan Kirman, and Antonio Palestrini. Whatâs that got to do with the price of fish? buyers behavior on the ancona fish market. *Journal of Economic Behavior & Organization*, 80(1):20–33, 2011.

[173] José Moran, Antoine Fosset, Michael Benzaquen, and Jean-Philippe Bouchaud. Schrödinger's ants: A continuous description of Kirman's recruitment model. *arXiv preprint arXiv:2004.06667*, 2020.

[174] Robert MacArthur. Species packing and competitive equilibrium for many species. *Theoretical population biology*, 1(1):1–11, 1970.

[175] Robert Mac Arthur. Species packing, and what competition minimizes. *Proceedings of the National Academy of Sciences*, 64(4):1369–1371, 1969.

[176] Nicolas Bacaër. Lotka, volterra and the predator–prey system (1920–1926). In *A short history of mathematical population dynamics*, pages 71–76. Springer, 2011.

[177] Milton Abramowitz and Irene A Stegun. *Handbook of mathematical functions with formulas, graphs, and mathematical tables*, volume 55. US Government printing office, 1948.

Titre : Crises de liquidité endogènes dans les marchés financiers

Mots clés : microstructure, carnet d'ordres, instabilités, métastabilité, processus de Hawkes

Résumé : De récentes analyses empiriques ont révélé l'existence de l'effet Zumbach. Cette découverte a conduit à l'élaboration des processus de Hawkes quadratique, adpaté pour reproduire cet effet. Ce modèle ne faisant pas de lien avec le processus de formation de prix, nous l'avons étendu au carnet d'ordres avec un processus de Hawkes quadratique généralisé (GQ-Hawkes). En utilisant des données de marchés, nous avons montré qu'il existe un effet de type Zumbach qui diminue la liquidité future. Microfondant l'effet Zumbach, il est responsable d'une potentielle déstabilisation des marchés financiers. De plus, la calibration exacte d'un processus GQ-Hawkes nous indique que les marchés sont aux bords de la criticité. Ces preuves empiriques nous ont donc incité à faire une analyse d'un modèle de carnet d'ordres construit avec un couplage de type Zumbach. Nous avons donc introduit le modèle de Santa Fe quadratique et prouvé numériquement qu'il existe une transition de phase entre un marché stable et un marché instable sujet à des crises de liquidité. Grâce à une analyse de taille finie nous avons pu déterminer les exposants critiques de cette transition, appartenant à une nouvelle classe d'universalité. N'étant pas analytiquement soluble, cela nous a conduit à introduire des modèles plus simples pour décrire les crises de liquidités. En mettant de côté la microstructure du carnet d'ordres, nous obtenons une classe de modèles de spread où nous avons calculé les paramètres critiques de leurs transitions. Même si ces exposants ne sont pas ceux de la transition du Santa Fe quadratique, ces modèles ouvrent de nouveaux horizons pour explorer la dynamique de spread. L'un d'entre eux possède un couplage non-linéaire faisant apparaître un état métastable. Ce scénario alternatif élégant n'a pas besoin de paramètres critiques pour obtenir un marché instable, même si les données empiriques ne sont pas en sa faveur. Pour finir, nous avons regardé la dynamique du carnet d'ordres sous un autre angle : celui de la réaction-diffusion. Nous avons modélisé une liquidité qui se révèle dans le carnet d'ordres avec une certaine fréquence. La résolution de ce modèle à l'équilibre révèle qu'il existe une condition de stabilité sur les paramètres au-delà de laquelle le carnet d'ordres se vide totalement, correspondant à une crise de liquidité. En le calibrant sur des données de marchés nous avons pu analyser qualitativement la distance à cette région instable.

Title : Endogenous liquidity crises in financial markets

Keywords : market microstructure, limit order book, instability, metastability, Hawkes process

Abstract : Recent empirical analyses have revealed the existence of the Zumbach effect. This discovery has led to the development of quadratic Hawkes processes, which are suitable for reproducing this effect. Since this model is not linked with the price formation process, we extended it to order book modeling with a generalized quadratic Hawkes process (GQ-Hawkes). Using market data, we showed that there is a Zumbach-like effect that decreases future liquidity. Microfounding the Zumbach effect, it is responsible for a destabilization of financial markets. Moreover, the exact calibration of a GQ-Hawkes process tells us that the markets are on the verge of criticality. This empirical evidence therefore prompted us to analyse an order-book model constructed upon a Zumbach-like feedback. We therefore introduced the quadratic Santa Fe model and proved numerically that there is a phase transition between a stable market and an unstable market subject to liquidity crises. Thanks to a finite size scaling we were able to determine the critical exponents of this transition, which appears to belong to a new universality class. As this was not analytically tractable, it led us to introduce simpler models to describe liquidity crises. Setting aside the microstructure of the order book, we obtain a class of spread models where we computed the critical parameters of their transitions. Even if these exponents are not those of the quadratic Santa Fe transition, these models open new horizons for modelling spread dynamics. One of them has a non-linear coupling that reveals a metastable state. This elegant alternative scenario does not need critical parameters to obtain an unstable market, even if the empirical evidence is not in its favour. Finally, we looked at the order book dynamics from another point of view : the reaction-diffusion one. We have modelled a liquidity that appears in the order book with a certain frequency. The resolution of this model at equilibrium reveals that there is a condition of stability on the parameters beyond which the order book empties completely, corresponding to a liquidity crisis. By calibrating it on market data we were able to qualitatively analyse the distance to this unstable region.

Institut Polytechnique de Paris
91120 Palaiseau, France